Charles University / Univerzita Karlova

Faculty of Science / Přírodovědecká fakulta

Study programme / Studijní program: Geology / Geologie

Branch of study / Studijní obor: Geology / Geologie

Mgr. Igor Soejono

Evolution of accretionary orogenic systems – the nature and geodynamics of the western Mongolian Altai

Vývoj akrečních orogenních systémů – povaha a geodynamika Západního Mongolského Altaje

Supplementary material to the doctoral thesis (Chapters I–III)

Supervisor / Školitel: Doc. Mgr. Vojtěch Janoušek, Ph.D.

Co-supervisor / Konzultant: Doc. Mgr. Ondrej Lexa, Ph.D.

Praha, 2019

Chapter I

A reworked Lake Zone margin: chronological and geochemical constraints from the Ordovician arc-related basement of the Hovd Zone (western Mongolia)

by Igor Soejono, David Buriánek, Vojtěch Janoušek, Martin Svojtka, Pavel Čáp, Vojtěch Erban, Nyamtsetseg Ganpurev

Graphical abstract

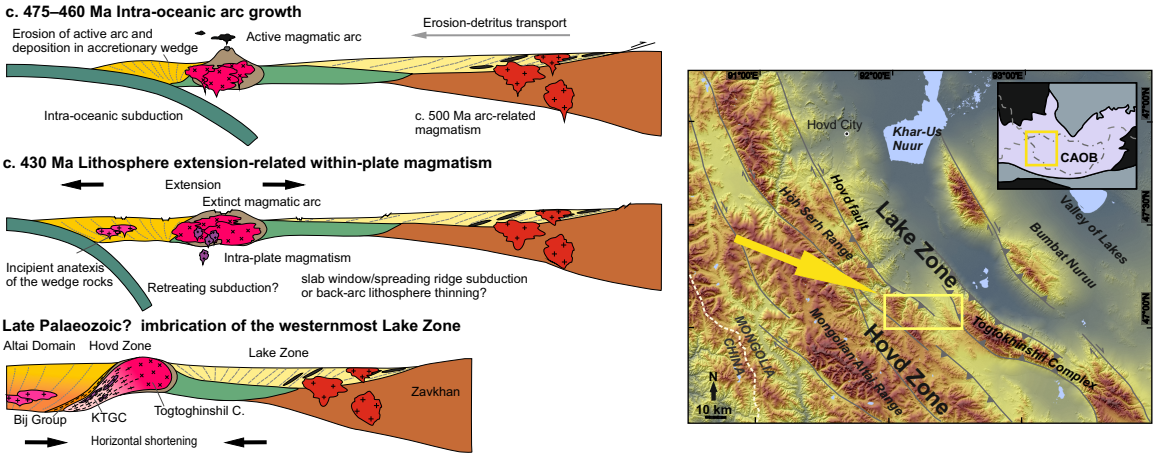

Keywords: *Ordovician magmatic arc, Mid-Silurian intra-plate magmatism, Hovd Zone, reworked Lake Zone*

Supplementary materials are available at https://doi.org/10.1016/j.liths.2017.08.014

Lithos 294–295 (2017) 112–132

Contents lists available at ScienceDirect

Lithos

journal homepage: www.elsevier.com/locate/lithos

A reworked Lake Zone margin: Chronological and geochemical constraints from the Ordovician arc-related basement of the Hovd Zone (western Mongolia)

Igor Soejono [a,b,*], David Buriánek [a], Vojtěch Janoušek [a,b], Martin Svojtka [c], Pavel Čáp [a], Vojtěch Erban [a], Nyamtsetseg Ganpurev [d]

[a] Czech Geological Survey, Klárov 3, 118 21 Prague 1, Czech Republic
[b] Institute of Petrology and Structural Geology, Faculty of Science, Charles University, Albertov 6, 128 43 Prague 2, Czech Republic
[c] Institute of Geology of the CAS, v. v. i., Rozvojová 269, 165 00 Prague 6, Czech Republic
[d] Plagioclase LLC, 16th khoroo-19, Bayanzurkh district, Ulaanbaatar, Mongolia

ARTICLE INFO

Article history:
Received 3 July 2017
Accepted 21 August 2017
Available online 04 September 2017

Keywords:
Ordovician magmatic arc
Mid-Silurian intra-plate magmatism
Hovd Zone
Reworked Lake Zone

ABSTRACT

The primary relationships and character of the boundaries between principal lithotectonic domains in the Mongolian tract of the Central Asian Orogenic Belt (CAOB) are still poorly constrained. This brings much uncertainty in understanding of the orogeny configuration and the complete accretionary history. The plutonic Khuurai Tsenkher Gol Complex and the mainly metasedimentary Bij Group represent associated medium- to high-grade basement complexes exposed in the Hovd Zone close to its boundary with the Lake Zone in western Mongolia. The Khuurai Tsenkher Gol Complex is composed of variously deformed acid to basic magmatic rocks intimately associated with the metamorphosed sedimentary and volcanic rocks of the Bij Group.

Results of our field work, new U–Pb zircon ages and whole-rock geochemical data suggest an existence of two separate magmatic events within the evolution of the Khuurai Tsenkher Gol Complex. Early to Mid-Ordovician (476 ± 5 Ma and 467 ± 4 Ma protoliths) normal- to high-K calc-alkaline orthogneisses, metadiorites and metagabbros predominate over Mid-Silurian (430 ± 3 Ma) tholeiitic–mildly alkaline quartz monzodiorites. Whereas the geochemical signature of the former suite unequivocally demonstrates its magmatic-arc origin, that of the latter quartz monzodiorite suggests an intra-plate setting. As shown by Sr–Nd isotopic data, the older arc-related magmas were derived from depleted mantle and/or were generated by partial melting of juvenile metabasic crust. Detrital zircon age populations of the metasedimentary rocks together with geochemical signatures of the associated amphibolites imply that the Bij Group was a volcano-sedimentary sequence, formed probably in the associated fore-arc wedge basin. Moreover, our data argue for an identical provenance of the Altai and Hovd domains, overall westward sediment transport during the Early Palaeozoic and the east-dipping subduction polarity. The obvious similarities of the Khuurai Tsenkher Gol Complex (Hovd Zone) with the neighbouring Togtokhinshil Complex (Lake Zone) suggest that both magmatic complexes originally belonged to the same magmatic arc, related to the Palaeo-Asian subduction system. The geodynamic cause of the later, within-plate magmatic pulse is unclear, but was probably still related to the effects of retreating subduction (slab window/ocean ridge subduction or back-arc lithosphere thinning). The Khuurai Tsenkher Gol Complex was subsequently separated from the western margin of the Lake Zone and imbricated into the Hovd Zone mélange. It is proposed that the Lake/Hovd zones boundary in the study area represents a younger deformation zone rather than a true terrane boundary/suture. This could be a general feature of the suture zones within this part of the CAOB.

1. Introduction

Accretionary-type (also called Pacific-, Cordilleran- or Miyashiro-type) orogens rank among the most important sites where the new continental crust is generated (Cawood et al., 2009; Maruyama, 1997; Santosh et al., 2010). The Central Asian Orogenic Belt (CAOB: Mossakovsky et al., 1994; Şengör et al., 1993) is an extensive accretionary system assembled during the Late Proterozoic to Early Mesozoic times (Safonova et al., 2011; Windley et al., 2007; Xiao et al., 2009), and showing many features resembling the modern subduction–accretion configurations in the SW Pacific.

A characteristic attribute of the long-term evolution of the CAOB was the successive incorporation of continental blocks, magmatic arcs, ophiolites, back-arc basins and accretionary wedges into a single

* Corresponding author at: Czech Geological Survey, Klárov 3, 118 21 Prague 1, Czech Republic.
E-mail address: igor.soejono@geology.cz (I. Soejono).

http://dx.doi.org/10.1016/j.lithos.2017.08.014
0024-4937/

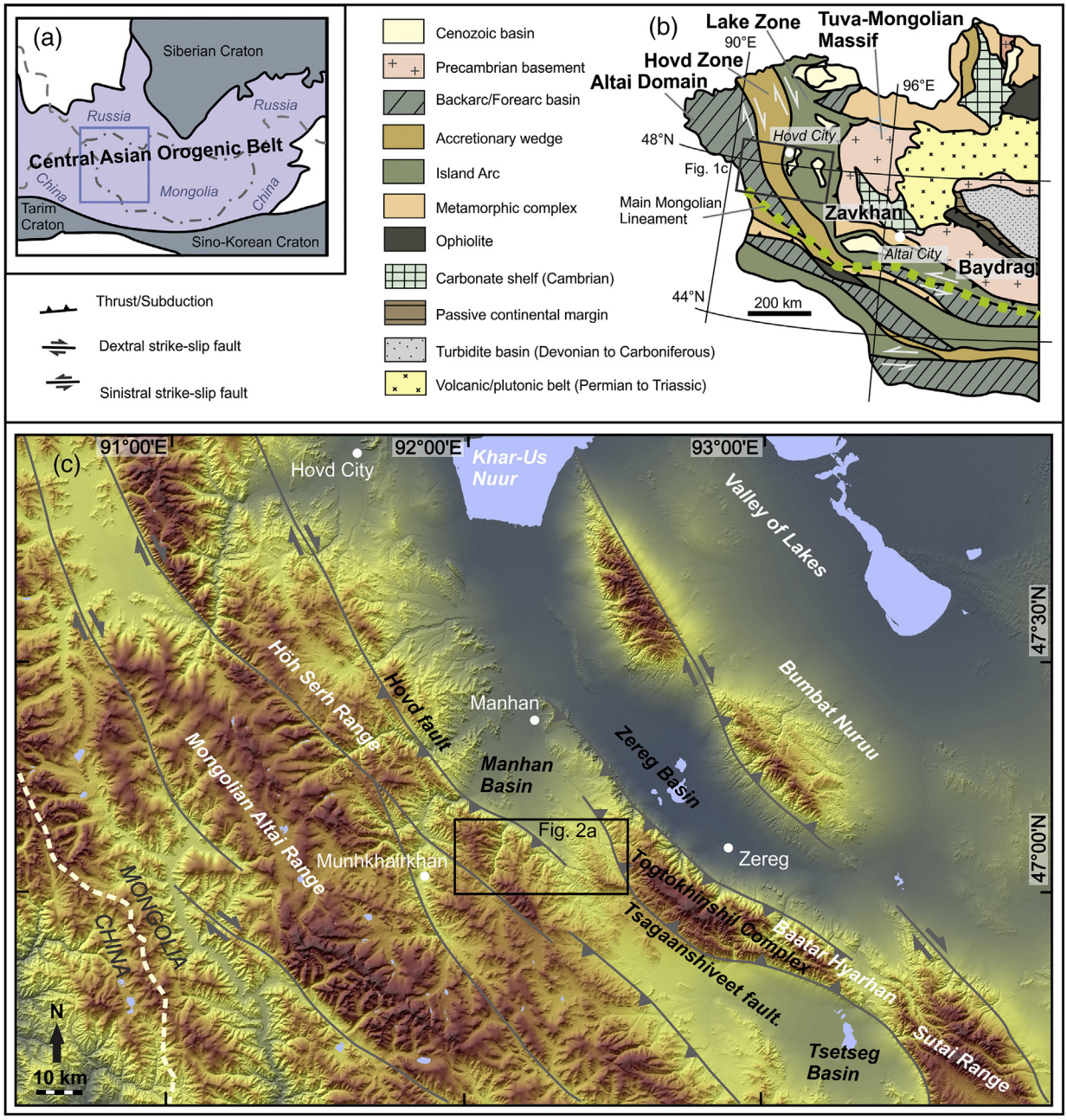

Fig. 1. (a) Schematic tectonic map of the Central Asian Orogenic Belt (modified after Şengör et al., 1993). (b) Overview geological map showing main lithotectonic domains and sutures of the western Mongolia (after Badarch et al., 2002). (c) Location of the study area (black rectangle) in the Mongolian Altai Mountain Range. The figure shows topography, geographical names and major faults.

orogenic system (Badarch et al., 2002; Rojas-Agramonte et al., 2011; Wilhem et al., 2012; Xiao and Santosh, 2014). The volumetric proportion of individual crustal types is uncertain; however, the formation of magmatic arc-related complexes and their amalgamation clearly played a crucial role in the geodynamic evolution (Kröner et al., 2014; Safonova et al., 2017; Şengör and Natal'in, 1996).

Many basic aspects of the CAOB architecture remain unresolved, including the nature, formation ages and provenance of many basement complexes. These variable-sized high- to medium-grade units, often containing metamorphosed and deformed magmatic and sedimentary rocks, are frequently surrounded by generally low-grade envelopes. Countless geochronological as well as geochemical data have been recently published from the CAOB; however, their thorough integration with detailed field work is necessary in order to fully establish their real geologic context.

The present paper focuses on the magmatic Khuurai Tsenkher Gol Complex, newly defined in this paper, and the associated volcano-sedimentary Bij Group (Baatarhuyag and Gansukh, 1999; Žáček et al., 2016). These examples of little-known high-grade magmatic/volcano-sedimentary complexes are located in the easternmost part of the Hovd Zone, at the contact with the Lake Zone. New field observations closely linked with geochemical data and U–Pb zircon ages are used to reveal the nature, primary tectonic setting and evolution of these basement complexes, as well as to constrain the character of the Lake/Hovd zones boundary. Additionally, the detrital zircon ages from the Bij Group metasedimentary rocks are applied to determine their depositional ages

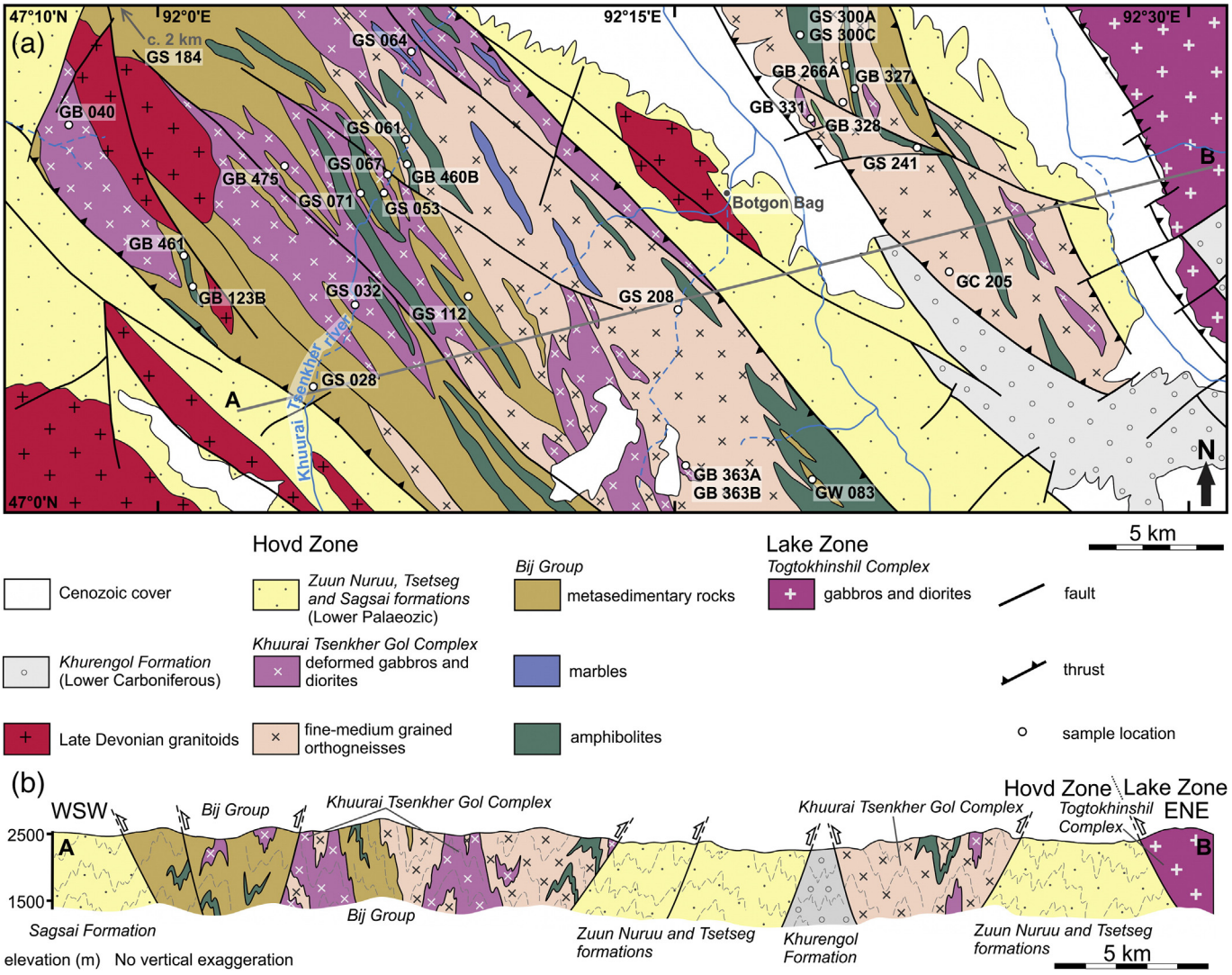

Fig. 2. (a) Geological map of the study area. White points indicate localization of geochemical and geochronological samples. Sample GS 184 is situated outside of the displayed area. (b) Idealized structural cross-section along the line A–B. Interrupted lines show solid-state foliation in magmatic rocks, metamorphic foliation in the metasedimentary rocks and bedding in the sedimentary rocks.

and provenance. Using a combination of these results and comparison with published data from the neighbouring units we further show that the Khuurai Tsenkher Gol Complex in fact constitutes a reworked western continuation of the Lake Zone. We also discuss the composition and likely genesis of this magmatic arc, located within the Lake/Hovd zones suture zone, as a member of the gigantic Cambro–Ordovician Ikh-Mongol Arc System bordering the outer margin of the chain of the Precambrian microcontinents (Tuva–Mongolia, Zavkhan and Baydrag) in the heart of the Mongolian tract of the CAOB (Janoušek et al., in print).

2. Geological setting

2.1. Regional overview of Western Mongolia

The CAOB occupies an enormous territory between the Siberian Craton in the north, the Tarim Craton in the southwest and the Sino-Korean Craton in the south (Fig. 1a) and was assembled in Late Proterozoic to Early Triassic times (Safonova et al., 2011; Windley et al., 2007; Xiao et al., 2009). The overall geological structure of Mongolia is divided into two principal domains differing mainly in the age of their formation and accretion: the Early Palaeozoic northern and the Late Devonian to Early Carboniferous southern parts (Badarch et al., 2002; Windley et al., 2007; Xiao et al., 2004; Zonenshain, 1973). The western Mongolian tract of the CAOB is built by three main lithotectonic regions (terranes) of different lithological, geochronological and structural features: Zavkhan and Baydrag microcontinents in the east, Lake Zone in the centre, and Hovd and Altai domains in the west (Fig. 1b) (Badarch et al., 2002; Xiao et al., 2004). These units display westward younging trend and form NW–SE elongated belts bounded by the sutures and/or by strike-slip fault zones (Badarch et al., 2002).

The *Zavkhan and Baydrag blocks* belong to a belt of microcontinental segments mostly with Precambrian basement, the so-called Tuva–Mongolian continental ribbon (Bold et al., 2016; Buslov et al., 2001; Demoux et al., 2009).

The *Lake Zone* is dominated by metavolcanic and metasedimentary rocks with relicts of Neoproterozoic ophiolites (Dijkstra et al., 2006; Jian et al., 2014; Khain et al., 2003; Zonenshain and Kuzmin, 1978) intruded by Cambrian–Ordovician arc-related magmatic rocks (Janoušek et al., in print; Rudnev et al., 2012; Soejono et al., 2016; Yarmolyuk et al., 2011). This tectonic collage is interpreted as a Neoproterozoic accretionary wedge (Kovach et al., 2011; Windley et al., 2007) or passive continental margin (Buriánek et al., 2017) hosting the Early Palaeozoic arc-system associated with the formation and closure of the Palaeo-Asian Ocean (Buslov et al., 2001; Xiao et al., 2004).

The *Hovd and Altai domains* are mainly composed of Lower Palaeozoic sedimentary and volcano-sedimentary sequences together with low- to

Fig. 3. Main rock-types from the KTGC. (a) Strongly deformed medium-grained metadiorite to metatonalite (GS 101). (b) Round mafic microgranular enclaves (MME) with lobate, chilled contacts against the host granodiorite (GS 029). (c) Alternation of K-feldspar-rich cumulate layers and MME accumulations (GS 080). (d) Coarse-grained amphibole cumulate of gabbroic composition (GS 271).

high-grade metamorphic complexes (Badarch et al., 2002; Kröner et al., 2010; Xiao et al., 2004) intruded by Devonian–Permian granitic bodies (Buriánek et al., 2016; Cai et al., 2015; Wang et al., 2006; Zhang et al., 2017). These domains have been mostly interpreted as a large Cambrian–Silurian accretionary wedge associated with the Lake Zone arc-system (Kröner et al., 2010; Xiao and Santosh, 2014).

The Early Palaeozoic accretionary evolution of Mongolian part of the CAOB was characterized by thrusting of Neoproterozoic passive margin and ophiolites over the Precambrian continental segments. Convergence between the Siberian Craton and Palaeo-Asian oceanic plate resulted in long-lasting subduction and development of the associated magmatic arc (Buriánek et al., 2017; Wilhem et al., 2012). The Late Palaeozoic final amalgamation was followed by a magmatic and deformational evolution until the Early Mesozoic (Guy et al., 2014a; Wilhem et al., 2012; Windley et al., 2007; Xiao et al., 2009).

2.2. Geology of the study area

The present study focusses on the newly established Khuurai Tsenkher Gol Intrusive Complex (KTGC), which belongs to the Hovd Plutonic Complex (or Hovd Batholith) (Cai et al., 2015; Gavrilova et al., 1975), and the volcano-sedimentary Bij Group (BG) (Bij Formation after Baatarhuyag and Gansukh, 1999; see Žáček et al., 2016). Both complexes are located in the easternmost part of the Hovd Zone (Fig. 1b), and occupy the southern part of the Höh Serh Range (Munhkhairkhan and Manhan soums, Hovd aimag) (Fig. 1c). New term Khuurai Tsenkher Gol Complex is used in an effort to avoid confusion between the Hovd Plutonic Complex and the Hovd Zone. The studied rock assemblages are directly juxtaposed to the Togtokhinshil Complex (western margin of the Lake Zone) further in the east.

The KTGC is composed mainly of variably deformed basic to acid igneous rocks interfolded with low- to high-grade metasedimentary and metavolcanic rocks of the BG. Due to absence of geochronological and geochemical data, the ages and character of these two units have not been well constrained.

The KTGC, together with the BG, form two NW–SE trending belts (Fig. 1c, 2a) separated from the Lower Palaeozoic flysch sequences of Zuun Nuruu, Tsetseg and Sagsai formations, Carboniferous sediments of the Khurengol Formation and Cenozoic Manhan and Tsetseg basins by the Cenozoic thrust faults (Figs. 1c, 2a–b) (Žáček et al., 2016). All these rocks were intruded by the Late Devonian granitoid plutons (Baatarhuyag and Gansukh, 1999; Cai et al., 2015). The whole domain has been polyphase metamorphosed and deformed under amphibolite-facies conditions in the Silurian–Devonian times (Soejono et al., 2015).

3. Field relations

3.1. Khuurai Tsenkher Gol Complex (KTGC)

The KTGC forms several NW–SE-elongated bodies (Fig. 2a) intimately associated with the metamorphosed sedimentary and volcanic rocks of the BG. Contacts between these two units are predominantly sharp and concordant with the penetratively developed foliation. The KTGC is mainly composed of variably deformed metagabbros, metadiorites to quartz metadiorites and metagranodiorites to orthogneisses. Minor body of deformed quartz monzodiorite, identified only according to its

Fig. 4. Main rock-types from the BG. (a) Boudin of medium-grained gabbro within the amphibolite schists (GS 300). (b) Banded amphibolite with orthogneiss layers (GS 066). (c) Alternation of orthogneisses and amphibolites (GS 241). (d) Quartz-rich Grt–Sill–Bt paragneiss (GS 125).

different age and geochemical signature, is difficult to distinguish from the dominant metadiorites in the field.

All these magmatic rocks range from relatively undeformed to mylonitic (Fig. 3a). Rarely, primary relations and textures are well-preserved in less deformed domains. Different rock types often form layers, several m thick, alternating with the BG rocks within the foliation. Contacts of the metagranitoids and metadiorites are locally characterized by mingling textures providing an evidence for interaction between two compositionally contrasting magmas.

The eastern part of the KTGC is dominated by metagranitoids to orthogneisses which contain numerous mafic microgranular enclaves (MME) (Fig. 3b). These enclaves of round or elliptical shapes are 1–10 cm in size, and display lobate or irregular contacts with sharp, chilled margins against their host rock. In contrast, in the western part are abundant discrete intrusions of diorites and gabbros (Fig. 2a). Gabbros form oval-shaped bodies, up to several km across, with sharp contacts against the surrounding rocks. Relict cumulate textures and magmatic layering are in places preserved as hornblende- or plagioclase-rich, up to 30 cm thick, bands (Figs. 3c–d). Peridotite and serpentinite locally form lenticular bodies up to 30 m in size and represent ultramafic cumulate within the gabbros.

3.2. Bij Group (BG)

The rock assemblage of the BG occurs mainly in the western part of the study area (Fig. 2a) and consists of paragneisses, micaschists, greenschists and amphibolites, with rare bodies of marbles and calc-silicate rocks. Amphibolites form a few, up to several hundred m wide, foliation-parallel bodies (Figs. 4a–c). The metamorphic grade in the metasedimentary rocks, as well as intensity of deformation within the magmatic rocks, decreases gradually from the centre to both NE and SW flanks of the study area.

3.3. Structural pattern

The primary emplacement/depositional structures in the rocks of both complexes were polyphase reworked into the heterogeneously developed sub-vertical ~NW–SE trending deformational fabrics. Metamorphic foliation in amphibolites is defined by preferred orientation of amphibole and plagioclase, concordant with those in the surrounding metapelites and orthogneisses (Fig. 4c). All the metasedimentary rocks have well-developed foliation (Fig. 4d) defined by alternating mica-rich and quartz–feldspar layers and/or by shape-preferred orientation of rock-forming minerals. Moreover, the entire area was affected by NW–SE trending ductile shear zones, and subsequently rearranged by the numerous Cenozoic NW–SE trending thrust faults and NE–SW trending strike-slip faults (Fig. 2a–b).

4. Petrography

This study focuses on the KTGC (meta-)igneous and the BG metavolcanic and metasedimentary rocks. Localities with brief petrological descriptions of the individual samples are given in Table 1 and representative mineral compositions listed in Supplementary Material A (see also Fig. 2a for sample locations).

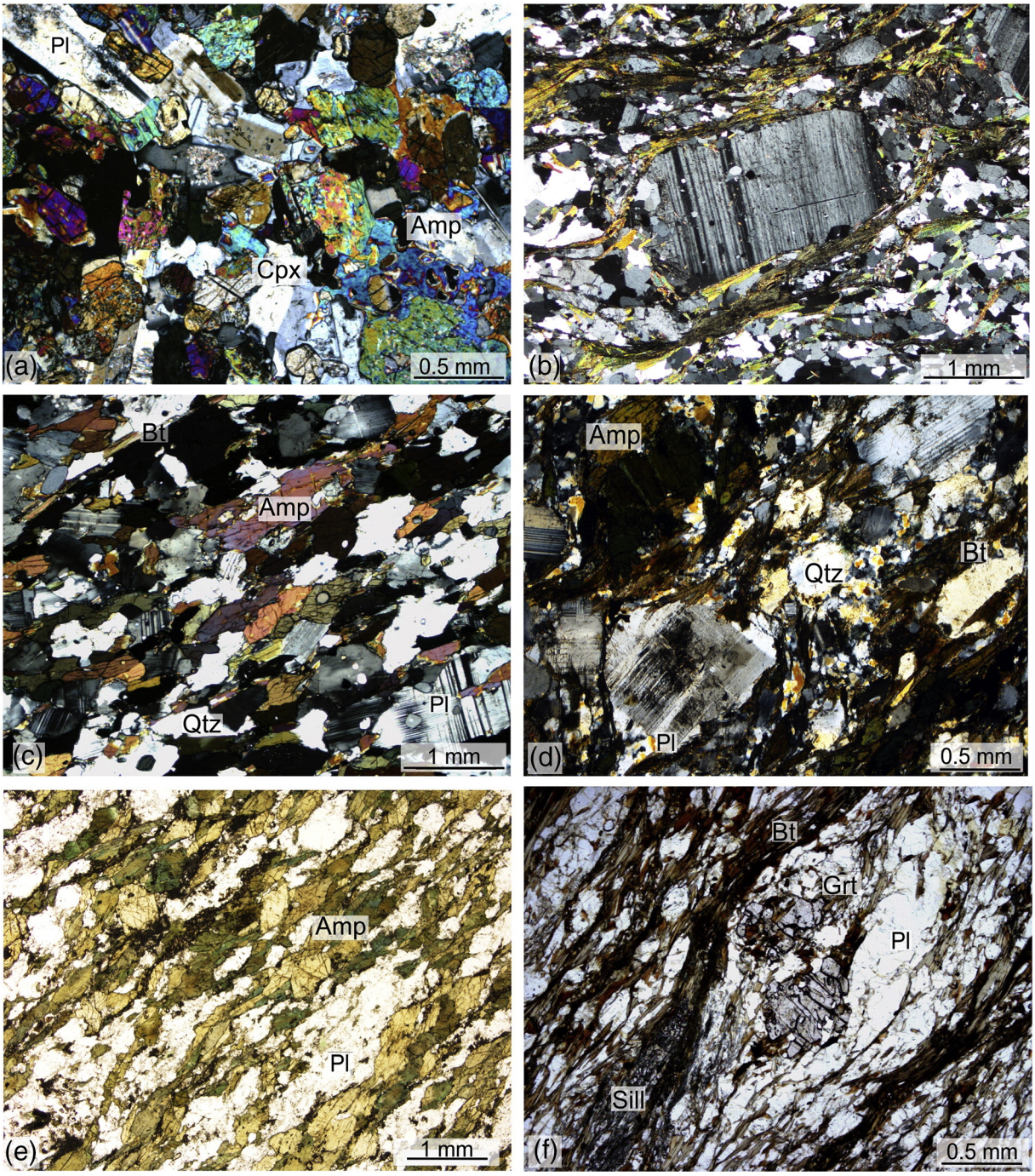

Fig. 5. Photomicrographs for magmatic rocks from the KTGC (a–d) and the BG (e–f). (a) Granular texture of the clinopyroxene–amphibole metagabbro (XPL, GB 040). (b) Plagioclase porphyroclast in the orthogneiss (XPL, GS 235). (c) Biotite–amphibole metatonalite (XPL, GB 191). (d) Biotite–amphibole monzodiorite (XPL, GS 032). (e) Plagioclase and amphibole in amphibolite arranged parallel to the metamorphic foliation (PPL, GS 073). (f) Paragneiss with sillimanite–biotite- and quartz–feldspar dominated layers and garnet porphyroblasts (PPL, GB 367).

4.1. Petrography of the Khuurai Tsenkher Gol Complex rocks

4.1.1. Metagabbros

Medium- to coarse-grained pyroxene–amphibole metagabbros are composed of plagioclase (32–48 vol.%), amphibole (14–52 vol.%), variable amounts of diopside (4–32 vol.%) and enstatite (0–1 vol.%); apatite, Cr-magnetite and Fe–Ti oxides are common accessories. The texture of metagabbros is typically hypidiomorphic granular to subophitic (Fig. 5a). Plagioclase has been considerably recrystallized to the aggregates of oligoclase ($An_{24–30}$; Fig. 6a), carbonate, clinozoisite and white mica. Magnesiohornblende (Fig. 6b; Si = 6.88–7.47 apfu; X_{Mg} = 0.60–0.71), enstatite (Ca = 0.04–0.06 apfu; X_{Fe} = 0.41–0.42) with diopside (Ca = 0.28 apfu; X_{Fe} = 0.85) are present as subhedral to euhedral crystals (Fig. 5a). Locally is enstatite, partly to completely, altered to magnesiohornblende.

Medium-grained plagioclase or olivine–pyroxene cumulates are massive, dark green rocks that consist of polygonal mosaic of olivine (45–78 vol.%) and clinopyroxene (11–62 vol.%). Accessory minerals are represented by chromite, magnetite and Ni–Fe sulphides.

4.1.2. Orthogneisses

Medium-grained, often porphyroclastic, muscovite–biotite, biotite or amphibole–biotite orthogneisses to metagranodiorites consist of euhedral to subhedral plagioclase (31–40 vol.%), anhedral quartz

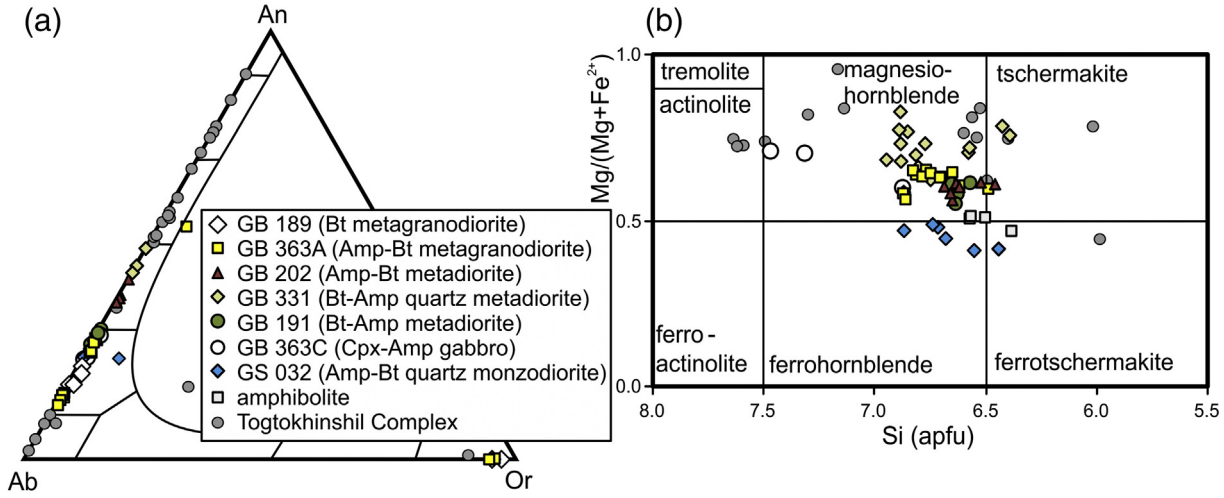

Fig. 6. Compositions of selected rock-forming minerals. (a) Ternary diagram Ab–An–Or for feldspars. (b) Si vs. Mg/(Mg + Fe^{2+}) (apfu) classification diagram for calcic amphiboles (Leake et al., 1997) with $Ca_B \geq 1.5$, $(Na + K)_A < 0.5$, $Ca_A < 0.5$.

(17–28 vol.%), anhedral K-feldspar (12–28 vol.%), subhedral amphibole (0–6 vol.%), subhedral biotite (3–12 vol.%) or muscovite (0–5 vol.%). Typical accessories are magnetite, titanite, epidote/allanite, apatite and zircon. This rock type shows variable degree of recrystallization with hypidiomorphic granular to blastomylonitic (Fig. 5b) textures. Many plagioclase crystals (Fig. 6a; $An_{13–49}$) are polysynthetically twinned and exhibit oscillatory or discontinuous zoning with altered cores. Myrmekite often occurs along grain boundaries between plagioclase and perthitic K-feldspar ($Ab_{2–6}$). Subhedral biotite (^{IV}Al = 2.29–2.44 apfu; X_{Fe} = 0.52–0.59) flakes are partially replaced by chlorite. Composition of subhedral amphibole ranges from magnesiohornblende to tschermakite (Fig. 6b; Si = 6.49–6.87 apfu; X_{Mg} = 0.56–0.65). Subhedral magnetite grains, up to 3 mm across, rarely form inclusions in ilmenite. Equigranular MME of dioritic composition consist of plagioclase (40–52 vol.%), amphibole (38–46 vol.%), biotite (3–10 vol.%) and minor quartz with K-feldspar.

4.1.3. Metadiorites to quartz metadiorites

Biotite–amphibole metadiorite to quartz metadiorite is medium- to fine-grained rock, with plagioclase (37–54 vol.%) and amphibole (32–46 vol.%), dominating over quartz (1–18 vol.%) and biotite (5–11 vol.%); magnetite, titanite, apatite, zircon and epidote/allanite are the common accessories. Subhedral, normally zoned plagioclase (Fig. 6a, $An_{24–49}$) is the major component of matrix and sometimes also occurs as euhedral porphyroclasts (up to 2 mm). Plagioclase is extensively altered to sericite; biotite (^{IV}Al = 2.27–2.36 apfu; X_{Fe} = 0.45–0.49) is also partially replaced by chlorite. Amphibole (magnesiohornblende to tschermakite, Fig. 6b; Si = 6.39–6.95 apfu;

Table 1
Location and brief petrological description of geochemical and geochronological samples from the KTGC and the BG.

Sample (rock type)	Latitude (N)	Longitude (E)	Mineral composition
Khuurai Tsenkher Gol Complex			
GB 040 (gabbro)	47.127575	91.957460	Amp, Pl, Cpx, (Opq, Ap)
GB 328 (orthogneiss)	47.133861	92.332950	Qtz, Pl, Kfs, Bt, Ms, (Ap), *Ep*, *Chl*
GB 331 (quartz metadiorite)	47.132013	92.314844	Pl, Amp, Qtz, Bt, (Opq, Ap, Zrn), *Chl*
GB 363A (metagranodiorite)	47.015201	92.255346	Qtz, Pl, Kfs, Bt, Amf, (Ap), *Chl*
GS 363B (gabbro)	47.015202	92.255347	Pl, Amp, Cpx, Bt, (Opq), *Amp*, *Ep*
GB 475 (quartz metadiorite)	47.112980	92.063547	Pl, Amp, Bt, Qtz, (Opq, Ap), *Chl*
GC 205 (quartz metadiorite)	47.081612	92.381177	Pl, Amp, Qtz, Bt, (Ap, Zrn, Aln), *Chl*
GS 032 (quartz monzodiorite)	47.069725	92.094645	Pl, Amp, Bt, Qtz, (Opq, Ap, Zrn, Mag), *Ep*
GS 061 (orthogneiss)	47.121414	92.120944	Pl, Kfs, Qtz, Bt, Ms, (Ap, Opq, Zrn), *Chl*
GS 064 (metadiorite)	47.151080	92.124269	Pl, Amp, Qtz, Bt, (Ttn, Opq, Ap), *Chl*, *Ep*
GS 208 (orthogneiss)	47.067639	92.252436	Pl, Kfs, Qtz, Bt, Amp, (Mag, Ttn, Ep, Ap)
GS 300C (gabbro)	47.158763	92.310608	Amp, Pl, Cpx, Qtz, (Rt, Ap), *Ep*, *Chl*
Bij Group			
GB 123B (amphibolite)	47.074254	92.013674	Pl, Amp, (Opq, Ap)
GB 327 (amphibolite)	47.134955	92.337791	Amp, Pl, Bt, Qtz, (Opq), *Chl*
GB 460B (amphibolite)	47.114348	92.120316	Pl, Amp, (Opq, Ap)
GB 461 (amphibolite)	47.081859	92.013164	Pl, Amp, Qtz, (Opq)
GS 241 (amphibolite)	47.119827	92.373706	Pl, Amp, (Opq)
GS 300 (amphibolite)	47.158763	92.310608	Amp, Pl, Qtz, (Ttn, Opq), *Ep*
GS 028 (greenschist)	47.041421	92.075310	Pl, Chl, Cal, Ep, (Ttn, Zrn, Opq)
GS 053 (micaschist)	47.105589	92.108417	Qtz, Bt, Pl, Ms, Grt, (Ap, Zrn, Tur, Mnz, Opq)
GS 067 (paragneiss)	47.111489	92.111051	Pl, Qtz, Bt, (Ap, Zrn, Opq), *Chl*
GS 184 (paragneiss)	47.225079	91.927068	Pl, Qtz, Bt, Amp, (Ap, Zrn, Opq), *Chl*
GW 083 (micaschist)	47.007979	92.321436	Qtz, Bt, Pl, Grt, St, Sill, Ms, (Ap, Ilm, Tur), *Chl*
GS 071 (paragneiss)	47.107648	92.103729	Qtz, Pl, Bt, Grt, (Opq, Ap, Zrn), *Chl*
GB 266A (paragneiss)	47.141374	92.334689	Qtz, Bt, Ms, Pl, Grt, St, Sill, (Ap, Ilm), *Chl*
GS 112 (paragneiss)	47.141374	92.334689	Pl, Qtz, Bt, Sill, Grt, (St, Ap, Zrn, Opq), *Chl*

The abbreviations of mineral names are after Kretz (1983). Accessory minerals are listed in parentheses and secondary minerals in italic.

Table 2
Estimated P–T conditions, oxygen fugacity and water content for magmas of rocks from the KTGC.

Rock	Metadiorite Bt–Amp	Metadiorite Bt–Amp	Metagranodiorite Amp–Bt	Metadiorite Amp–Bt	Monzonite Amp–Bt
Sample	GB 191	GB 331	GB 363A	GB 202	GS 032
Amphibole thermobarometry (Ridolfi et al., 2010)					
T (°C)	847 to 964	790 to 867	788	–	–
Uncertainty*	22	22	22	–	–
P (GPa)	0.18 to 0.21	0.13 to 0.22	0.12	–	–
Uncertainty (Max error)	0.02 to 0.05	0.01 to 0.08	0.01	–	–
Log fO_2	−12.7 to −12.3	−13.0 to −10.8	−13.8	–	–
Uncertainty*	0.4	0.4	0.4	–	–
H_2O melt (wt.%)	5.5 to 6.4	6.2 to 7.6	6.1	–	–
Uncertainty*	0.4	0.4 to 1.1	0.4	–	–
Amp–Pl thermometry (Holland and Blundy, 1994)					
T (°C) ±32 °C	494 to 500	442 to 564	410 to 545	468 to 520	547 to 592
Amp–Pl barometry (Molina et al., 2015); *temperature according to Amp–Pl thermometry* (Holland and Blundy, 1994)					
P (GPa)	0.21 to 0.23	0.41 to 0.59	0.43 to 0.58	0.47 to 0.59	0.45 to 0.52

* Estimated standard errors.

X_{Mg} = 0.55–0.83) in the groundmass is euhedral to subhedral (Fig. 5c) up to 1 mm in size; amphibole porphyroclasts are subhedral and up to 2 mm in length. Their cores contain scattered ilmenite inclusions, while the rims are inclusions-free. Primary magmatic textures (Fig. 5c) are locally recrystallized into the solid-state deformation fabric.

4.1.4. Quartz monzodiorite

Medium- to fine-grained biotite–amphibole quartz monzodiorite (Fig. 5d) consists of plagioclase (54 vol.%), amphibole (19 vol.%), K-feldspar (9 vol.%) and subordinate biotite (8 vol.%) with quartz (6 vol.%). Subhedral biotite (^{IV}Al = 2.40–2.71 apfu; X_{Fe} = 0.13–0.14) is commonly associated with amphibole and hosts inclusions of apatite and zircon. Composition of long prismatic amphibole crystals ranges from ferrohornblende to ferrotschermakite (Fig. 6b; Si = 6.45–6.87 apfu; X_{Mg} = 0.41–0.49). Subhedral plagioclase shows faint zoning (Fig. 6a; $An_{23–27}$). Accessory minerals are represented by apatite, zircon, magnetite, epidote and titanite.

4.2. Petrography of the Bij Group rocks

4.2.1. Amphibolites

Medium-grained amphibolites have mostly nematogranoblastic texture (Fig. 5e) and consist mainly of amphibole (36–68 vol.%) and plagioclase (30–47 vol.%); they also contain biotite, quartz, magnetite, apatite and epidote. Both the plagioclase grains in the matrix and the porphyroblasts show a normal zoning ($An_{23–39}$). In some samples are present up to 4 mm long aggregates formed mainly by fine-grained plagioclase. Composition of acicular to prismatic amphibole corresponds to magnesiohornblende or ferrotschermakite (Si = 6.35–6.58; X_{Mg} = 0.46–0.51). In some samples occurs also fine-grained biotite.

With increasing contents of biotite in the rock, the amphibolites pass to amphibolitic gneisses. Amphibole of these gneisses (Si = 6.46–6.69; X_{Mg} = 0.56–0.61) and plagioclase ($An_{37–42}$) have chemical compositions similar to those of the matching phases in the amphibolites. Accessory minerals are represented by apatite, magnetite and ilmenite.

4.2.2. Metasedimentary rocks and greenschists

Fine-grained paragneisses are dominant rock-type composed mainly of quartz (20–55 vol.%), plagioclase (10–30 vol.%) and biotite (12–35 vol.%). Sometimes also contain minor amounts of muscovite, garnet, staurolite, sillimanite and cordierite (Fig. 5f). Accessory minerals are represented by amphibole, apatite, zircon and ore minerals. Fine- to medium-grained micaschists form only few narrow (up to hundred m thick) bodies and are composed of quartz (25–55 vol.%), plagioclase (10–40 vol.%), biotite (10–25 vol.%), muscovite (8–20 vol.%) and chlorite (5–15 vol.%), with variable amounts of garnet, sillimanite, staurolite and/or cordierite; accessory minerals are tourmaline, apatite, zircon and monazite. Greenschists are fine-grained rocks composed mainly of plagioclase (20–55 vol.%), chlorite (5–25 vol.%), actinolite (8–20 vol.%) and epidote (up to 10 vol.%), in places calcite, quartz and clinopyroxene. Accessory minerals are represented by titanite, zircon and ore minerals.

4.3. Geothermobarometry

The calcic amphibole thermobarometry (Ridolfi et al., 2010) was used for determination of P–T conditions of magmatic crystallization of the amphibole cores from some metadiorites and metagranodiorites of the KTGC. However, the application of geothermobarometry to the studied samples is complicated due to their common metamorphic overprint.

The estimated P–T conditions of magmatic crystallization for these (meta-)igneous rocks are 788–964 °C and 0.12–0.22 GPa (Table 2). The Ridolfi et al. (2010) formulation also provides an estimate of oxygen fugacity (−13.8 to −11.8) and water contents (5.5–7.6 wt.%) in the melt during the amphibole crystallization.

In order to estimate the P–T conditions of metamorphic recrystallization were applied amphibole–plagioclase thermometer (Holland and Blundy, 1994) and amphibole–plagioclase barometer (Molina et al., 2015). The P–T conditions 410–564 °C and 0.41–0.59 GPa were calculated for the rims of the partially recrystallized plagioclase and amphibole grains (Table 2). The relatively low obtained pressure (0.21–0.23 GPa) for the metadiorite GB 191 could be considered as a result of subsequent low-grade re-equilibration. The P–T conditions of the quartz monzodiorite GS 032 (547–592 °C and 0.45–0.52 GPa) are comparable with other samples.

5. Whole-rock geochemistry

The geochemical dataset consists of 19 whole-rock major- and trace-element analyses of various magmatic rocks (Fig. 2a; Table 1). The KTGC is represented by three metagabbros, four metadiorites (metadiorites to quartz metadiorites), four orthogneisses (metagranodiorites to orthogneisses) and one quartz monzodiorite. The BG is characterized by six amphibolites. Analytical methods are listed in the Supplementary Material B. The whole-rock major- and trace-element data are listed in the Supplementary Materials C and D, respectively. This dataset was compared with previously published chemical analyses of the gabbro–diorite suite from the Togtokhinshil Complex (Soejono et al., 2016).

5.1. Major elements

5.1.1. The Khuurai Tsenkher Gol Complex

The studied (meta-)igneous rocks from the KTGC are basic to acid (SiO_2 = 51–71 wt.%). On the basis of Total Alkali–Silica (TAS) diagram (Cox et al., 1979), they can be classified as gabbros, diorites, quartz

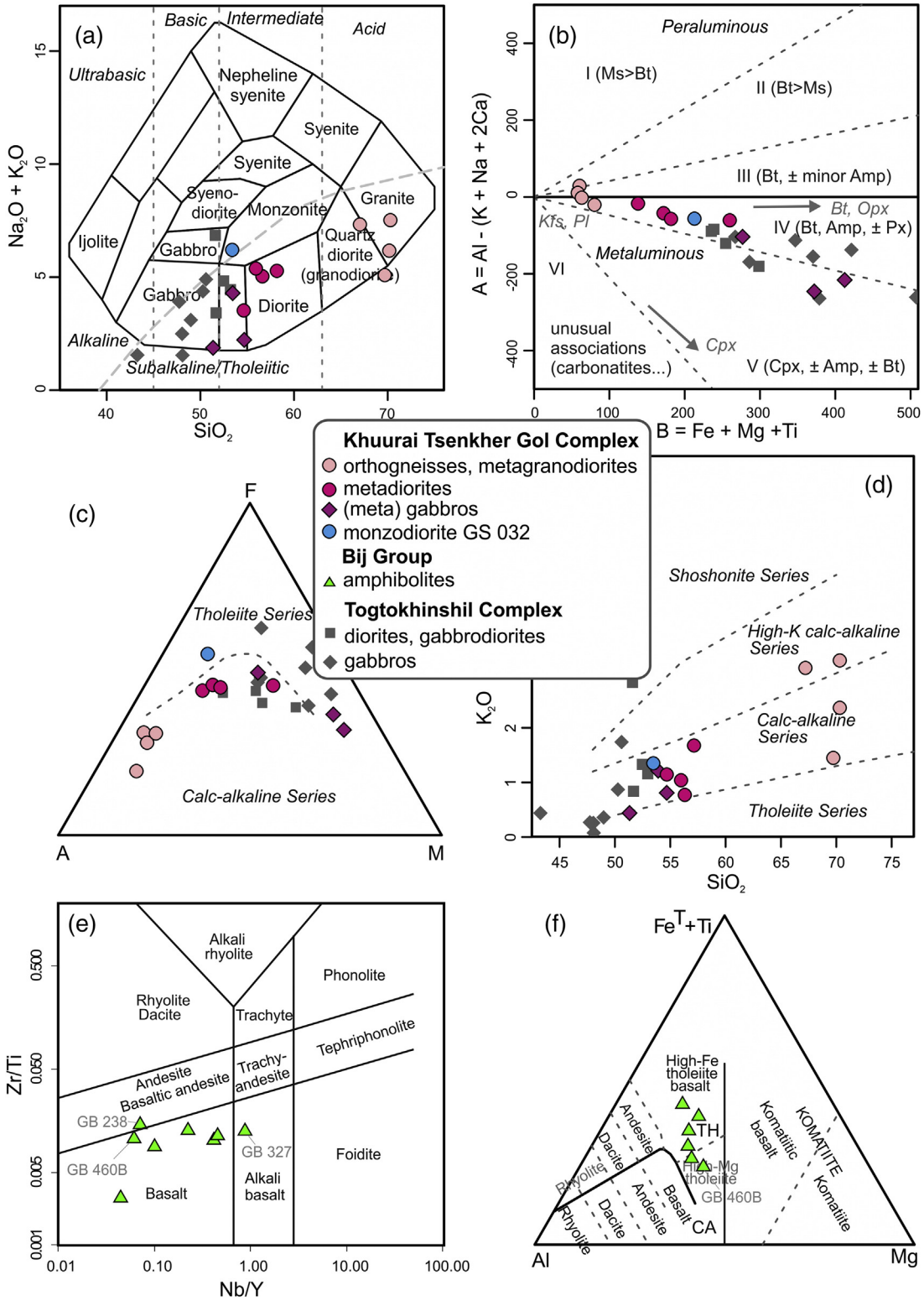

Fig. 7. Classification diagrams for magmatic rocks of the KTGC, the BG and the gabbro–diorite suite of the Togtokhinshil Complex (Soejono et al., 2016). (a) TAS diagram (Cox et al., 1979) with dashed line denoting the boundary between alkaline and subalkaline rocks according to Irvine and Baragar (1971). (b) Multielement B–A diagram (Debon and Le Fort, 1983). B represents the content of mafic minerals and A the balance of aluminium vs. alkalis with calcium. Typical of each of the sectors is a characteristic mineral assemblage (also marked). (c) AFM ternary diagram (Irvine and Baragar, 1971); A: $Na_2O + K_2O$, F: FeOt, M: MgO in wt.%. (d) SiO_2 vs. K_2O diagram in wt.% (Peccerillo and Taylor, 1976). (e) Classification diagram Nb/Y vs. Zr/Ti (Pearce, 1996). (f) Triangular plot Al–Fe^T + Ti–Mg (Jensen, 1976).

diorites and granodiorites to granites (Fig. 7a). All the samples from the KTGC are generally subalkaline, except the quartz monzodiorite GS 032 that however plots right next to the dividing line of Irvine and Baragar (1971) (Fig. 7a). Metagabbros, metadiorites as well as the monzodiorite are metaluminous (A/CNK = 0.50–0.96; $\frac{Al_2O_3}{CaO+Na_2O+K_2O}$ [mol.%]), whereas orthogneisses are generally subaluminous (A/CNK = 0.94–1.10), as documented also by the multi-element B–A diagram of Debon and Le Fort (1983) (Fig. 7b). The K_2O/Na_2O ratios (based on wt.%) range from 0.18 to 0.57 in gabbros, metadiorites and monzodiorite and from 0.40 to 0.75 in orthogneisses. In the AFM triangular plot of Irvine and

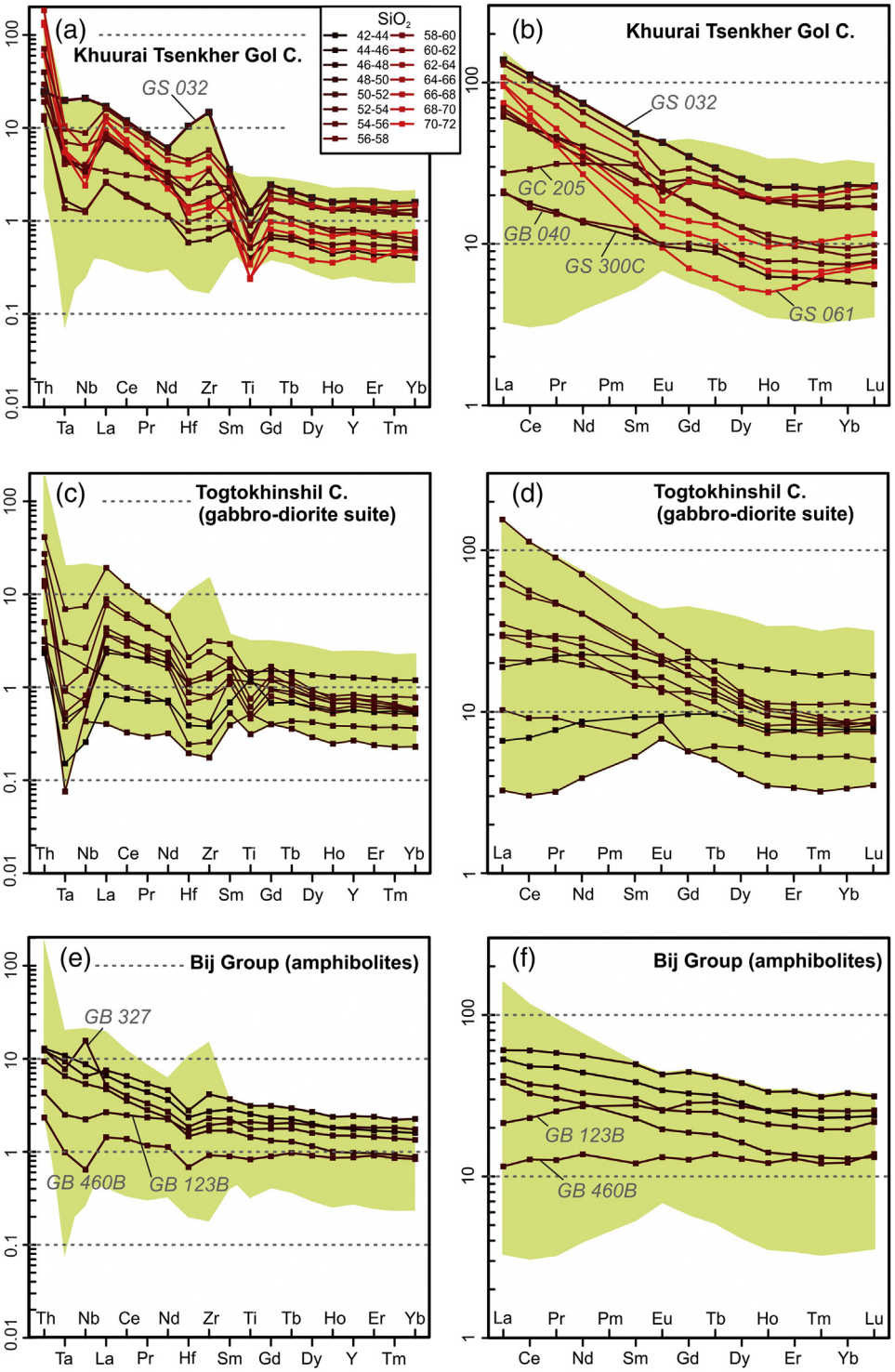

Fig. 8. Multielement diagrams of the magmatic rocks of the KTGC, the gabbro–diorite suite of the Togtokhinshil Complex (Soejono et al., 2016) and the BG amphibolites colour-coded by silica contents (wt.%). (a, c, e) NMORB-normalized (Sun and McDonough, 1989) trace-element patterns. Note that only presumably immobile elements are plotted (Pearce, 2008). (b, d, f) Chondrite-normalized (Boynton, 1984) REE patterns. The yellow field represents the range of chemical composition of all samples. (For interpretation of the references to colour in this figure legend, the reader is referred to the web version of this article.)

Baragar (1971) (Fig. 7c), all the samples from the KTGC seem to form a single calc-alkaline trend, even though the composition of gabbros may be affected by accumulation of MgO-rich phases. In addition, the overall normal- to high-K calc-alkaline character is documented by the SiO_2–K_2O binary diagram (Peccerillo and Taylor, 1976) (Fig. 7d). In general, the major-element compositions of more mafic types from the KTGC fit well with those from the gabbro–diorite suite of the Togtokhinshil Complex (Soejono et al., 2016).

Specific chemistry displays the quartz monzodiorite GS 032. It has a character transitional between subalkaline (tholeiitic) and alkaline (Fig. 7a, c; see also elevated Nb/Y ratio of 1.06). Compared to all other samples from the KTGC, its shows distinctly higher contents of TiO_2,

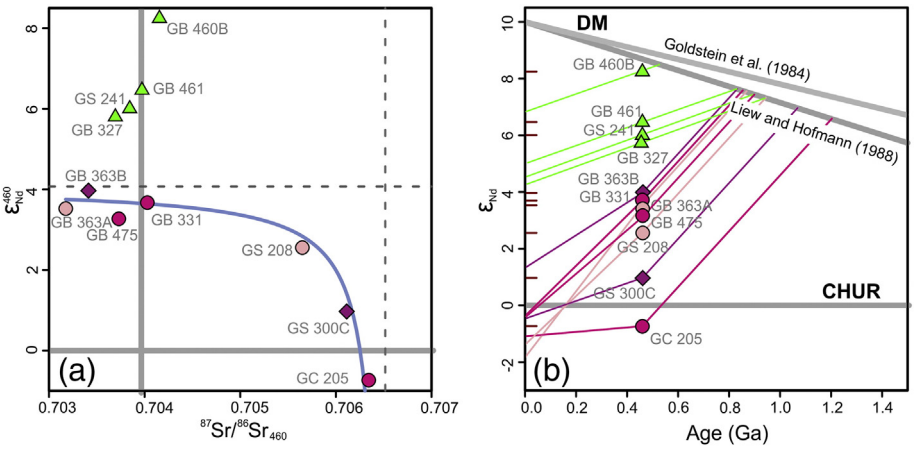

Fig. 9. Whole-rock Sr–Nd isotopic compositions. (a) Binary plot of $^{87}Sr/^{86}Sr_{460}$ vs. ε_{Nd}^{460} for BG and KTGC samples. The KTGC data are fitted by a binary mixing hyperbola using the least-squares approach and R code by Janoušek et al. (2016, exercise 19.1). The calculated asymptotes indicate that the mantle end-member had to have ε_{Nd}^{460}[B] < +4.1, and the crustal one $^{87}Sr/^{86}Sr_{460}$ [A] < 0.7065; from the available data also follows that $^{87}Sr/^{86}Sr_{460}$ [B] < 0.7035 and ε_{Nd}^{460}[A] < −0.5. (b) Two-stage Nd evolution diagram. DM = Depleted Mantle evolution lines after Goldstein et al. (1984) and Liew and Hofmann (1988). The extra tick marks on the ordinate denote ε_{Nd}^{460} values.

$Fe_2O_{3\ tot}$, P_2O_5 and lower mg# ($100\frac{MgO}{FeOt+MgO}$ [mol.%]) (Supplementary Material C).

5.1.2. The Bij Group amphibolites

Based on the Zr/Ti–Nb/Y plot (Pearce, 1996) (Fig. 7e), the BG amphibolites correspond to subalkaline basalts, except for mildly alkaline sample GB 327. Most have low silica contents (SiO_2 = 45–49 wt.%) and K_2O/Na_2O ratios (0.09–0.69). Their MgO ranges from 4.6 to 7.4 wt.% and mg# from 33.5 to 55.5. However, the sample GB 460B has distinctly higher SiO_2 (52.0 wt.%, if recast to anhydrous basis) and MgO (8.2 wt.%) as well as lower TiO_2 (1.1 wt.%) contents; also its mg# is high (60). Based on $Al–Fe^T + Ti–Mg$ triangular plot (Jensen, 1976) (Fig. 7f), all amphibolites consistently show tholeiitic character.

5.2. Trace elements

5.2.1. The Khuurai Tsenkher Gol Complex

The normal mid-ocean ridge basalt (N-MORB; Sun and McDonough, 1989) normalized multi-element patterns (Fig. 8a) feature mostly enrichment in Th and in Light Rare Earth Elements (LREE). Characteristic of nearly all patterns are deep negative anomalies of some High Field Strength Elements (HFSE; Ta, Nb and Ti). Only the pattern of monzodiorite GS 032 is different mainly by lacking the negative Ta and Nb anomalies (in fact, there is a slight enrichment in Nb) and by showing expressive hump in Hf and Zr.

All chondrite-normalized (Boynton, 1984) REE patterns (Fig. 8b), except that for the sample GC 205, have broadly similar gently sloping (rocks with lower SiO_2) or U-shaped (rocks with higher SiO_2) trends (Fig. 8b) with slight LREE enrichment (La_N/Yb_N = 1.4–13.9). Only several, as a rule less silicic, samples show negative Eu anomalies (Eu/Eu^* = 0.6–1.1). Compared to the rest of the dataset, the gabbros GB 040 and GS 300C have generally lower REE contents and orthogneiss GS 061 shows obvious depletion in Gd–Er.

In general, the mafic samples from the KTGC (except the monzodiorite GS 032), and those from the Togtokhinshil Complex, show broadly matching trace-element contents and distributions (Fig. 8a–d).

5.2.2. The Bij Group amphibolites

The trace-element contents of nearly all BG amphibolites are generally mutually well comparable. The N-MORB normalized multi-element patterns mostly show slight enrichment in Th and LREE and relatively weak negative Hf anomalies (Fig. 8e). Only the samples GB 123B and GB 460B display distinctly negative Ta and Nb anomalies, and conversely, the sample GB 327 a positive Nb anomaly. Compared with chondrite (Fig. 8f), the REE patterns of all amphibolites are uniformly flat, practically lacking any Eu anomalies (La_N/Yb_N = 0.8–3.0; Eu/Eu^* = 0.91–1.06).

5.3. Sr–Nd isotopes

The Sr–Nd isotopic data of the seven (meta-)igneous rocks from the KTGC and four amphibolites from the BG, age-corrected to 460 Ma, are given in Table 3. Relevant analytical methods are described in the Supplementary Material B.

5.3.1. The Khuurai Tsenkher Gol Complex

The Sr–Nd isotopic compositions from the KTGC do not directly correlate with petrology or silica contents (Table 3). Four of the analysed gabbro to orthogneiss samples are relatively primitive, showing only limited variations in both $^{87}Sr/^{86}Sr_{460}$ (0.7032–0.7057) and ε_{Nd}^{460} (+4.0 to +2.6) (Fig. 9a). These correspond to relatively low two-stage Nd model ages ($T_{DM\ 2stage}^{Nd}$ = 0.83–0.94 Ga) (Fig. 9b). Their parental magmas could have been generated by partial melting of depleted mantle or relatively geochemically unevolved juvenile source, such as young metabasic lower crust.

In contrast, gabbro GS 300C and metadiorite GC 205 display less primitive, CHUR-like isotopic compositions, translating to somewhat higher Nd model ages ($^{87}Sr/^{86}Sr_{460}$ ~ 0.706; ε_{Nd}^{460} = +1.0 and −0.7; $T_{DM\ 2stage}^{Nd}$ = 1.07 and 1.20 Ga). This points to a CHUR-like mantle source, or considerable degree of contamination of depleted-mantle derived melts by crustal material.

5.3.2. The Bij Group

The amphibolites from the BG display uniform, fairly primitive, Sr–Nd isotopic compositions ($^{87}Sr/^{86}Sr_{460}$ = 0.7037–0.7042; ε_{Nd}^{460} = + 8.3 to +5.9) (Fig. 9a). This is reflected by low single-stage Nd model ages ($T_{DM\ 1stage}^{Nd}$ = 0.54–1.03 Ga) (Fig. 9b). Such an isotopic signature documents a relatively recent derivation of the protolith of BG amphibolites directly from a strongly depleted mantle reservoir.

6. U–Pb zircon geochronology

U–Pb ages of three samples of KTGC magmatic rocks and four samples of detrital zircon in BG metasedimentary rocks (Fig. 2; Table 1) were determined using laser ablation inductively coupled mass

Table 3
Whole-rock Sr–Nd isotopic data for selected samples of the KTGC and BG.

Sample (rock type)	Rb (ppm)	Sr (ppm)	$^{87}Rb/^{86}Sr$	$^{87}Sr/^{86}Sr$[a]	2 se	$^{87}Sr/^{86}Sr_{460}$[b]	Sm (ppm)	Nd (ppm)	$^{147}Sm/^{144}Nd$	$^{143}Nd/^{144}Nd$[a]	2 s Nd	$(^{143}Nd/^{144}Nd)_{460}$[b]	εNd_{460}	$T_{Nd}DM_{1stg}$[c]	$T_{Nd}DM_{2stg}$[d]
Khuurai Tsenkher Gol Complex															
GB 363B (gabbro)	44	242	0.5262	0.706861	0.000010	0.703413	6.05	24.1	0.1518	0.512706	0.000008	0.512249	4.0	1.01	0.83
GB 331 (quartz metadiorite)	18	923	0.0564	0.704398	0.000015	0.704028	4.81	22.8	0.1275	0.512619	0.000008	0.512235	3.7	0.89	0.85
GB 363A (metagranodiorite)	87	248	1.0156	0.709830	0.000009	0.703175	3.82	21.9	0.1055	0.512544	0.000007	0.512226	3.5	0.82	0.87
GS 208 (orthogneiss)	101	217	1.3480	0.714499	0.000012	0.705665	7.06	32.9	0.1297	0.512567	0.000005	0.512176	2.6	1.00	0.94
GS 300c (gabbro)	29	183	0.4587	0.709119	0.000016	0.706113	2.38	8.35	0.1723	0.512614	0.000006	0.512095	1.0	1.75	1.07
GC 205 (quartz metadiorite)	36	362	0.2878	0.708229	0.000008	0.706343	5.96	18.9	0.1906	0.512582	0.000008	0.512008	−0.7	3.04	1.20
GB 475 (quartz metadiorite)	29	536	0.1565	0.704637	0.000009	0.703611	4.63	20.8	0.1346	0.512618	0.000007	0.512213	3.3	0.96	0.89
Bij Group															
GB 460B (amphibolite)	1	150	0.0193	0.704281	0.000013	0.704155	2.35	8.23	0.1726	0.512988	0.000006	0.512468	8.3	0.54	
GB 461 (amphibolite)	5	169	0.0856	0.704533	0.000010	0.703972	9.67	33.6	0.1740	0.512901	0.000004	0.512377	6.5	0.85	
GS 241 (amphibolite)	6	219	0.0793	0.704363	0.000018	0.703844	7.49	26.4	0.1715	0.512870	0.000004	0.512353	6.0	0.90	
GB 327 (amphibolite)	6	227	0.0765	0.704247	0.000018	0.703746	5.91	19.7	0.1814	0.512896	0.000005	0.512350	5.9	1.03	

[a] Followed by error (2 standard errors of the mean).
[b] Subscripts '460' indicate age-corrected isotopic ratios.
[c] Single-stage Nd model ages (Ga), using the depleted mantle parameters of Liew and Hofmann (1988).
[d] Two-stage depleted mantle Nd model ages (Ga) calculated after Liew and Hofmann (1988).

spectrometry (LA-ICP-MS) technique. Analytical methods are described in the Supplementary Material B and isotopic data with corresponding ages are provided in the Supplementary Material E.

6.1.1. The Khuurai Tsenkher Gol Complex

The *orthogneiss GS 061* contains mostly pale brown to light pink and prismatic, euhedral zircon grains, mostly 50 to 130 μm long. Oscillatory zoning observed in cathodoluminescence (CL) images corresponds to the crystallization from melt (Fig. 10a). Dating of sample GS 061 yielded a concordia age of 467 ± 4 Ma (2σ, 11 analyses; Fig. 11a), interpreted as timing the Mid-Ordovician intrusion of the protolith to the orthogneisses.

Zircon grains from the *orthogneiss GS 208* are mainly transparent, pale pink and euhedral, prismatic, mostly with oscillatory zoning. The grain sizes of the zircons from this sample range from 100 to 350 μm. In cases were observed thin and CL-bright outer rims, possibly related to the metamorphic resorption (Fig. 10b). Analyses of zircons from this orthogneiss yielded concordant or near concordant ages of 468 Ma to 486 Ma combined into a single concordia age of 476 ± 5 Ma (2σ, 27 analyses; Fig. 11b), most likely timing the magmatic crystallization.

Zircon population of the *quartz monzodiorite GS 032* contains yellow to brown, mostly euhedral, both short- and long-prismatic grains, 80–300 μm long. In CL images, most grains have euhedral to subhedral, unzoned or irregular patchy zoned cores (Fig. 10c). Moreover, some show a thin oscillatory zoning in the rims. Dating yielded ages scattering between 421 Ma and 438 Ma. They can be combined into a single concordia age of 430 ± 3 Ma (2σ, 20 analyses; Fig. 11c), interpreted to reflect the Mid-Silurian magmatic crystallization of the studied monzodiorite.

6.1.2. The Bij Group

The sample of the *epidote–calcite–chlorite greenschist GS 028* contains mostly subhedral, pale brown to pink, short prismatic zircon grains with relicts of crystal faces. Most are 100–360 μm long. The majority of crystals show well developed igneous oscillatory zoning (Fig. 10d). A few discordant analyses yielded ages varying between 240 and 300 Ma, which is taken as a consequence of Pb loss due to a metamorphic disturbance, and these ages are not further discussed here. Age spectrum of 66 grains shows two large peaks at c. 510 Ma and c. 780–950 Ma, a small maximum at c. 375 Ma and rare data at c. 1770 Ma (Fig. 12a). Analyses of zircons from the sample GS 028 that yielded the Devonian ages ranging between 373 and 401 Ma apparently reflect the metamorphic recrystallization. Remaining data are considered as representing a detrital zircon population. Their maximum depositional age (YZD) is Mid-Ordovician, 461 (+4.6/−3.8) Ma.

The majority of zircons from the *muscovite–biotite micaschist GS 053* are brown, long-prismatic and rounded, only rarely showing relicts of crystal faces. The grain sizes range from 80 to 260 μm. Cathodoluminescence images show often truncated igneous oscillatory or sector zoning and some grains contain older corroded and zoned cores overgrown by oscillatory-zoned or unzoned rims (Fig. 10e). U–Pb dating of 77 grains yielded a main peak at c. 520 Ma, broad sub-peak at c. 700–970 Ma and a few single Mesoproterozoic to Palaeoproterozoic ages (Fig. 12b). Several younger, c. 370 Ma ages likely represent metamorphic event, recorded also in the sample GS 028. Maximum depositional age (YDZ) calculated for the sample GS 053 is 475 (+6.7/−7.8) Ma.

Zircon population of the *biotite paragneiss GS 067* contains wide spectrum of colour and morphological types: clear or light pink to brown, stubby or short- to long-prismatic. The grains, 60–230 μm long, are partly rounded and occasionally show well preserved crystal faces. Two types of internal structures revealed by CL resemble those in the sample GS 053. First type, the relatively thick rims of the prismatic grains, are often formed by oscillatory-zoned overgrowths of mostly rounded cores with variable zoning patterns (Fig. 10f). Second type, mostly long-prismatic zircons, show well developed oscillatory zoning.

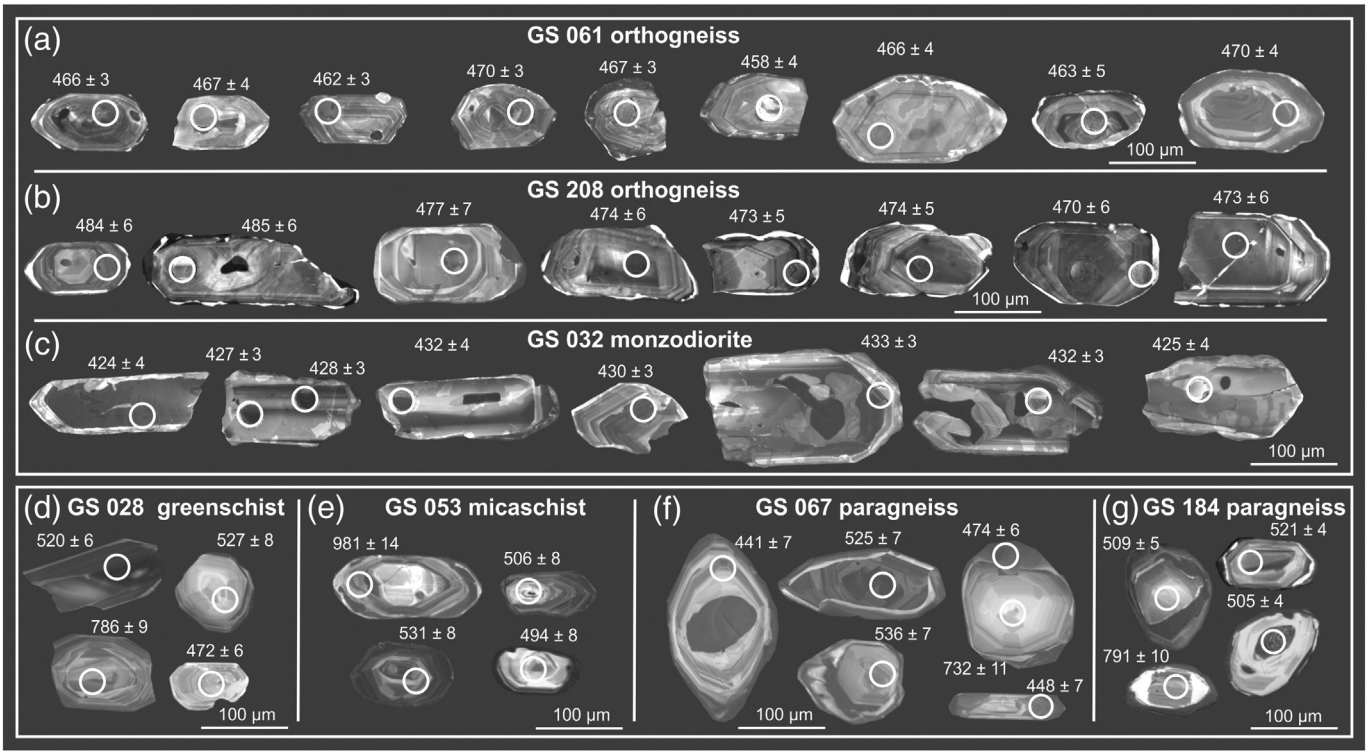

Fig. 10. Representative cathodoluminescence images of the typical zircon grains from the magmatic rocks of the KTGC (a–c) and metasedimentary rocks of the Bij Group (d–g). Laser-ablation ICP-MS analysis spots marked with concordant $^{206}Pb/^{238}U$ ages ± 2σ uncertainties (laser spot-size was 30 μm).

Analyses of 66 grains provided a wide spectrum of concordia ages, with two large peaks at c. 465 Ma and c. 520 Ma and several minor peaks at c. 770 Ma, 910 Ma and 1090 Ma (Fig. 12c). Analyses placed outside the cores and in the homogenous grains without the corroded cores yielded exclusively the youngest ages (c. 465 Ma), whereas the dating of the frequent inherited cores gave the c. 520 Ma and older ages. Maximum depositional age is 435 (+2.8/−5) Ma.

The zircon grains from *migmatitized paragneiss GS 184* are pale pink to yellow, mostly prismatic, 40–200 μm long, with rounded edges of the crystal faces. Common corroded and rounded cores are overgrown by oscillatory-zoned outer rims of variable thickness (Fig. 10g). U–Pb dating (22 analyses) provided similar age spectrum as the remaining BG samples with a major peak at c. 530 Ma, broad subordinate group at c. 780–950 Ma, two ages at c. 450 Ma and one age at c. 390 Ma (Fig. 12d). Our results indicate that the sample has a maximum depositional age of 505 (+2.9/−2.6) Ma.

7. Discussion

7.1. Ages, petrogenesis and tectonic setting of the Khuurai Tsenkher Gol Complex

The age and tectonic evolution of the high-grade basement from the eastern Hovd Zone have, so far, remained largely unconstrained. The studied (meta-)igneous rocks are major components of the newly described Khuurai Tsenkher Gol Complex exposed along the eastern margin of Hovd Zone. Based on the new U–Pb zircon ages, two diachronous igneous suites have been recognised in the KTGC: the prevalent orthogneisses, metadiorites and metagabbros with Early to Mid-Ordovician (c. 470 Ma) protoliths and, volumetrically subordinate, Mid-Silurian (c. 430 Ma) monzodiorites.

The vast majority of the KTGC rocks are calk-alkaline, uniformly showing major- and trace-element geochemical signatures typical of a magmatic-arc setting (Fig. 13a–d). The observed mingling textures between felsic and more mafic members suggest a nearly simultaneous emplacement of contrasting magmas within the same magmatic-arc system.

The Sr–Nd isotopic compositions and Depleted Mantle Nd model ages (c. 0.8–1.2 Ga) correspond to the published data for the arc-related magmatic rocks from the Lake Zone forming the so-called Ikh-Mongol Arc System (Janoušek et al., in print; Kovach et al., 2011; Rudnev et al., 2009; Yarmolyuk et al., 2011).

The whole-rock geochemical and Sr–Nd isotopic signatures provide evidence that the parental magmas of the KTGC originated directly from depleted mantle and/or by partial melting of young (not older than Tonian), juvenile metabasic crust. The latter could have been formed by an older basic magmatic phase of the same arc. In either case, the scope for contamination by mature crustal material is severely limited.

In contrast, the younger monzodiorite shows clearly a distinct, post-collisional whole-rock geochemical signature, as documented for instance in the multi-element R_1–R_2 plot of Batchelor and Bowden (1985) (Fig. 13a). The monzodiorite resembles within-plate magmatic rocks by its tholeiitic–mildly alkaline chemistry and lack of HFSE impoverishment (Fig. 13a–d).

7.2. Sedimentation age and setting of the Bij Group

Due to scarcity of geochronological data, the depositional age of the BG metasedimentary rocks has been poorly constrained so far. Age spectra of all four samples presented here are mutually well comparable, showing the dominance of detrital zircons of Neoproterozoic – Ordovician age. Moreover, two of samples, GS 028 and GS 053, also yielded a few Mesoproterozoic and Palaeoproterozoic ages.

All the samples from the BG show the calculated maximum depositional ages in the interval between c. 505 and 436 Ma, constraining the lower age limit of sedimentation. The maximum depositional ages obtained from the BG metasedimentary rocks are broadly similar to, or even slightly younger than, the intrusive ages of the arc-related magmatic suite of the KTGC. The newly obtained detrital zircon age spectra

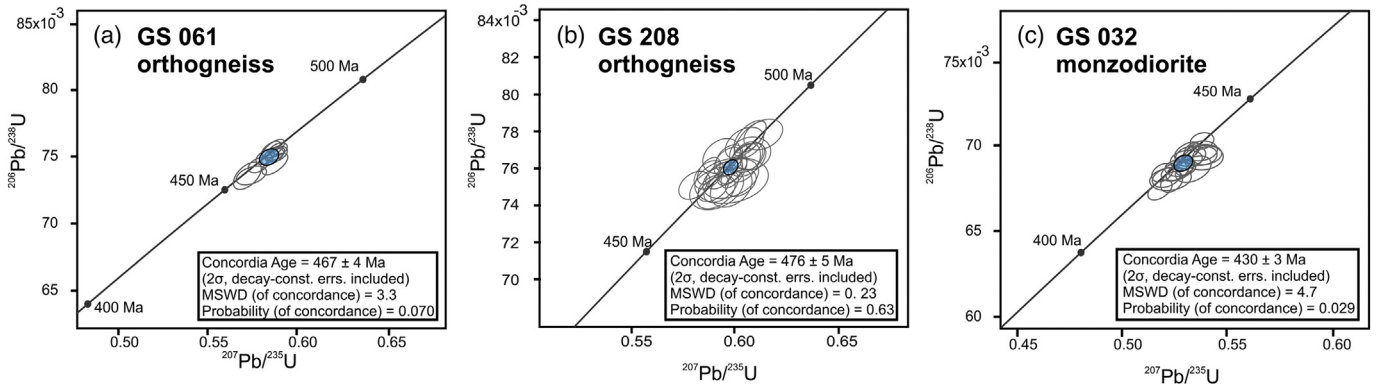

Fig. 11. U–Pb concordia diagrams and calculated concordia ages (in blue) for magmatic zircons (LA-ICP-MS data) from the studied samples of the KTGC. (For interpretation of the references to colour in this figure legend, the reader is referred to the web version of this article.)

thus indicate that much of the clastic material was probably derived directly from the KTGC.

The whole-rock geochemical and Sr–Nd isotopic signatures of the BG amphibolites do not show subduction-related features and unequivocally indicate derivation of their protolith from a strongly to moderately depleted mantle source. In the Th–Zr/117–Nb/16 ternary diagram of Wood (1980) and Nb/Yb–Th/Yb binary plot of Pearce (2008), most of the BG amphibolites fall close to the N-MORB and E-MORB fields (Fig. 13b, d). Still, a single sample GB 460B shows a weak volcanic-arc affinity (Fig. 13b, d). Its significance remains doubtful, though; such a signature, together with elevated SiO_2, can also reflect a crustal contamination.

The Hf vs. La/Th discrimination diagram of Floyd and Leveridge (1987) implies that the protoliths of the studied metasedimentary rocks were derived mainly from the acid arc-related magmatic source (Fig. 13e). The La/Sc vs. Ti/Zr diagram of Bhatia and Crook (1986) indicates that the BG metasedimentary rocks were deposited in continental island arc and/or active continental margin settings (Fig. 13f).

Taken together, the BG could be interpreted as a rock assemblage originally consisting of both volcanic and sedimentary rocks accompanying the magmatic arc, originated most likely from the coeval, and somewhat younger, parts of neighbouring accretionary wedge.

7.3. Provenance of the Bij Group metasedimentary rocks

Analogous detrital zircon age populations from all four samples (Fig. 12) indicate their similar sources. The prevalence of the c. 570–460 Ma age group (Fig. 14a) with igneous-looking zircon morphology and internal zoning demonstrates that the detritus was mainly derived from the Ediacaran to Mid-Ordovician magmatic rocks. As discussed above, the c. 470 Ma sub-peak implies that the KTGC was likely one of the sources. Indeed, most of these zircon grains have subhedral to euhedral habitus (Fig. 10b), compatible with short transport.

Broad peak at c. 1020–700 Ma (Fig. 14a) shows that the next important contribution of clastic material was provided from Grenvillean-age and late Tonian sources. These ages were often detected in the subrounded or corroded grains or cores, indicating longer transport than in the case of the proximal KTGC-derived detritus. Distinct age gap at c. 750–650 Ma further implies lack of magmatic activity within the (future) source areas. Only a few detected ages suggest a minor input of the Meso- and Palaeoproterozoic zircons.

The youngest ages grouping around 375 Ma are interpreted as a result of metamorphic overprint, in accord with the evidence for Late Devonian metamorphism provided by the electron-microprobe monazite dating of the BG metapelites (c. 360 Ma: Soejono et al., 2015).

As indicated by BG detrital zircon ages, the magmatic activity in the source region(s) concentrated into several pulses during Neoproterozoic–Ordovician. The Neoproterozoic to Early Palaeozoic magmatic complexes are widespread throughout the units adjacent to the Hovd Zone, both the westerly Altai Domain and the easterly Lake Zone. Ages of granitic rocks reported from the Chinese and Mongolian Altai predominantly range from c. 470 to 260 Ma (Cai et al., 2011a, 2011b, 2012; Sun et al., 2009; Wang et al., 2006; Zhang et al., 2017), whereas the main period of the magmatic-arc activity within the Lake Zone was between c. 570 and 460 Ma (Janoušek et al., in print; Kovach et al., 2011; Rudnev et al., 2012; Soejono et al., 2016). Moreover, the Ediacaran ophiolites are exposed in the eastern Lake Zone (Jian et al., 2014; Khain et al., 2003). The fairly consistent dominant zircon ages in the studied BG samples thus make the Lake Zone and the adjacent KTGC a proper candidate for the major sediment source.

The other age peak (c. 1020–700 Ma) can be linked most likely with the widespread Grenvillean-age (early Tonian) continental-arc magmatism (Buriánek et al., 2017; Demoux et al., 2009) and late Tonian rift-related volcanism (Levashova et al., 2010; Yarmolyuk et al., 2008) along the western margin of the Precambrian basement blocks. The microcontinental segments (Tuva-Mongolian, Zavkhan and Baydrag), located to the east of the Lake Zone, represent the most significant potential sources of the Tonian detritus within the wider vicinity of the studied area. Also the Meso- and Palaeoproterozoic zircons only rarely detected in our samples could have been directly contributed by, or at least recycled from, these Precambrian basement blocks (Bold et al., 2016; Demoux et al., 2009; Rojas-Agramonte et al., 2011).

Additionally, nearly identical detrital zircon age patterns, characterized by two major age peaks (Tonian and Ediacaran–Early Palaeozoic) were found in the (meta-)sedimentary rocks of both the Mongolian and Chinese Altai (Fig. 14b) (Chen et al., 2015; Jiang et al., 2011; Long et al., 2010; Wang et al., 2014).

In summary, the resemblance of detrital zircon age populations suggests identical provenance for Early Palaeozoic basins in the Altai and Hovd zones. The Lake Zone and the easterly Precambrian continental blocks were the closest plausible source regions of such a sedimentary material (Fig. 14b).

7.4. Correlation of the Khuurai Tsenkher Gol Complex (Hovd Zone) and the Togtokhinshil Complex (Lake Zone)

The Early to Mid-Ordovician arc-related plutonites of the KTGC display many whole-rock geochemical and Sr–Nd isotopic similarities with the gabbro–diorite suite of the Togtokhinshil Complex at the western margin of the Lake Zone (Figs. 7, 8, 13a–d). Also the protolith ages of the two KTGC orthogneisses (476 ± 5 and 467 ± 4 Ma) roughly correspond to the U–Pb zircon age of 459 ± 2 Ma reported from the Togtokhinshil Complex (Soejono et al., 2016). Lastly, the geochemical signatures point to an analogous magmatic-arc origin of both magmatic complexes (Fig. 13a–d).

In the KTGC, the amphibole-based P–T estimates (Ridolfi et al., 2010) indicate crystallization of metadiorites and metagranodiorites at c. 790–960 °C and 0.12–0.22 GPa (Table 2). This pressure range

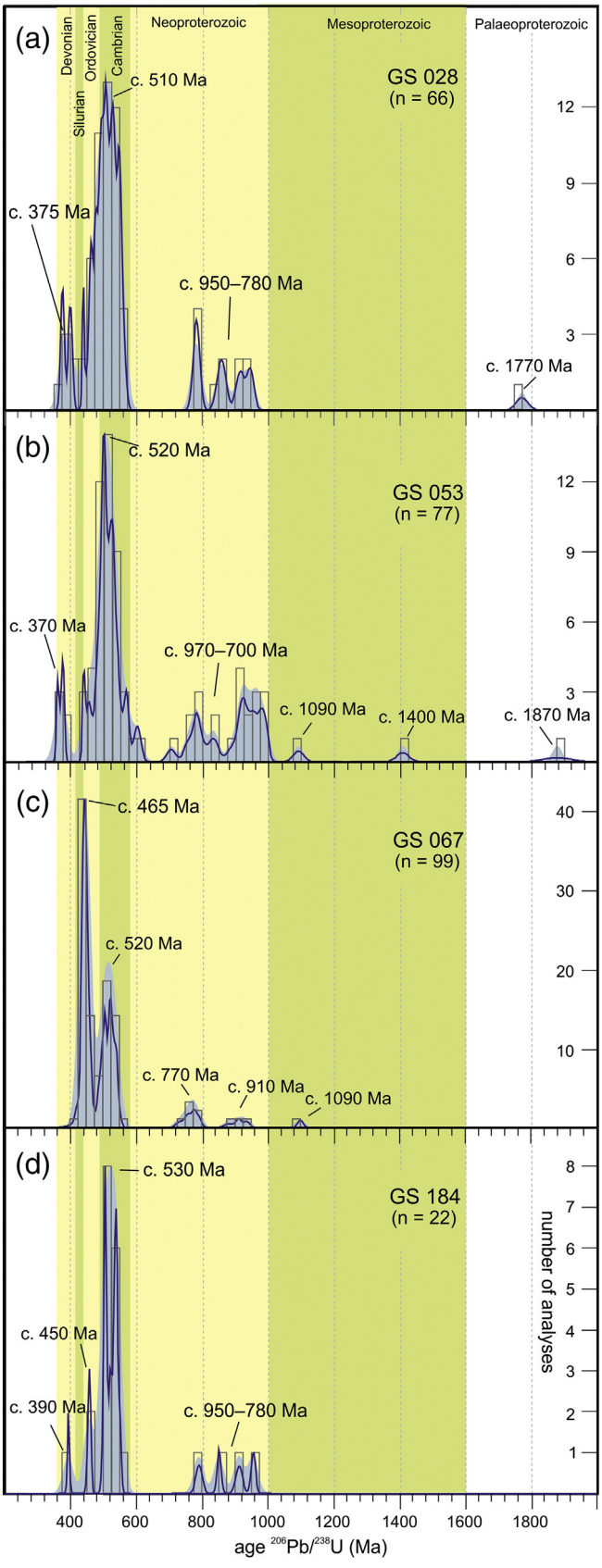

Fig. 12. Kernel density estimates (blue areas), frequency histograms (bin width = 25 Ma) and probability density plots (dark blue) showing U–Pb zircon concordia age distributions in the studied BG metasedimentary rocks; n — number of analyses. Only data less than 10% discordant were used. (For interpretation of the references to colour in this figure legend, the reader is referred to the web version of this article.)

corresponds to a depth of c. 4–8 km, i.e. roughly the same crustal levels as for the Togtokhinshil Complex (c. 5–12 km; Soejono et al., 2016). However, amphiboles from the KTGC (meta-)igneous rocks suffered metamorphic recrystallization under amphibolite-facies conditions (410–560 °C and 0.4–0.6 GPa), whereas the amphiboles from the Togtokhinshil Complex diorites have been only locally recrystallized due to the low-grade overprint.

7.5. Geodynamic implications

7.5.1. Regional context of Ordovician magmatic arc at the Lake and Hovd zones boundary

The present study reveals that the basement at the eastern edge of the Hovd Zone, newly defined as the KTGC, was formed within an Early to Mid-Ordovician magmatic arc. Our results thus support the conclusions of recent works, showing that many of the basement complexes exposed in the southern–central and western Mongolia as well as in the Chinese Altai originated in the Early Palaeozoic magmatic-arc setting (Janoušek et al., in print; Kovach et al., 2011; Rudnev et al., 2012; Soejono et al., 2016; Yarmolyuk et al., 2011).

Due to strong reworking of the studied region, it is difficult to constrain the exact geotectonic context and life-span of the arc, extent of the subducted oceanic domain and subduction polarity (see discussion in Soejono et al., 2016 and references therein). The Sr–Nd isotopic signatures allow two possibilities: either the arc was purely intra-oceanic or it was founded on geochemically primitive, juvenile continental crust. As discussed above, the BG is in any case interpreted as a fragment of the nearby accretionary wedge. The detrital zircon spectra require significant contributions from other sources, apart from the magmatic arc itself. They thus imply relative proximity and availability of the exposed older continental crust. Hence the magmatic arc likely developed upon the young continental crustal segment composed of the Neoproterozoic–Early Palaeozoic arcs and ophiolites of the Lake Zone freshly accreted to the neighbouring Precambrian nuclei, or at least in vicinity of the continent. In contrast, the morphology and internal features of the abundant Proterozoic zircons from studied samples argue for a relatively long transport and/or recycling.

The remarkable similarities in petrology, field relationships, magmatic ages, geochemistry, and crystallization conditions of the KTGC to the gabbro–diorite suite of the Togtokhinshil Complex suggest an idea that the KTGC was originally integral constituent of the Lake Zone. Thus, the KTGC could have been separated from the (current) western margin of the Lake Zone only during the subsequent tectonic evolution. The Hovd Zone basement thus could represent, at least in the study area, reworked marginal part of the Lake Zone, rather than a fully independent unit.

The western margin of the Lake Zone could originally have been a member of the westward (in the western Mongolia, present-day coordinates) younging Cambro–Ordovician magmatic-arc system, driven by the continuous closure of the Palaeo-Asian oceanic domain in the west (Buslov et al., 2001). Progressive roll-back of the subducting Palaeo-Asian oceanic plate is considered to be a reason for different configurations of magmatic arcs (from the continental through the transitional to the typical intra-oceanic) documented in the Lake Zone along the strike of the this Ikh-Mongol Arc System (Janoušek et al., in print).

Comparison of our detrital zircon age spectra with published data (Fig. 14) suggests that the Early Palaeozoic sedimentary rocks in the Hovd and Altai domains most likely shared identical sources. Westward sediment transport indicates the absence of available source rocks west of the Hovd Zone area, which was most likely occupied by an oceanic domain at that time. Exclusively westward transport of the clastic material into the Hovd/Altai sedimentary basin (wedge) supports east-dipping subduction beneath the Lake Zone and the Precambrian microcontinents during the Early to Mid-Ordovician.

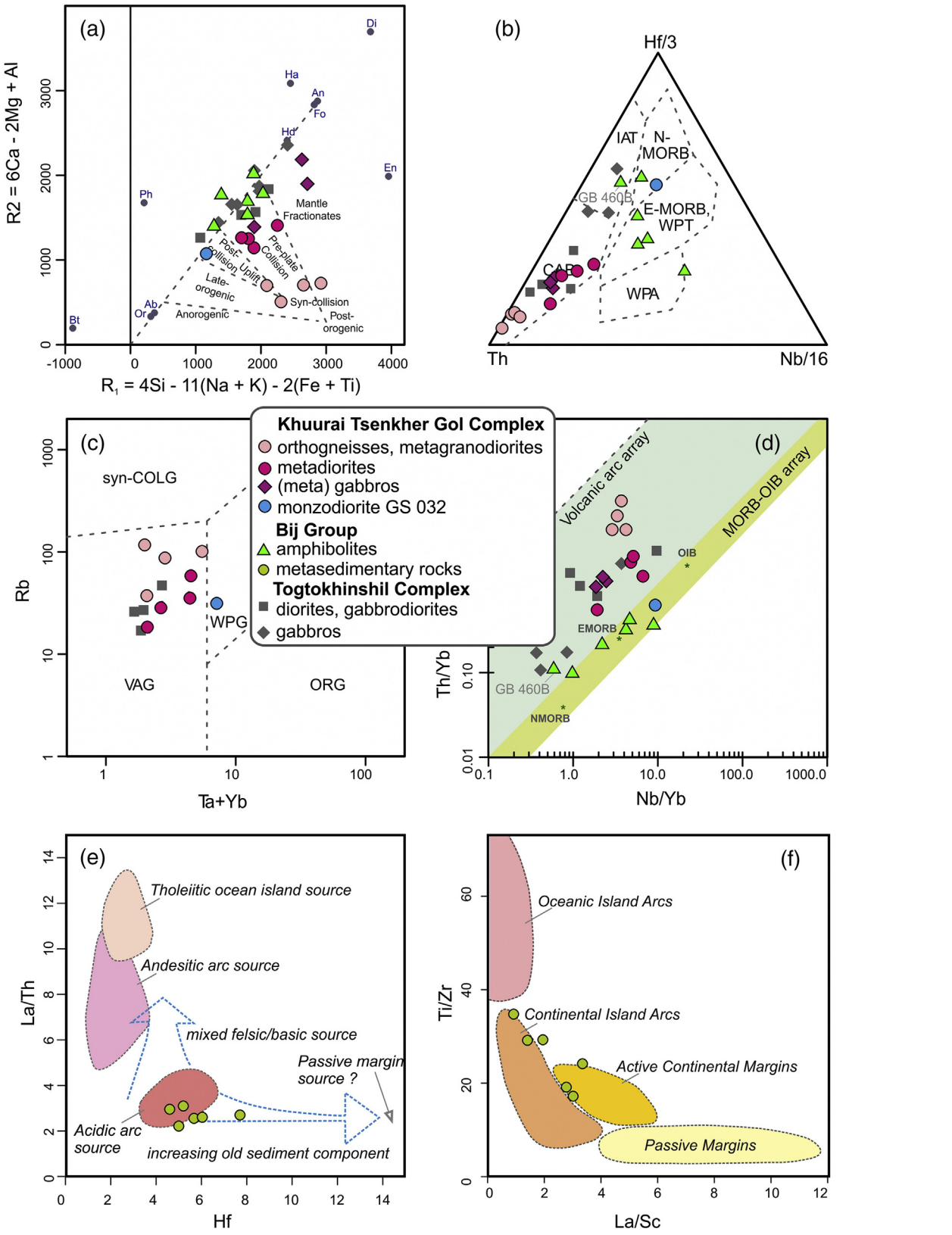

Fig. 13. Geotectonic diagrams for the rocks of the KTGC, amphibolites, metasedimentary rocks of the BG and the gabbro–diorite suite of the Togtokhinshil Complex (Soejono et al., 2016). (a) Multielement R_1–R_2 plot (Batchelor and Bowden, 1985). (b) Ternary diagram Th–Hf/3–Nb/16 of Wood (1980); IAT: Island-Arc Tholeiites; CAB: Calc-Alkaline Basalts; WPT: Within-Plate Tholeiites; WPA: Within-Plate Alkaline basalts. (c) Binary plot Ta + Yb vs. Rb (Pearce et al., 1984). ORG: Ocean Ridge Granites, VAG: Volcanic Arc Granites, syn-COLG: Syncollisional Granites, WPG: Within Plate Granites. (d) Nb/Yb vs. Th/Yb discrimination diagram (Pearce, 2008). OIB: Ocean-Island Basalt; E- and N-MORB: Enriched and Normal Mid-Ocean Ridge Basalts. (e) Hf vs. La/Th discrimination diagram for sediment sources (Floyd and Leveridge, 1987). (f) La/Sc vs. Ti/Zr diagram for tectonic setting of sedimentary rocks (Bhatia and Crook, 1986).

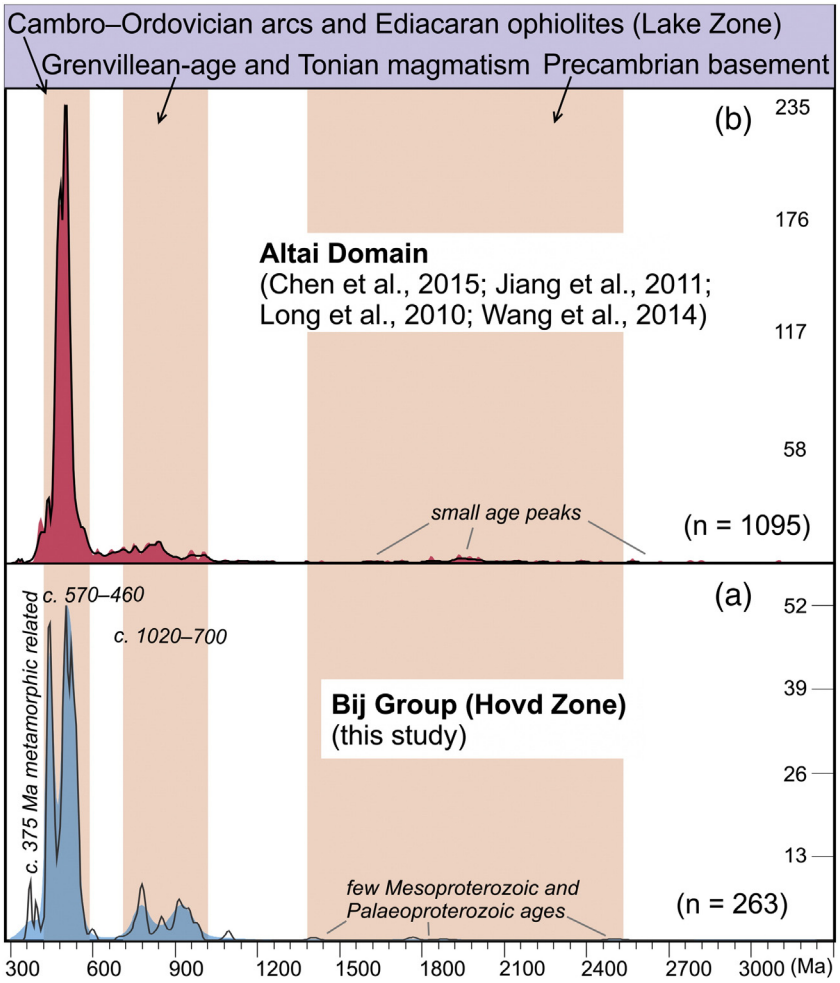

Fig. 14. Comparison of kernel density estimates (coloured areas) and probability density plots (black lines) for detrital zircon ages for the BG (this work) and Archaean–Early Palaeozoic (meta-)sedimentary rocks from the Mongolian, Chinese and Russian Altai (published data with references indicated). The age peaks of the studied samples are denoted by pink rectangles; n — number of analyses. Possible source areas are marked on the top.

7.5.2. Significance of Mid-Silurian intra-plate magmatism in the Khuurai Tsenkher Gol Complex

The dating of quartz monzodiorite GS 032 from the KTGC at c. 430 Ma provides first evidence of Mid-Silurian intra-plate magmatic activity in the region. Unfortunately, macroscopic similarity of this monzodiorite with the older metadiorites did not allow its field identification and thus the real proportion of such magmatic rocks remains uncertain. In any case, common occurrence of well-preserved mingling textures between Ordovician metadiorites and orthogneisses indirectly indicates the prevalence of the older suite.

Poor knowledge of field relationships and the fact that only one sample is available do not permit an unequivocal geotectonic interpretation of the newly detected Late Silurian within-plate magmatic activity. In any case, this magmatic episode obviously followed the culmination of arc activity. The Late Silurian magmatism in the KTGC could reflect crustal thinning and decompression melting of the mantle in the back-arc region. Alternatively, if the arc became extinct, such a basic, mildly alkaline magmatism may have been a hallmark of incipient intracontinental rifting during regional extension caused by far-field forces. Moreover, only slightly older maximum depositional age (c. 436 Ma) obtained from the youngest detrital zircon sample from the BG (GS 067) and the occurrence of unambiguously depleted-mantle derived associated amphibolites mostly lacking any subduction imprint also indicate significant extension and late mantle input.

In the Silurian–Mid-Devonian, an asthenospheric mantle upwelling facilitated by slab window or spreading ridge subduction (Davies and von Blanckenburg, 1995; Thorkelson, 1996) was proposed as mechanism of the widespread partial melting of accretionary wedge in the neighbouring Chinese Altai (Jiang et al., 2010, 2016; Long et al., 2010). Alternatively, elevated heat flow and crustal anatexis resulting from lithosphere thinning of a supra-subduction system or back-arc extension (Collins, 2002; Hyndman et al., 2005) have also been recently proposed for this area (Hanžl et al., 2016; Jiang et al., 2016).

7.5.3. Nature of the Lake and Hovd zones boundary

The primary configuration of the principal domains within the CAOB separated by oceans is generally accepted (Badarch et al., 2002; Xiao et al., 2004). However, the existence of these oceanic domains, their real extent and life-span are often a matter of debate. The Lake Zone is interpreted as the Neoproterozoic passive margin of the Precambrian Zavkhan, Baydrag and Tuva–Mongolian microcontinents (Buriánek et al., 2017) whereas the Hovd Zone is considered as the Early Palaeozoic accretionary wedge (Kröner et al., 2010; Xiao and Santosh, 2014).

The exact timing of the Lake Zone and Hovd Zone (or rather Altai Domain) assembly is poorly constrained. In general, Early Palaeozoic progressive accretion is supposed (Badarch et al., 2002; Windley et al., 2007; Xiao et al., 2004). Our data provide the maximum age limit for this process initiation, as the Early to Mid-Ordovician arc-related KTGC had to pre-date it. On the contrary, the Devonian to Early Carboniferous granites, widespread in the western Mongolia and the Chinese Altai, post-dated the main stage of the accretionary processes in this tract of the CAOB (Cai et al., 2015; Glorie et al., 2011; Soejono et al., 2016).

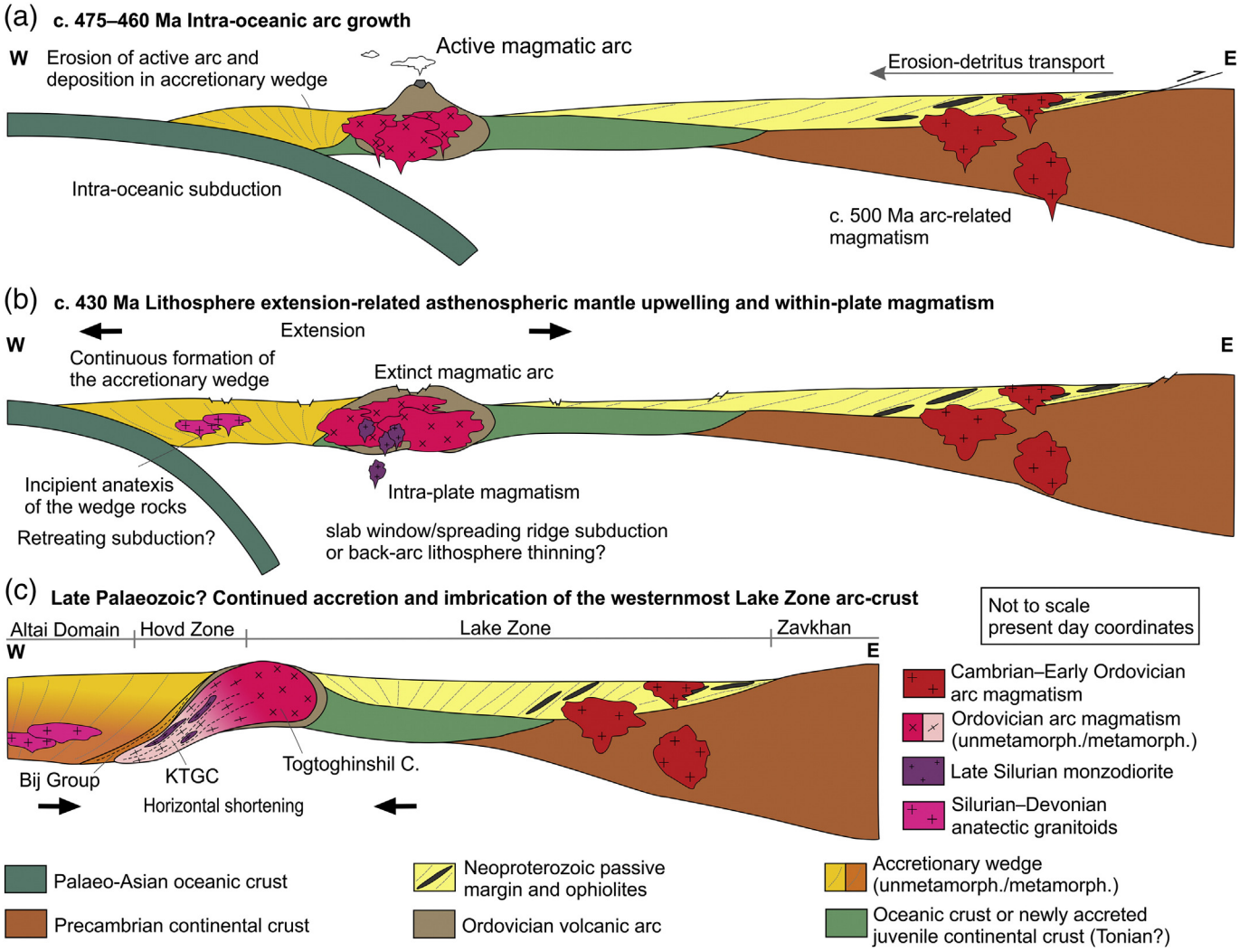

Fig. 15. Schematic geodynamic model for evolution of the western Mongolian tract of the CAOB. (a) Magmatic-arc stage in Ordovician. (b) Mid-Silurian arc extension and related tholeiitic–mildly alkaline magmatic activity. (c) Late Palaeozoic imbrication of the western part of the arc complex and formation of the Lake and Hovd zones.

The accretion had to be completed by the latest Palaeozoic/Early Mesozoic (Guy et al., 2014a; Xiao et al., 2009).

Our study thus demonstrates that the Hovd Zone basement and the Lake Zone margin shared many similar features. Based on field evidence, petrological character, ages and geochemical characteristics, we correlate the KTGC with the Togtokhinshil Complex. In view of the generally similar nature and mutual affinity, an existence of a putative, substantial oceanic domain in between both units seems highly improbable. The Hovd Zone basement thus should represent imbricated western margin of the Lake Zone decorated by the Ordovician magmatic-arc belt. This younger reworking could be result of the Late Palaeozoic NE–SW horizontal shortening reported from the whole Mongolian Altai region (Guy et al., 2014a; Lehmann et al., 2010).

The terrane model, based on the tectonostratigraphic contrasts and the idea of deeply rooted sutures containing oceanic crust fragments between these domains, was recently challenged by geophysical study in southern Mongolia (Guy et al., 2014b) and the structural analysis in the southeastern Mongolian Altai (Hanžl et al., 2016). These authors suggested that the terrane boundaries constitute the Late Permian deformation zones rather than true suture. Similarly, our results show that the Lake/Hovd zones boundary represents a complex structural feature. Our concept thus also casts some doubts on the validity of the CAOB subdivision in western Mongolia into more or less independent terranes separated by the relics of oceanic domains (Badarch et al., 2002; Windley et al., 2007; Xiao et al., 2004). In fact, the mutual relationships are much more complicated and the boundaries between individual domains are broad zones rather than discrete interfaces. Intense younger reworking obscured, or at least extensively modified the primary suture zones and caused present-day configuration — a situation commonly characterizing contacts of major lithotectonic domains in the CAOB.

7.6. Tectonic evolution of the eastern Hovd Zone

The KTGC, BG as well as the Togtokhinshil Complex, located within the Lake and Hovd suture zone, are typical components of western Mongolian branch of the CAOB accretionary system. All above discussed data allow us to compile a potential evolutionary model of the region (Fig. 15).

The KTGC/Togtokhinshil magmatic arc developed above the Early- to Mid-Ordovician east-dipping subduction zone, probably as a somewhat younger continuation of the long-lasting magmatic-arc system of the Palaeo-Asian oceanic domain in the Lake Zone (Fig. 15a). Simultaneously and shortly thereafter, the BG sedimentary precursors were deposited in the accretionary wedge. In the Mid-Silurian, the small body of transitional (tholeiitic–mildly alkaline) quartz monzodiorite intruded the older calc-alkaline suite of the

KTGC. The geodynamic cause for the latter magmatic phase is uncertain, but the slab window/ocean ridge subduction or back-arc lithosphere thinning with attendant asthenospheric mantle upwelling, seem to be plausible mechanisms (Fig. 15b). The subsequent, most likely Late Palaeozoic, accretionary evolution caused that the KTGC and BG were jointly broken off from the Togtokhinshil Complex, imbricated, and incorporated into the future Hovd Zone (Fig. 15c).

In conclusion, we propose that the accretionary processes and geodynamic evolution in the west Mongolian part of the CAOB were dominated by continuous evolution of the Ikh-Mongol Arc System: from the magmatic arc-stage through the intra-plate magmatic episode to the final reworking of the involved complexes. Clearly, much more detailed geochronological, geochemical and structural studies are needed in order to clarify primary relations and possible connections of dismembered crystalline complexes in the studied region. Well-founded knowledge of the primary configuration would, in turn, enable unravelling its complete accretionary history.

8. Conclusions

The combined petrological, whole-rock geochemical and geochronological study of metaigneous and metasedimentary rocks from the Khuurai Tsenkher Gol Complex and Bij Group (Hovd Zone, western Mongolia) has brought the following main conclusions:

1) The Khuurai Tsenkher Gol Complex is composed of two distinct igneous rock suites: (i) dominant low- to medium-grade, calc-alkaline, basic to acid igneous rocks related to the Early–Mid-Ordovician magmatic-arc magmatism and (ii) subordinate transitional (tholeiitic–mildly alkaline) quartz monzodiorite, a product of the Mid-Silurian intra-plate magmatic activity.
2) The Bij Group assemblage consists of metavolcanic and metasedimentary rocks, most likely formed in the accretionary wedge broadly coeval with the arc activity. Detrital zircon age populations of the Bij Group imply identical provenance of the Altai and Hovd domains and overall westward sediment transport. Moreover, they indicate the east-dipping subduction polarity in the Early Palaeozoic.
3) The overall similarity of the Khuurai Tsenkher Gol Complex (Hovd Zone) with the neighbouring Togtokhinshil Complex (Lake Zone) suggests that both magmatic complexes originally belonged to the same magmatic arc, probably the youngest member of the Palaeo-Asian subduction system.
4) The geotectonic reason of the Mid-Silurian intra-plate magmatic event is uncertain, but was likely connected with the continued but retreating subduction (slab window/spreading ridge subduction or back-arc lithosphere thinning).
5) The two complexes were then separated from the western margin of the Lake Zone and imbricated along the current Lake/Hovd zones boundary. This intense modification of the primary configuration was related to the Late Palaeozoic accretionary evolution. We propose that at least some basement complexes of the Hovd Zone represent reworked western margin of the Lake Zone Ikh-Mongol Arc System.
6) Our results challenge the terrane subdivision of the western Mongolia. Similar, diffuse and broad deformation zones are to be expected to form contacts of other major lithotectonic domains in the CAOB as well.

Supplementary data to this article can be found online at http://dx.doi.org/10.1016/j.lithos.2017.08.014.

Acknowledgements

We thank M. Racek and P. Halodová for the CL images, P. Gadas for the assistance with the electron-microprobe analyses and Y. Kochergina for the Sr–Nd isotopic chemistry. We also thank O. Gerel for the discussions, S. Vrána for the help with microscopy and V. Žáček, K. Verner, V. Fürych, O. Oyun-Enkh, and B. Janzanpagma for field assistance. We also acknowledge Xian-Hua Li for the editorial handling of this manuscript and two anonymous referees for their constructive comments. This work was supported by the internal grant of Czech Geological Survey no. 321660 and by the Czech Science Foundation (GAČR) (17-17540S to K. Schulmann and O. Lexa). The Scientific Programme RVO67985831 of the Institute of Geology, The Czech Academy of Sciences is also acknowledged.

References

Baatarhuyag, A., Gansukh, L., 1999. Geological Map of the Mongolia on the Scale 1:200 000, Map Sheet L-46-IX. Geological Information Center, MRAM, Ulaanbaatar (in Mongolian).
Badarch, G., Cunningham, W.D., Windley, B.F., 2002. A new terrane subdivision for Mongolia: implications for the Phanerozoic crustal growth of Central Asia. Journal of Asian Earth Sciences 21, 87–110.
Batchelor, R.A., Bowden, P., 1985. Petrogenetic interpretation of granitic rock series using multicationic parameters. Chemical Geology 48, 43–55.
Bhatia, M.R., Crook, K.A.W., 1986. Trace element characteristics of greywackes and tectonic setting discrimination of sedimentary basins. Contributions to Mineralogy and Petrology 92, 181–193.
Bold, U., Crowley, J.L., Smith, E.F., Sambuu, O., Macdonald, F.A., 2016. Neoproterozoic to early Paleozoic tectonic evolution of the Zavkhan Terrane of Mongolia: implications for continental growth in the Central Asian Orogenic Belt. Lithosphere 8, 729–750.
Boynton, W.V., 1984. Cosmochemistry of the rare earth elements: meteorite studies. In: Henderson, P. (Ed.), Rare Earth Element Geochemistry. Elsevier, Amsterdam, pp. 63–114.
Buriánek, D., Janoušek, V., Hanžl, P., Jiang, Y., Schulmann, K., Lexa, O., Altanbaatar, B., 2016. Petrogenesis of the Late Carboniferous Sagsai Pluton in the SE Mongolian Altai. Journal of Geosciences 61, 67–92.
Buriánek, D., Schulmann, K., Hrdličková, K., Hanžl, P., Janoušek, V., Gerdes, A., 2017. Geochemical and geochronological constraints on distinct Early-Neoproterozoic and Cambrian accretionary events along southern margin of the Baydrag Continent in western Mongolia. Gondwana Research 47, 200–227.
Buslov, M.M., Safonova, I., Watanabe, T., Obut, O., Fujiwara, Y., Iwata, K., Semakov, N.N., Sugai, Y., Smirnova, L.V., Kazansky, Yu., 2001. Evolution of the Paleo-Asian Ocean (Altai–Sayan region, Central Asia) and collision of possible Gondwana-derived terranes with the southern marginal part of the Siberian Continent. Geosciences Journal 5, 203–224.
Cai, K., Sun, M., Yuan, C., Zhao, G., Xiao, W.J., Long, X., Wu, F., 2011a. Prolonged magmatism, juvenile nature and tectonic evolution of the Chinese Altai, NW China: evidence from zircon U–Pb and Hf isotopic study of Paleozoic granitoids. Journal of Asian Earth Sciences 42, 949–968.
Cai, K., Sun, M., Yuan, C., Zhao, G., Xiao, W.J., Long, X., Wu, F., 2011b. Geochronology, petrogenesis and tectonic significance of peraluminous granites from the Chinese Altai, NW China. Lithos 127, 261–281.
Cai, K., Sun, M., Yuan, C., Xiao, W., Zhao, G., Long, X., Wu, F., 2012. Carboniferous mantle-derived felsic intrusion in the Chinese Altai, NW China: implications for geodynamic change of the accretionary orogenic belt. Gondwana Research 22, 681–698.
Cai, K., Sun, M., Jahn, B., Xiao, W.J., Yuan, C., Long, X., Chen, H., Tumurkhuu, D., 2015. A synthesis of zircon U–Pb ages and Hf isotopic compositions of granitoids from southwest Mongolia: implications for crustal nature and tectonic evolution of the Altai Superterrane. Lithos 232, 131–142.
Cawood, P.A., Kröner, A., Collins, W.J., Kusky, T.M., Mooney, W.D., Windley, B.F., 2009. Accretionary orogens through Earth history. In: Cawood, P.A., Kröner, A. (Eds.), Earth Accretionary Systems in Space and Time. Geological Society London Special Publications vol. 318, pp. 1–36.
Chen, M., Sun, M., Cai, K., Buslov, M.M., Zhao, G., Rubanova, E.S., Voytishek, E.E., 2015. Detrital zircon record of the early Paleozoic meta-sedimentary rocks in Russian Altai: implications on their provenance and the tectonic nature of the Altai–Mongolian Terrane. Lithos 233, 209–222.
Collins, W.J., 2002. Hot orogens, tectonic switching, and creation of continental crust. Geology 30, 535–538.
Cox, K.G., Bell, J.D., Pankhurst, R.J., 1979. The Interpretation of Igneous Rocks. George Allen & Unwin, London.
Davies, J.H., von Blanckenburg, F., 1995. Slab breakoff: a model of lithosphere detachment and its test in the magmatism and deformation of collisional orogens. Earth and Planetary Science Letters 129, 85–102.
Debon, F., Le Fort, P., 1983. A chemical–mineralogical classification of common plutonic rocks and associations. Transactions of the Royal Society of Edinburgh: Earth Sciences 73, 135–149.
Demoux, A., Kröner, A., Badarch, G., Jian, P., Tomurhuu, D., Wingate, M.T.D., 2009. Zircon ages from the Baydrag Block and the Bayankhongor Ophiolite Zone: time constraints on Late Neoproterozoic to Cambrian subduction and accretion related magmatism in Central Mongolia. Journal of Geology 117, 377–397.
Dijkstra, A., Buchan, C., Dijkstra, A., Brouwer, F., Cunningham, W., Badarch, G., Mason, P., 2006. Late Neoproterozoic proto-arc ocean crust in the Dariv Range, Western Mongolia: a supra-subduction zone end-member ophiolite. Journal of the Geological Society 163, 363–373.
Floyd, P.A., Leveridge, B.E., 1987. Tectonic environment of the Devonian Gramscatho Basin, south Cornwall: framework mode and geochemical evidence from turbiditic sandstones. Journal of the Geological Society 144, 531–542.

Gavrilova, S.P., Zaitsev, N.S., Pavlov, V.P., Yashina, R.M., 1975. Granitoid and Alkaline Formations in the Structures of Western and Northern Mongolia. Transactions 14. Nauka, Moscow (in Russian).
Glorie, S., De Grave, J., Buslov, M.M., Zhimulev, F.I., Izmer, A., Vandoorne, W., Ryabinin, A., Van den Haute, P., Vanhaecke, F., Elburg, M.A., 2011. Formation and Palaeozoic evolution of the Gorny–Altai–Altai–Mongolia suture zone (south Siberia): zircon U/Pb constraints on the igneous record. Gondwana Research 20, 465–484.
Goldstein, S.L., O'Nions, R.K., Hamilton, P.J., 1984. A Sm–Nd isotopic study of atmospheric dusts and particulates from major river systems. Earth and Planetary Science Letters 70, 221–236.
Guy, A., Schulmann, K., Clauer, N., Hasalová, P., Seltmann, R., Armstrong, R., Lexa, O., Benedicto, A., 2014a. Late Paleozoic–Mesozoic tectonic evolution of the Trans-Altai and South Gobi zones in southern Mongolia based on structural and geochronological data. Gondwana Research 25, 309–337.
Guy, A., Schulmann, K., Munschy, M., Miehe, J.-M., Edel, J.-B., Lexa, O., Fairhead, D., 2014b. Geophysical constraints for terrane boundaries in southern Mongolia. Journal of Geophysical Research — Solid Earth 119, 7966–7991.
Hanžl, P., Schulmann, K., Janoušek, V., Lexa, O., Hrdličková, K., Jiang, Y., Buriánek, D., Altanbaatar, B., Ganchuluun, T., Erban, V., 2016. Making continental crust: origin of Devonian orthogneisses from SE Mongolian Altai. Journal of Geosciences 61, 25–50.
Holland, T.J.B., Blundy, J.D., 1994. Non-ideal interactions in calcic amphiboles and their bearing on amphibole–plagioclase thermometry. Contributions to Mineralogy and Petrology 116, 433–447.
Hyndman, R.D., Currie, C.A., Mazzotti, S.P., 2005. Subduction zone backarcs, mobile belts, and orogenic heat. GSA Today 15, 4–10.
Irvine, T.N., Baragar, W.R.A., 1971. A guide to the chemical classification of the common volcanic rocks. Canadian Journal of Earth Sciences 8, 523–548.
Janoušek, V., Moyen, J.F., Martin, H., Erban, V., Farrow, C., 2016. Geochemical Modelling of Igneous Processes – Principles and Recipes in R Language. Bringing the Power of R to a Geochemical Community. Springer-Verlag, Berlin.
Janoušek, V., Jiang, Y.D., Buriánek, D., Schulmann, K., Hanžl, P., Soejono, I., Kröner, A., Altanbaatar, B., Erban, V., Lexa, O., Ganchuluun, T., Košler, J., 2017. Cambrian–Ordovician magmatism of the Ikh-Mongol Arc System exemplified by the Khantaishir Magmatic Complex (Lake Zone, south-central Mongolia). Gondwana Research (in print).
Jensen, L.S., 1976. A New Cation Plot for Classifying Subalkalic Volcanic Rocks. Ontario Geological Survey, Miscellaneous Paper 66.
Jian, P., Kröner, A., Jahn, B.M., Windley, B.F., Shi, Y., Zhang, W., Zhang, F., Miao, L., Tomurhuu, D., Liu, D., 2014. Zircon dating of Neoproterozoic and Cambrian ophiolites in West Mongolia and implications for the timing of orogenic processes in the central part of the Central Asian Orogenic Belt. Earth-Science Reviews 133, 62–93.
Jiang, Y.D., Sun, M., Zhao, G., Yuan, C., Xiao, W.J., Xia, X., Long, X., Wu, F., 2010. The ~390 Ma high-T metamorphic event in the Chinese Altai: a consequence of ridge-subduction? American Journal of Science 310, 1421–1452.
Jiang, Y.D., Sun, M., Zhao, G., Yuan, C., Xiao, W.J., Xia, X., Long, X., Wu, F., 2011. Precambrian detrital zircons in the Early Paleozoic Chinese Altai: their provenance and implications for the crustal growth of central Asia. Precambrian Research 189, 140–154.
Jiang, Y.D., Schulmann, K., Sun, M., Štípská, P., Guy, A., Janoušek, V., Lexa, O., Yuan, C., 2016. Anatexis of accretionary wedge, Pacific type magmatism, and formation of vertically stratified continental crust in the Altai Orogenic Belt. Tectonics 35, 3095–3118.
Khain, E.V., Bibikova, E.V., Sal'nikova, E.B., Kröner, A., Gibsher, A.S., Didenko, A.N., Degtyarev, K.E., Fedotova, A.A., 2003. The Palaeo-Asian Ocean in the Neoproterozoic and early Palaeozoic: new geochronologic data and palaeotectonic reconstructions. Precambrian Research 122, 329–358.
Kovach, V.P., Yarmolyuk, V.V., Kovalenko, V.I., Kozlovskyi, A.M., Kotov, A.B., Terent'eva, L.B., 2011. Composition, sources, and mechanisms of formation of the continental crust of the Lake Zone of the Central Asian Caledonides. II. Geochemical and Nd isotope data. Petrology 19, 399–425.
Kretz, R., 1983. Symbols for rock-forming minerals. American Mineralogist 68, 277–279.
Kröner, A., Lehmann, J., Schulmann, K., Demoux, A., Lexa, O., Tomurhuu, D., Štípská, P., Liu, D., Wingate, M.T.D., 2010. Lithostratigraphic and geochronological constraints on the evolution of the Central Asian Orogenic Belt in SW Mongolia: Early Paleozoic rifting followed by Late Paleozoic accretion. American Journal of Science 310, 523–574.
Kröner, A., Kovach, V., Belousova, E., Hegner, E., Armstrong, R., Dolgopolova, A., Seltmann, R., Alexeiev, D.V., Hoffmann, J.E., Wong, J., Sun, M., Cai, K., Wang, T., Tong, Y., Wilde, S.A., Degtyarev, K.E., Rytsk, E., 2014. Reassessment of continental growth during the accretionary history of the Central Asian Orogenic Belt. Gondwana Research 25, 103–125.
Leake, B.E., Woolley, A.R., Arps, C.E.S., Birch, W.D., Gilbert, M.C., Grice, J.D., Hawthorne, F.C., Kato, A., Kisch, H.J., Krivovichev, V.G., Linthout, K., Laird, J., Mandarino, J., Maresch, W.V., Nickel, E.H., Rock, N.M.S., Schumacher, J.C., Smith, J.C., Stephenson, N.C.N., Whittaker, E.J.W., Youzhi, G., 1997. Nomenclature of amphiboles: report of the Subcommittee on Amphiboles of the International Mineralogical Association Commission on New Minerals and Mineral Names. Mineralogical Magazine 61, 295–321.
Lehmann, J., Schulmann, K., Lexa, O., Corsini, M., Kröner, A., Štípská, P., Tomurhuu, D., Otgonbator, D., 2010. Structural constraints on the evolution of the Central Asian Orogenic Belt in SW Mongolia. American Journal of Science 310, 575–628.
Levashova, N.M., Kalugin, V.M., Gibsher, A.S., Yff, J., Ryabinin, A.B., Meert, J.G., Malone, S.J., 2010. The origin of the Baydaric microcontinent, Mongolia: constraints from paleomagnetism and geochronology. Tectonophysics 485, 306–320.
Liew, T.C., Hofmann, A.W., 1988. Precambrian crustal components, plutonic associations, plate environment of the Hercynian Fold Belt of Central Europe: indications from a Nd and Sr isotopic study. Contributions to Mineralogy and Petrology 98, 129–138.
Long, X., Yuan, C., Sun, M., Xiao, W.J., Zhao, G., Wang, Y., Cai, K., Xia, X., Xie, L., 2010. Detrital zircon ages and Hf isotopes of the early Paleozoic flysch sequence in the Chinese Altai, NW China: new constrains on depositional age, provenance and tectonic evolution. Tectonophysics 480, 213–231.
Maruyama, S., 1997. Pacific-type orogeny revisited: Miyashiro-type orogeny proposed. Island Arc 6, 91–120.
Molina, J.F., Moreno, J.A., Castro, A., Rodríguez, C., Fershtater, G.B., 2015. Calcic amphibole thermobarometry in metamorphic and igneous rocks: new calibrations based on plagioclase/amphibole Al–Si partitioning and amphibole/liquid Mg partitioning. Lithos 232, 286–305.
Mossakovsky, A.A., Ruzhentsev, S.V., Samygin, S.G., Kheraskova, T.N., 1994. Central Asian Fold Belt: geodynamic evolution and formation history. Geotectonics 27, 445–474.
Pearce, J.A., 1996. A user's guide to basalt discrimination diagrams. In: Wyman, D.A. (Ed.), Trace Element Geochemistry of Volcanic Rocks: Applications for Massive Sulphide Exploration. Geological Association of Canada, Short Course Notes vol. 12, pp. 79–113.
Pearce, J.A., 2008. Geochemical fingerprinting of oceanic basalts with applications to ophiolite classification and the search for Archean oceanic crust. Lithos 100, 14–48.
Pearce, J.A., Harris, N.B.W., Tindle, A.G., 1984. Trace element discrimination diagrams for the tectonic interpretation of granitic rocks. Journal of Petrology 25, 956–983.
Peccerillo, A., Taylor, S.R., 1976. Geochemistry of Eocene calc-alkaline volcanic rocks from the Katamonu area, northern Turkey. Contributions to Mineralogy and Petrology 58, 63–81.
Ridolfi, F., Renzulli, A., Puerini, M., 2010. Stability and chemical equilibrium of amphibole in calc-alkaline magmas: an overview, new thermobarometric formulations and application to subduction-related volcanoes. Contributions to Mineralogy and Petrology 160, 45–66.
Rojas-Agramonte, Y., Kröner, A., Demoux, A., Xia, X., Wang, W., Donskaya, T., Liu, D., Sun, M., 2011. Detrital and xenocrystic zircon ages from Neoproterozoic to Palaeozoic arc terranes of Mongolia: significance for the origin of crustal fragments in the Central Asian Orogenic Belt. Gondwana Research 19, 751–763.
Rudnev, S.N., Izokh, A.E., Kovach, V.P., Shelepaev, R.A., Terent'eva, L.B., 2009. Age, composition, sources, and geodynamic environments of the origin of granitoids in the northern part of the Ozernaya Zone, western Mongolia: growth mechanisms of the Paleozoic continental crust. Petrology 17, 439–475.
Rudnev, S., Izokh, E., Borisenko, S., Shelepaev, R., Orihashi, Y., Lobanov, K., Vishnevsky, V., 2012. Early Paleozoic magmatism in the Bumbat-Hairhan area of the Lake Zone in western Mongolia (geological, petrochemical, and geochronological data). Russian Geology and Geophysics 53, 425–441.
Safonova, I., Seltmann, R., Kröner, A., Gladkochub, D., Schulmann, K., Xiao, W., Kim, J., Komiya, T., Sun, M., 2011. A new concept of continental construction in the Central Asian Orogenic Belt. Episodes 34, 186–196.
Safonova, I., Kotlyarov, A., Krivonogov, S., Xiao, W.J., 2017. Intra-oceanic arcs of the Paleo-Asian Ocean. Gondwana Research 50, 167–194.
Santosh, M., Maruyama, S., Komiya, T., Yamamoto, S., 2010. Orogens in the evolving Earth: from surface continents to "lost continents" at the core–mantle boundary. In: Kusky, T.M., Zhai, M., Xiao, W. (Eds.), The Evolving Continents: Understanding Processes of Continental Growth. Geological Society of London, Special Publications vol. 338, pp. 77–116.
Şengör, A.M.C., Natal'in, B.A., 1996. Turkic-type orogeny and its role in the making of the continental crust. Annual Review of Earth and Planetary Sciences 24, 263–337.
Şengör, A., Natal'in, B., Burtman, V., 1993. Evolution of the Altaid tectonic collage and Paleozoic crustal growth in Eurasia. Nature 364, 299–307.
Soejono, I., Čopjaková, R., Čáp, P., Buriánek, D., Verner, K., 2015. Lower Palaeozoic tectonometamorphic evolution of the Bij Formation, Hovd Zone, western Mongolia. In: Lexa, O., Hasalová, P., Jeřábek, P. (Eds.), CETEG 2015 — 13th Meeting of the Central European Tectonic Groups and 20th Meeting of the Czech Tectonic Studies Group (ČTS), Kadaň, 22–25 April, 2015, Abstract Volume. Czech Geological Survey, Prague, p. 82.
Soejono, I., Buriánek, D., Svojtka, M., Žáček, V., Čáp, P., Janoušek, V., 2016. Mid-Ordovician and late Devonian magmatism in the Togtokhinshil Complex: new insight into the formation and accretionary evolution of the Lake Zone (Western Mongolia). Journal of Geosciences 61, 5–23.
Sun, S.S., McDonough, W.F., 1989. Chemical and isotopic systematics of oceanic basalts: implications for mantle composition and processes. In: Saunders, A.D., Norry, M. (Eds.), Magmatism in the Ocean Basins. Geological Society, London, Special Publications vol. 42, pp. 313–345.
Sun, M., Long, X.P., Cai, K. Da, Jiang, Y. De, Wang, B.Y., Yuan, C., Zhao, G.C., Xiao, W.J., Wu, F.Y., 2009. Early Paleozoic ridge subduction in the Chinese Altai: insight from the abrupt change in zircon Hf isotopic compositions. Science in China, Series D: Earth Sciences 52, 1345–1358.
Thorkelson, D.J., 1996. Subduction of diverging plates and the principles of slab window formation. Tectonophysics 255, 47–63.
Wang, T., Hong, D., Jahn, B.M., Tong, Y., Wang, Y., Han, B., Wang, X., 2006. Timing, petrogenesis, and setting of Paleozoic synorogenic intrusions from the Altai Mountains, northwest China: implications for the tectonic evolution of an accretionary orogen. Journal of Geology 114, 735–751.
Wang, Y., Long, X., Wilde, S.A., Xu, H., Sun, M., Xiao, W.J., Yuan, C., Cai, K., 2014. Provenance of Early Paleozoic metasediments in the central Chinese Altai: implications for tectonic affinity of the Altai-Mongolia Terrane in the Central Asian Orogenic Belt. Lithos 210, 57–68.
Wilhem, C., Windley, B.F., Stampfli, G.M., 2012. The Altaids of Central Asia: a tectonic and evolutionary innovative review. Earth-Science Reviews 113, 303–341.
Windley, B.F., Alexeiev, D.V., Xiao, W.J., Kröner, A., Badarch, G., 2007. Tectonic models for accretion of the Central Asian Orogenic Belt. Journal of the Geological Society 164, 31–47.

Wood, D.A., 1980. The application of a Th–Hf–Ta diagram to problems of tectonomagmatic classification and to establishing the nature of crustal contamination of basaltic lavas of the British Tertiary Volcanic Province. Earth and Planetary Science Letters 50, 11–30.

Xiao, W.J., Santosh, M., 2014. The western Central Asian Orogenic Belt: a window to accretionary orogenesis and continental growth. Gondwana Research 25, 1429–1444.

Xiao, W.J., Windley, B.F., Badarch, G., Sun, S., Li, J., Qin, K., Wang, Z., 2004. Palaeozoic accretionary and convergent tectonics of the southern Altaids: implications for the growth of Central Asia. Journal of the Geological Society 161, 339–342.

Xiao, W.J., Windley, B.F., Huang, B.C., Han, C.M., Yuan, C., Chen, H.L., Sun, M., Sun, S., Li, J.L., 2009. End-Permian to mid-Triassic termination of the accretionary processes of the southern Altaids: implications for the geodynamic evolution, Phanerozoic continental growth, and metallogeny of Central Asia. International Journal of Earth Sciences 98, 1189–1217.

Yarmolyuk, V.V., Kovalenko, V.I., Anisimova, I.V., Sal'nikova, E.B., Kovach, V.P., Kozakov, I.K., Kozlovsky, A.M., Kudryashova, E.A., Kotov, A.B., Plotkina, Y., Terent'eva, L.B., Yakovleva, S.Z., 2008. Late Riphean alkali granites of the Zabhan microcontinent: evidence for the timing of Rodinia breakup and formation of microcontinents in the Central Asian Fold belt. Doklady Earth Sciences 420, 583–588.

Yarmolyuk, V.V., Kovach, V.P., Kovalenko, V.I., Sal'nikova, E.B., Kozlovskii, A.M., Kotov, A.B., Yakovleva, S.Z., Fedoseenko, A.M., 2011. Composition, sources, and mechanism of continental crust growth in the Lake Zone of the Central Asian Caledonides: I. Geological and geochronological data. Petrology 19, 55–78.

Žáček, V., Břízová, E., Bohdálek, P., Buriánek, D., Čáp, P., Enkhjargal, M., Franců, J., Gelegjamts, A., Guy, A., Hanžl, P., Havlíček, P., Henrion, E., Hošek, J., Jelének, J., Knésl, I., Karenová, J., Kociánová, L., Kotková, J., Krejčí, Z., Mixa, P., Mrlina, J., Pecina, V., Pécskay, Z., Prudhomme, A., Soejono, I., Svojtka, M., Šimůnek, Z., Škoda, R., Verner, K., Vondrovic, L., Vorel, T., Vrána, S., Čopjaková, R., 2016. Geological mapping 1: 50,000 and assessment of economic potential of selected region in Western Mongolia (Mongol Altai 50, Ma-50). Final Report, Czech Geological Survey, Prague, Mineral Resources Authority of Mongolia, pp. 1–518.

Zhang, J., Wang, T., Tong, Y., Zhang, Z., Song, P., Zhang, L., Huang, H., Guo, L., Hou, Z., 2017. Tracking deep ancient crustal components by xenocrystic/inherited zircons of Palaeozoic felsic igneous rocks from the Altai–East Junggar Terrane and adjacent regions, western Central Asian Orogenic Belt and its tectonic significance. International Geology Review (in print). http://dx.doi.org/10.1080/00206814.2017.1308841.

Zonenshain, L.P., 1973. The evolution of Central Asiatic geosynclines through sea-floor spreading. Tectonophysics 19, 213–232.

Zonenshain, L.P., Kuzmin, M.I., 1978. Khan–Taishir ophiolite complex in western Mongolia and problems of ophiolites. Geotectonics 1, 19–42.

Chapter II

Cambrian–Ordovician magmatism of the Ikh-Mongol Arc System exemplified by the Khantaishir Magmatic Complex (Lake Zone, south–central Mongolia)

by Vojtěch Janoušek, Yingde Jiang, David Buriánek, Karel Schulmann, Pavel Hanžl, Igor Soejono, Alfred Kröner, Battushig Altanbaatar, Vojtěch Erban, Ondrej Lexa, Turbat Ganchuluun, Jan Košler

Graphical abstract

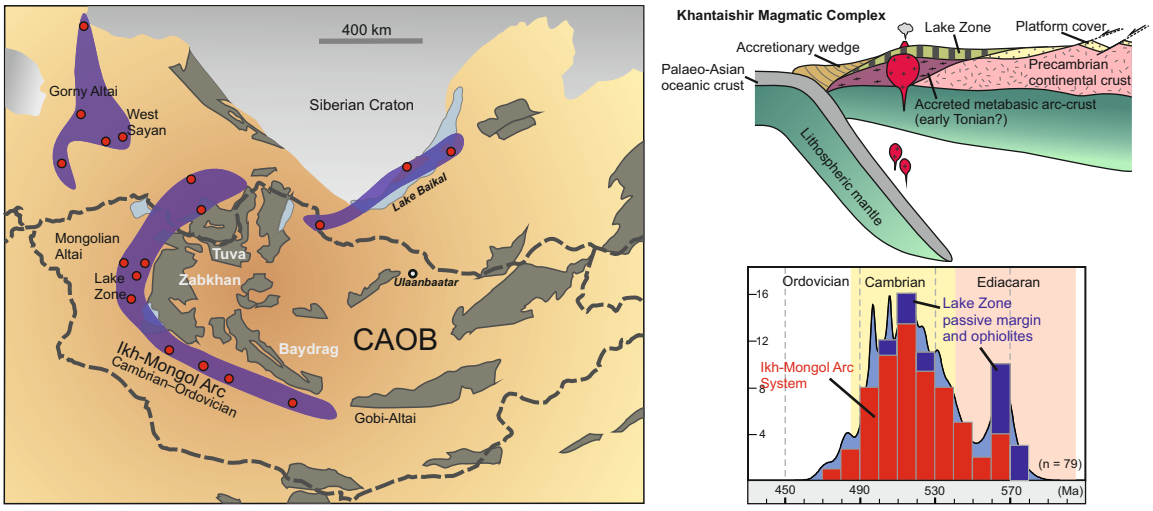

Keywords: *subduction; Lake Zone; whole-rock geochemistry; zircon dating; Ikh-Mongol Arc System*

Supplementary materials are available at https://doi.org/10.1016/j.gr.2017.10.003

Gondwana Research 54 (2018) 122–149

Contents lists available at ScienceDirect

Gondwana Research

journal homepage: www.elsevier.com/locate/gr

Cambrian–Ordovician magmatism of the Ikh-Mongol Arc System exemplified by the Khantaishir Magmatic Complex (Lake Zone, south–central Mongolia)

Vojtěch Janoušek [a,*], Yingde Jiang [b], David Buriánek [a], Karel Schulmann [a], Pavel Hanžl [a], Igor Soejono [a,c], Alfred Kröner [d,e], Battushig Altanbaatar [f], Vojtěch Erban [a], Ondrej Lexa [c], Turbat Ganchuluun [g], Jan Košler [h,1]

[a] Czech Geological Survey, Klárov 3, 118 21 Prague 1, Czech Republic
[b] State Key Laboratory of Isotope Geochemistry, Guangzhou Institute of Geochemistry, Chinese Academy of Sciences, Guangzhou 510640, China
[c] Institute of Petrology and Structural Geology, Charles University, Albertov 6, 128 43 Prague 2, Czech Republic
[d] Department of Geosciences, University of Mainz, D-55099 Mainz, Germany
[e] Beijing SHRIMP Centre, Chinese Academy of Geological Sciences, 26 Baiwanzhuang Road, 100037 Beijing, China
[f] Institute of Paleontology and Geology, Mongolian Academy of Sciences, P.O. Box 45/650,Ulaanbaatar 15160, Mongolia
[g] School of Geology and Mining Engineering, MUST, P.O. Box 654, Ulaanbaatar, Mongolia
[h] Department of Earth Science, University of Bergen, Allégaten 41, 5007 Bergen, Norway

ARTICLE INFO

Article history:
Received 6 December 2016
Received in revised form 17 August 2017
Accepted 12 October 2017
Available online 18 October 2017

Handling Editor: S.J. Liu

Keywords:
Subduction
Lake Zone
Whole-rock geochemistry
Zircon dating
Ikh-Mongol Arc System

ABSTRACT

The Khantaishir Magmatic Complex (KMC) (south–central Mongolia) exposes a section of a magmatic system consisting of deep crustal, ultramafic cumulates (coarse-grained Amp gabbros and hornblendites; *c.* 0.35–0.5 GPa) to shallower crustal levels dominated by Amp–Bt tonalites (*c.* 0.1–0.2 GPa). The magmatic rocks were emplaced during most of the Cambrian (*c.* 538–495 Ma) and are mostly geochemically primitive (Mg# ~ 50), Na-rich and metaluminous. The (normal-) calc-alkaline signature and characteristic trace-element enrichment in hydrous-fluid mobile large-ion lithophile elements (LILE) relative to high-field strength elements (HFSE) suggest an origin within a magmatic arc. Multiple intrusions of basic magma derived from a subduction-modified depleted mantle developed by fractional crystallization and/or accumulation of (Ol, Cpx) Amp + Bt, later joined by Pl. Magma mixing with, or without, exchange of xenocrysts between compositionally dissimilar melt batches was also important. Over time, partial melting of older, lower crustal metabasic rocks became increasingly significant, again with a strong subduction signature. The lack of zircon inheritance in the magmatic products and rather high zircon ε_{Hf}^{t} values (all >+3, but for most samples > +8) as well as whole-rock Sr–Nd isotopic compositions imply that the arc was not founded on mature continental crust. It was probably located at the margin of the Baydrag microcontinent, dominated by accreted metabasic rocks of an older (early Tonian?) island arc covered by a thin layer of subordinate metasediments containing detrital zircons with Tonian and ill-defined Palaeoproterozoic ages. The KMC represents a small vestige of an extensive Cambrian–Ordovician subduction system (termed here the Ikh-Mongol Arc System), bordering the western margin of a chain of Precambrian microcontinents (Tuva-Mongolia, Zabkhan and Baydrag) that, together with accreted Neoproterozoic marginal basins (the Lake Zone), defines the external part of the Mongolian orocline.

1. Introduction

The timescales and key mechanism(s) driving crustal growth are of fundamental geotectonic importance and thus justly a subject of heated debate in the current literature. The inferred composition of the average continental crust – in particular its intermediate silica contents, calc-alkaline chemistry and characteristic strong enrichment of Large Ion Lithophile Elements (LILE) relative to the High Field Strength Elements (HFSE) – resembles that of many Phanerozoic magmatic arcs (e.g., Rudnick and Gao, 2003; Taylor and McLennan, 2009; Weaver and Tarney, 1984). This is taken as evidence that at least post-Archaean continental crustal growth occurred mainly in such arcs (e.g., Jagoutz and Schmidt, 2012; Kelemen, 1995), an idea that is still a matter of discussion, though (Condie and Kröner, 2013).

The average crust is relatively siliceous (andesitic ± dacitic: see Taylor and McLennan, 2009 for review) and poor in ferromagnesian

* Corresponding author.
E-mail address: vojtech.janousek@geology.cz (V. Janoušek).
[1] Deceased.

https://doi.org/10.1016/j.gr.2017.10.003
1342-937X/

components (Rudnick and Gao, 2003; Taylor, 1967; Taylor and McLennan, 1995). However, the net juvenile input into arcs, as a product of partial melting of mantle peridotite, would be characterized by low SiO_2, high FeOt + MgO, and Mg#, i.e. significantly different from bulk continental crust estimates. This so-called 'continental crust paradox' has attracted explanations that can be subdivided into two broad groups (Castro et al., 2013; Jagoutz and Kelemen, 2015; Tatsumi, 2005).

The first group of models invokes rather silicic, high-Mg andesitic parental magmas (Taylor, 1967). These can be generated by slab melting (Rapp et al., 2010; Yogodzinski et al., 2001), by partial melting of previously depleted, but subsequently metasomatised, hydrous mantle peridotite (Grove et al., 2012), or by reaction between ascending melts and mantle peridotite (Kelemen, 1995). From mantle domains contaminated by subducted oceanic crust the material can be transported into the melting region by mixed mantle wedge diapirs (Castro and Gerya, 2008; Castro et al., 2013).

The second possibility is that some additional open-system process comes into play, transforming the primary basaltic magma into andesitic/dacitic continental crust:

(1) Hybridization between a mafic melt and crustally-derived felsic magma, including the early metabasic products of arc activity melted by subsequent basaltic injections (Annen et al., 2006; Atherton and Petford, 1993; Huppert and Sparks, 1988). Arcs often provide ample evidence for the operation of magma mixing/mingling in the form of variously hybrid mafic enclaves or larger igneous units, whole-rock geochemical and isotopic variation as well as microtextural record for chemical and thermal disequilibria and exchange of xenocrysts (Didier and Barbarin, 1991a; Bateman, 1995; Hibbard, 1995; Janoušek et al., 2004; Wiebe, 1996).
(2) Extensive fractionation of basaltic magma or partial melting of metabasic lower crust produces hydrous melts which have low viscosity and thus ascend to shallower crustal levels (e.g., Annen et al., 2006; Lee and Bachmann, 2014). These two processes are inevitably connected with formation of dense mafic cumulates or basic granulitic residua dominated by hornblende, clinopyroxene ± garnet. The mass balance requires subsequent foundering of the lowermost, garnet-bearing crust into the asthenospheric mantle (Arndt and Goldstein, 1989; Jagoutz and Behn, 2013; Kay and Kay, 1993; Lee and Anderson, 2015; Zandt et al., 2004).
(3) Relamination of deeply recycled felsic crustal material at the bottom of the arc crust (Castro et al., 2013; Hacker et al., 2011, 2015; Kelemen and Behn, 2016; Schulmann et al., 2014). Such recycling may include subduction of sediments deposited on the oceanic slab, arc/forearc subduction, subduction erosion of the overriding plate and deep underplating of felsic continental crust during continent–continent collision (Carswell and Compagnoni, 2003; Dobrzhinetskaya et al., 2011; Chopin, 1984; Hacker et al., 2011). However, the significance, applicability and details of the crustal relamination model still largely remain to be investigated (Dymkova et al., 2016; Guy et al., 2015; Kusbach et al., 2015; Maierová et al., 2016).

The gigantic (*c.* 9 mil. km^2) Central Asian Orogenic Belt (CAOB) represents the product of unprecedented late Mesoproterozoic–Phanerozoic continental growth, the exact mechanism of which is still poorly understood (e.g., Kröner et al., 2014; Xiao and Santosh, 2014). In any case, Neoproterozoic to Carboniferous magmatic arcs form an essential component of the CAOB (Şengör and Natal'in, 1996) and have been variably interpreted as Andean-type or purely intra-oceanic (Kröner et al., 2014; Xiao et al., 2015). These giant magmatic units are of great interest as they can be used to characterize the plate configuration, polarity and spatio-temporal evolution of migrating Palaeo-Asian subduction zones (Şengör et al., 1993; Wilhem et al., 2012; Windley et al., 2007).

This paper deals with Cambrian magmatic arc rocks located in the Lake Zone of Mongolia (Fig. 1a), a region critical for the Neoproterozoic to early Palaeozoic evolution of the CAOB. We describe a more or less continuous section from deep crustal ultramafic cumulates to shallower arc levels, built by quartz diorites to tonalites in the eastern Khantaishir Range (south–central Mongolia, Fig. 1b). Moreover, we present petrological, whole-rock geochemical and Sr–Nd isotopic data, as well as *in-situ* zircon U–Pb and Hf isotopic data. These datasets are integrated to provide an insight into the nature, likely petrogenesis and geotectonic setting of the arc magmas.

The Khantaishir Magmatic Complex (KMC) provides an excellent opportunity to study the important Cambrian period of arc-related magmatism and crustal growth in the Mongolian CAOB as well as the anatomy and internal workings of immature continental magmatic arcs in general. We demonstrate that the Khantaishir Magmatic Complex forms a part of the largest arc system in the Mongolian and Russian tracts of the CAOB, termed here the Ikh-Mongol Arc System. Its character varies from Andean-type to purely intra-oceanic along the strike of the Tuva–Mongolian continental ribbon (Yakubchuk, 2004) (Fig. 1a).

2. Geological setting

2.1. Central Asian Orogenic Belt (CAOB)

The CAOB (Mossakovsky et al., 1994; Yanshin, 1965) developed between the Siberian, Tarim and Sino–Korean blocks in latest Mesoproterozoic to early Triassic times (Fig. 1a) (e.g., Dergunov, 2001; Şengör et al., 1993; Xiao et al., 2009a). The Mongolian tract of the CAOB formed by accretion of Neoproterozoic, Cambrian, Ordovician and Devonian–Carboniferous arcs, back-arcs and accretionary wedges (Badarch et al., 2002; Kröner et al., 2007; Lamb and Badarch, 2001; Windley et al., 2007) to Archaean to early Tonian microcontinents (Tuva-Mongolian, Zabkhan, and Baydrag) (Bold et al., 2016; Buriánek et al., 2017; Demoux et al., 2009a; Kozakov et al., 2007; Kuzmichev et al., 2001; Rojas-Agramonte et al., 2011). This so-called Mongolian collage (Xiao et al., 2015) is thought to having been shaped by three major accretionary events: the late Proterozoic and early Palaeozoic, forming a tectonic province in the north, and the Late Devonian to early Carboniferous, during which vast oceanic domains evolved in the south (Xiao et al., 2004; Zonenshain, 1973; Zonenshain et al., 1976).

In detail, the Mongolian collage consists of several Precambrian continental fragments of both Siberian (Barguzin; Gladkochub et al., 2008) and Gondwanan (Tuva Mongol, Zavkhan, Baydrag and Erguna, Parfenov et al., 2003) provenance that have been amalgamated to the north-eastern margin of Siberian Continent during Baikalian orogenic cycle at 560–540 Ma (Dobretsov et al., 2003). The intervening oceanic domains were accreted to both Siberian margin and to Precambrian fragments in form of several ophiolite sheets and accretionary oceanic arc complexes forming the Lake Zone (Khain et al., 2003; Kovach et al., 2011). Altogether, thus freshly formed Mongolian collage was affected by ca. 500 Ma magmatic and HT/LP metamorphic event during the second, late Cambrian–early Ordovician cycle (Dobretsov et al., 2003; Kozakov et al., 2015). The Devono–Carboniferous orogenic cycle represented a specific accretionary convergent event that was responsible for shortening of external oceanic units (Lehmann et al., 2010). It is only later (in Carboniferous to Permian times) when the whole system was rotated clockwise to the current position, together with opening of the Mongol-Okhotsk Ocean (Domeier and Torsvik, 2014) and formation of Mongolian ribbon continent orthogonal to the Siberian margin (Zorin, 1999). Finally, in Permian to Jurassic the whole Mongolian ribbon system was compressed in between jaws of Siberian and North China cratons in course of the Mongol-Okhotsk oceanic basin closure (Lehmann et al., 2010).

The early Cambrian accretion in the CAOB could be interpreted as a consequence of thrusting of oceanic fragments of Neoproterozoic age over the southern margin of the Siberian Craton (Khain et al., 2003) or accretion of Neoproterozoic ophiolitic sequences onto the peri-Siberian

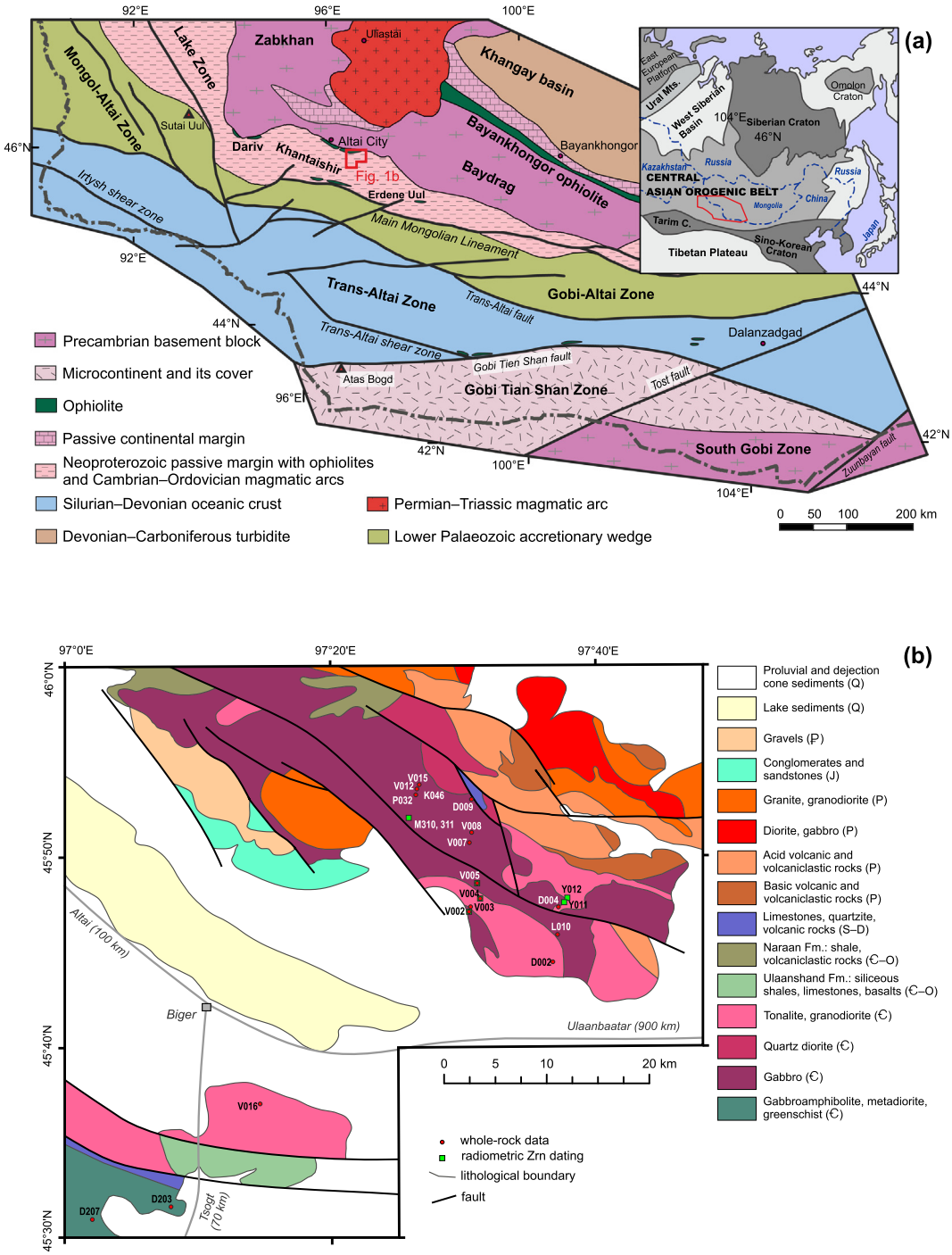

Fig. 1. (a) – Simplified map of the major tectonic zones of SW Mongolia with location of the study area. Inset shows location of the CAOB in the frame of adjacent tectonic elements. Modified from Kröner et al. (2010) and Buriánek et al. (2017). (b) – Geological sketch map of the Khantaishir Magmatic Complex based on Czech Geological Survey field work with sample locations shown.

Tuva–Mongolian continental ribbon (Domeier and Torsvik, 2014; Štípská et al., 2010). In any case, this event hallmarked the onset of convergence between the "Palaeo-Asian" oceanic plate and the Siberian Continent after break-up of the Rodinia supercontinent (Domeier and Torsvik, 2014; Wilhem et al., 2012). A relatively well preserved early Palaeozoic suture is represented by isolated occurrences of ophiolitic sequences in central Kazakhstan (Khain et al., 2003), the Gorny Altai of Russia (Buslov and De Grave, 2015; Volkova and Sklyarov, 2007; Wilhem et al., 2012), and in the Lake Zone of northwestern and south-central Mongolia (Jian et al., 2014 and references therein).

2.2. Lake Zone

The Lake Zone is a narrow, continuous belt decorating the western and southern rims of the Zabkhan and Baydrag microcontinents; its southern boundary with the late Palaeozoic units of the Gobi Altai and Mongolian Altai ranges is known as the Main Mongolian Lineament (Badarch et al., 2002; Marinov et al., 1973). The Lake Zone was interpreted by Badarch et al. (2002) as a Neoproterozoic accretionary wedge (Kovach et al., 2011 Windley et al., 2007) composed of volcanic, volcano-sedimentary and sedimentary sequences with

imbricated ophiolitic remnants (Buchan et al., 2002; Dijkstra et al., 2006; Jian et al., 2014; Zonenshain and Kuzmin, 1978).

The Dariv ophiolite has been dated as late Neoproterozoic using the U–Pb and Pb–Pb methods on zircon: 571 ± 4 Ma (Khain et al., 2003), 573 ± 6 Ma (Kozakov et al., 2002) and 515 ± 8 Ma (Dijkstra et al., 2006). Recent SHRIMP dating of zircon yielded $^{206}Pb/^{238}U$ ages of 568 ± 5 Ma, 567 ± 4 Ma, 560 ± 8 Ma (Jian et al., 2014). Likewise, the plagiogranites from the Khantaishir ophiolite gave U–Pb and Pb–Pb zircon ages of 568 ± 4 Ma (Khain et al., 2003), 573 ± 8 Ma and 566 ± 7 Ma (SHRIMP $^{206}Pb/^{238}U$ ages of Jian et al., 2014).

During the early Cambrian, the ophiolites were thrust over the continental basement in the hanging wall of eclogitic units (Štípská et al., 2010), described from the Zamtyn Nuruu (Buriánek et al., 2017) and the Dariv (Dijkstra et al., 2006) mountain ranges. These high-pressure units are interpreted as remnants of subduction channels which sampled a sedimentary matrix scraped off the Ediacaran to early Cambrian cover of the Baydrag and Zabkhan continental blocks (Buriánek et al., 2017). The related phengite-bearing foliation in eclogite and high-pressure fabrics in the associated metapelites yielded $^{40}Ar/^{39}Ar$ cooling ages of *c.* 540 Ma (Štípská et al., 2010), timing the overthrusting. In any case, thrusting took place before intrusion of a syn- to post-tectonic diorite in the Dariv ophiolite, dated at 514.7 ± 7.6 Ma (U–Pb SHRIMP on zircon, Dijkstra et al., 2006).

Deformed but unmetamorphosed upper Cambrian to Ordovician siliciclastic sequences rest upon the metamorphic rocks and ophiolites in the Erdene Uul–Zamtyn Nuruu area (Hrdličková et al., 2010; Kröner et al., 2010).

The Lake Zone is characterized by an abundance of mostly Cambrian mafic to intermediate plutons which can be traced from the Zamtyn Nuruu Range (Buriánek et al., 2017) towards the NW to the Khantaishir (Matsumoto and Tomurtogoo, 2003 and the current paper) and the Dariv ranges (Dijkstra et al., 2006), where they were described as ophiolite-related (Jian et al., 2014). Exposures of Cambrian to Ordovician plutons in the northwestern continuation of the Lake Zone were reported, among others, by Rudnev et al. (2009, 2013b), Yarmolyuk et al. (2011) and Soejono et al. (2016). However, Cambrian arc-related magmatic complexes are also known from the underlying continental blocks (e.g., Sal'nikova et al., 2001).

3. Materials and methods

Please note that this is just an abbreviated version focusing mostly on data interpretation; full analytical details are given in the Electronic Appendix 1.

3.1. Sampling, petrology and mineral chemistry

The studied magmatic complex was described in the eastern Khantaishir Mountain Range (NE of Biger, southern–central Mongolia, Fig. 1b) during the Czech Geological Survey (CGS) expedition in 2012. Twenty-four samples of the major igneous rock types selected for petrological study are listed in Electronic Appendix 2, and their locations are shown in Fig. 1b.

Electron-microprobe analyses (EMPA) were performed using the Cameca SX-100 instrument at Masaryk University (Brno, Czech Republic). The empirical formulae of feldspars and micas were recalculated to 8 and 22 oxygen atoms, respectively. The amphibole formulae were obtained on the basis of 23 oxygen atoms (Leake et al., 1997). The Fe^{2+}/Fe^{3+} ratios in amphiboles were estimated assuming the cation sum of 13 without Ca, Na and K (13 eCNK). Pyroxenes are classified according to Morimoto (1988); the formulae were obtained on the basis of 4 cations and the ferric iron estimated after Droop (1987). The abbreviations of the mineral names are taken from Whitney and Evans (2010).

3.2. Whole-rock geochemistry

In total, 19 whole-rock samples, each 5–10 kg in weight, were obtained in the field (see Fig. 1b for locations). After conventional crushing and homogenization, the powders produced in an agate mill were analyzed at ActLabs (Vancouver, Canada), using the 4Lithoresearch procedure (http://www.actlabs.com). Major-element concentrations were obtained by Inductively-Coupled Plasma Optical Emission Spectrometry (ICP-OES) and trace-element concentrations by Inductively-Coupled Plasma Mass Spectrometry (ICP-MS), following lithium metaborate/tetraborate fusion and weak nitric acid dissolution. Such a procedure ensures that the entire sample is digested, including refractory phases such as zircon and sphene.

Recalculation and plotting were facilitated using the R software package *GCDkit* (Janoušek et al., 2006). In this work, the Mg number (Mg#) is defined as $100\,\frac{MgO}{FeOt+MgO}$ [mol%] and the A/CNK index (Shand, 1943) as $\frac{Al_2O_3}{CaO+Na_2O+K_2O}$ [mol%]. For description of chondrite-normalized REE patterns serves the Eu/Eu* ratio, reflecting the magnitude of the Eu anomaly ($\frac{Eu}{Eu^*} = {}^{Eu_N}/_{\sqrt{Sm_N Gd_N}}$), where N refers to concentrations normalized to chondritic abundances (Boynton, 1984). Moreover, their curvature is expressed using the Dy/Dy* parameter (Davidson et al., 2013) defined as $\frac{Dy}{Dy^*} = \frac{Dy_N}{La_N^{4/13} Yb_N^{9/13}}$. The magnitude of the Ti anomaly on the NMORB-normalized plots is quantified by the Ti/Ti* ratio. Note that while the overall philosophy of the Ti/Ti* parameter calculation follows Davidson et al. (2013), our calculation formula is different: $\frac{Ti}{Ti^*} = \frac{Ti_N}{Gd_N^{4/5} Sm_N^{1/5}}$, where N refers to values normalized to average NMORB of Sun and McDonough (1989).

3.3. Whole-rock Sr–Nd isotopic compositions

Isotopic analyses of Sr and Nd were performed on a Finnigan MAT 262 thermal ionization mass spectrometer housed at CGS. The decay constants applied to age-correct the isotopic ratios are from Steiger and Jäger (1977 – Sr) and Lugmair and Marti (1978 – Nd). The ε_{Nd} values were obtained using Bulk Earth parameters of Jacobsen and Wasserburg (1980). In order to compensate for the effects of crystal accumulation upon the $^{147}Sm/^{144}Nd$ ratios, we calculated not only single-stage ($T^{Nd}_{DM.1stg}$) but also two-stage Depleted Mantle Nd model ages ($T^{Nd}_{DM.2stg}$), using the Depleted Mantle parameters and the general approach of Liew and Hofmann (1988). However, the $^{147}Sm/^{144}Nd$ ratio of the intermediate average reservoir has been set to 0.138 in order to better reflect the basic sources involved.

3.4. U–Pb geochronology

Except for samples M310 and M311, zircon dating used an ArF excimer 193 nm laser ablation system (Resolution M-50), coupled with a Nu Plasma HR MC-ICP-MS at the Department of Earth Sciences, University of Hong Kong, following the analytical procedure of Xia et al. (2011). The age calculations and concordia plots were performed using ISOPLOT (version 3.0, Ludwig, 2003). Individual analyses are presented with 1σ error in the concordia diagrams, and uncertainties in mean age calculations are quoted at the 95% level (2σ).

For measurement of U/Pb and Pb/Pb isotopic ratios in zircons from samples M310 and M311, a Thermo-Finnigan Element 2 sector field ICP-MS, coupled to a 193 ArF Excimer laser (Resonetics RESOlution M50-LR) at Bergen University, Norway was used following the technique described by Košler et al. (2002). Details of raw data reduction and corrections are described in Košler et al. (2002) and Košler and Sylvester (2003). The calculations and plotting on concordia diagrams were done using Isoplot 4.15 (Ludwig, 2012).

3.5. Zircon Lu–Hf isotope analyses

In-situ zircon Lu–Hf isotopic analyses were carried out on a Neptune Plus multi-collector ICP-MS equipped with a Resolution M-50-LR laser-ablation system at the Guangzhou Institute of Geochemistry, Chinese Academy of Sciences. Detailed instrumental settings and analytical procedures were described by Zhang et al. (2015).

All Hf-in-zircon isotopic data were calculated with the decay constant of 1.867×10^{-11} yr^{-1} (Söderlund et al., 2004). The chondritic values of $^{176}Hf/^{177}Hf = 0.282772$ and $^{176}Lu/^{177}Hf = 0.0332$ reported by Blichert-Toft and Albaréde (1997) were employed for the calculation of ε_{Hf}^{f} values. The depleted-mantle evolution line is defined by present-day $^{176}Hf/^{177}Hf$ of 0.28325 and $^{176}Lu/^{177}Hf$ of 0.0384 (Griffin et al., 2000). A "crustal" Hf model age (T_{DM}^{HfC}) is considered to be more meaningful for the studied rocks than a depleted mantle model age. This model age (T_{DM}^{HfC}) was calculated separately for each zircon grain, assuming a mean basaltic $^{176}Lu/^{177}Hf$ ratio of 0.022 for the 2nd stage of the model (Lancaster et al., 2011). In the calculation, $^{206}Pb/^{238}U$ ages were

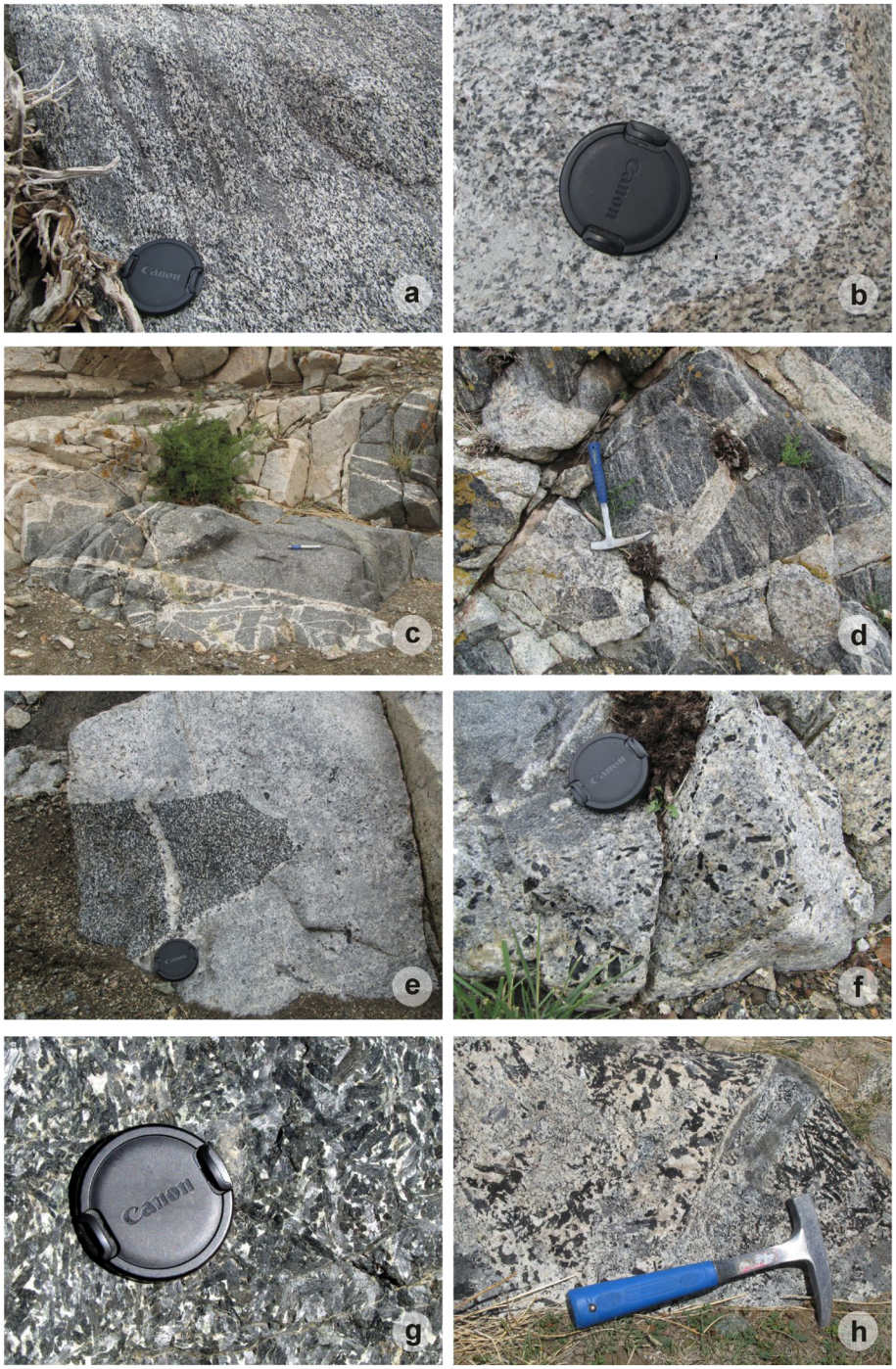

Fig. 2. (a) – Amp–Bt tonalite showing strong fabric and intensely deformed MME (site V008); (b) – Coarse-grained Amp leucodiorite (sample V004); (c) – Angular fragments of coarse-grained Amp quartz diorite to gabbro, net veined by felsic magma also Amp-bearing; the top-left part of the photo occupies a younger felsic dyke with a stepped contact (site V009); (d) – Angular xenoliths of cumulate quartz gabbros (sample V008a) showing distinct layering broken by, and enclosed in, fresh leucocratic intrusion, the latter also Amp-bearing; (e) – Large angular xenolith of coarse-grained Amp gabbro enclosed by Amp–Bt tonalite (site V008); (f) – Resorbed amphibole xeno/antecrysts in later intrusion of leucocratic Amp–Bt tonalite (sample V008c); (g) – Coarse-grained amphibole-dominated cumulate (site V012); (h) – Pegmatoid facies with unidirectional solidification structure, indicating strong undercooling (site V012).

used for analyses younger than 1.0 Ga, and $^{207}Pb/^{206}Pb$ ages for older grains.

4. Results

4.1. Structural setting and field relations

The Khantaishir Magmatic Complex (Fig. 1b) is exposed along both sides of the Cenozoic Biger Basin, in the central part of the Neoproterozoic accretionary wedge of the Lake Zone. It is underthrusted southwards beneath the Palaeozoic volcano-sedimentary prism of the Gobi Altai Zone (Lehmann et al., 2010). All magmatic rocks show variably developed NNE–SSW trending, sub-vertical magmatic fabric defined by mafic minerals. The deepest gabbroic cumulates exhibit a weak shape-preferred orientation of amphiboles which is parallel to a locally strong mineral foliation developed in tonalites higher up in the section (Fig. 2a).

The KMC is mainly composed of several types of gabbro/hornblendite and, higher up in the sequence, quartz diorite and tonalite. Mingling textures are commonly observed between mafic and more felsic lithologies. Hybrid mafic microgranular enclaves (MME; Didier and Barbarin, 1991b) of variable shapes and sizes are locally abundant (Fig. 2a), whereas elsewhere the felsic rocks are pristine and homogeneous (Fig. 2b). The MME often cluster into monogenic enclave swarms (Didier and Barbarin, 1991b); rarely, load-cast structures were observed at the bottom of mafic layers along mafic/felsic interfaces (Wiebe and Collins, 1998; Žák et al., 2009). Some MME exhibit lobate contacts and/or chilled margins against their host; others contain xenocrysts derived from the surrounding granitoid such as mantled plagioclases and rapakivi K-feldspars (Hibbard, 1991, 1995).

The mafic rocks, hornblendites and hornblende gabbros, often display cumulate textures and conspicuous magmatic layering, pointing to a predominant amphibole accumulation. Numerous syn-magmatic shear zones and mafic or felsic veins cut the layering (Fig. 2c–d). Late dykes (up to *c.* 1 m wide) of aplite and pegmatite are dominated by plagioclase, with <10 vol% of hornblende (Fig. 2c).

In places, the already solidified hornblendite/gabbro of the layered mafic complex was broken into angular fragments and net veined by the invading felsic magma (Fig. 2c–d). Some mafic blocks were arrested in the process of fragmentation, and the contacts are accentuated by felsic rims (Fig. 2e). The felsic rocks contain variable amounts of relatively large, prismatic hornblende crystals that have been resorbed in the host magma (Fig. 2f) and thus seem to be xenocrystic in origin. The texture of the mafic rocks varies from microgabbro to coarse-grained gabbro (columnar amphibole crystals up to a few centimetres long) in the more homogeneous, isolated mafic bodies (Fig. 2g).

In one of the valleys cutting the KMC N of Biger, spectacular comb layering (Moore and Lockwood, 1973) was observed. This Unidirectional Solidification Texture (UST) is defined by large feather-like amphibole crystals growing perpendicular to the margins of late, otherwise fine-grained (quenched) sheets that cut the Amp-rich gabbro–hornblendite; plagioclase forms large grains but is only interstitial (Fig. 2h).

4.2. Petrology and mineral chemistry

Representative electron-microprobe analyses of amphibole, plagioclase, olivine, pyroxenes and biotite are given in Electronic Appendix 3a–c.

Amphibole–biotite tonalites are commonly medium-grained, grey to reddish rocks. They are composed of plagioclase, quartz, biotite, amphibole, clinopyroxene and minor K-feldspar (Fig. 3a). Typical accessories are monazite, apatite, zircon, titanite and magnetite.

Subhedral to euhedral plagioclase (52–59 vol%) from tonalite V005 is usually oscillatory-zoned andesine (An_{36-42}); however plagioclase in tonalite D002 is unzoned oligoclase (An_{21-22}). The content of anhedral K-feldspar (Ab_{4-8} Or_{92-96}) varies from 2 to 4 vol%. Biotite (7–12 vol%) occurs as aggregates up to 3 mm or as single flakes up to 1 mm across and exhibits a fairly wide range of chemical composition (Fe/(Fe + Mg) = 0.39–0.49; ^{IV}Al = 2.29–2.43 apfu). These chemical characteristics are typical of biotite in I-type calc-alkaline granitoids from volcanic arcs (Abdel-Rahman, 1994). Subhedral amphibole (5–10 vol%) is classified as magnesiohornblende (Si = 6.69–7.24 apfu; Mg/(Fe + Mg) = 0.59–0.75; Fig. 4a). Anhedral diopside (Fe/(Fe + Mg) = 0.21–0.24) is pushed back by magnesiohornblende (Fig. 3a). Biotite slightly altered to pale green-brown chlorite occurs locally. Secondary white mica appears as inclusions in the central parts of plagioclase grains. A replacement of plagioclase by secondary interstitial K-feldspar is seen in the reddish tonalite (sample D002).

Biotite–amphibole to amphibole–clinopyroxene quartz diorites (Fig. 3b) are medium-grained, equigranular, grey rocks composed of plagioclase (55–61 vol%), amphibole (22–27 vol%), quartz (7–11 vol%), biotite and/or clinopyroxene (5–12 vol%). Texturally the quartz diorites resemble the tonalites. Locally they contain amphibole or clinopyroxene-rich layers, 5 to 10 cm thick (Fig. 3b). Typical accessories are monazite, apatite, zircon, titanite and magnetite. Slightly altered plagioclase and chloritized biotite are locally present.

The main rock types of the KMC are medium- to coarse-grained biotite–amphibole gabbro to hornblendite which locally pass into amphibole gabbro with olivine or pyroxene. These mafic to ultramafic rocks chiefly consist of amphibole and variable amounts of plagioclase (Fig. 3c–f). Subordinate biotite, clinopyroxene and/or olivine are also present. Magnetite, apatite, ilmenite, rutile, chalcopyrite and spinel are common accessory minerals.

Biotite–amphibole gabbros to hornblendites are usually massive or layered with a cumulate texture. Massive gabbro is dominantly hypautomorphic granular (Fig. 3c). Very common are several cm to dm thick layers with variable proportions of amphibole (36–94 vol%) and plagioclase (63–5 vol%). Felsic mesocumulate to adcumulate layers consist of euhedral to subhedral plagioclase crystals (Fig. 3d) with interstitial amphibole, whereas mafic adcumulates consist of columnar or polygonal amphibole crystals with small amounts of interstitial plagioclase (0–12 vol%) and/or biotite (0–5 vol%). The plagioclase crystals usually show normal zoning (An_{89-93}). The amphiboles (pargasite; Si = 6.21–6.35 apfu; Mg/(Fe + Mg) = 0.74–0.76; Fig. 4b) occur as subhedral crystals, either individually or in aggregates. Apatite, magnetite and ilmenite usually form inclusions in amphibole. Late feldspar-rich felsic veins cutting mafic cumulate (Y011) in places also break or wrap up the mafic cumulate layers.

Amphibole gabbros with olivine and/or pyroxene display hypautomorphic granular, poikilitic or orthocumulate textures. Columnar amphibole (pargasite; Si = 6.15–6.37 apfu; Mg/(Fe + Mg) = 0.67–0.86; Fig. 4b) is often preferentially oriented (Fig. 3e). The cores of plagioclase grains usually show normal zoning (An_{77-94}) but rarely are replaced by younger oligoclase (An_{24}). Diopside (Fe/(Fe + Mg) = 0.17) is only present in the amphibole gabbro as strongly resorbed relicts in centres of amphibole crystals (Fig. 3e). Olivine ($Fo_{74-76}Fa_{24-25}Tp_1$) is a rare early phase of the gabbros (V013). Olivine is completely surrounded by amphibole (Fig. 3f) and often rimed by small magnetite, spinel and/or enstatite grains, next to small relicts of plagioclase. Enstatite (Fe/(Fe + Mg) = 0.20–0.21) is present as up to 0.1 mm thick layers adjacent to olivine, locally in association with small anhedral grains of spinel (Sp_{58-59} Hc_{31-32}) and magnetite. Spinel and clinopyroxene do not form inclusions in olivine. Large magnetite grains are in direct contact with small anhedral grains of ilmenite, whereas fine trellis ilmenite lamellae sometimes occur in magnetite. Magnetite and chalcopyrite are also present as interstices of olivine and/or amphibole. Secondary Fe–Ti oxides occur as alteration products of ilmenite and magnetite. Symplectites of rutile and hematite after ilmenite are very common.

Olivine is often partially replaced by thin veins of a serpentinite group mineral and magnetite grains. Biotite and amphibole are partially altered to chlorite (rarely also K-feldspar, hematite and prehnite) and plagioclase to sericite and/or zoisite, albite and prehnite.

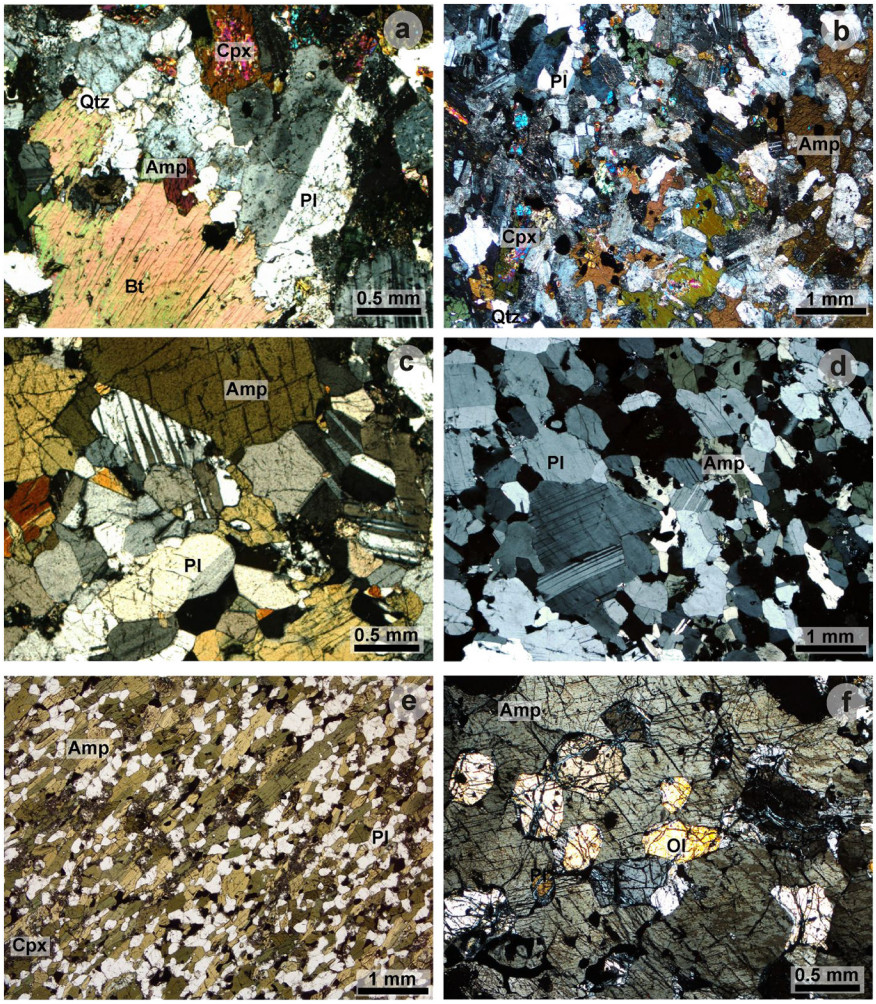

Fig. 3. Photomicrographs in cross-polarized light (XPL, except panel e) showing typical petrology and textures in rocks of the KMC: (a) – Incomplete replacement of clinopyroxene by amphibole in Amp-Bt tonalite with Cpx (D002); (b) – Contact between clinopyroxene and amphibole-rich layers in Cpx–Amp quartz diorite (D009b); (c) – Subhedral amphibole in Amp gabbro (D016); (d) – Plagioclase crystals with interstitial amphibole in Amp gabbro with a mesocumulate texture (D015); (e) – Magmatic foliation subparallel to layering in cumulate Cpx–Amp gabbro (P032); (f) – Olivine phenocrysts enclosed in amphibole of Amp–Ol gabbro (V013).

4.3. Thermobarometry

According to the thermobarometer of Ridolfi et al. (2010), amphiboles from gabbros to hornblendites were equilibrated at higher P–T conditions (0.35–0.51 GPa and 931–976 °C; Table 1) than those from tonalites (P = 0.11–0.20 GPa and 808–844 °C) (Fig. 4c). The amphibole–plagioclase barometry of Molina et al. (2015) provided slightly higher pressure estimates for gabbros to hornblendites (0.49–0.53 GPa; Table 1) and a wider range of generally similar pressures (0.08–0.13 GPa) for tonalite sample D002. For the tonalite sample V005, however, this calculation yielded unrealistically low results. Temperatures calculated using the Holland and Blundy (1994) edenite–richterite (model B) plagioclase–amphibole thermometer are comparable to the results of Ridolfi et al. (2010) formulation for the gabbros to hornblendites (914–1098 °C). Again, we obtained only 664–725 °C for the tonalites, probably due to subsolidus reequilibration during cooling (e. g., Cornejo and Mahood, 1997).

Disequilibrium texture between olivine and plagioclase (V013) explains the formation of spinel–enstatite–magnetite rims as a result of sub-solidus reactions (Claeson, 1998; Mongkoltip and Ashworth, 1983; Turner and Stüwe, 1992). Temperatures of formation of orthopyroxene and spinel in the olivine rims were estimated at 725 to 742 °C (Table 1), using the orthopyroxene geothermometer (Witt-Eickschen and Seck, 1991).

4.4. Oxygen fugacity and water contents in the magma

The Ridolfi et al. (2010) formulation also provides an estimate of oxygen fugacity during crystallization of amphibole. For gabbros to hornblendites, it varies from log fO_2 − 10.7 to 9.2 (±0.4 log units; equal to NNO +0.4 to +1.0) and for tonalites from log fO_2 −13.1 to −12.3 (±0.4 log units; equal to NNO +0.2 to +1.8). The water content in the magma was evaluated using the amphibole compositions (Ridolfi et al., 2010) and is higher for the ultrabasic to basic rocks (7.1–8.4 wt%) than for the tonalites (4.2–6.2 wt%) (Fig. 4d).

Additionally, temperatures and fO_2 were estimated using the ilmenite–magnetite geothermometer and oxygen geobarometer (Andersen et al., 1993) and range from 517 to 534 °C and −22.5 to −23.9, respectively. The observed ilmenite–magnetite intergrowths suggest a eutectic relationship. Low calculated temperatures probably reflect subsolidus reequilibration during cooling.

4.5. U–Pb zircon ages and in-situ Hf isotopes

4.5.1. Zircon internal structures

Zircons from three quartz diorite–tonalite samples (V002, V003 and V004) display mutually similar morphological and internal structures. They form clear, euhedral and long prismatic crystals, mainly ranging from 250 to 450 μm in length. These zircons commonly show clearly igneous-related oscillatory zoning without inherited cores in CL images

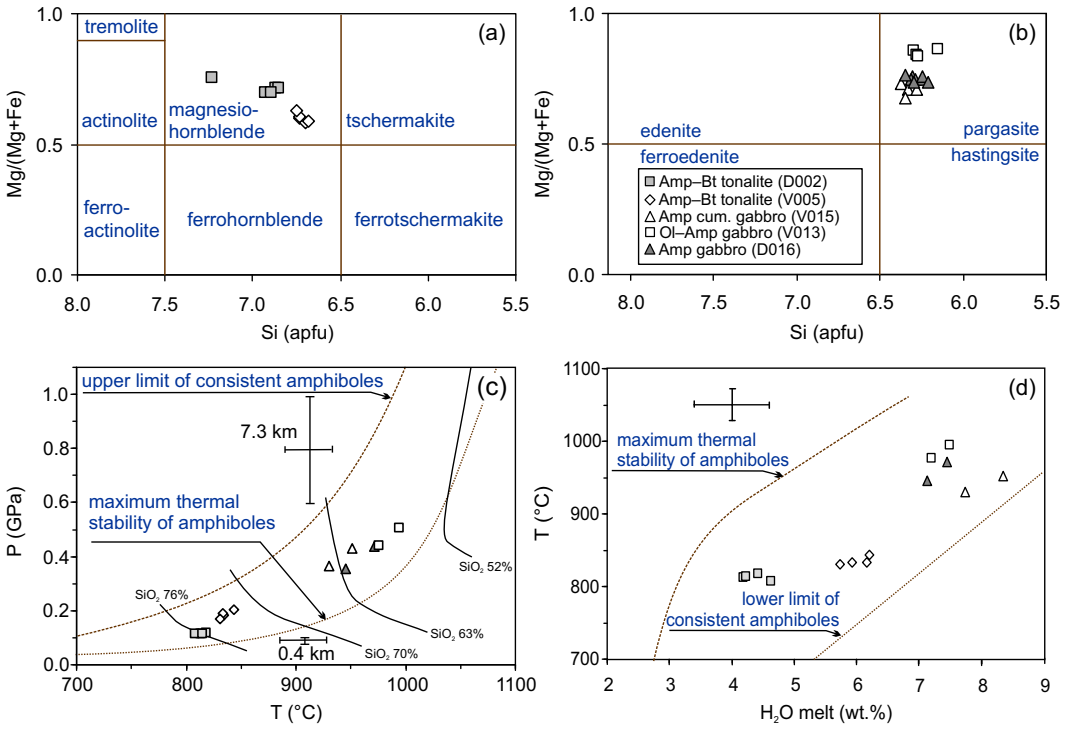

Fig. 4. (a–b) – Si vs. Mg/(Mg + Fe^{2+}) classification plot for calcic amphiboles (Leake et al., 1997); (c) – P–T diagram; isopleths show anhydrous SiO_2 (wt%) content of the melt and consistent amphiboles are defined according to Ridolfi et al. (2010); (d) – H_2O in melt diagram vs. T. Error bars represent the expected uncertainty in T (±22 °C), for H_2O in the melt (±1 wt%), and representative errors for P, indicating the variation in accuracy.

(Fig. 5a–c). Zircons from the tonalite V005 are dominated by euhedral and stubby prismatic crystals, ranging from 150 to 300 μm in length with a length/width ratio lower than 2:1. These grains also show concentric oscillatory zoning, suggesting an igneous origin (Fig. 5d).

Zircons from the gabbro Y011 are euhedral and short-prismatic. These grains vary between 150 and 300 μm in length and most clearly display igneous growth zoning in CL images (Fig. 5e). The majority of zircons from the leucogabbro M310 are long-prismatic with slightly rounded terminations, but short, stubby grains also occur. The CL images reveal broad, striped zonation (Fig. 6a) due to high-T crystallization typical of gabbroic rocks (Corfu et al., 2003). Some grains have very narrow high-luminescence (low-U) rims or embayments, indicating metamorphic overgrowth or partial recrystallization. The zircons of the quartz diorite dyke M311 are similar in morphology, but their terminations are mostly well

Table 1
Composition of amphiboles, estimated P–T conditions, oxygen fugacities and water contents for rocks from the KMC.

Rock	Gabbroic dyke	Hornblendite	Amp gabbro	Cpx–Amp tonalite	Bt–Amp tonalite
Sample	V015	V013	D016	D002	V005
Mineral assemblage	Amp, Pl, Mgt, Ap	Amp, Ol, Pl, Opx, Ilm, Mgt, Ap	Pl, Amp, Ilm, Rt, Mgt, Ap, Ccp	Pl, Bt, Amp, Qtz, Cpx, Kfs, Mgt, Ttn, Ap, Ccp	Pl, Qtz, Amp, Bt, Mgt, Ttn, Ap
Secondary minerals	Sericite, Zo		Hem		
Amphibole					
X_{Mg}	0.67 to 0.73	0.83 to 0.86	0.74 to 0.76	0.70 to 0.75	0.58 to 0.63
Si	6.28 to 6.37	6.15 to 6.30	6.21 to 6.35	6.85 to 7.24	6.69 to 6.75
Amp thermobarometry (Ridolfi et al., 2010)					
T (°C)	931 to 952	976 to 995	945 to 971	808 to 818	831 to 844
Uncertainty (σ_{est})	22	22	22	22	22
P (GPa)	0.36 to 0.43	0.44 to 0.51	0.35 to 0.43	0.11 to 0.12	0.17 to 0.20
Uncertainty (max error)	0.04	0.05	0.04	0.01	0.04 to 0.05
log fO_2	−10.7 to −10.5	−9.2 to −9.6	−10.3 to −10.2	−13.1 to −12.3	−12.8 to −12.7
Uncertainty (σ_{est})	0.4	0.4	0.4	0.4	0.4
H_2O melt (wt%)	7.7 to 8.4	7.2 to 7.5	7.1 to 7.5	4.2 to 4.6	5.7 to 6.2
Uncertainty (σ_{est})	1.2 to 1.3	1.1	1.1	0.4	0.4
Pl–Amp thermometry (Holland and Blundy, 1994); pressure according Amp barometry (Ridolfi et al., 2010)					
T (°C) ±32 °C	914 to 939	1030 to 1052	954 to 1098	664 to 699	683 to 725
Amp barometry (Molina et al., 2015); temperature according to Amp thermometry (Ridolfi et al., 2010)					
P (GPa)	0.49 to 0.50	0.50 to 0.53	0.52 to 0.53	0.08 to 0.13	–
Al in Opx geothermometer (Witt-Eickschen and Seck, 1991)					
T (°C)	–	725 to 742	–	–	–
Fe–Ti two-oxide geothermometer and oxygen barometer (Andersen et al., 1993)					
T (°C)	–	517 to 534	–	–	–
log fO_2	–	−22.5 to −23.9	–	–	–

rounded (Fig. 6b). Striped zonation is also abundant, and some grains show very homogeneous domains. As in sample M310, very narrow low-U rims occur on some grains.

Zircons from the migmatite Y012 (Fig. 7a) are dominated by euhedral and stubby to elongated prismatic crystals (100–200 μm long), some with variably corroded surfaces. In CL images, they can broadly be subdivided into two groups. One generally exhibits simple oscillatory zoning but commonly with dull luminescence in the narrow outermost part, whereas the other shows core–rim structures with corroded, angular or rounded cores surrounded by weakly zoned, low-luminescent rims (Fig. 7b–c).

4.5.2. Zircon U–Pb ages and Hf isotopic compositions

4.5.2.1. Quartz diorites–tonalites. **Bt–Amp tonalite V002c:** thirty-one analyses were made on oscillatory zoned zircons. Except for three discordant ones, the remaining twenty-eight points form a cluster with $^{206}Pb/^{238}U$ ages between 484 and 505 Ma. Their weighted mean age of 495 ± 3 Ma (Electronic Appendix 4; Fig. 5a) is interpreted as timing the magmatic crystallization.

Bt–Amp quartz diorite V003: twenty-eight zircons with oscillatory zoning were selected for U–Pb isotopic analyses. Nearly all the data are concordant (Fig. 5b), yielding $^{206}Pb/^{238}U$ ages between 477 and 512 Ma. Their weighted mean age of 494 ± 3 Ma is interpreted to reflect the crystallization of the quartz diorite.

Leucocratic Bt–Amp quartz diorite V004: a total of thirty-one zircon grains were analyzed, twenty-nine of which were concordant. These concordant analyses gave $^{206}Pb/^{238}U$ ages ranging from 502 Ma to 525 Ma, defining an age cluster with a weighted mean of 511 ± 2 Ma (Fig. 5c). This is considered to represent the crystallization age of the quartz diorite.

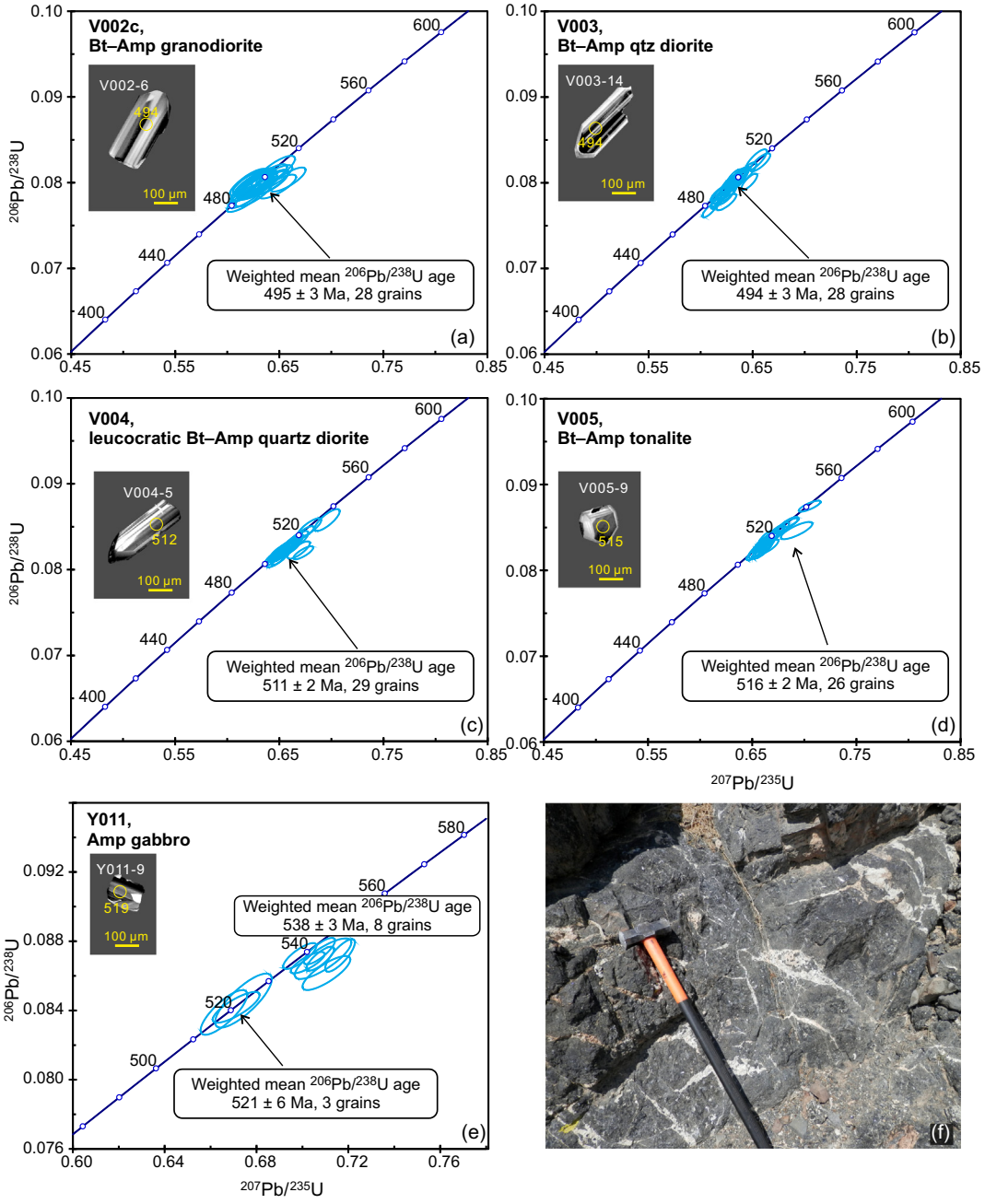

Fig. 5. (a–e) U–Pb concordia plots for studied zircons from igneous samples of the KMC (dated at the University of Hong Kong). Insets: characteristic CL images. (f) Field photograph of the outcrop situation of the sample Y011.

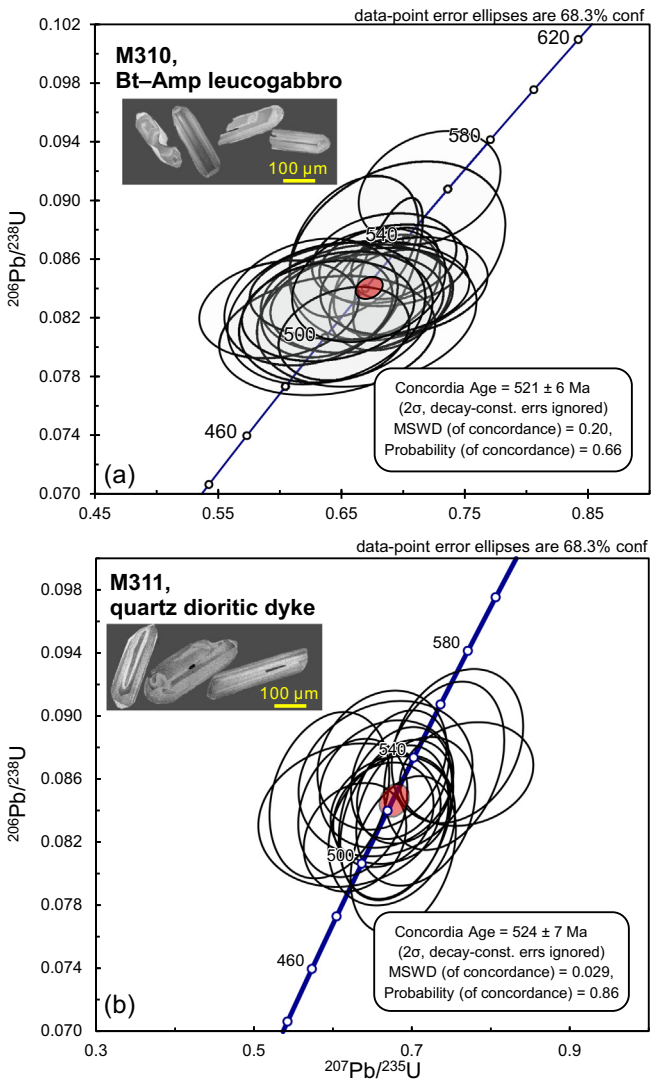

Fig. 6. U–Pb concordia plots for studied zircons from basic magmatic rocks of the KMC (dated at the University of Bergen).

Bt–Amp tonalite V005: zircons from this sample show well-defined magmatic oscillatory zoning; thirty of them were selected for U–Pb isotopic analyses. Twenty-eight analyses gave $^{206}Pb/^{238}U$ ages ranging from 508 Ma to 541 Ma, twenty-six of which define an age cluster with a weighted mean age of 516 ± 2 Ma (Fig. 5d). We interpret this age to reflect the crystallization of the tonalite.

Although zircons from these four samples yielded consistent ages, they show large variations in their initial $^{176}Hf/^{177}Hf$ ratios. In general, Hf isotopic compositions from the tonalite (V002c) and two quartz diorites (V003 and V004) exhibit similar Hf isotopic characteristics, with strongly positive initial ε^{t}_{Hf} values (+8.4 to +14.3) and young T^{HfC}_{DM} model ages (0.59–1.12 Ga) (Electronic Appendix 5; Fig. 8a–c; Fig. 9). This may imply derivation through (near) closed-system fractionation from little modified, depleted-mantle derived magmas. In contrast, zircons in the Bt–Amp tonalite V005 yield less radiogenic Hf isotopic characteristics (ε^{t}_{Hf} = +2.5 to +6.2; T^{HfC}_{DM} = 1.34–1.67 Ga, Fig. 8d; Fig. 9). This may indicate an origin from a distinct, less depleted or perhaps slightly metasomatised mantle domain or, more likely, by remelting of pre-existing, but still rather juvenile, metabasic crust.

4.5.2.2. Gabbro. Net-veined gabbro Y011 yielded two zircon populations, 521 ± 6 Ma and 538 ± 3 Ma, although these show similar features in CL images (Fig. 5e). The *in-situ* Hf initial isotopic ratios vary widely (ε^{t}_{Hf} =

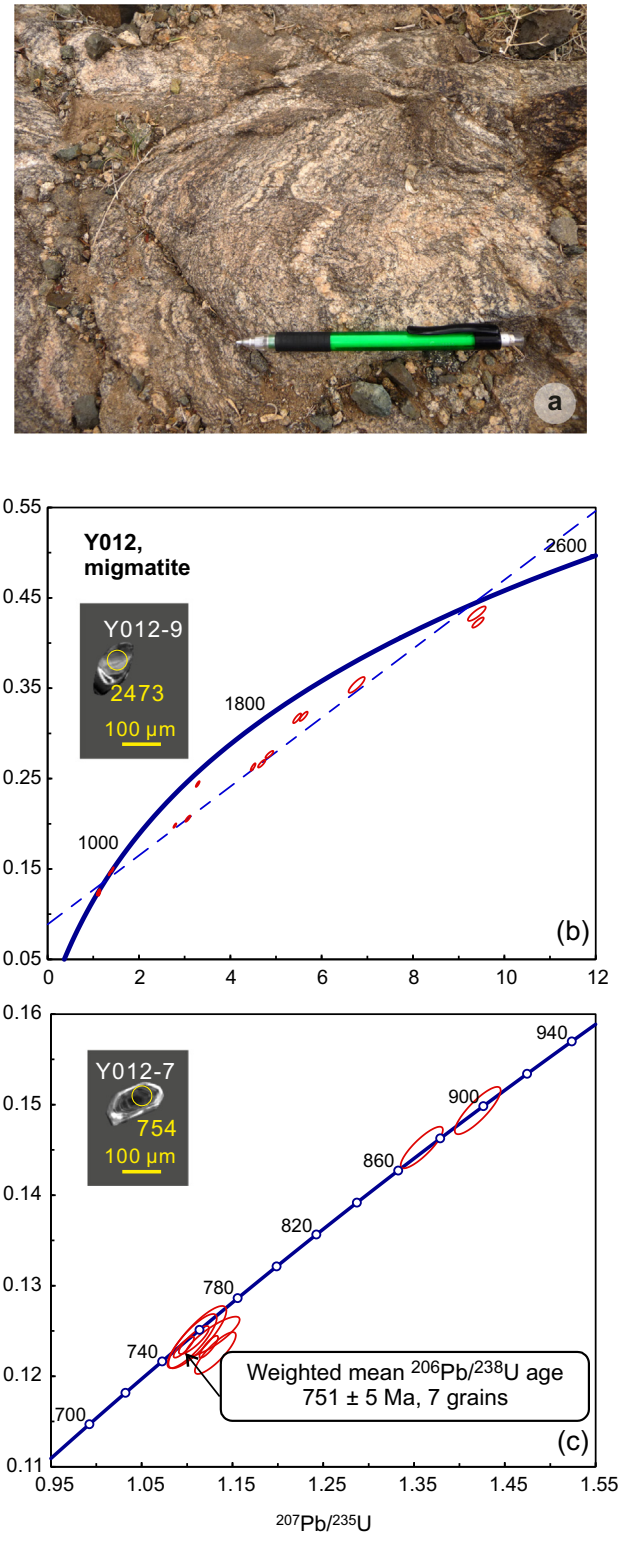

Fig. 7. Zircon age data for migmatite from roof of the KMC (sample Y012). (a) Field appearance of the migmatite. (b) U–Pb concordia plot, including detail at around the presumed migmatitization age (~750 Ma) (d) (dated at the University of Hong Kong).

+4.3 to +13.3; Fig. 8e). The zircons contain both, the more and less radiogenic, Hf components distinguished in the more siliceous samples (Fig. 9a). However, there seems to be no simple relation between the ages of individual zircon grains and their Hf isotopic compositions (Fig. 9a). The T^{HfC}_{DM} crustal model ages in the gabbro Y011 again vary widely between 0.70 and 1.52 Ga, almost covering the range of all the more siliceous samples studied (Fig. 9b).

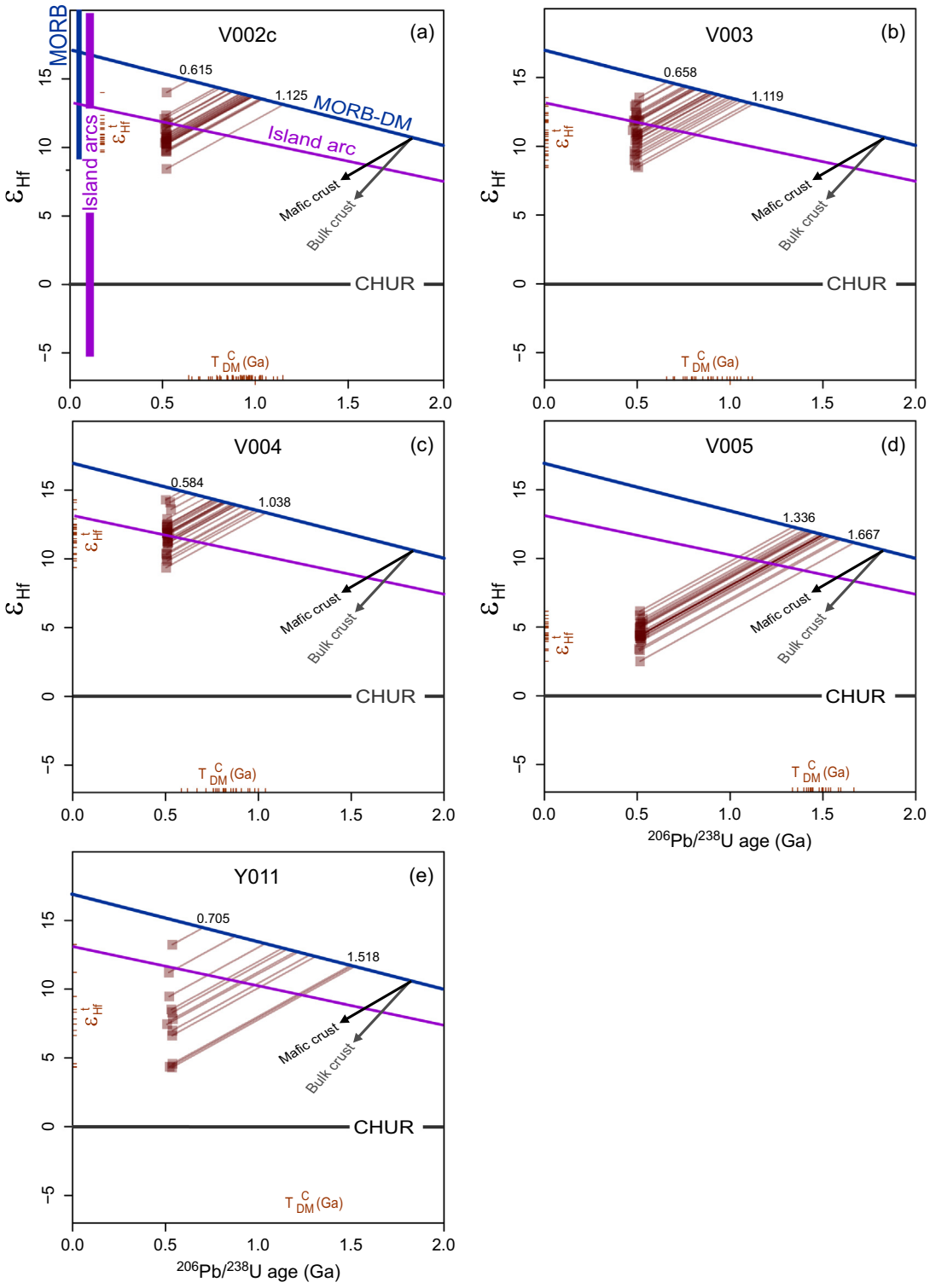

Fig. 8. Two-stage Hf evolution diagram for dated zircons from samples V003, V004, V005 and Y011 (a–d). The Depleted Mantle line is after Griffin et al. (2000) and Belousova et al. (2010), the composition of CHUR from Blichert-Toft and Albaréde (1997). The evolution line for the average mantle source to modern island-arc magmas, as well as intervals ε^{t}_{Hf} of modern Mid-Ocean Ridge Basalt (MORB) and Island-Arc Basalts are from Kemp and Hawkesworth (2014 and references therein).

Twenty-eight analyses of zircons from leucogabbro sample M310 produced well-grouped results with a concordia age of 521 ± 6 Ma (Fig. 6a) that we interpret to reflect the time of gabbro crystallization. Similarly, 19 analyses of zircons from quartz diorite vein M311 also yielded a tight cluster of error ellipses with a concordia age of 524 ± 7 Ma (Fig. 6b), identical, within error, to the gabbro data. These ages may imply that the two rocks were coeval, and thus perhaps also cogenetic.

4.5.2.3. Migmatite. The U–Pb analyses of the oscillatory-zoned zircon grains of migmatite sample Y012 (Fig. 7b–c) yielded ages clustering around 750 Ma (751 ± 5 Ma, n = 7; Electronic Appendix 4). The narrow dull outermost rims were too thin to be analyzed. Given the lack of younger ages, the near-euhedral shape, oscillatory zoning and high Th/U ratios (0.65–2.21) of these zircons, they can be theoretically interpreted as igneous, resulting from crustal melting during the

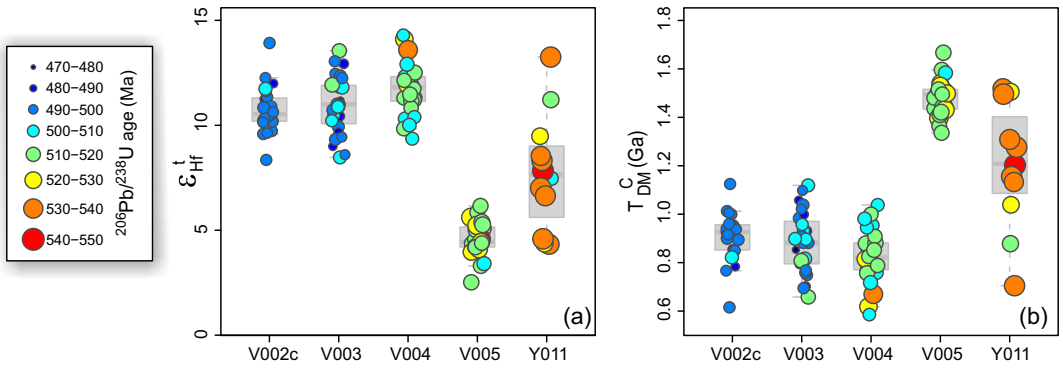

Fig. 9. 'Strip box plots' (Janoušek et al., 2016) illustrating the statistical distribution of ε^{t}_{Hf} values (a) and "crustal" model ages (T^{HfC}_{DM}) for individual zircons in each of the dated samples (b). The variously sized and coloured circles depict the distribution of intrusive ($^{206}Pb/^{238}U$) ages. For calculation of crustal model ages (T^{HfC}_{DM}), a basaltic $^{176}Lu/^{177}Hf$ ratio of 0.022 (Lancaster et al., 2011) was employed.

migmatitization. However, the ~750 Ma zircons can equally well be viewed as an igneous, detrital component in the sediment whose migmatitization was younger than 750 Ma and remained undetected by the U–Pb dating.

The remaining zircon population in Y012 is characterized by rather complicated core–rim structures. Dating the zircon cores mostly provided old $^{207}Pb/^{206}Pb$ ages, typically discordant due to Pb-loss or partial recrystallization. They vary between 1.6 Ga and 2.5 Ga and this scatter is taken as a consequence of metamorphic disturbance. Again, no ages could have been obtained from the rather narrow rims.

4.6. Whole-rock geochemistry

In the following section, the dataset will be split into four groups based on the silica contents, differences in appearance, petrology, the salient geochemical signatures and likely genesis as follows: Group 1: ultrabasic cumulates (SiO_2 < 42 wt%), Group 2: gabbros (42 < SiO_2 < 50 wt%), Group 3: quartz diorites (50 < SiO_2 < 57 wt%) and Group 4: tonalitic rocks (SiO_2 > 57 wt%).

4.6.1. Major and minor elements

The studied magmatic rocks are ultrabasic to intermediate in composition, rarely straddling the boundary of the acid domain (SiO_2 = 40.2–63.6 wt%; data from Electronic Appendix 6 recast on a volatile-free basis). They are geochemically rather primitive (Mg# = 58–30, but mostly constant at ~50) amphibole-bearing gabbros and hornblendites to Amp–Bt tonalites with quartz dioritic types prevailing (Fig. 10a). All samples are metaluminous to subaluminous (Fig. 10b), with A/CNK values (Shand, 1943) rising continuously from 0.61 to 0.98 with increasing SiO_2 (not shown).

Using the CIPW norm (Hutchison, 1975), the three ultrabasic samples (V015, V012a and P032) contain up to 9.5% normative *Ne*, together with *Ol* (Electronic Appendix 6). The more acidic compositions are characterized by the presence of normative *Q*, *Hy* and *Pl*; only in samples D004 and L010b appears some normative *Ol* instead of *Q*. The bulk of the dataset is thus subalkaline, except for the ultrabasic types that are slightly alkaline.

As there is no significant change in FeOt/MgO during differentiation for most of the samples (Fig. 10c), they do not represent a tholeiitic but a calc-alkaline suite (Miyashiro, 1974). The rocks are all Na-rich (Na_2O = 1.8–6.6 wt%, Na_2O/K_2O = 1.3–9.7 by weight). They classify mostly as normal-K calc-alkaline in the diagram of Peccerillo and Taylor (1976) (Fig. 10d); only the most siliceous samples enter the high-K calc-alkaline field.

Harker plots show mostly negative correlations, except for those involving alkalis and phosphorus that have positive slopes (Fig. 11). For FeOt and CaO negative trends are well defined over the entire silica range. On the other hand, plots with TiO_2 and MgO display excess scatter for the (ultra-) basic samples. The trend for Al_2O_3 is clearly inflexed; a strongly scattered positive correlation for (ultra-) basic samples gives way to a negative one at about 50 wt% SiO_2 and 19 wt% Al_2O_3.

4.6.2. Trace elements

The complete trace-element data are presented in Electronic Appendix 7. The elemental concentrations were normalized to the average composition of Normal Mid-Ocean Ridge Basalt (NMORB) (Sun and McDonough, 1989) (Fig. 12) and chondrite (Boynton, 1984) (REE; Fig. 13). The former multi-element plots are invariably characterized by the presence of deep negative anomalies of Nb and Ta, and, except for the least siliceous samples, a fair enrichment in LILE (including K, Pb and Sr).

The **ultrabasic rocks** (**Group 1**) are extremely poor in many incompatible elements (Rb 1–3, Cs < 0.1, Th < 0.05–0.06, U 0.02–0.04, Nb < 0.2–0.3, Ta < 0.01–0.004 ppm). The Sr concentrations are somewhat elevated, leading to low Rb/Sr ratios of 0.001–0.004. The contents of transition metals are variable (Cr < 20, Ni < 20–50, Pb < 5 ppm but Co 43–62, Sc 34–99, and V 422–751 ppm). The NMORB-normalized patterns (Fig. 12a) show normalized contents, for most elements, significantly lower than unity (Th, Nb, Ta – if above the respective detection limits – as well as P, Zr, Hf, HREE) or approaching it (U, LREE + MREE). The only more abundant elements are Rb, Ba, K, Sr ± Ti.

The chondrite-normalized REE patterns for the three ultrabasic samples are concave down, with maxima reached at Sm and Eu (Fig. 13a). Hence, the Dy/Dy* values are high (1.35–1.58). Total REE contents are consistently low (ΣREE = 26.8–28.3 ppm). Normalized contents of La and Yb are mutually comparable (La_N/Yb_N = 0.96–1.04, Yb_N = 5.6–6.1), and the Eu anomaly is insignificantly positive (Eu/Eu* = 1.09–1.16).

Compared with the previous group, three of the **Group 2 gabbros** (Fig. 12b) contain much higher LILE (Cs, Rb, Ba, K), LREE and HFSE (Nb, Ta, Ti, Zr, Hf). The normalized contents of the said elements mostly exceed unity. Still, the distribution pattern for the fourth sample V016 is more depleted and does not differ greatly from that of the ultrabasic group.

For the three gabbros, the total REE contents are higher than those in the Group 1 (ΣREE = 51.0–107.7 ppm), and the Eu anomalies are negligible to clearly negative (Eu/Eu* = 0.97–0.72) (Fig. 13b). The sample V007 is very different, showing distinctly lower ΣREE of 31.8 ppm and a strong positive Eu anomaly (Eu/Eu* = 1.41). The patterns of Group 2 invariably display weak LREE over HREE enrichment (La_N/Yb_N = 2.26–6.05, Yb_N = 4.7–9.1) and are gently concave up at Dy (Dy/Dy* = 0.93–0.80).

The **Group 3 quartz diorites** yielded NMORB-normalized multi-element patterns that are strongly enriched in incompatible elements (particularly Cs and Rb; Fig. 12c); the contents of the most compatible elements are only slightly below unity. Superimposed on the patterns are strong spikes in Ba, K, Pb, Sr and P as well as deep troughs in Nb and Ta as well as – much less pronounced – Ti.

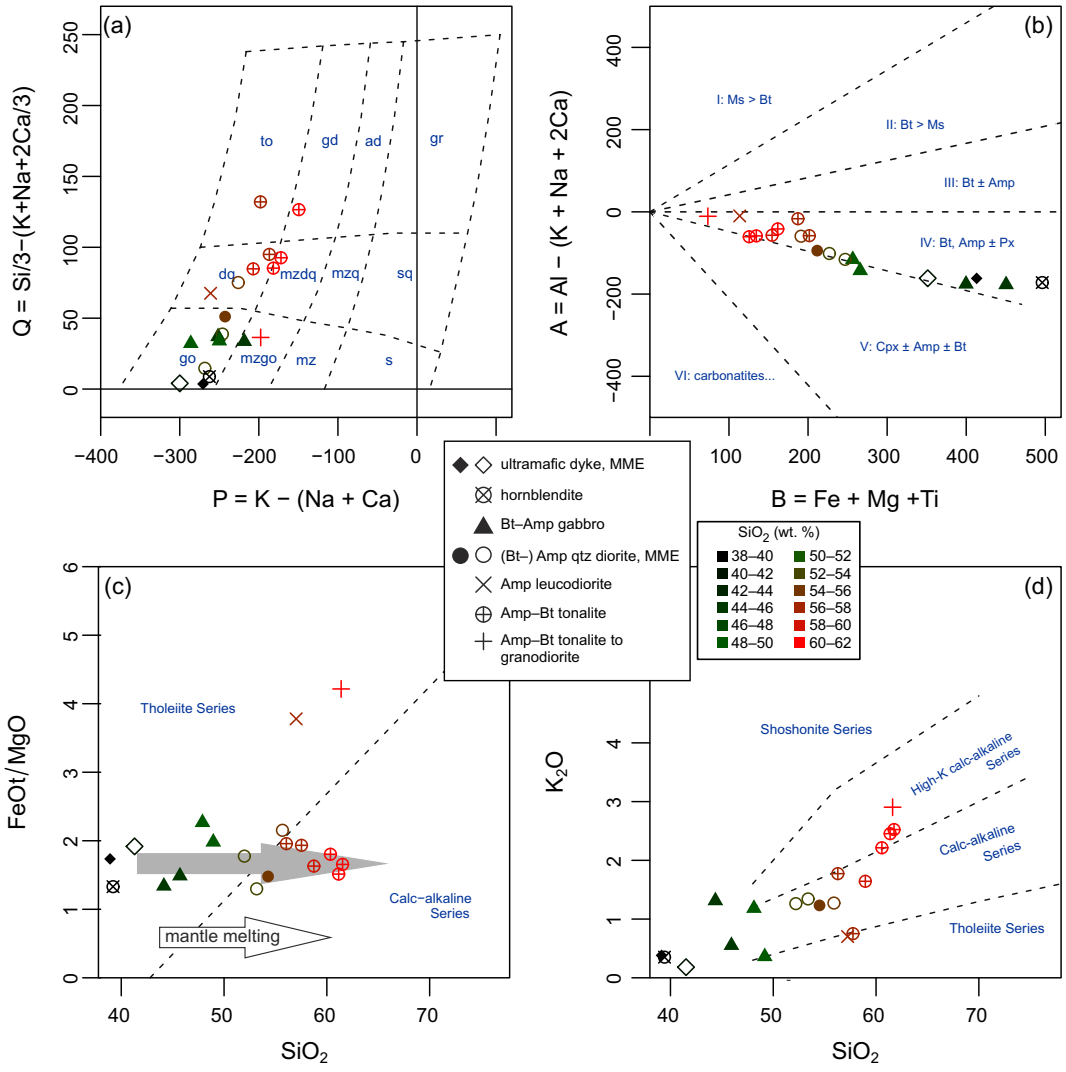

Fig. 10. Major-element based classification plots with the plotting symbols colour-coded according to silica contents. (a) Multicationic P–Q diagram of Debon and Le Fort (1983). gr = granite, ad = adamellite, gd = granodiorite, to = tonalite, sq = quartz syenite, mzq = quartz monzonite, mzdq = quartz monzodiorite, dq = quartz diorite, s = syenite, mz = monzonite, mzgo = monzogabbro, go = gabbro. (b) Multicationic B–A diagram of the same authors. Sectors (I–VI) reflect alumina balance of samples: I, muscovite > biotite; II, biotite > muscovite; III, biotite ± amphibole; IV, biotite, amphibole ± pyroxene; V, clinopyroxene ± amphibole ± biotite; VI, unusual mineral associations (carbonatites). (c) Binary plot of SiO_2 vs. FeOt/MgO (wt%) of Miyashiro (1974) showing the calc-alkaline affinity of the KMC. The global mantle melting array is based on the compilation of Grove et al. (2012). (d) SiO_2–K_2O plot with discrimination boundaries between the tholeiitic, calc-alkaline, high-K calc-alkaline and shoshonitic rocks of Peccerillo and Taylor (1976).

The REE patterns are subparallel for the entire group (Fig. 13c; La_N/Yb_N = 4.94–9.10). They exhibit no or slightly negative Eu anomalies (Eu/Eu^* = 1.00–0.80) and are clearly curved, concave up (Dy/Dy^* = 0.72–0.65). However, the total contents are variable (ΣREE = 59.9–123.5 ppm, Yb_N = 6.8–10.8).

The NMORB-normalized spiderplots for the felsic **Group 4** do not differ greatly from the previous one, even though the LILE enrichment reaches its highest values here. An interesting feature is a strong Zr and Hf enrichment in the felsic samples V002c and V008c as well as considerable variability in the HREE + Y contents of the whole group.

The REE patterns are very variable (Fig. 13d) in terms of total REE (62.8–191.8 ppm), the HREE contents (Yb_N = 3.6–10.1) and the degree of the LREE/HREE enrichment (La_N/Yb_N = 6.45–20.14). The magnitude of the Eu anomaly is also variable (Eu/Eu^* = 1.24–0.78), but all curves are clearly concave up (Dy/Dy^* = 0.65–0.54).

4.7. Sr–Nd isotopes

In order to shed more light on sources and subsequent development of the studied plutonic association, Sr–Nd isotopic analyses were undertaken for seven representative whole-rock samples (Table 2, Fig. 14). In view of the newly obtained intrusive ages, the isotopic data were age-corrected to 500 Ma. Overall they show a rather narrow range of initial Sr isotopic compositions ($^{87}Sr/^{86}Sr_{500}$ = 0.7034–0.7044), but the Nd isotopic variability is significantly broader (ε_{Nd}^{500} = +5.8 to −4.9).

The most primitive, clearly Depleted Mantle-derived samples are the ultrabasic dyke V015, gabbro V007 and quartz diorite V003 ($^{87}Sr/^{86}Sr_{500}$ = 0.7035–0.7038, ε_{Nd}^{500} = +4.7 to +3.5). The hornblendite V012a has slightly less radiogenic Nd ($^{87}Sr/^{86}Sr_{500}$ = 0.7036, ε_{Nd}^{500} = +2.6). Due to elevated $^{147}Sm/^{144}Nd$ ratios in the cumulate rocks, the two-stage Nd model ages represent only rather rough estimates ($T_{DM}{}^{Nd}{}_{.2stg}$ = 0.87–1.07 Ga).

The more siliceous rocks represent a rather heterogeneous group. Two of these (leucocratic hybrid Amp–Bt tonalite V008c and Amp–Bt tonalite V005) show primitive Sr but immature crust-like Nd isotopic compositions ($^{87}Sr/^{86}Sr_{500}$ = 0.7043 and 0.7044, ε_{Nd}^{500} = −4.9 and −0.6, $T_{DM\cdot 2stg}^{Nd}$ = 1.79 and 1.38 Ga). On the other hand, coarse-grained leucocratic Amp–Bt quartz diorite V004 has a composition resembling the Depleted Mantle and is the least evolved among the samples investigated ($^{87}Sr/^{86}Sr_{500}$ = 0.7034, ε_{Nd}^{500} = +5.8, $T_{DM}{}^{Nd}{}_{.2stg}$ = 0.77 Ga).

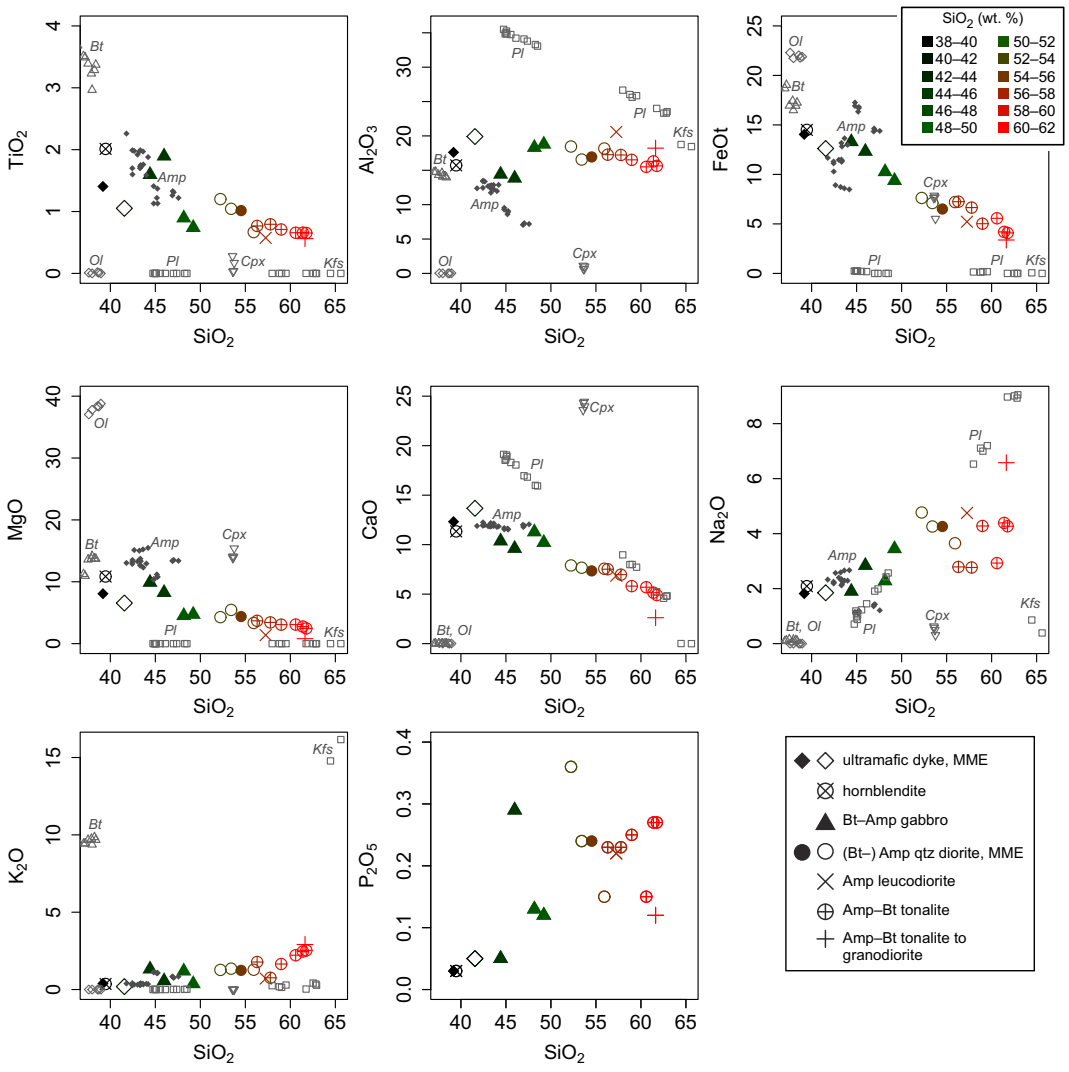

Fig. 11. Harker plots for the studied magmatic rocks from the KMC. Also plotted are typical electron-microprobe analyses of the main rock-forming minerals.

5. Discussion

5.1. Geotectonic context

The studied samples from the Khantaishir Magmatic Complex are mostly subalkaline, except for the ultrabasic types gradually becoming alkaline in character, most likely due to accumulation of amphibole crystals. The (normal-K) calc-alkaline chemistry of the more siliceous rock types, as well as characteristic trace-element enrichment in hydrous-fluid mobile LILE (Cs, Rb, Ba, K, Pb and Sr), with Th and U, relative to the "conservative" HFSE (Nb, Ta and Ti) suggest an origin within a magmatic arc (Fig. 12) (e.g., Pearce and Peate, 1995; Tatsumi and Eggins, 1995).

Indeed, in the Th–Hf/3–Ta ternary plot of Wood (1980) (Fig. 15a), the samples fall exclusively into the arc-related (CAB and IAT) fields. Also, the binary plots Ti–V of Shervais (1982) and Zr–Ti of Pearce (1982) demonstrate an arc affinity of the studied samples (Fig. 15b–c). In the binary diagram Nb/Yb vs. Th/Yb (Pearce, 2008, 2014) (Fig. 15d) all samples plot well above the 'NMORB–OIB array', into the region occupied by arc-related magmas. Moreover, this plot demonstrates that the arc was rather mature, producing magmas with relatively high Nb and Th contents.

One should be aware of possible limitations concerning the interpretation of geotectonic diagrams, though. Especially for the felsic igneous rocks, the Nb, Ta and Ti depletion and LILE enrichment may merely imply remelting of older, arc-related crustal sources (Arculus, 1987; Förster et al., 1997; Janoušek et al., 2010; Roberts and Clemens, 1993). In fact, these characteristics are inherent to the continental crust as a whole (see Introduction). The chemistry of the magmatic rocks can also be profoundly modified by crystal accumulation, peritectic phase entrainment, assimilation or hybridization (e.g., Clemens and Stevens, 2012; Deering and Bachmann, 2010; Didier and Barbarin, 1991a). Still, the whole-rock geochemical signature for most of the KMC dataset (mafic–intermediate rocks) seems to consistently indicate an affinity to subduction-modified mantle melts, or their fractionates.

5.2. Petrogenesis of the Khantaishir Magmatic Complex

5.2.1. Magma evolution

As shown above, the Harker plots for non-cumulate rocks show negative correlations of TiO_2, Al_2O_3, FeOt, MgO and CaO with SiO_2 (Fig. 11), but the ultrabasic cumulates often define scattered oblique trends (e.g., Al_2O_3). Such a variation can be modelled by fractionation dominated by ferromagnesian phases (mainly amphibole) with, or without, their crystal accumulation. This is in line with the field and microtextural evidence that points to a particularly important role for amphibole accumulation (and hence also fractional crystallization) in the petrogenesis of the KMC.

Plagioclase was probably only a late crystallizing phase, as shown by distinct inflections at SiO_2 ~ 50 wt%, especially in the SiO_2–Al_2O_3 and

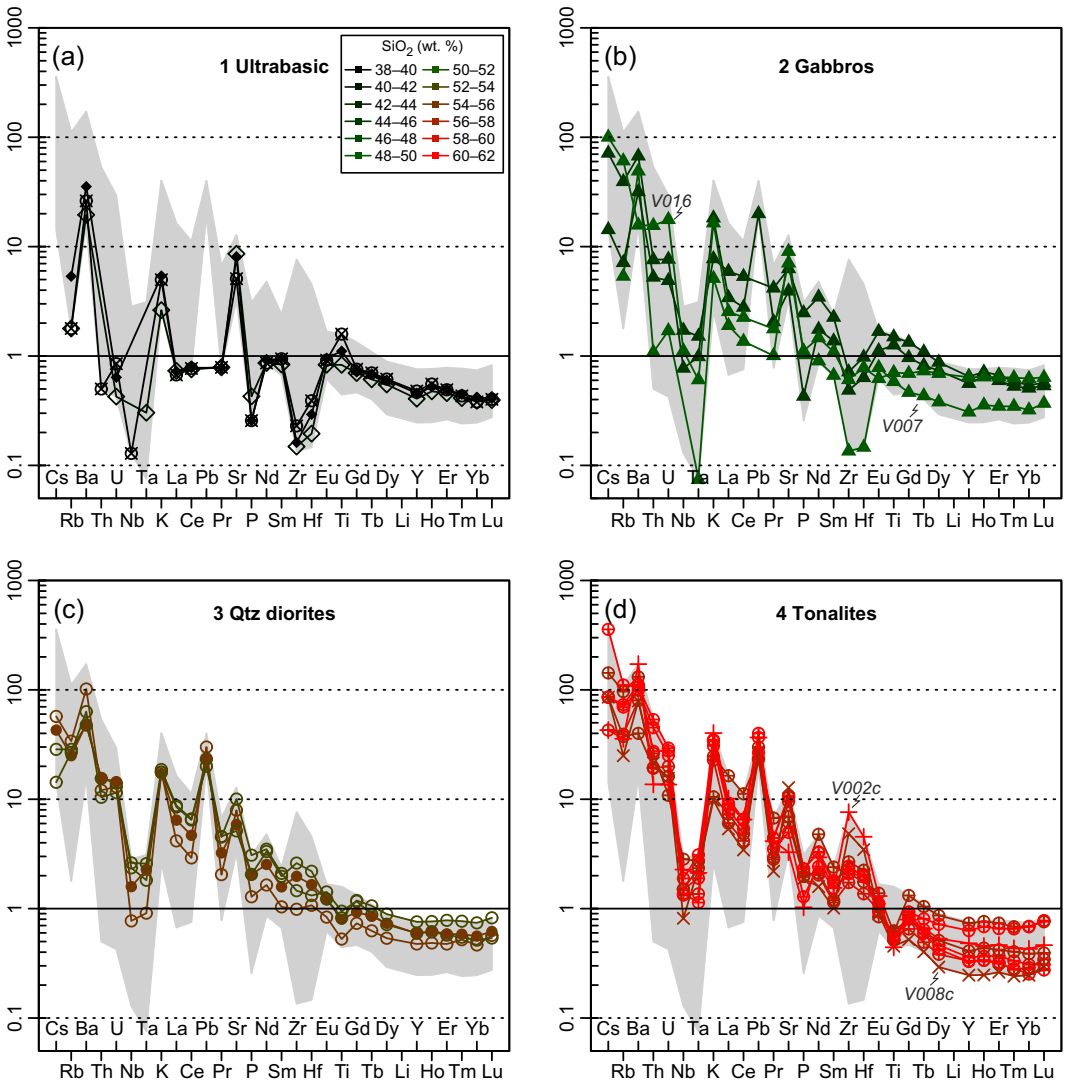

Fig. 12. Normal Mid-Ocean Ridge Basalt (NMORB) (Sun and McDonough, 1989) normalized spiderplots colour-coded by silica contents. The grey background field indicates the overall variability in the dataset. Plotting symbols as in Fig. 10.

SiO_2–MgO plots (Fig. 11) as well as the general lack of Eu anomalies, especially in more mafic rock types (Fig. 13). Indeed, delayed crystallization of plagioclase is a common feature of water-rich calc-alkaline magmas at continental margins (Dessimoz et al., 2012; Grove et al., 2012).

Theoretically also garnet could have been involved during deep crustal crystallization (Alonso-Perez et al., 2009), or partial melting. Given the preference of amphibole and, to a lesser extent, clinopyroxene for the MREE and garnet for the HREE, the nature of the key ferromagnesian phase can be best assessed using the shapes of the REE patterns and their change in course of differentiation. In this context the observed positive SiO_2–La_N/Yb_N correlation (Fig. 16a) is equivocal as it could be interpreted as being due to either garnet or amphibole control (Davidson et al., 2007).

Fortunately Dy/Dy* and Ti/Ti*, the parameters expressing the curvature of the MREE–HREE segments of the REE patterns (Fig. 13) and the magnitude of the Ti anomaly in the NMORB-normalized multi-element plots (Fig. 12), respectively, are capable of distinguishing between the two possibilities (Davidson et al., 2013). According to these authors, garnet fractionation should cause a rise in Dy/Dy* (increasingly concave down patterns), but amphibole should have the opposite effect. In the KMC, all non-cumulate rocks are characterized by Dy/Dy* < 1, further sharply decreasing with rising SiO_2 (Fig. 16b).

In addition, the amphibole control (± magnetite) should result in a progressively developing negative Ti anomaly in the NMORB-normalized multi-element plot (Fig. 12), and thus a positive Ti/Ti*–Dy/Dy* correlation. Therefore, the binary plots involving the Dy/Dy* and Ti/Ti* parameters (Fig. 16c–d) corroborate the amphibole control for most of the studied rocks. Moreover, they confirm that the amphibole-rich ultrabasic samples are truly cumulates (see e.g., the low SiO_2, La_N/Yb_N, high Dy/Dy* (≫1) and Ti/Ti*).

5.2.2. Water contents in the magma

As pointed out by Grove et al. (2012), primary arc magmas are commonly water-rich, with 6–8 wt% H_2O or more, bearing a witness to the profusion of water in their subduction-modified mantle sources. The major effect of H_2O is to suppress the crystallization of plagioclase at mid- to lower-crustal pressures in favour of Fe–Mg-rich silicates. Hence the distinctive enrichment in SiO_2, typical of these magmatic suites, is primarily driven by the early crystallization of olivine, pyroxene and/or amphibole. Moreover, the late-crystallizing plagioclase is An-rich (and thus Ca–Al-rich and Si-poor), further promoting a rapid evolution to siliceous residual liquids rich in alkalis (Grove et al., 2012).

Using the amphibole compositions as a proxy (Ridolfi et al., 2010), the Khantaishir magma was probably water-rich; gabbros and hornblendites could have had *c.* 7.0 to 8.5 wt% H_2O, tonalites somewhat

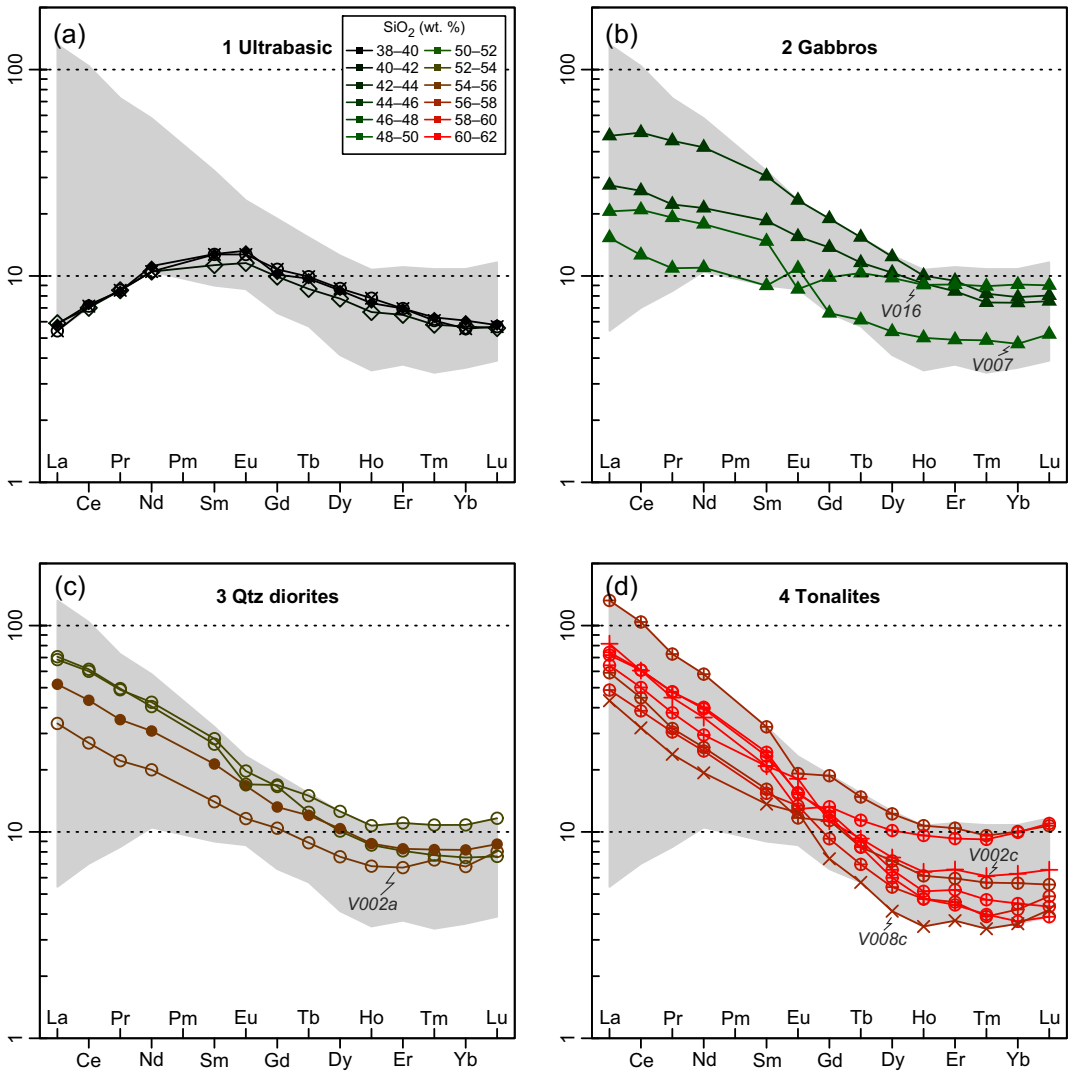

Fig. 13. Chondrite (Boynton, 1984) normalized REE patterns colour-coded by silica contents. The grey background field indicates the overall variability in the dataset. Plotting symbols as in Fig. 10.

less, down to 4 wt% (Table 1). The former values correspond to vapour saturation of a basaltic magma at depths of about 15–25 km (Plank et al., 2013), which is in good agreement with calculated pressures for the gabbros and hornblendites (Table 1).

Most parental magmas in subduction zones fractionate amphibole as a result of elevated H_2O during crystallization (Grove et al., 2012; Müntener et al., 2001). But this mineral could also be a product of a late-stage peritectic reaction of clinopyroxene with melt (hydrous melt + clinopyroxene + Fe–Ti oxides + Ca-rich plagioclase = amphibole + quartz + Na-rich plagioclase; Beard et al., 2004).

Still, high initial H_2O contents of the basic intrusions into the Khantaishir arc are confirmed by the occurrence of comb layering (Fig. 2h). Based on extensive experimental work, these textures have been explained by the loss of H_2O from the crystallizing mafic system (nearly) saturated in water into the adjacent water-poor (felsic) magma or wall rock (Pistone et al., 2015). In this model, the mafic part of the system would be 'chemically quenched' just by the H_2O loss, even if the loss was isothermal. The undercooling front migrates inwards, away from the interface between both domains. The nucleation takes place on the interface, and the steady undercooling regime promotes perpendicular, inward growth of large crystals, such as amphiboles in the present case.

The rock sequence in the KMC preserves evidence for a fractionation trend typical of arc magmas with early olivine crystallization, followed by clinopyroxene and/or amphibole (e.g., Smith, 2014). Mainly at the more advanced stages, the crystallization produced assemblages with higher proportions of amphibole at the expense of clinopyroxene. The studied mafic or intermediate magmas would be saturated at 4 wt% H_2O at relatively shallow depths (~6 km) which is a common storage depth beneath arc volcanoes, based on geodetic and seismic observations (e.g., Cervelli et al., 2010; Lu et al., 2010; Plank et al., 2013).

Similar to our case, the importance of hornblende-dominated fractional crystallization in the production of intermediate arc magmas was emphasized by several authors (e.g., Davidson et al., 2007; Dessimoz et al., 2012; Lee and Bachmann, 2014). Clearly also in the KMC, the basic melts were responsible for H_2O transfer from a water-rich mantle wedge to the lower–middle arc crust, where they were subject to fractional crystallization forming the amphibole "sponge" *sensu* Davidson et al. (2007).

5.2.3. Depleted mantle contribution

The whole-rock geochemical and Sr–Nd isotopic signatures some of the (ultra-) basic samples, namely the ultrabasic dyke V015, microgabbro V007 and hornblendite V012a, requires direct fractionation (with variable degree of crystal accumulation) from primary melts derived from a depleted mantle wedge, overprinted by subduction fluids ($^{87}Sr/^{86}Sr_{500}$ = 0.7038 to 0.7036, ε_{Nd}^{500} = +4.5 to +2.6, $T_{DM\ .2stg}^{Nd}$ = 0.89–1.07 Ga).

Table 2
Whole-rock Sr–Nd isotopic data for selected samples of the KMC.

Sample ID	Petrology	SiO_2 (wt%)	Rb (ppm)	Sr (ppm)	$^{87}Rb/^{86}Sr$	$^{87}Sr/^{86}Sr$ [a]	2 se	$^{87}Sr/^{86}Sr_{500}$ [b]	Sm (ppm)	Nd (ppm)	$^{147}Sm/^{144}Nd$	$^{143}Nd/^{144}Nd$ [a]	2 se	$(^{143}Nd/^{144}Nd)_{500}$ [b]	ε_{Nd}^{500}	$T_{DM.1stg}^{Nd}$ [c]	$T_{DM.2stg}^{Nd}$ [d]
V015	Fine-grained ultrabasic dyke	39.18	3	728	0.0119	0.703911	0.000005	0.70383	2.49	6.7	0.2247	0.512907	0.000007	0.51217	+3.5	−6.69	0.99
V012a	Hornblendite	39.47	1	458	0.0063	0.703688	0.000012	0.70364	2.48	6.3	0.2380	0.512908	0.000010	0.51213	+2.6	−1.97	1.07
V007	Fine-grained Amp gabbro from the mingling zone	49.21	3	813	0.0107	0.703707	0.000017	0.70363	1.75	6.6	0.1608	0.512753	0.000005	0.51223	+4.5	1.04	0.89
V003	Bt–Amp qtz diorite	54.53	14	530	0.0764	0.703997	0.000009	0.70345	4.16	18.5	0.1359	0.512679	0.000005	0.51223	+4.7	0.87	0.88
V008c	Leucocratic Amp–Bt tonalite with Amp xenocrysts	57.26	14	1149	0.0352	0.704530	0.000009	0.70428	2.66	11.6	0.1386	0.512197	0.000010	0.51174	−4.9	1.80	1.79
V005	Amp–Bt tonalite	60.59	62	448	0.4004	0.707260	0.000012	0.70441	4.06	17.7	0.1387	0.512419	0.000004	0.51196	−0.6	1.39	1.38
V004	Leucocratic Amp–Bt quartz diorite	61.77	41	936	0.1267	0.704275	0.000009	0.70337	4.54	23.7	0.1158	0.512669	0.000005	0.51229	+5.8	0.71	0.77

[a] Followed by error (2 standard errors of the mean).
[b] Subscripts '500' indicate age-corrected isotopic ratios.
[c] Single-stage Nd model ages (Ga) using the Depleted Mantle parameters of Liew and Hofmann (1988).
[d] Two-stage Nd model ages (Ga) using the Depleted Mantle parameters and the general approach of Liew and Hofmann (1988); however, $^{147}Sm/^{144}Nd_{CC} = 0.138$ (metabasic crust).

However, the chemistry of the more siliceous samples is more equivocal. The crustal Hf model ages (T_{DM}^{HfC}) for the quartz diorite V003, leucocratic quartz diorite V004 and tonalite V002c are low, ranging between 0.59 and 1.12 Ga. Also, the whole-rock Sr–Nd isotopic signatures of the former two samples are in accord with a short crustal residence time of their source ($^{87}Sr/^{86}Sr_{500} \sim 0.7035$, $\varepsilon_{Nd}^{500} = +4.7$ and $+5.8$, $T_{DM\cdot2stg}^{Nd} = 0.88$ and 0.77 Ga, respectively). The plausible genetic scenarios thus include remelting of a recently formed basaltic underplate at the bottom of the magmatic arc (Atherton and Petford, 1993), or direct fractionation from primary melts derived from a metasomatized depleted-mantle wedge. Another viable alternative is partial melting of a relatively young and geochemically primitive metabasic crust; given the HFSE depletion, it could have formed a recently accreted island-arc (Rapp and Watson, 1995).

5.2.4. Anatexis of pre-existing crust?

In contrast, the Hf and Nd isotopic compositions of the two remaining felsic samples disclose a longer crustal history of their sources. Tonalite V005 contains exclusively old Hf ($T_{DM}^{HfC} = 1.34$–1.67 Ga, median 1.5 Ga), and its Nd is significantly less radiogenic than in the more basic rock types ($\varepsilon_{Nd}^{500} = -0.6$, $T_{DM.2stg}^{Nd} = 1.38$ Ga). Even more clear-cut is the case of tonalite V008c, which requires a crustal source with a still older Mesoproterozoic mean Nd residence age ($\varepsilon_{Nd}^{500} = -4.9$, $T_{DM.2stg}^{Nd} = 1.79$).

At the same time, both samples do not have particularly high $^{87}Sr/^{86}Sr_{500}$ ratios (~0.7044). This points to a source with low time-integrated Rb/Sr, such as metabasic rocks. In view of the Hf isotopic composition of the V005 zircons, as well as of the whole geochemical signature (esp. distinct HFSE depletion), the most likely candidate would again be previously accreted, significantly older island-arc rocks.

Nevertheless, there is also evidence for the presence of some, truly metasedimentary country rocks in the roof of the KMC. The migmatite sample Y012 gives *c.* 750 Ma ages for near-euhedral zircons that can be most plausibly interpreted as a detrital component in Neoproterozoic sediment deposited, after short transport, from a homogenous Tonian magmatic source. The migmatitization could have been of Cambrian age, being caused by the heat input from the voluminous mafic magmas of the KMC.

Even though the number of dated zircons from the migmatite is very limited, the strongly discordant inherited component with ill-defined upper intercept age(s) suggests an abundance of Palaeoproterozoic detritic zircon in the sedimentary source of its protolith, resembling the age spectra known from the nearby Baydrag Continent (e.g., Demoux et al., 2009a; Kozakov et al., 1993). This does not seem to imply that the Khantaishir arc was founded on an ancient crustal segment, though. The evidence to the contrary is provided by the lack of typical ('S-type') anatectic granites in the KMC, its rather primitive Sr isotopic signature as well as (mostly) short crustal residence times shown by the whole-rock Nd and zircon Hf model ages. The migmatite is thus interpreted as a minor sedimentary component overlying the local, mostly metabasic crust. The sedimentary material of its protolith could have been transported from a Palaeoproterozoic core of the continent, perhaps not very far away. These metasediments, however, apparently played a negligible role in the genesis of the arc itself.

5.2.5. Mutual interaction of mantle- and crustally-derived magmas

Field and petrographic observations suggest that hybridization between crustal and mantle-derived melts was significant in the genesis at least some of the studied quartz diorites and tonalites. Its importance is documented by the abundance of MME commonly with lobate contacts and chilled margins (e.g., Barbarin, 2005; Didier and Barbarin, 1991a) as well as by the presence of some microtextures, most notably mantled plagioclases and rapakivi feldspars (e.g., Hibbard, 1991; Janoušek et al., 2004; Vernon, 1984).

The variation in the Sr–Nd isotopic data (Fig. 14) indicates heterogeneity of the sample set that can be interpreted in terms of contrasting

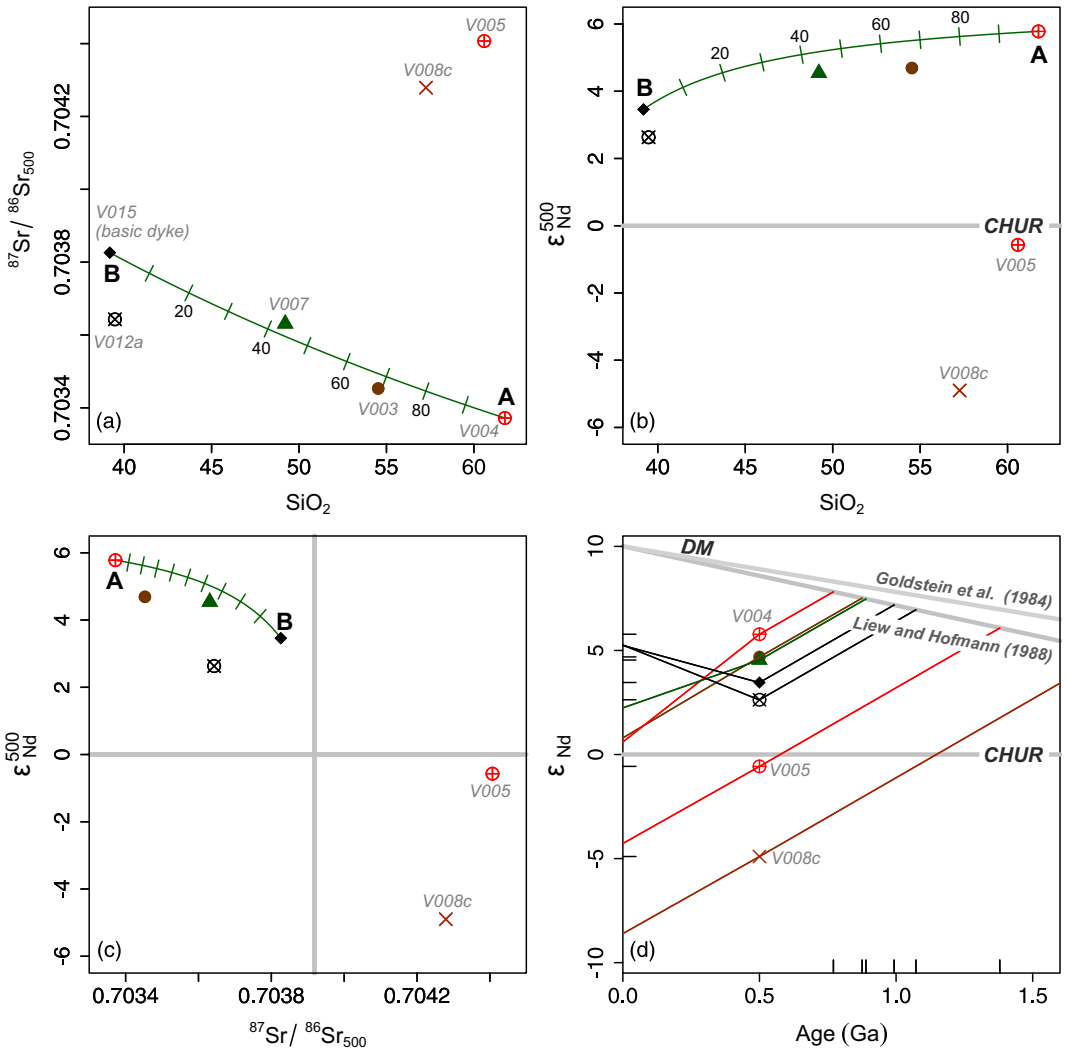

Fig. 14. Whole-rock Sr–Nd isotopic compositions. (a) – SiO_2 vs. $^{87}Sr/^{86}Sr_{500}$ plot. (b) – SiO_2 vs. ε_{Nd}^{500} plot. (c) Binary plot of $^{87}Sr/^{86}Sr_{500}$ vs. ε_{Nd}^{500} for KMC rocks. (d) Two-stage Nd evolution diagram. DM = Depleted Mantle evolution lines after Goldstein et al. (1984) and Liew and Hofmann (1988). The extra tick marks on the ordinate denote ε_{Nd}^{500} values, on the abscissa the two-stage Depleted Mantle model ages, $T_{DM\text{-}2stg}^{Nd}$ (Liew and Hofmann, 1988). Plotting symbols as in Fig. 10. Binary mixing hyperbolae in (a–c) indicate weight proportions of assumed felsic end-member V004 (10% tick marks) mixed with a mafic magma with composition of dyke V015 (see Janoušek et al., 2016 for the principles and R code employed). Independent position of felsic samples V005 and V008c, probably derived by anatexis of older metabasic crust, is clearly visible. For explanation see text.

mantle and crustal sources for individual rock types. Moreover, the position of samples V015, V007, V003 and V004 in Fig. 14a–c does not seem fortuitous but rather reflects the operation of open-system processes. Rather curiously, strontium becomes *less* and neodymium *more* radiogenic with increasing silica in this sequence (Fig. 14a–b).

Assuming that the basic mantle-derived end-member had a composition of dyke V015 and the felsic crustal melt of leucocratic quartz diorite V004, binary mixing hyperbolae require that the microgabbro V007 contains *c.* 40 wt%, and the Bt–Amp quartz diorite V003 *c.* 70 wt% of the crustal component (Fig. 14a–c). The negligible curvature in the SiO_2 vs. $^{87}Sr/^{86}Sr_{500}$ plot makes it to appear nearly linear (Fig. 14a). Indeed, the two samples presumably dominated by the felsic component (V003 and V004) yielded exclusively low Hf model ages (T_{DM}^{HfC}) of 0.59 to 1.12 Ga, with medians at 0.8–0.9 Ga (Fig. 9b). The U–Pb dating proves that these two samples were contemporaneous at *c.* 495 Ma (late Cambrian).

Nonetheless, binary plots of SiO_2 vs. Al_2O_3 and MgO (Fig. 11) are clearly inflexed. On this basis, simple binary mixing, but also partial melting or fractional crystallization with a constant proportion of minerals in the residue/crystallizing cumulate can be discounted. These processes are all governed by mass balance, leading to simple linear relationships (Janoušek and Moyen, 2014). On this basis, as well as of field, petrological and geochemical arguments given above, fractional crystallization had to be an important process, but there also had to be a major change in the fractionating assemblage (plagioclase in?) at *c.* SiO_2 ~ 50 wt%.

Taken together, neither simple binary mixing nor closed-system fractional crystallization alone can account for the observed Sr–Nd isotopic, major- and trace-element variations. Hence, the two mechanisms had to be coupled into a single process, such as Assimilation and Fractional Crystallization (AFC) (DePaolo, 1981; O'Hara, 1977) most likely with changing fractionating assemblages and thus also bulk distribution coefficients (Janoušek et al., 2000; Powell, 1984). The operation of complex multistage fractional crystallization/crystal accumulation in combination with variable open-system processes is typical of many magmatic arcs (Otamendi et al., 2012).

The amphibole gabbro Y011 contains two zircon populations of dissimilar ages (521 ± 6 and 538 ± 3 Ma), giving a broad range of *in-situ* ε_{Hf}^{t} values (Fig. 9a). The field relations indicate that the already solidified mafic igneous rock has been invaded by younger, felsic magma (Fig. 5f). The likely mechanism thus appears to be recycling of *c.* 538 Ma xenocrysts/antecrysts from an earlier, more mafic magma pulse and mixing with the *c.* 521 Ma magmatic crystals from the more felsic system (e.g., Davidson et al., 2007; Larrea et al., 2013).

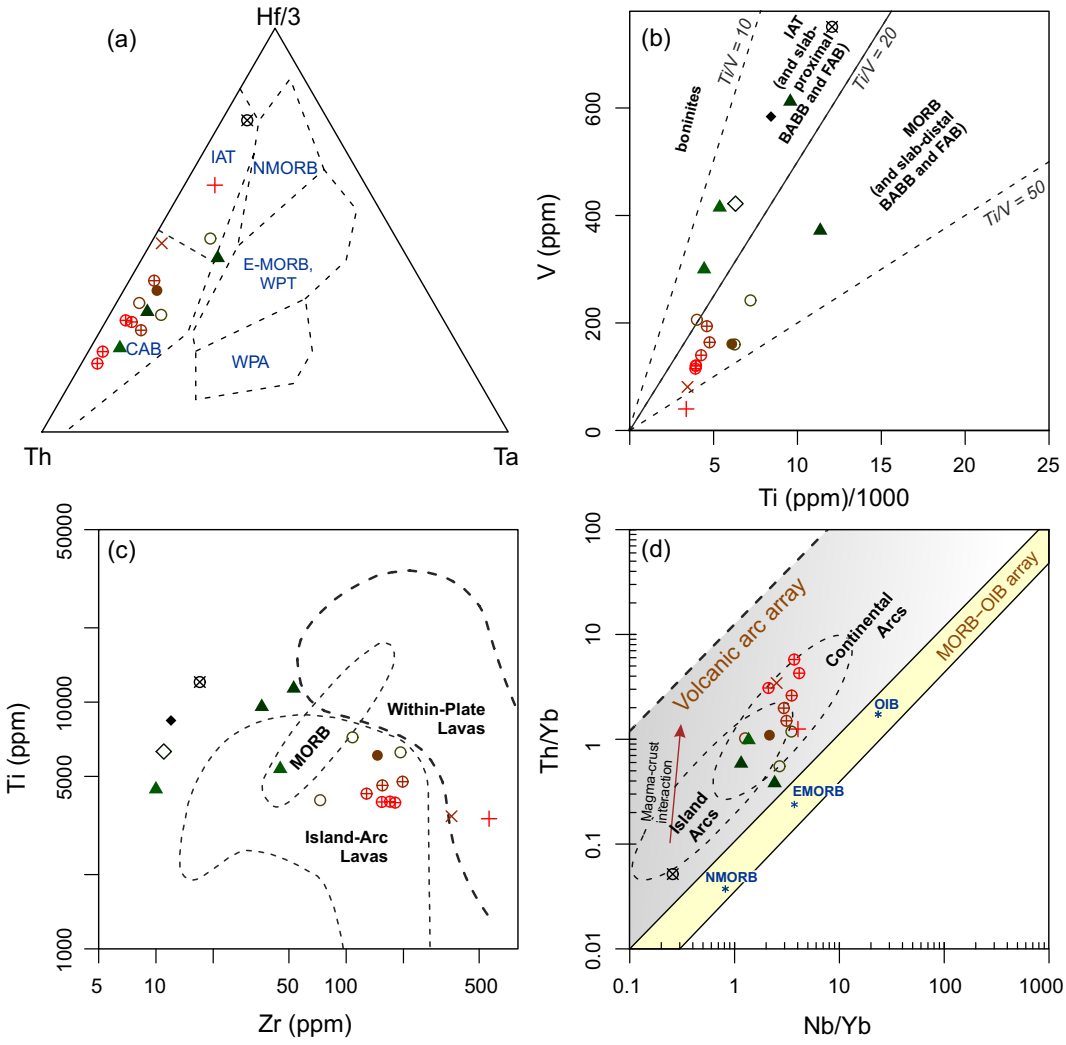

Fig. 15. Geotectonic diagrams based on whole-rock geochemical compositions. (a) – Triangular plot Th–Hf/3–Ta of Wood (1980). IAT – Island-Arc Tholeiites, CAB – Calc-Alkaline Basalts, N-MORB – Normal Mid-Ocean Ridge Basalts, E-MORB – Enriched Mid-Ocean Ridge Basalts, WPT – Within-Plate Tholeiites, WPA – Within-Plate Alkali Basalts. (b) – Binary plot Ti–V of Shervais (1982) modified by Pearce (2014). IAT – Island-Arc Tholeiites, BABB – Back-Arc Basin Basalts, FAB – Fore-Arc Basalts. (c) – Binary plot Zr vs. Ti of Pearce (1982). (d) – Binary diagram Nb/Yb vs. Th/Yb (Pearce, 2008, 2014). The 'MORB–OIB array' is defined by average NMORB, EMORB and OIB compositions taken from Sun and McDonough (1989). Plotting symbols and colours as in Fig. 10.

The felsic samples V005 and V008c show a position different from the main trend in Fig. 14, having comparably radiogenic Sr and non-radiogenic Nd. In particular in the $^{87}Sr/^{86}Sr_{500}$ – ε_{Nd}^{500} plot (Fig. 14c), they fall on the other side of the magma mixing array compared to the inferred crustal end-member (V004). This is in line with the fact that their Nd model ages ($T_{DM\text{-}2stg}^{Nd}$) are Mesoproterozoic and that the former sample yields rather high T_{DM}^{HfC} (1.34–1.67 Ga). The tonalite V005 was dated at 516 ± 2 Ma, but for the leucotonalite V008c we have no direct age information. However, based on field relations, sample V008c needs to be younger that the layered gabbro/hornblendite (Fig. 2d) because it contains amphibole xenocrysts/antecrysts derived from the gabbro (Fig. 2f). This can be taken as a field evidence for recycling of amphibole crystals from the older, more mafic into the younger, felsic members of the magmatic suite (e.g., Paterson et al., 2008; Solgadi and Sawyer, 2008).

5.3. Age and temporal development of the Khantaishir Magmatic Complex

The pressures for KMC rocks, estimated from the amphibole compositions (Ridolfi et al., 2010) are considerably higher for the ultrabasic cumulates and gabbros (*c.* 0.35–0.5 GPa) than for the quartz diorites and tonalites (*c.* 0.1–0.2 GPa). The former correspond to a depth of *c.* 13–19 km, the latter to *c.* 4–8 km. As the typical thickness of arc crust ranges from 15 to 35 km (intra-oceanic arc) to 30–70 km (continental arc) (Spandler and Pirard, 2013), the studied amphibole-rich cumulates record crystallization at middle to lower crustal levels.

Field evidence, together with the whole-rock Sr–Nd isotopes, argue for the presence of several generations of (ultra-) basic magmas as well as magma mixing/mingling between some of the contrasting magma batches. However, among the samples dated by the U–Pb method on zircon, the most mafic rock types preceded somewhat the more siliceous magmatic activity. Sample Y011 shows two age populations, at 538 ± 3 and 521 ± 6 Ma. Leucogabbro sample M310 yielded a well-defined age of 521 ± 6 Ma, and the quartz diorite dyke M311 cutting it has an identical age, within error, of 524 ± 7 Ma. On the other hand, four quartz diorites to tonalites are on average younger, ranging between 516 ± 2 and 494 ± 3 Ma.

Such a temporal shift from deeper, mafic to shallower, more felsic magmatic activity may reflect upward growth of the magmatic arc (Otamendi et al., 2012). The growth would be linked to increasing importance of crustal melting with time, an inevitable consequence of progressive heating by, and/or water release from, the periodically incoming, hot and hydrous mantle-derived basaltic melts (Annen et al., 2006; Dufek and Bergantz, 2005; Hildreth and Moorbath, 1988). This could go hand in hand with the establishment of larger magma

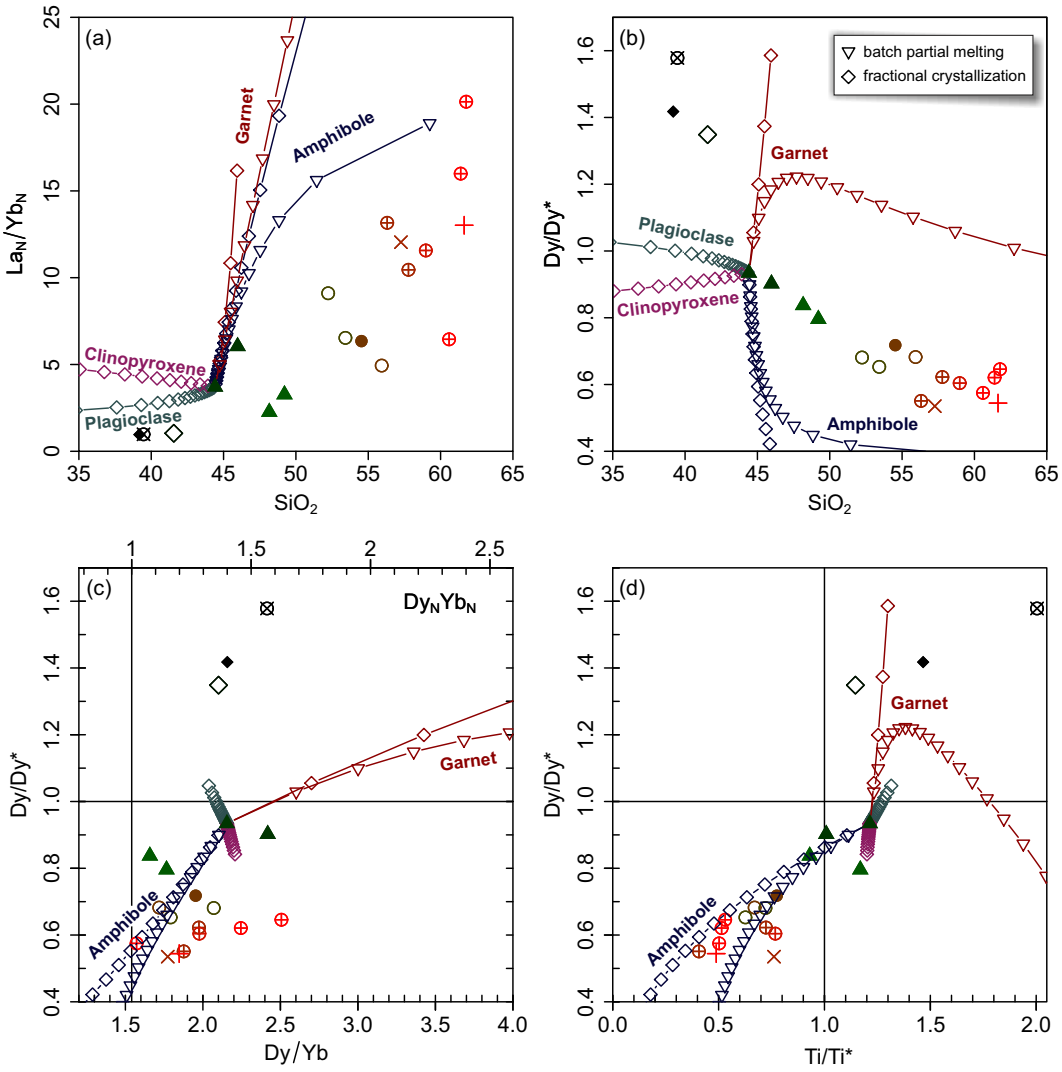

Fig. 16. Binary plots underlining the important petrogenetic role played by amphibole. (a) – SiO_2 (wt%) vs. the La_N/Yb_N ratio; (b) – SiO_2 (wt%) vs. the Dy/Dy* parameter (Davidson et al., 2013); (c) – Dy/Yb vs. Dy/Dy*; Ti/Ti* vs. Dy/Dy* diagram. Plotting symbols as in Fig. 10. Please note that while the rationale of the Ti/Ti* value follows Davidson et al. (2013), the calculation formula is different (see Analytical Techniques). For consistency with Figs 12 and 13, the normalizing values for Ti are based on average NMORB composition of Sun and McDonough (1989), and those for the REE are chondritic (Boynton, 1984). Also shown are trends of fractional crystallization (diamonds) and batch partial melting (triangles) (5% tick interval in both cases) for single mineral phases: amphibole, garnet, clinopyroxene and plagioclase. The partition coefficients are from Sisson (1994) (Amp), Johnson (1998) (Grt), Hart and Dunn (1993) with Johnson (1998) (Cpx) and McKenzie and O'Nions (1991) (Pl). For further discussion see text.

chambers that would have greater potential for fractionation and crustal contamination. However, it cannot be ruled out that this temporal evolution of compositions is just an artefact and that it simply reflects ongoing Cambrian erosion of the magmatic products down to the older arc roots, accompanied by contemporaneous intrusion by younger, inevitably shallower magma pulses. The former hypothesis still seems more likely thanks to the preserved vertical distribution of igneous rocks in a column > 1000 m high which is characterized by mafic cumulates in a deeply incised valley and tonalites close to the crest of the Khantaishir Mountain Range.

Apart from a few discordant analyses, most likely reflecting variable Pb loss, no older xenocrysts or cores were found in the studied zircons from the magmatic rocks. This seems to reflect the fact that the magmas were hot and mafic, with enhanced zircon solubility not favourable for unmelted zircon preservation (Janoušek, 2006; Watson and Harrison, 1983). Indeed Zr behaves incompatibly in the studied samples over the whole silica range, demonstrating that zircon saturation was never reached close to the liquidus. Thus the zircon grew relatively late in the dated samples. If present in the metabasic source, zircons were likely fully dissolved in the partial melt. In any case, substantial amounts of zirconium could have been stored also in other phases, such as rutile, garnet, or hornblende (Kohn et al., 2015).

5.4. Regional correlation

Based on the petrologic, geochemical and age similarities, the newly discovered Cambrian arc-related magmatism in the Khantaishir Range could be correlated with similar occurrences in adjacent regions of Mongolia and Russia. The Cambrian subduction-related magmatic complexes can be traced through terranes bordering the Precambrian Tuva-Mongolia, Zabkhan, and Baydrag microcontinental segments (Badarch et al., 2002; Buslov et al., 2001; Demoux et al., 2009a; Kröner et al., 2011; Kuzmichev et al., 2001), as well as the southern and southwestern margin of the Siberian Craton (in present coordinates) (Fig. 17).

The north-easternmost occurrences of Cambrian magmatic-arc complexes (Fig. 18a) in the eastern CAOB are the Uda–Vitim island arc (Gordienko et al., 2010), the Tsagan-Zaba Complex in the Olkhon Terrane (Gladkochub et al., 2014) and the Dzhida Zone (Gordienko et al., 2006, 2007, 2015) of Transbaikalia. These complexes have been interpreted as parts of an island-arc system that bordered the southern

margin of the Siberian Craton (Gladkochub et al., 2014; Gordienko et al., 2006, 2010).

The second, separate group of arc-related magmatic bodies occurs in the eastern part of the Gorny Altai (Glorie et al., 2011; Kruk et al., 2007; Rudnev et al., 2008), considered as components of an Ediacaran–Cambrian island arc (named Kuznetsk-Altai arc) formed along the Siberian margin (Buslov et al., 2001, 2013; Dobretsov et al., 2004; Kruk et al., 2010, 2011; Ota et al., 2007). Fragments of island arcs of comparable age are also exposed in the Gornya Shoria and West Sayan (Rudnev et al., 2005, 2013a), in the Tannu-Ola Zone (*c.* 520 Ma, Mongush et al., 2011) and in the Kaakhem Batholith (563–535 Ma, Rudnev et al., 2006) of eastern Tuva (Fig. 18a).

A similar situation has been reported from other areas in western and southwestern Mongolia. In the Lake Zone, numerous island-arc complexes of Cambrian age have been described from the Kharanur and Sharatologoi plutons (Rudnev et al., 2009), Ureg Nuur area (Izokh et al., 2011), Bumbat-Hairhan Pluton, Bayan-Tsagaan-Nuur Ridge (Rudnev et al., 2012), Dariv Range (Kovalenko et al., 2014), Tugrik Pluton (Rudnev et al., 2013b) and the Bayan-Khairkhan Massif (Yarmolyuk et al., 2011).

Another similar age of *c.* 540 Ma from the Zamtyn Nuruu Complex (Fig. 19a) was interpreted as timing the intrusion of a primitive continental magmatic arc (Buriánek et al., 2017). Widespread and generally island-arc related magmatism in the Lake Zone took place during the Cambrian (*c.* 555–495 Ma), whereas at the western margin of the Lake Zone, a mid-Ordovician island-arc (*c.* 460 Ma) was recently found (Soejono et al., 2016).

Moreover, several studies of detrital zircons (dominant age peak at *c.* 520 Ma) from the Gorny Altai (Chen et al., 2015, 2016), Chinese Altai (Jiang et al., 2011; Long et al., 2010; Sun et al., 2008), Tseel (Jiang et al., 2012), Gobi Altai (Gibson et al., 2013) and the margin of the Baydrag microcontinent (Kröner et al., 2011) suggest an existence of a large Cambrian magmatic-arc system, both in western Mongolia and in the Gorny Altai.

However, it needs to be stressed that both ophiolite- and arc-related magmatic evolution of the units bordering the Precambrian Tuva-Mongolia, Zabkhan, and Baydrag microcontinental segments started at *c.* 570 Ma; however, the major period of the magmatic activity culminated at *c.* 510 Ma (Fig. 18b). In general, the late Neoproterozoic–Ordovician isotope province and corresponding crust-forming event were previously identified and well established in the central part of the CAOB (Kovalenko et al., 2004), the Lake Zone (Kovach et al., 2011) and Altay-Sayan region (Rudnev et al., 2013b). We suggest here, that the whole crust-forming event can be divided into two episodes (Dobretsov et al., 2003; Kozakov et al., 2013, 2015) and we focus here solely onto the younger, late Cambrian–Early Ordovician one.

Moreover, Neoproterozoic–Cambrian ophiolites and magmatic arc complexes have been described from the opposite side of the Baydrag

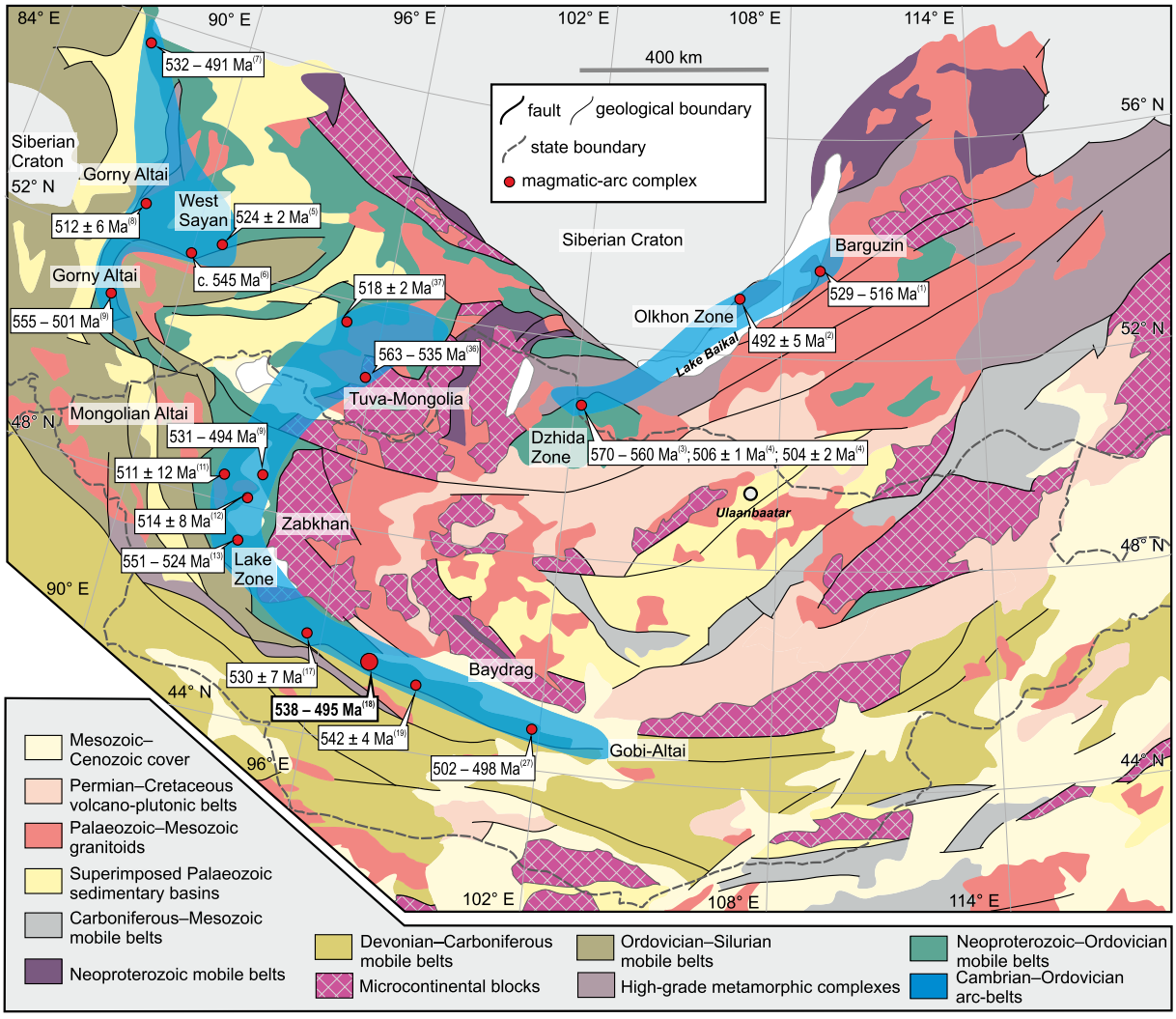

Fig. 17. Simplified tectonic map of the central CAOB depicting main lithotectonic domains (modified from Parfenov et al., 2003) and spatial distribution of Cambrian to Ordovician magmatic arcs; their zircon ages are also shown. Numbers in top-right corner of each box refer to references given in Fig. 18.

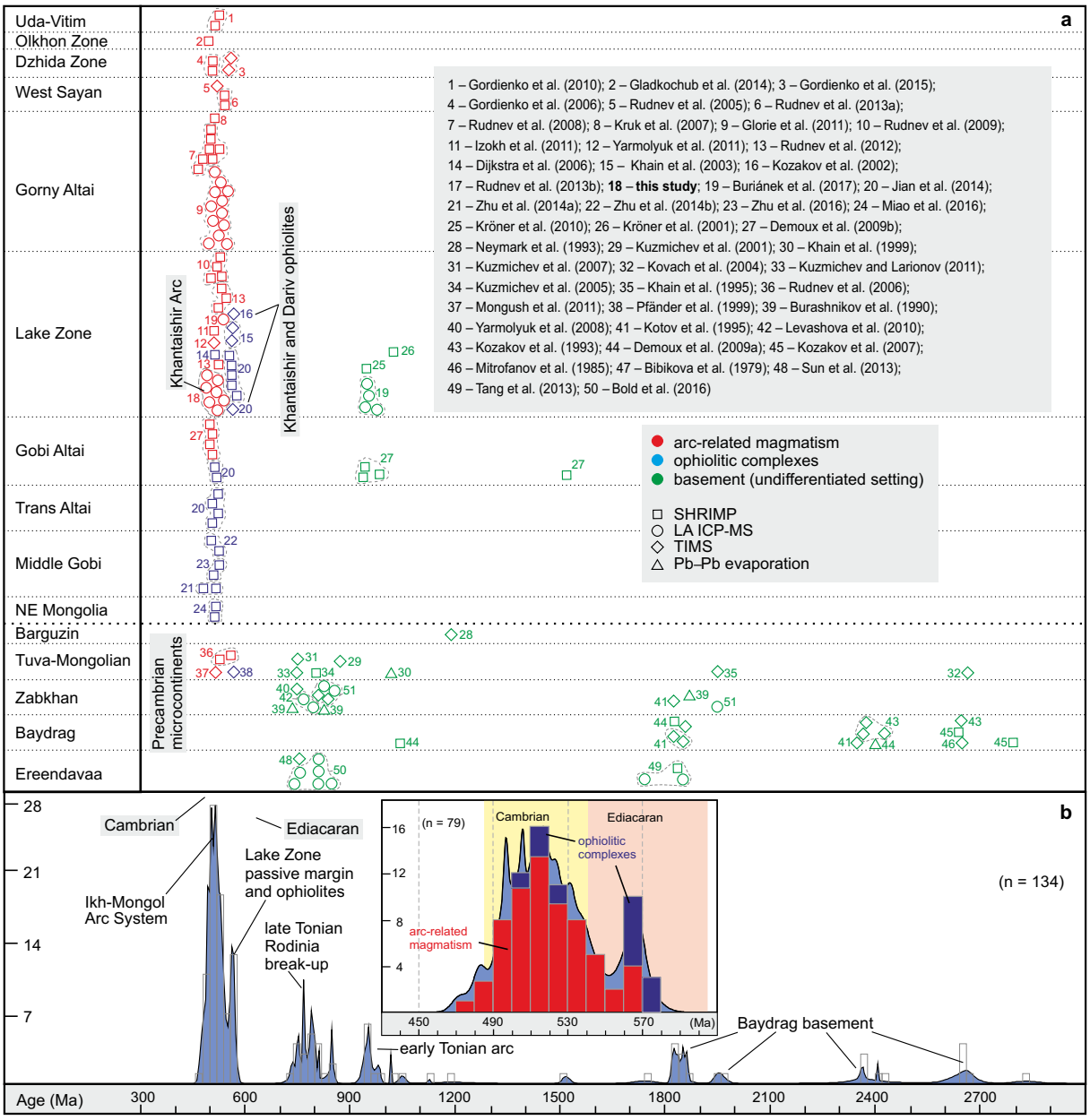

Fig. 18. (a) Correlation of U–Pb and Pb–Pb zircon ages arranged by individual microcontinents. For each, a range of basement ages, arc magmatism and ophiolites are given (in online version of this figure distinguished by colour). (b) – Frequency histograms and probability density plots of published zircon crystallization ages used in panel a, n – number of samples. Inset shows the detail of the main age peak. The density plots were produced by DensityPlotter (Vermeesch, 2012). Data sources: 1 – Gordienko et al. (2010); 2 – Gladkochub et al. (2014); 3 – Gordienko et al. (2015); 4 – Gordienko et al. (2006); 5 – Rudnev et al. (2005); 6 – Rudnev et al. (2013a); 7 – Rudnev et al. (2008); 8 – Kruk et al. (2007); 9 – Glorie et al. (2011); 10 – Rudnev et al. (2009); 11 – Izokh et al. (2011); 12 – Yarmolyuk et al. (2011); 13 – Rudnev et al. (2012); 14 – Dijkstra et al. (2006); 15 – Khain et al. (2003); 16 – Kozakov et al. (2002); 17 – Rudnev et al. (2013b); 18 – this study; 19 – Buriánek et al. (2017); 20 – Jian et al. (2014); 21 – Zhu et al. (2014a); 22 – Zhu et al. (2014b); 23 – Zhu et al. (2016); 24 – Miao et al. (2016); 25 – Kröner et al. (2010); 26 – Kröner et al. (2001); 27 – Demoux et al. (2009b); 28 – Neymark et al. (1993); 29 – Kuzmichev et al. (2001); 30 – Khain et al. (1999); 31 – Kuzmichev et al. (2007); 32 – Kovach et al. (2004); 33 – Kuzmichev and Larionov (2011); 34 – Kuzmichev et al. (2005); 35 – Khain et al. (1995); 36 – Rudnev et al. (2006); 37 – Mongush et al. (2011); 38 – Pfänder et al. (1999); 39 – Burashnikov (1990); 40 – Yarmolyuk et al. (2008); 41 – Kotov et al. (1995); 42 – Levashova et al. (2010); 43 – Kozakov et al. (1993); 44 – Demoux et al. (2009a); 45 – Kozakov et al. (2007); 46 – Mitrofanov et al. (1985); 47 – Bibikova et al. (1979); 48 – Sun et al. (2013); 49 – Tang et al. (2013); 50 – Bold et al. (2016).

Block as well (Demoux et al., 2009a; Kozakov et al., 2008, 2015; Jian et al., 2010; Kröner et al., 2011). This indicates the possible presence of an independent, (near?) contemporaneous and broadly parallel subduction zone there – again, this structure has not been a subject of the current study.

5.5. Synthesis and definition of the Ikh-Mongol Arc System

All the above data point to a major importance of ocean crust formation, subduction and associated magmatic activity within the Neoproterozoic and early Palaeozoic oceanic system of the central CAOB (Fig. 18a). Unfortunately, direct correlation of these dismembered complexes is difficult and thus a potential continuation from the KMC to the eastern–central parts of the CAOB is, in part, speculative. Still, the studied KMC fits well into a belt of Cambrian arc-related magmatic complexes in terms of its position, composition and age (Fig. 18a–b). This belt, >1800 km in length, borders the outer margin of the Mongolian Precambrian ribbon continent, defining the western, external part of the Mongolian orocline (Xiao et al., 2015 and references therein) (Fig. 17). The spatial distribution indicates that many of the Cambrian

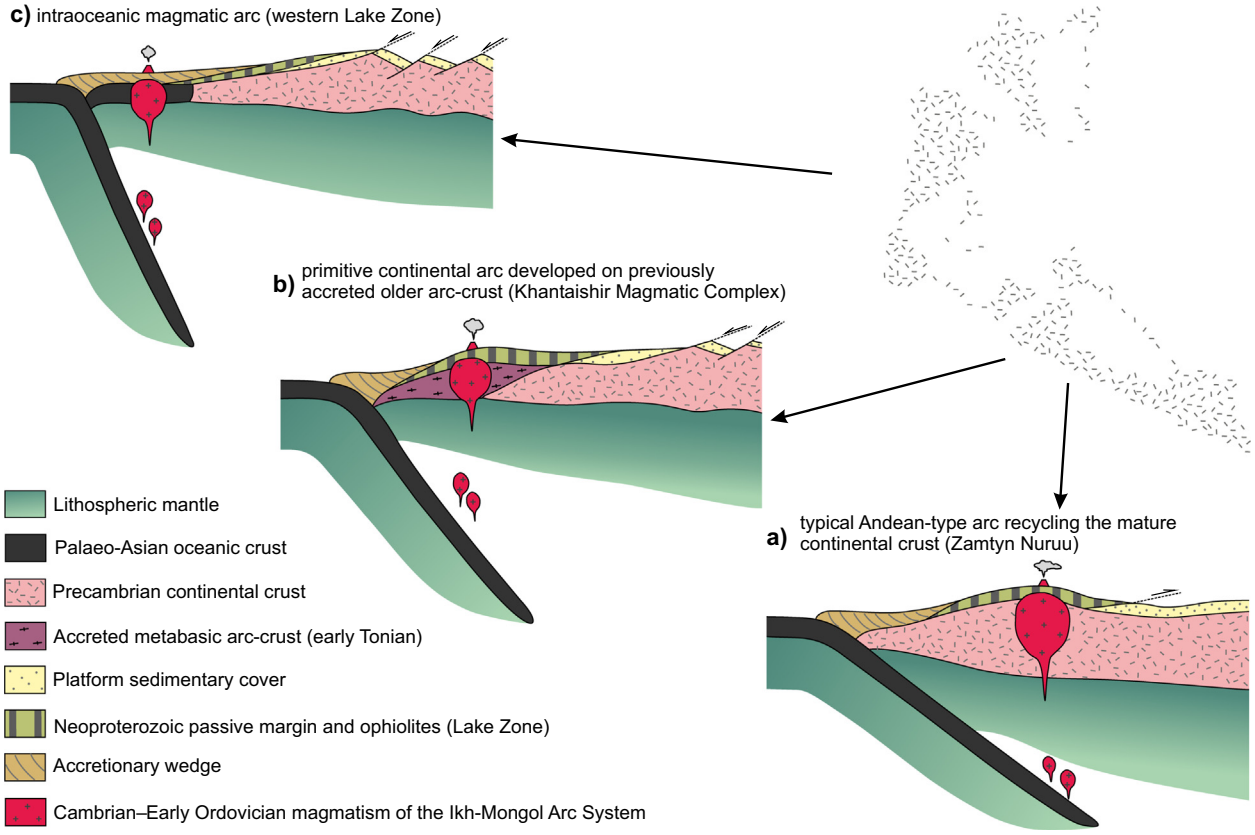

Fig. 19. Interpretative cross sections depicting different configurations of three known sections of the Ikh-Mongol Arc System. (a) Typical continental magmatic arc in the Zamtyn Nuruu founded on mature crust of the Baydrag Continent (Buriánek et al., 2017); (b) primitive continental arc developed on previously accreted older (early Tonian) arc in the Khantaishir Magmatic Complex (this study); (c) intraoceanic magmatic arc in the western Lake Zone (Rudnev et al., 2012; Soejono et al., 2016; Yarmolyuk et al., 2011).

to Ordovician magmatic complexes within this belt constituted a huge single subduction system.

This view agrees well with the concept of magmatic-arc systems, having operated in the Palaeo-Asian Ocean in late Neoproterozoic to Cambrian times (Dobretsov and Buslov, 2007; Şengör and Natal'in, 1996). Şengör et al. (1993) assumed the existence of a single and persistent Tuva-Mongol arc active over much of the early Palaeozoic. However, we argue that the main episode of magmatism and associated crustal growth was restricted to the interval of *c.* 530 to 490 Ma (Fig. 18b) and that the magmatic activity could have been related to a more complicated arc system, rather than to a single, continuous arc. Thus in order to avoid confusion, we coin the new term Ikh-Mongol Arc System for this giant Cambrian to early Ordovician structure.

In the quest for elucidating the petrogenesis of the Khantaishir segment of the Ikh-Mongol Arc System it is important to discuss the previous geological history of the Baydrag continental margin in the study area. There is growing evidence for an important early Tonian (*c.* 1000–850 Ma) subduction-related magmatism affecting the Palaeoproterozoic continental margin (Buriánek et al., 2017; Demoux et al., 2009b; Kozakov et al., 2014). In addition, the former authors showed that the Baydrag continental margin in the present-day Zamtyn Nuruu Range was the location of yet another (Cambrian) Andean-type subduction event. The magma sources of the Cambrian arc have been sought dominantly in the Palaeoproterozoic basement with a small contribution from the early Tonian arc (Fig. 19a).

Our data also fit a similar scenario; apart from the obvious mantle contribution, the KMC magmas also recycled the older, late Palaeoproterozoic mafic metaigneous arc crust (Fig. 19b). Based on Hf and Nd model ages, but lacking precise age data, we can only speculate that it could have been the same early Tonian Andean-type arc material as proposed by Buriánek et al. (2017). On the other hand, we found no evidence for Baydrag basement-derived detritus except for the migmatite in the roof of the KMC that contains *c.* 750 Ma igneous-looking zircons. Similar ages were reported from extension-related rhyolite–andesite volcanic suite of the Baydrag Continent by Levashova et al. (2010, 2011). Some authors interpreted such a bimodal, extension-related igneous activity as a testimony of Rodinia break-up (Dobretsov et al., 2003; Yarmolyuk et al., 2008; Kheraskova et al., 2010).

The new data presented here improve the scenario proposed by Buriánek et al. (2017, their Fig. 17). The probability age distribution for arc-derived magmatic rocks and ophiolite complexes (Fig. 18b) shows that the Baydrag Continent formed at 2.7 to 1.8 Ga, followed by early Tonian active margin magmatism at around 950–930 Ma and late Tonian volcanism related to the Rodinia break-up at 800–700 Ma.

More importantly, we see a strong concentration of ages between 600 and 480 Ma that define two peaks: a narrow Ediacaran (with a *c.* 570 Ma maximum) and a wide Cambrian (*c.* 510 Ma). The former is interpreted in terms of ophiolites formation, back-arc and oceanic-arc magmatism of short-lived supra-subduction marginal basins finally obducted onto the Baydrag Continent in early Cambrian times (Khain et al., 2003; Štípská et al., 2010). The latter reflects voluminous arc magmatism affecting the entire Tuva-Mongol, Zabkhan and Baydrag continental margin, including the newly accreted units of the Lake Zone with ca. 570 Ma ophiolites.

Therefore it seems likely that the late Proterozoic ophiolite sequences and Precambrian continents formed a single, unified tectonic unit before the intrusion of Ikh-Mongol Arc System (Sal'nikova et al., 2001; Kovach et al., 2011; Bold et al., 2016; Buriánek et al., 2017). Depending on the exact position, the arc acquired a character of a typical Andean arc recycling the mature Palaeoproterozoic continental crust (e.g., Zamtyn Nuruu, Fig. 19a), of a primitive continental arc developed on previously accreted older (?early Tonian) arc crust (Khantaishir

Magmatic Complex, Fig. 19b) or of a typical intraoceanic arc (western Lake Zone, Fig. 19c).

In general, this paper represents a cautionary tale; the character of subduction (intraoceanic vs. Andean-type), and thus of the magma sources, may change dramatically along strike of an arc. This has grave consequences for models of crustal recycling in that the remelted recently accreted mafic arc-type contributions would be difficult to recognize by conventional (Hf–Nd) isotopic approaches and could easily be mistaken for a juvenile input (Kröner et al., 2014, 2017).

The Ikh-Mongol Arc System magmatism affected different regions of an extended continental margin in Cambrian to Early Ordovician times (Fig. 19). This magmatism heralded the onset of slab roll-back, related extension and formation of a giant accretionary sedimentary wedge forming the future Mongol Altai Terrane (Xiao and Santosh, 2014; Xiao et al., 2009b). Taken together, the Cambro–Ordovician Ikh-Mongol Arc System magmatism and associated formation of a giant accretionary sedimentary wedge represented the most important period of crustal growth in the Tuva-Mongolian realm of the CAOB.

6. Conclusions

The newly described Cambrian Khantaishir Magmatic Complex (KMC) occurs in the eastern Khantaishir Range (south–central Mongolia). Combined petrological and whole-rock geochemical research, complemented by *in-situ* U–Pb zircon ages and Hf isotopic compositions, yielded the following conclusions:

1. The KMC exhibits a section from deeper, ultramafic cumulates (coarse-grained Amp gabbros and hornblendites; *c.* 0.35–0.5 GPa) to shallower crustal levels with intermediate rock types (mainly Amp–Bt tonalites; *c.* 0.1–0.2 GPa).
2. U–Pb zircon dating provides evidence for long-lived Cambrian (538 ± 3 to 494 ± 3 Ma) magmatism, whereby the dominant mafic plutons mostly preceded the subordinate felsic igneous activity.
3. The (normal-) calc-alkaline geochemical signature and a characteristic enrichment in large-ion lithophile elements (LILE: including Li, Rb, K, Sr, and Pb) and U with Th relative to the high-field strength elements (HFSE: Nb and Ta) indicate an origin within an igneous arc.
4. The lack of significant zircon inheritance in the magmatic products and rather primitive zircon ε_{Hf}^{t} values (> +3 but for most samples > +8), as well as whole-rock Sr–Nd isotopic compositions imply that the arc was not founded on mature continental crust.
5. Even for the tonalite with the least radiogenic Hf, the two-stage whole-rock Nd and *in-situ* Hf-in-zircon crustal model ages preclude partial melting of metabasic crust older than *c.* 1.5 Ga.
6. Multiple intrusions of mafic magmas developed by fractional crystallization and/or accumulation of (Ol, Cpx), Amp + Bt, later joined by plagioclase. An important role is also ascribed to the magma mixing and to the exchange of xenocrysts/antecrysts between compositionally different melt batches derived from depleted mantle and lower crustal metabasic sources (remelting of the early Tonian arc?).
7. The KMC is only a small fragment of a belt of Cambrian–Ordovician arc-related magmatic complexes exceeding 1800 km in length – termed here the Ikh-Mongol Arc System. It decorates the outer margin of a chain of Precambrian microcontinents (Tuva-Mongolia, Zabkhan and Baydrag) that, together with accreted late Neoproterozoic marginal basins (Lake Zone), defines the western, external part of the Mongolian orocline.
8. We argue that the Cambro–Ordovician was the most important period of crustal growth in the Mongolian tract of the CAOB.

Supplementary data to this article can be found online at https://doi.org/10.1016/j.gr.2017.10.003.

Acknowledgements

The authors would like to thank Jitka Míková (Czech Geological Survey, Prague) for assistance with the Sr–Nd isotopic separations and Petr Gadas (Masaryk University, Brno) for help with the electron-microprobe analyses. The manuscript was improved significantly by detailed reviews of Wenjiao Xiao and Victor Kovach, and benefited from careful editorial work of Shoujie Liu. This research was financially supported by the Czech Science Foundation (GAČR) (P210/12/2205 and 17-17540S). The International Partnership (132744KYSB20160005) and the 100 Talents programs of the Chinese Academy of Sciences (both to Y.D.J.) are also acknowledged. This paper is dedicated to Prof. O. Gerel on occasion of her 75th birthday.

References

Abdel-Rahman, A.M., 1994. Nature of biotites from alkaline, calc-alkaline and peraluminous magmas. Journal of Petrology 35, 525–541.
Alonso-Perez, R., Müntener, O., Ulmer, P., 2009. Igneous garnet and amphibole fractionation in the roots of island arcs: experimental constraints on andesitic liquids. Contributions to Mineralogy and Petrology 157, 541–558.
Andersen, D.J., Lindsley, D.H., Davidson, P.M., 1993. QUILF: a Pascal program to assess equilibria among Fe–Mg–Mn–Ti oxides, pyroxenes, olivine, and quartz. Computers & Geosciences 19, 1333–1350.
Annen, C., Blundy, J.D., Sparks, R.S.J., 2006. The genesis of intermediate and silicic magmas in deep crustal hot zones. Journal of Petrology 47, 505–539.
Arculus, R.J., 1987. The significance of source versus process in the tectonic controls of magma genesis. Journal of Volcanology and Geothermal Research 32, 1–12.
Arndt, N.T., Goldstein, S.L., 1989. An open boundary between lower continental crust and mantle: its role in crust formation and crustal recycling. Tectonophysics 161, 201–212.
Atherton, M., Petford, N., 1993. Generation of sodium-rich magmas from newly underplated basaltic crust. Nature 362, 144–146.
Badarch, G., Cunningham, W.D., Windley, B.F., 2002. A new terrane subdivision for Mongolia: implications for the Phanerozoic crustal growth of Central Asia. Journal of Asian Earth Sciences 21, 87–110.
Barbarin, B., 2005. Mafic magmatic enclaves and mafic rocks associated with some granitoids of the central Sierra Nevada Batholith, California: nature, origin, and relations with the hosts. Lithos 80, 155–177.
Bateman, R., 1995. The interplay between crystallization, replenishment and hybridization in large felsic magma chambers. Earth-Science Reviews 39, 91–106.
Beard, J.S., Ragland, P.C., Rushmer, T., 2004. Hydration crystallization reactions between anhydrous minerals and hydrous melt to yield amphibole and biotite in igneous rocks: description and implications. The Journal of Geology 112, 617–621.
Belousova, E.A., Kostitsyn, Y.A., Griffin, W.L., Begg, G.C., O'Reilly, S.Y., Pearson, N.J., 2010. The growth of the continental crust: constraints from zircon Hf-isotope data. Lithos 119, 457–466.
Bibikova, E.V., Gracheva, T.V., Makarov, V.A., Vorobjev, V.S., 1979. Geochronological borders for the southern part of East Transbaikalia from data of U–Pb method dating (in Russian). Geochimiya 2, 204–215.
Blichert-Toft, J., Albaréde, F., 1997. The Lu–Hf isotope geochemistry of chondrites and the evolution of the mantle–crust system. Earth and Planetary Science Letters 148, 243–258.
Bold, U., Crowley, J.L., Smith, E.F., Sambuu, O., Macdonald, F.A., 2016. Neoproterozoic to early Paleozoic tectonic evolution of the Zavkhan Terrane of Mongolia: implications for continental growth in the Central Asian Orogenic Belt. Lithosphere 8, 729–750.
Boynton, W.V., 1984. Cosmochemistry of the rare earth elements: meteorite studies. In: Henderson, P. (Ed.), Rare Earth Element Geochemistry. Elsevier, Amsterdam, pp. 63–114.
Buchan, C., Pfänder, J., Kröner, A., Brewer, T.S., Tomurtogoo, O., Tomurhuu, D., Cunningham, D., Windley, B.F., 2002. Timing of accretion and collisional deformation in the Central Asian Orogenic Belt: implications of granite geochronology in the Bayankhongor Ophiolite Zone. Chemical Geology 192, 23–45.
Burashnikov, V.V., 1990. Tectonics of the Urgamal Zone, Early Caledonides of Western Mongolia. Unpublished Ph.D. Thesis. Geological Institute, Russian Academy of Sciences, Moscow.
Buriánek, D., Schulmann, K., Hrdličková, K., Hanžl, P., Janoušek, V., Gerdes, A., Lexa, O., 2017. Geochemical and geochronological constraints on distinct early-Neoproterozoic and Cambrian accretionary events along southern margin of the Baydrag Continent in western Mongolia. Gondwana Research 47, 200–227.
Buslov, M.M., De Grave, J., 2015. Tectonics and geodynamics of the Altai-Sayan Foldbelt (southern Siberia). In: Kröner, A. (Ed.), The Central Asian Orogenic Belt. Beitrage zur regionalen Geologie der Erde vol. 32. Borntraeger Science Publishers, Stuttgart, pp. 93–154.
Buslov, M.M., Saphonova, I.Y., Watanabe, T., Obut, O.T., Fujiwara, Y., Iwata, K., Semakov, N.N., Sugai, Y., Smirnova, L.V., Kazansky, A.Y., 2001. Evolution of the paleo-Asian Ocean (Altai-Sayan region, Central Asia) and collision of possible Gondwana-derived terranes with the southern marginal part of the Siberian Continent. Geosciences Journal 5, 203–224.
Buslov, M.M., Geng, H., Travin, A.V., Otgonbaatar, D., Kulikova, A.V., Ming, C., Stijn, G., Semakov, N.N., Rubanova, E.S., Abildaeva, M.A., Voitishek, E.E., Trofimova, D.A., 2013. Tectonics and geodynamics of Gorny Altai and adjacent structures of the Altai-Sayan folded area. Russian Geology and Geophysics 54, 1250–1271.

Carswell, D.A., Compagnoni, R. (Eds.), 2003. Ultrahigh Pressure Metamorphism. EMU Notes in Mineralogy vol. 5. Eötvös University Press, Budapest.
Castro, A., Gerya, T.V., 2008. Magmatic implications of mantle wedge plumes: experimental study. Lithos 103, 138–148.
Castro, A., Vogt, K., Gerya, T., 2013. Generation of new continental crust by sublithospheric silicic-magma relamination in arcs: a test of Taylor's andesite model. Gondwana Research 23, 1554–1566.
Cervelli, P.F., Fournier, T.J., Freymueller, J.T., Power, J.A., Lisowski, M., Pauk, B.A., 2010. Geodetic constraints on magma movement and withdrawal during the 2006 eruption of Augustine Volcano. In: Power, J.A., Coombs, M.L., Freymueller, J.T. (Eds.), The 2006 Eruption of Augustine Volcano, Alaska. U.S. Geological Survey Professional Papers 1769, Reston, VA, pp. 427–452.
Chen, M., Sun, M., Buslov, M.M., Cai, K., Zhao, G.C., Zheng, J.P., Rubanova, E.S., Voytishek, E.E., 2015. Neoproterozoic–middle Paleozoic tectono-magmatic evolution of the Gorny Altai Terrane, northwest of the Central Asian Orogenic Belt: constraints from detrital zircon U–Pb and Hf-isotope studies. Lithos 233, 223–236.
Chen, M., Sun, M., Cai, K., Buslov, M.M., Zhao, G.C., Jiang, Y.D., Rubanova, E.S., Kulikova, A.V., Voytishek, E.E., 2016. The early Paleozoic tectonic evolution of the Russian Altai: implications from geochemical and detrital zircon U–Pb and Hf isotopic studies of meta-sedimentary complexes in the Charysh-Terekta-Ulagan-Sayan suture zone. Gondwana Research 34, 1–15.
Chopin, C., 1984. Coesite and pure pyrope in high-grade blueschists from western Alps: a first record and some consequences. Contributions to Mineralogy and Petrology 86, 107–118.
Claeson, D.T., 1998. Coronas, reaction rims, symplectites and emplacement depth of the Rymmen Gabbro, Transscandinavian igneous belt, southern Sweden. Mineralogical Magazine 62, 743–757.
Clemens, J.D., Stevens, G., 2012. What controls chemical variation in granitic magmas? Lithos 134–135, 317–329.
Condie, K.C., Kröner, A., 2013. The building blocks of continental crust: evidence for a major change in the tectonic setting of continental growth at the end of the Archean. Gondwana Research 23, 394–402.
Corfu, F., Hanchar, J.M., Hoskin, P.W.O., Kinny, P., 2003. Atlas of zircon textures. In: Hanchar, J.M., Hoskin, P.W.O. (Eds.), Zircon. Reviews in Mineralogy and Geochemistry 53. Mineralogical Society of America and Geochemical Society, Washington, pp. 469–503.
Cornejo, P.C., Mahood, G.A., 1997. Seeing past the effects of re-equilibration to reconstruct magmatic gradients in plutons: La Gloria Pluton, central Chilean Andes. Contributions to Mineralogy and Petrology 127, 159–175.
Davidson, J., Turner, S., Handley, H., Macpherson, C., Dosseto, A., 2007. Amphibole "sponge" in arc crust? Geology 35, 787–790.
Davidson, J., Turner, S., Plank, T., 2013. Dy/Dy*: variations arising from mantle sources and petrogenetic processes. Journal of Petrology 54, 525–537.
Davidson, J.P., Morgan, D.J., Charlier, B.L.A., Harlou, R., Hora, J.M., 2007. Microsampling and isotopic analysis of igneous rocks: implications for the study of magmatic systems. Annual Review of Earth and Planetary Sciences 35, 273–311.
Debon, F., Le Fort, P., 1983. A chemical–mineralogical classification of common plutonic rocks and associations. Transactions of the Royal Society of Edinburgh, Earth Sciences 73, 135–149.
Deering, C.D., Bachmann, O., 2010. Trace element indicators of crystal accumulation in silicic igneous rocks. Earth and Planetary Science Letters 297, 324–331.
Demoux, A., Kröner, A., Badarch, G., Jian, P., Tomurhuu, D., Wingate, M.T.D., 2009a. Zircon ages from the Baydrag Block and the Bayankhongor Ophiolite Zone: time constraints on late Neoproterozoic to Cambrian subduction- and accretion-related magmatism in Central Mongolia. The Journal of Geology 117, 377–397.
Demoux, A., Kröner, A., Liu, D., Badarch, G., 2009b. Precambrian crystalline basement in southern Mongolia as revealed by SHRIMP zircon dating. International Journal of Earth Sciences 98, 1365–1380.
DePaolo, D.J., 1981. Trace element and isotopic effects of combined wallrock assimilation and fractional crystallization. Earth and Planetary Science Letters 53, 189–202.
Dergunov, A.B. (Ed.), 2001. Tectonics, Magmatism, and Metallogeny of Mongolia. Routledge, London and New York.
Dessimoz, M., Müntener, O., Ulmer, P., 2012. A case for hornblende dominated fractionation of arc magmas: the Chelan Complex (Washington Cascades). Contributions to Mineralogy and Petrology 163, 567–589.
Didier, J., Barbarin, B. (Eds.), 1991a. Enclaves and Granite Petrology. Elsevier, Amsterdam.
Didier, J., Barbarin, B., 1991b. The different types of enclaves in granites – nomenclature. In: Didier, J., Barbarin, B. (Eds.), Enclaves and Granite Petrology. Elsevier, Amsterdam, pp. 19–24.
Dijkstra, A.H., Brouwer, F.M., Cunningham, W.D., Buchan, C., Badarch, G., Mason, P.R.D., 2006. Late Neoproterozoic proto-arc ocean crust in the Dariv Range, Western Mongolia: a supra-subduction zone end-member ophiolite. Journal of the Geological Society (London) 163, 363–373.
Dobretsov, N.L., Buslov, M.M., 2007. Late Cambrian–Ordovician tectonics and geodynamics of Central Asia. Russian Geology and Geophysics 48, 71–82.
Dobretsov, N.L., Buslov, M.M., Vernikovsky, V.A., 2003. Neoproterozoic to Early Ordovician evolution of the Paleo-Asian Ocean: implications to the break-up of Rodinia. Gondwana Research 6, 143–159.
Dobretsov, N.L., Buslov, M.M., Yu, U., 2004. Fragments of oceanic islands in accretion–collision areas of Gorny Altai and Salair, southern Siberia, Russia: early stages of continental crustal growth of the Siberian Continent in Vendian–early Cambrian time. Journal of Asian Earth Sciences 23, 673–690.
Dobrzhinetskaya, L.F., Faryad, S.W., Wallis, S., Cuthbert, S. (Eds.), 2011. Ultra-high Pressure Metamorphism. 25 years After the Discovery of Coesite and Diamond. Elsevier, Amsterdam.
Domeier, M., Torsvik, T.H., 2014. Plate tectonics in the late Paleozoic. Geoscience Frontiers 5, 303–350.
Droop, G.T.R., 1987. A general equation for estimating Fe^{3+} concentrations in ferromagnesian silicates using stoichiometric criteria. Mineralogical Magazine 51, 431–435.
Dufek, J., Bergantz, G.W., 2005. Lower crustal magma genesis and preservation: a stochastic framework for the evaluation of basalt–crust interaction. Journal of Petrology 46, 2167–2195.
Dymkova, D., Gerya, T., Burg, J.P., 2016. 2D thermomechanical modelling of continent–arc–continent collision. Gondwana Research 32, 138–150.
Förster, H.-J., Tischendorf, G., Trumbull, R.B., 1997. An evaluation of the Rb vs. (Y + Nb) discrimination diagram to infer tectonic setting of silicic igneous rocks. Lithos 40, 261–293.
Gibson, T.M., Myrow, P.M., Macdonald, F.A., Minjin, C., Gehrels, G.E., 2013. Depositional history, tectonics, and detrital zircon geochronology of Ordovician and Devonian strata in southwestern Mongolia. GSA Bulletin 125, 877–893.
Gladkochub, D.P., Donskaya, T.V., Wingate, M.T.D., Poller, U., Kröner, A., Fedorovsky, V.S., Mazukabzov, A.M., Todt, W., Pisarevsky, S.A., 2008. Petrology, geochronology, and tectonic implications of c. 500 Ma metamorphic and igneous rocks along the northern margin of the Central Asian Orogen (Olkhon Terrane, Lake Baikal, Siberia). Journal of the Geological Society (London) 165, 235–246.
Gladkochub, D.P., Donskaya, T.V., Fedorovskii, V.S., Mazukabzov, A.M., Sklyarov, E.V., Lavrenchuk, A.V., Lepekhina, E.N., 2014. Fragment of the early Paleozoic (~500 Ma) island arc in the structure of the Olkhon Terrane, Central Asian fold belt. Doklady Earth Sciences 457, 905–909.
Glorie, S., De Grave, J., Buslov, M.M., Zhimulev, F.I., Izmer, A., Vandoorne, W., Ryabinin, A., van den Haute, P., Vanhaecke, F., Elburg, M.A., 2011. Formation and Palaeozoic evolution of the Gorny-Altai–Altai-Mongolia suture zone (South Siberia): zircon U/Pb constraints on the igneous record. Gondwana Research 20, 465–484.
Goldstein, S.L., O'Nions, R.K., Hamilton, P.J., 1984. A Sm–Nd isotopic study of atmospheric dusts and particulates from major river systems. Earth and Planetary Science Letters 70, 221–236.
Gordienko, I.V., Kovach, V.P., Gorokhovsky, D.V., Plotkina, Y.V., 2006. Composition, U–Pb age, and geodynamic setting of island-arc gabbroids and granitoids of the Dzhida Zone. Russian Geology and Geophysics 47, 948–955.
Gordienko, I.V., Filimonov, A.V., Minina, O.R., Gornova, M.A., Medvedev, A.Y., Klimuk, V.S., Elbaev, A.L., Tomurtogoo, O., 2007. Dzhida island-arc system in the Paleoasian Ocean: structure and main stages of Vendian–Paleozoic geodynamic evolution. Russian Geology and Geophysics 48, 91–106.
Gordienko, I.V., Bulgatov, A.N., Ruzhentsev, S.V., Minina, O.R., Klimuk, V.S., Vetluzhskikh, L.I., Nekrasov, G.E., Lastochkin, N.I., Sitnikova, V.S., Metelkin, D.V., Goneger, T.A., Lepekhina, E.N., 2010. The late Riphean–Paleozoic history of the Uda-Vitim island arc system in the Transbaikalian sector of the Paleoasian Ocean. Russian Geology and Geophysics 51, 461–481.
Gordienko, I.V., Gorokhovskiy, D.V., Elbaev, A.L., Bayanova, T.B., 2015. New data on the early Paleozoic gabbroid and granitoid magmatism age within the Dzhida Zone of Caledonides (southwestern Transbaikalia, North Mongolia). Doklady Earth Sciences 463, 817–821.
Griffin, W.L., Pearson, N.J., Belousova, E., Jackson, S.E., van Achterbergh, E., O'Reilly, S.Y., Shee, S.R., 2000. The Hf isotope composition of cratonic mantle: LAM-MC-ICPMS analysis of zircon megacrysts in kimberlites. Geochimica et Cosmochimica Acta 64, 133–147.
Grove, T.L., Till, C.B., Krawczynski, M.J., 2012. The role of H_2O in subduction zone magmatism. Annual Review of Earth and Planetary Sciences 40, 413–439.
Guy, A., Schulmann, K., Janoušek, V., Štípská, P., Armstrong, R., Belousova, E., Dolgopolova, A., Seltmann, R., Lexa, O., Jiang, Y., Hanžl, P., 2015. Geophysical and geochemical nature of relaminated arc-derived lower crust underneath oceanic domain in southern Mongolia. Tectonics 34, 1030–1053.
Hacker, B.R., Kelemen, P.B., Behn, M.D., 2011. Differentiation of the continental crust by relamination. Earth and Planetary Science Letters 307, 501–516.
Hacker, B.R., Kelemen, P.B., Behn, M.D., 2015. Continental lower crust. Annual Review of Earth and Planetary Sciences 43, 167–205.
Hart, S.R., Dunn, T., 1993. Experimental Cpx/melt partitioning of 24 trace elements. Contributions to Mineralogy and Petrology 113, 1–8.
Hibbard, M.J., 1991. Textural anatomy of twelve magma-mixed granitoid systems. In: Didier, J., Barbarin, B. (Eds.), Enclaves and Granite Petrology. Elsevier, Amsterdam, pp. 431–444.
Hibbard, M.J., 1995. Mixed magma rocks. Petrography to Petrogenesis. Prentice Hall, New Jersey, pp. 242–260.
Hildreth, W., Moorbath, S., 1988. Crustal contributions to arc magmatism in the Andes of Central Chile. Contributions to Mineralogy and Petrology 98, 455–489.
Holland, T.J.B., Blundy, J.D., 1994. Non-ideal interactions in calcic amphiboles and their bearing on amphibole–plagioclase thermometry. Contributions to Mineralogy and Petrology 116, 433–447.
Hrdličková, K., Gerdes, A., Gilíková, H., Bat-Ulzii, D., Hanžl, P., 2010. Burd Gol Granite Massif as a product of the late Cambrian post-orogenic magmatism in the SE part of the Lake Zone, Gobi Altay, SW Mongolia. Journal of Geosciences 55, 369–386.
Huppert, H.E., Sparks, R.S.J., 1988. The generation of granitic magmas by intrusion of basalt into continental crust. Journal of Petrology 29, 599–624.
Hutchison, C.S., 1975. The norm, its variations, their calculation and relationships. Schweizerische Mineralogische und Petrographische Mitteilungen 55, 243–256.
Izokh, A.E., Vishnevskii, A.V., Polyakov, G.V., Shelepaev, R.A., 2011. Age of picrite and picrodolerite magmatism in western Mongolia. Russian Geology and Geophysics 52, 7–23.
Jacobsen, S.B., Wasserburg, G.J., 1980. Sm–Nd isotopic evolution of chondrites. Earth and Planetary Science Letters 50, 139–155.

Jagoutz, O., Behn, M.D., 2013. Foundering of lower island-arc crust as an explanation for the origin of the continental Moho. Nature 504, 131–134.
Jagoutz, O., Kelemen, P.B., 2015. Role of arc processes in the formation of continental crust. Annual Review of Earth and Planetary Sciences 43, 363–404.
Jagoutz, O., Schmidt, M.W., 2012. The formation and bulk composition of modern juvenile continental crust: the Kohistan arc. Chemical Geology 298–299, 79–96.
Janoušek, V., 2006. *Saturnin*, R language script for application of accessory-mineral saturation models in igneous geochemistry. Geologica Carpathica 57, 131–142.
Janoušek, V., Moyen, J.F., 2014. Mass balance modelling of magmatic processes in *GCDkit*. In: Kumar, S., Singh, R.N. (Eds.), Modelling of Magmatic and Allied Processes. Society of Earth Scientists Series 83. Springer, Berlin, pp. 225–238.
Janoušek, V., Bowes, D.R., Rogers, G., Farrow, C.M., Jelínek, E., 2000. Modelling diverse processes in the petrogenesis of a composite batholith: the Central Bohemian Pluton, Central European Hercynides. Journal of Petrology 41, 511–543.
Janoušek, V., Braithwaite, C.J.R., Bowes, D.R., Gerdes, A., 2004. Magma-mixing in the genesis of Hercynian calc-alkaline granitoids: an integrated petrographic and geochemical study of the Sázava intrusion, Central Bohemian Pluton, Czech Republic. Lithos 78, 67–99.
Janoušek, V., Farrow, C.M., Erban, V., 2006. Interpretation of whole-rock geochemical data in igneous geochemistry: introducing Geochemical Data Toolkit (GCDkit). Journal of Petrology 47, 1255–1259.
Janoušek, V., Konopásek, J., Ulrich, S., Erban, V., Tajčmanová, L., Jeřábek, P., 2010. Geochemical character and petrogenesis of Pan-African Amspoort suite of the Boundary Igneous Complex in the Kaoko Belt (NW Namibia). Gondwana Research 18, 688–707.
Janoušek, V., Moyen, J.F., Martin, H., Erban, V., Farrow, C., 2016. Geochemical Modelling of Igneous Processes – Principles and Recipes in R Language. Bringing the Power of R to a Geochemical Community. Springer-Verlag, Berlin, Heidelberg.
Jian, P., Kröner, A., Windley, B.F., Shi, Y., Zhang, F., Miao, L., Tomurhuu, D., Zhang, W., Liu, D., 2010. Zircon ages of the Bayankhongor ophiolite mélange and associated rocks: time constraints on Neoproterozoic to Cambrian accretionary and collisional orogenesis in Central Mongolia. Precambrian Research 177, 162–180.
Jian, P., Kröner, A., Jahn, B.M., Windley, B.F., Shi, Y., Zhang, W., Zhang, F., Miao, L., Tomurhuu, D., Liu, D., 2014. Zircon dating of Neoproterozoic and Cambrian ophiolites in West Mongolia and implications for the timing of orogenic processes in the central part of the Central Asian Orogenic Belt. Earth-Science Reviews 133, 62–93.
Jiang, Y.D., Sun, M., Zhao, G.C., Yuan, C., Xiao, W.J., Xia, X.P., Long, X.P., Wu, F.Y., 2011. Precambrian detrital zircons in the early Paleozoic Chinese Altai: their provenance and implications for the crustal growth of central Asia. Precambrian Research 189, 140–154.
Jiang, Y.D., Sun, M., Kröner, A., Tumurkhuu, D., Long, X.P., Zhao, G.C., Yuan, C., Xiao, W.J., 2012. The high-grade Tseel Terrane in SW Mongolia: an early Paleozoic arc system or a Precambrian sliver? Lithos 142–143, 95–115.
Johnson, K.T.M., 1998. Experimental determination of partition coefficients for rare earth and high-field-strength elements between clinopyroxene, garnet, and basaltic melt at high pressures. Contributions to Mineralogy and Petrology 133, 60–68.
Kay, R.W., Kay, S.M., 1993. Delamination and delamination magmatism. Tectonophysics 219, 177–189.
Kelemen, P.B., 1995. Genesis of high Mg# andesites and the continental crust. Contributions to Mineralogy and Petrology 120, 1–19.
Kelemen, P.B., Behn, M.D., 2016. Formation of lower continental crust by relamination of buoyant arc lavas and plutons. Nature Geoscience 9, 197–205.
Kemp, A.I.S., Hawkesworth, C.J., 2014. 4.11 – growth and differentiation of the continental crust from isotope studies of accessory minerals. In: Holland, H.D., Turekian, K.K. (Eds.), Treatise on Geochemistry, Second Edition Elsevier, Oxford, pp. 379–421.
Khain, E.V., Neimark, L.A., Amelin Yu, V., 1995. The Caledonian stage of remobilization of the Precambrian basement of the Gargan block, the Eastern Sayan (isotopic geochronological data) (in Russian). Doklady Akademii Nauk 342, 776–780.
Khain, E.V., Bibikova, E.V., Degtyarev, K., Gibsher, A.S., Didenko, A.N., Klochko, A.N., Rytsk, E.Y., Sal'nikova, E.B., Fedotova, A.A., 1999. The Paleo-Asian Ocean in the Neoproterozoic and early Paleozoic: new isotope geochronological data. Geological Development of Proterozoic Pericratonic and Palaeoceanic Structures of Northern Eurasia, pp. 175–181 Abstract Volume. St. Petersburg.
Khain, E.V., Bibikova, E.V., Sal'ikova, E.B., Kröner, A., Gibsher, A.S., Didenko, A.N., Degtyarev, K.E., Fedotova, A.A., 2003. The Palaeo-Asian Ocean in the Neoproterozoic and early Palaeozoic: new geochronologic data and palaeotectonic reconstructions. Precambrian Research 122, 329–358.
Kheraskova, T.N., Bush, V.A., Didenko, A.N., Samygin, S.G., 2010. Breakup of Rodinia and early stages of evolution of the Paleoasian Ocean. Geotectonics 44, 3–24.
Kohn, M.J., Corrie, S.L., Markley, C., 2015. The fall and rise of metamorphic zircon. American Mineralogist 100, 897–908.
Košler, J., Sylvester, P.J., 2003. Present trends and the future of zircon in geochronology: Laser ablation ICPMS. In: Hanchar, J.M., Hoskin, P.W.O. (Eds.), Zircon. Reviews in Mineralogy and Geochemistry 53. Mineralogical Society of America and Geochemical Society, Washington, pp. 243–275.
Košler, J., Fonneland, H., Sylvester, P.J., Tubrett, M., Pedersen, R.B., 2002. U–Pb dating of detrital zircons for sediment provenance studies – a comparison of laser ablation ICPMS and SIMS techniques. Chemical Geology 182, 605–618.
Kotov, A.B., Kozakov, I.K., Bibikova, E.V., Sal'nikova, E.B., Kirnozova, T.I., Kovach, V.P., 1995. Duration of regional metamorphic episodes in areas of polycyclic endogenic processes – a U–Pb geochronological study (in Russian). Petrology 3, 567–575.
Kovach, V.P., Matukov, D.I., Berezhnaya, N.G., 2004. Tectonics of Precambrian mobile belts. The 32nd IGC Florence, Session: T31.01. 1263.
Kovach, V.P., Yarmolyuk, V.V., Kovalenko, V.I., Kozlovskyi, A.M., Kotov, A.B., Terent'eva, L.B., 2011. Composition, sources, and mechanisms of formation of the continental crust of the Lake Zone of the Central Asian Caledonides. II. Geochemical and Nd isotope data. Petrology 19, 399–425.
Kovalenko, D.V., Mongush, A.A., Ageeva, O.A., Eenzhin, G., 2014. Sources and geodynamic environments of formation of Vendian–early Paleozoic magmatic complexes in the Daribi Range, Western Mongolia. Petrology 22, 389–417.
Kovalenko, V.I., Yarmolyuk, V.V., Kovach, V.P., Kotov, A.B., Kozakov, I.K., Sal'nikova, E.B., Larin, A.M., 2004. Isotope provinces, mechanisms of generation and sources of the continental crust in the Central Asian mobile belt: geological and isotopic evidence. Journal of Asian Earth Sciences 23, 605–627.
Kozakov, I.K., Bibikova, E., Neymark, L.A., Kimozova, T.I., 1993. The Baydaric Block. In: Rudnik, B.A., Sokolov, Y.M., Filatova, L.I. (Eds.), The Early Precambrian of the Central Asian Fold Belt. Nauka, St. Petersburg, pp. 118–137.
Kozakov, I.K., Sal'nikova, E.B., Khain, E.V., Kovach, V.P., Berezhnaya, N.G., Yakovleva, S.Z., Plotkina, Y.V., 2002. Early Caledonian crystalline rocks of the Lake Zone in Mongolia: formation history and tectonic settings as deduced from U–Pb and Sm–Nd datings. Geotectonics 36, 156–166.
Kozakov, I.K., Sal'nikova, E.B., Wang, T., Didenko, A.N., Plotkina, Y., Podkovyrov, V.N., 2007. Early Precambrian crystalline complexes of the Central Asian microcontinent: age, sources, tectonic position. Stratigraphy and Geological Correlation 15, 121–140.
Kozakov, I.K., Sal'nikova, E.B., Kovach, V.P., Yarmolyuk, V.V., Anisimova, I.V., Kozlovskii, A.M., Plotkina, Y.V., Myskova, T.A., Fedoseenko, A.M., Yakovleva, S.Z., Sugorakova, A.M., 2008. Vendian stage in formation of the early Caledonian superterrane in Central Asia. Stratigraphy and Geological Correlation 16, 360–382.
Kozakov, I.K., Sal'nikova, E.B., Yarmolyuk, V.V., Kovach, V.P., Kozlovskii, A.M., Anisimova, I.V., Plotkina, Y., Fedoseenko, A.M., Yakovleva, S.Z., Erdenezhargal, C., 2013. Crustal growth stages in the Songino block of the Early Caledonian superterrane in Central Asia: I. Geological and geochronological data. Petrology 21, 203–220.
Kozakov, I.K., Kovach, V.P., Bibikova, E.V., Kirnozova, T.I., Lykhin, D.A., Plotkina, Y., Tolmacheva, E.V., Fugzan, M.M., Erdenezhargal, C., 2014. Late Riphean episode in the formation of crystalline rock complexes in the Dzabkhan microcontinent: geological, geochronologic, and Nd isotopic-geochemical data. Petrology 22, 480–506.
Kozakov, I.K., Kovach, V.P., Yakovleva, S.Z., Anisimova, I.V., Kozlovsky, A.M., Fedoseenko, A.M., 2015. Main stages in the evolution and geodynamic setting of the South Hangay Metamorphic Belt, Central Asia. Petrology 23, 309–330.
Kröner, A., Tomurtogoo, O., Badarch, G., Windley, B.F., Kozakov, I.K., 2001. New zircon ages and significance for crustal evolution in Mongolia. In: Sklyarov, E.V. (Ed.), IGCP-440 Workshop, Guidebook and Abstract Volume. Irkutsk, pp. 142–145.
Kröner, A., Windley, B.F., Badarch, G., Tomurtogoo, O., Hegner, E., Jahn, B.M., Gruschka, S., Khain, E.V., Demoux, A., Wingate, M.T.D., 2007. Accretionary growth and crust formation in the Central Asian Orogenic Belt and comparison with the Arabian-Nubian Shield. In: Hatcher Jr., R.D., Carlson, M.P., McBride, J.H., Martínez Catalán, J.R. (Eds.), 4-D Framework of Continental Crust. Geological Society of America Memoirs 200, pp. 181–209.
Kröner, A., Lehmann, J., Schulmann, K., Demoux, A., Lexa, O., Tomurhuu, D., Štípská, P., Liu, D., Wingate, M.T.D., 2010. Lithostratigraphic and geochronological constraints on the evolution of the Central Asian Orogenic Belt in SW Mongolia: early Paleozoic rifting followed by late Paleozoic accretion. American Journal of Science 310, 523–574.
Kröner, A., Demoux, A., Zack, T., Rojas-Agramonte, Y., Jian, P., Tomurhuu, D., Barth, M., 2011. Zircon ages for a felsic volcanic rock and arc-related early Palaeozoic sediments on the margin of the Baydrag microcontinent, Central Asian Orogenic Belt, Mongolia. Journal of Asian Earth Sciences 42, 1008–1017.
Kröner, A., Kovach, V., Belousova, E., Hegner, E., Armstrong, R., Dolgopolova, A., Seltmann, R., Alexeiev, D.V., Hoffmann, J.E., Wong, J., Sun, M., Cai, K., Wang, T., Tong, Y., Wilde, S.A., Degtyarev, K.E., Rytsk, E., 2014. Reassessment of continental growth during the accretionary history of the Central Asian Orogenic Belt. Gondwana Research 25, 103–125.
Kröner, A., Kovach, V., Alexeiev, D., Wang, K.L., Wong, J., Degtyarev, K., Kozakov, I., 2017. No excessive crustal growth in the Central Asian Orogenic Belt: further evidence from field relationships and isotopic data. Gondwana Research 50, 135–166.
Kruk, N.N., Rudnev, S.N., Shokalsky, S.P., Babin, G.A., Kubida, M.L., Lepekhina, E.N., Kovach, V.P., 2007. Age and tectonic position of plagiogranites of Sarakoksha Massif (Altai Mountains) (in Russian). Litosfera 137–146.
Kruk, N.N., Vladimirov, A.G., Babin, G.A., Shokalsky, S.P., Sennikov, N.V., Rudnev, S.N., Volkova, N.I., Kovach, V.P., Serov, P.A., 2010. Continental crust in Gorny Altai: nature and composition of protoliths. Russian Geology and Geophysics 51, 431–446.
Kruk, N.N., Rudnev, S.N., Vladimirov, A.G., Shokal'sky, S.P., Kovach, V.P., Serov, P.A., Volkova, N.I., 2011. Early–middle Paleozoic granitoids in Gorny Altai, Russia: implications for continental crust history and magma sources. Journal of Asian Earth Sciences 42, 928–948.
Kusbach, V., Janoušek, V., Hasalová, P., Schulmann, K., Fanning, C.M., Erban, V., Ulrich, S., 2015. Importance of crustal relamination in origin of the orogenic mantle peridotite–high-pressure granulite association: example from the Náměšť Granulite Massif (Bohemian Massif, Czech Republic). Journal of the Geological Society (London) 172, 479–490.
Kuzmichev, A.B., Larionov, A.N., 2011. The Sarkhoi Group in East Sayan: Neoproterozoic (~770–800 Ma) volcanic belt of the Andean type. Russian Geology and Geophysics 52, 685–700.
Kuzmichev, A.B., Bibikova, E.V., Zhuravlev, D.Z., 2001. Neoproterozoic (~800 Ma) orogeny in the Tuva-Mongolia Massif (Siberia): island arc–continent collision at the northeast Rodinia margin. Precambrian Research 110, 109–126.
Kuzmichev, A.B., Kröner, A., Hegner, E., Dunyi, L., Yusheng, W., 2005. The Shishkhid ophiolite, northern Mongolia: a key to the reconstruction of a Neoproterozoic island-arc system in central Asia. Precambrian Research 138, 125–150.
Kuzmichev, A.B., Sklyarov, E., Postnikov, A., Bibikova, E., 2007. The Oka Belt (Southern Siberia and northern Mongolia): a Neoproterozoic analog of the Japanese Shimanto Belt? Island Arc 16, 224–242.
Lamb, M.A., Badarch, G., 2001. Paleozoic sedimentary basins and volcanic arc systems of southern Mongolia: new geochemical and petrographic constraints. In: Hendrix,

S.M., Davis, A.G. (Eds.), Paleozoic and Mesozoic Tectonic Evolution of Central and Eastern Asia: From Continental Assembly to Intracontinental Deformation. Geological Society of America Memoirs 194, pp. 117–149.
Lancaster, P.J., Storey, C.D., Hawkesworth, C.J., Dhuime, B., 2011. Understanding the roles of crustal growth and preservation in the detrital zircon record. Earth and Planetary Science Letters 305, 405–412.
Larrea, P., França, Z., Lago, M., Widom, E., Galé, C., Ubide, T., 2013. Magmatic processes and the role of antecrysts in the genesis of Corvo Island (Azores Archipelago, Portugal). Journal of Petrology 54, 769–793.
Leake, B.E., Woolley, A.R., Arps, C.E.S., Birch, W.D., Gilbert, M.C., Grice, J.D., Hawthorne, F.C., Kato, A., Kisch, H.J., Krivovichev, V.G., Linthout, K., Laird, J., Mandarino, J., Maresch, W.V., Nickel, E.H., Rock, N.M.S., Schumacher, J.C., Smith, J.C., Stephenson, N.C.N., Whittaker, E.J.W., Youzhi, G., 1997. Nomenclature of amphiboles: report of the Subcommittee on Amphiboles of the International Mineralogical Association Commission on New Minerals and Mineral Names. Mineralogical Magazine 61, 295–321.
Lee, C.T., Anderson, D.L., 2015. Continental crust formation at arcs, the arclogite 'delamination' cycle, and one origin for fertile melting anomalies in the mantle. Science Bulletin 60, 1141–1156.
Lee, C.T., Bachmann, O., 2014. How important is the role of crystal fractionation in making intermediate magmas? Insights from Zr and P systematics. Earth and Planetary Science Letters 393, 266–274.
Lehmann, J., Schulmann, K., Lexa, O., Corsini, M., Kröner, A., Štípská, P., Tomurhuu, D., Otgonbator, D., 2010. Structural constraints on the evolution of the Central Asian Orogenic Belt in SW Mongolia. American Journal of Science 310, 575–628.
Levashova, N.M., Kalugin, V.M., Gibsher, A.S., Yff, J., Ryabinin, A.B., Meert, J.G., Malone, S.J., 2010. The origin of the Baydaric microcontinent, Mongolia: constraints from paleomagnetism and geochronology. Tectonophysics 485, 306–320.
Levashova, N.M., Meert, J.G., Gibsher, A.S., Grice, W.C., Bazhenov, M.L., 2011. The origin of microcontinents in the Central Asian Orogenic Belt: constraints from paleomagnetism and geochronology. Precambrian Research 185, 37–54.
Liew, T.C., Hofmann, A.W., 1988. Precambrian crustal components, plutonic associations, plate environment of the Hercynian Fold Belt of Central Europe: indications from a Nd and Sr isotopic study. Contributions to Mineralogy and Petrology 98, 129–138.
Long, X.P., Yuan, C., Sun, M., Xiao, W.J., Zhao, G.C., Wang, Y.J., Cai, K., Xia, X.P., Xie, L.W., 2010. Detrital zircon ages and Hf isotopes of the early Paleozoic flysch sequence in the Chinese Altai, NW China: new constrains on depositional age, provenance and tectonic evolution. Tectonophysics 480, 213–231.
Lu, Z., Dzurisin, D., Biggs, J., Wicks, C., McNutt, S., 2010. Ground surface deformation patterns, magma supply, and magma storage at Okmok volcano, Alaska, from InSAR analysis: 1. Intereruption deformation, 1997–2008. Journal of Geophysical Research: Solid Earth 115. https://doi.org/10.1029/2009JB006969.
Ludwig, K.R., 2003. Isoplot/Ex Version 3.00. A Geochronological Toolkit for Microsoft Excel, User's Manual. Berkeley Geochronology Center Special Publications 4, Berkeley.
Ludwig, K.R., 2012. Isoplot/Ex Version 3.75. A geochronological toolkit for Microsoft Excel, User's Manual. Berkeley Geochronology Center Special Publications 5, Berkeley.
Lugmair, G.W., Marti, K., 1978. Lunar initial $^{143}Nd/^{144}Nd$: differential evolution line of the lunar crust and mantle. Earth and Planetary Science Letters 39, 349–357.
Maierová, P., Schulmann, K., Lexa, O., Guillot, S., Štípská, P., Janoušek, V., Čadek, O., 2016. European Variscan orogenic evolution as an analogue of Tibetan–Himalayan orogen – insights from petrology and numerical modeling. Tectonics 35, 1760–1780.
Marinov, N.A., Zonenshain, L.P., Blagonravov, V.A. (Eds.), 1973. Geology of the Mongolian People's Republic. 2. Magmatism, Metamorphism, Tectonics (in Russian). Nedra, Moscow.
Matsumoto, I., Tomurtogoo, O., 2003. Petrological characteristics of the Hantaishir Ophiolite Complex, Altai Region, Mongolia: coexistence of podiform chromitite and boninite. Gondwana Research 6, 161–169.
McKenzie, D., O'Nions, R.K., 1991. Partial melt distributions from inversion of rare earth element concentrations. Journal of Petrology 32, 1021–1091.
Miao, L., Baatar, M., Zhang, F., Anaad, C., Zhu, M.S., Yang, S., 2016. Cambrian Kherlen ophiolite in northeastern Mongolia and its tectonic implications: SHRIMP zircon dating and geochemical constraints. Lithos 261, 128–143.
Mitrofanov, F.P., Bibikova, E.V., Gracheva, T.V., Kozakov, I.K., Sumin, L.V., Shuleshko, I.K., 1985. Archaean isotope age of tonalite ("grey") gneisses within the Caledonian structures of Central Mongolia (in Russian). Doklady Akademii Nauk 284, 670–674.
Miyashiro, A., 1974. Volcanic rock series in island arcs and active continental margins. American Journal of Science 274, 321–355.
Molina, J.F., Moreno, J.A., Castro, A., Rodríguez, C., Fershtater, G.B., 2015. Calcic amphibole thermobarometry in metamorphic and igneous rocks: new calibrations based on plagioclase/amphibole Al–Si partitioning and amphibole/liquid Mg partitioning. Lithos 232, 286–305.
Mongkoltip, P., Ashworth, J.R., 1983. Quantitative estimation of an open-system symplectite-forming reaction: restricted diffusion of Al and Si in coronas around olivine. Journal of Petrology 24, 635–661.
Mongush, A.A., Lebedev, V.I., Kovach, V.P., Sal'nikova, E.B., Druzhkova, E.K., Yakovleva, S.Z., Plotkina, Y., Zagornaya, N.Y., Travin, A.V., Serov, P.A., 2011. The tectonomagmatic evolution of structure-lithologic complexes in the Tannu-Ola Zone, Tuva, in the late Vendian–early Cambrian (from geochemical, Nd isotope, and geochronological data). Russian Geology and Geophysics 52, 503–516.
Moore, J.G., Lockwood, J.P., 1973. Origin of comb layering and orbicular structure, Sierra Nevada Batholith, California. Geological Society of America Bulletin 84, 1–20.
Morimoto, N., 1988. Nomenclature of pyroxenes. Mineralogical Magazine 52, 535–550.
Mossakovsky, A.A., Ruzhentsev, S.V., Samygin, S.G., Kheraskova, T.N., 1994. Central Asian fold belt: geodynamic evolution and formation history. Geotectonics 27, 445–474.
Müntener, O., Kelemen, P.B., Grove, T.L., 2001. The role of H_2O during crystallization of primitive arc magmas under uppermost mantle conditions and genesis of igneous pyroxenites: an experimental study. Contributions to Mineralogy and Petrology 141, 643–658.
Neymark, L.A., Rytsk, E.Yu., Rizvanova, N.G., 1993. Hercynian age and Precambrian crustal protolith for Barguzin granitoids of Angaro-Bitimskii Batholith (in Russian). Doklady Akademii Nauk 331, 726–729.
O'Hara, M.J., 1977. Geochemical evolution during fractional crystallisation of a periodically refilled magma chamber. Nature 266, 503–507.
Ota, T., Utsunomiya, A., Uchio, Y., Isozaki, Y., Buslov, M.M., Ishikawa, A., Maruyama, S., Kitajima, K., Kaneko, Y., Yamamoto, H., Katayama, I., 2007. Geology of the Gorny Altai subduction–accretion complex, southern Siberia: tectonic evolution of an Ediacaran–Cambrian intra-oceanic arc–trench system. Journal of Asian Earth Sciences 30, 666–695.
Otamendi, J.E., Ducea, M.N., Bergantz, G.W., 2012. Geological, petrological and geochemical evidence for progressive construction of an arc crustal section, Sierra de Valle Fértil, Famatinian Arc, Argentina. Journal of Petrology 53, 761–800.
Parfenov, L.M., Khanchuk, A.I., Badarch, G., Miller, R.J., Naumova, V.V., Nokleberg, W.J., Ogasawara, M., Prokopiev, A.V., Yan, H., 2003. Preliminary Northeast Asia geodynamics map, sheet 2, scale 1:5,000,000. US Geological Survey Open-File Report 03-205.
Paterson, S.R., Žák, J., Janoušek, V., 2008. Growth of complex sheeted zones during recycling of older magmatic units into younger: Sawmill Canyon area, Tuolumne Batholith, Sierra Nevada, California. Journal of Volcanology and Geothermal Research 177, 457–484.
Pearce, J.A., 1982. Trace element characteristics of lavas from destructive plate boundaries. In: Thorpe, R.S. (Ed.), Andesites; Orogenic Andesites and Related Rocks. John Wiley & Sons, Chichester, pp. 525–548.
Pearce, J.A., 2008. Geochemical fingerprinting of oceanic basalts with applications to ophiolite classification and the search for Archean oceanic crust. Lithos 100, 14–48.
Pearce, J.A., 2014. Immobile element fingerprinting of ophiolites. Elements 10, 101–108.
Pearce, J.A., Peate, D.W., 1995. Tectonic implications of the composition of volcanic arc magmas. Annual Review of Earth and Planetary Sciences 23, 251–285.
Peccerillo, A., Taylor, S.R., 1976. Geochemistry of Eocene calc-alkaline volcanic rocks from the Kastamonu area, Northern Turkey. Contributions to Mineralogy and Petrology 58, 63–81.
Pfänder, J., Jochum, K.P., Todt, W., Kröner, A., 1999. Relationships between the mantle, lower crust and upper crust within the Agardagh-Tes Chem ophiolite, Central Asia: evidence from petrologic, trace element, and isotopic data. Ofioliti 24, 151–152.
Pistone, M., Blundy, J.D., Brooker, R.A., 2015. Textural and chemical consequences of interaction between hydrous mafic and felsic magmas: an experimental study. Contributions to Mineralogy and Petrology 171, 1–21.
Plank, T., Kelley, K.A., Zimmer, M.M., Hauri, E.H., Wallace, P.J., 2013. Why do mafic arc magmas contain ~4 wt% water on average? Earth and Planetary Science Letters 364, 168–179.
Powell, R., 1984. Inversion of the assimilation and fractional crystallization (AFC) equations; characterization of contaminants from isotope and trace element relationships in volcanic suites. Journal of the Geological Society (London) 141, 447–452.
Rapp, R.P., Watson, E.B., 1995. Dehydration melting of metabasalt at 8–32 kbar: implications for continental growth and crust–mantle recycling. Journal of Petrology 36, 891–931.
Rapp, R.P., Norman, M.D., Laporte, D., Yaxley, G.M., Martin, H., Foley, S.F., 2010. Continent formation in the Archean and chemical evolution of the cratonic lithosphere: melt–rock reaction experiments at 3–4 GPa and petrogenesis of Archean Mg-diorites (sanukitoids). Journal of Petrology 51, 1237–1266.
Ridolfi, F., Renzulli, A., Puerini, M., 2010. Stability and chemical equilibrium of amphibole in calc-alkaline magmas: an overview, new thermobarometric formulations and application to subduction-related volcanoes. Contributions to Mineralogy and Petrology 160, 45–66.
Roberts, M.P., Clemens, J.D., 1993. Origin of high-potassium, calc-alkaline, I-type granitoids. Geology 21, 825–828.
Rojas-Agramonte, Y., Kröner, A., Demoux, A., Xia, X., Wang, W., Donskaya, T., Liu, D., Sun, M., 2011. Detrital and xenocrystic zircon ages from Neoproterozoic to Palaeozoic arc terranes of Mongolia: significance for the origin of crustal fragments in the Central Asian Orogenic Belt. Gondwana Research 19, 751–763.
Rudnev, S.N., Babin, G.A., Vladimirov, A.G., Kruk, N.N., Shokal'sky, S.P., Borisov, S.M., Travin, A.V., Levchenkov, O.A., Terleev, A.A., Kuibida, M.L., 2005. Geologic setting, age, and geochemical model of the formation of West Sayan plagiogranitoids. Geologya i Geofizika 46, 170–187.
Rudnev, S.N., Vladimirov, A.G., Ponomarchuk, V.A., Bibikova, E.V., Sergeev, S.A., Plotkina, Y.V., Bayanova, T.B., 2006. The Kaakhem polychronous granitoid batholith, eastern Tuva: composition, age, sources, and geodynamic setting (in Russian). Litosfera 200, 3–33.
Rudnev, S.N., Borisov, S.M., Babin, G.A., Levchenkov, O.A., Makeev, A.F., Serov, P.A., Matukov, D.I., Plotkina, Y., 2008. Early Paleozoic batholiths in the northern part of the Kuznetsk Alatau: composition, age, and sources. Petrology 16, 395–419.
Rudnev, S.N., Izokh, A.E., Kovach, V.P., Shelepaev, R.A., Terent'eva, L.B., 2009. Age, composition, sources, and geodynamic environments of the origin of granitoids in the northern part of the Ozernaya Zone, western Mongolia: growth mechanisms of the Paleozoic continental crust. Petrology 17, 439–475.
Rudnev, S.N., Izokh, A.E., Borisenko, A.S., Shelepaev, R.A., Orihashi, Y., Lobanov, K.V., Vishnevsky, A.V., 2012. Early Paleozoic magmatism in the Bumbat–Hairhan area of the Lake Zone in western Mongolia (geological, petrochemical, and geochronological data). Russian Geology and Geophysics 53, 425–441.
Rudnev, S.N., Babin, G.A., Kovach, V.P., Kiseleva, V.Y., Serov, P.A., 2013a. The early stages of island-arc plagiogranitoid magmatism in Gornaya Shoriya and West Sayan. Russian Geology and Geophysics 54, 20–33.

Rudnev, S.N., Kovach, V.P., Ponomarchuk, V.A., 2013b. Vendian–early Cambrian island-arc plagiogranitoid magmatism in the Altai-Sayan folded area and in the Lake Zone of western Mongolia (geochronological, geochemical, and isotope data). Russian Geology and Geophysics 54, 1272–1287.
Rudnick, R.L., Gao, S., 2003. The composition of the continental crust. In: Holland, H.D., Turekian, K.K. (Eds.), Treatise on Geochemistry 3, The Crust (ed. R.L. Rudnick). Elsevier-Pergamon, Oxford, pp. 1–64.
Sal'nikova, E.B., Kozakov, I.K., Kotov, A.B., Kröner, A., Todt, W., Bibikova, E.V., Nutman, A., Yakovleva, S.Z., Kovach, V.P., 2001. Age of Palaeozoic granites and metamorphism in the Tuvino-Mongolian Massif of the Central Asian Mobile Belt: loss of a Precambrian microcontinent. Precambrian Research 110, 143–164.
Schulmann, K., Lexa, O., Janoušek, V., Lardeaux, J.M., Edel, J.B., 2014. Anatomy of a diffuse cryptic suture zone: an example from the Bohemian Massif, European Variscides. Geology 42, 275–278.
Şengör, A.M.C., Natal'in, B.A., 1996. Turkic-type orogeny and its role in the making of the continental crust. Annual Review of Earth and Planetary Sciences 24, 263–337.
Şengör, A.M.C., Natal'in, B.A., Burtman, V.S., 1993. Evolution of the Altaid tectonic collage and Palaeozoic crustal growth in Eurasia. Nature 364, 299–307.
Shand, S.J., 1943. Eruptive Rocks. Their Genesis, Composition, Classification, and Their Relation to Ore-Deposits With a Chapter on Meteorite. John Wiley & Sons, New York.
Shervais, J.W., 1982. Ti–V plots and the petrogenesis of modern and ophiolitic lavas. Earth and Planetary Science Letters 59, 101–118.
Sisson, T.W., 1994. Hornblende–melt trace-element partitioning measured by ion microprobe. Chemical Geology 117, 331–344.
Smith, D.J., 2014. Clinopyroxene precursors to amphibole sponge in arc crust. Nature Communications 5. https://doi.org/10.1038/ncomms5329.
Söderlund, U., Patchett, P.J., Vervoort, J.D., Isachsen, C.E., 2004. The ^{176}Lu decay constant determined by Lu–Hf and U–Pb isotope systematics of Precambrian mafic intrusions. Earth and Planetary Science Letters 219, 311–324.
Soejono, I., Buriánek, D., Svojtka, M., Žáček, V., Čáp, P., Janoušek, V., 2016. Mid-Ordovician and Late Devonian magmatism in the Togtokhinshil Complex: new insight into the formation and accretionary evolution of the Lake Zone (western Mongolia). Journal of Geosciences 61, 5–23.
Solgadi, F., Sawyer, E.W., 2008. Formation of igneous layering in granodiorite by gravity flow: a field, microstructure and geochemical study of the Tuolumne Intrusive Suite at Sawmill Canyon, California. Journal of Petrology 49, 2009–2042.
Spandler, C., Pirard, C., 2013. Element recycling from subducting slabs to arc crust: a review. Lithos 170-171, 208–223.
Steiger, R.H., Jäger, E., 1977. Subcommission on Geochronology; convention on the use of decay constants in geo- and cosmochronology. Earth and Planetary Science Letters 36, 359–362.
Štípská, P., Schulmann, K., Lehmann, J., Corsini, M., Lexa, O., Tomurhuu, D., 2010. Early Cambrian eclogites in SW Mongolia: evidence that the Palaeo-Asian Ocean suture extends further east than expected. Journal of Metamorphic Geology 28, 915–933.
Sun, L.X., Ren, B.F., Zhao, F.Q., Ji, S.P., Geng, J.Z., 2013. Late Paleoproterozoic magmatic records in Eerguna Massif: evidence from the zircon U–Pb dating of granitic gneisses (in Chinese with English abstract). Geological Bulletin of China 32, 341–352.
Sun, M., Yuan, C., Xiao, W.J., Long, X.P., Xia, X.P., Zhao, G.C., Lin, S.F., Wu, F.Y., Kröner, A., 2008. Zircon U–Pb and Hf isotopic study of gneissic rocks from the Chinese Altai: progressive accretionary history in the early to middle Palaeozoic. Chemical Geology 247, 352–383.
Sun, S.S., McDonough, W.F., 1989. Chemical and isotopic systematics of oceanic basalts: implications for mantle composition and processes. In: Saunders, A.D., Norry, M. (Eds.), Magmatism in the Ocean Basins. Geological Society of London Special Publications 42, pp. 313–345.
Tang, J., Xu, W.L., Wang, F., Wang, W., Xu, M.J., Zhang, Y.H., 2013. Geochronology and geochemistry of Neoproterozoic magmatism in the Erguna Massif, NE China: petrogenesis and implications for the breakup of the Rodinia supercontinent. Precambrian Research 224, 597–611.
Tatsumi, Y., 2005. The subduction factory: how it operates in the evolving Earth. GSA Today 15, 4–10.
Tatsumi, Y., Eggins, S., 1995. Subduction Zone Magmatism. Frontiers in Earth Sciences. Blackwell, Cambridge, Mass.
Taylor, S.R., 1967. The origin and growth of continents. Tectonophysics 4, 17–34.
Taylor, S.R., McLennan, S.M., 1995. The geochemical evolution of the continental crust. Reviews in Geophysics 33, 241–265.
Taylor, S.R., McLennan, S.M., 2009. Planetary Crusts: Their Composition, Origin and Evolution. Cambridge University Press, Cambridge.
Turner, S.P., Stüwe, K., 1992. Low-pressure corona textures between olivine and plagioclase in unmetamorphosed gabbros from Black Hill, South Australia. Mineralogical Magazine 56, 503–509.
Vermeesch, P., 2012. On the visualisation of detrital age distributions. Chemical Geology 312-313, 190–194.
Vernon, R.H., 1984. Microgranitoid enclaves in granites – globules of hybrid magma quenched in a plutonic environment. Nature 309, 438–439.
Volkova, N.I., Sklyarov, E.V., 2007. High-pressure complexes of Central Asian Fold Belt: geologic setting, geochemistry, and geodynamic implications. Russian Geology and Geophysics 48, 83–90.
Watson, E.B., Harrison, T.M., 1983. Zircon saturation revisited: temperature and composition effects in a variety of crustal magma types. Earth and Planetary Science Letters 64, 295–304.
Weaver, B.L., Tarney, J., 1984. Empirical approach to estimating the composition of the continental crust. Nature 310, 575–577.
Whitney, D.L., Evans, B.W., 2010. Abbreviations for names of rock-forming minerals. American Mineralogist 95, 185–187.
Wiebe, R.A., 1996. Mafic–silicic layered intrusions: the role of basaltic injections on magmatic processes and the evolution of silicic magma chambers. Transactions of the Royal Society of Edinburgh, Earth Sciences 87, 233–242.
Wiebe, R.A., Collins, W.J., 1998. Depositional features and stratigraphic sections in granitic plutons: implications for the emplacement and crystallization of granitic magma. Journal of Structural Geology 20, 1273–1289.
Wilhem, C., Windley, B.F., Stampfli, G.M., 2012. The Altaids of Central Asia: a tectonic and evolutionary innovative review. Earth-Science Reviews 113, 303–341.
Windley, B.F., Alexeiev, D., Xiao, W.J., Kröner, A., Badarch, G., 2007. Tectonic models for accretion of the Central Asian Orogenic Belt. Journal of the Geological Society (London) 164, 31–47.
Witt-Eickschen, G., Seck, H.A., 1991. Solubility of Ca and Al in orthopyroxene from spinel peridotite: an improved version of an empirical geothermometer. Contributions to Mineralogy and Petrology 106, 431–439.
Wood, D.A., 1980. The application of a Th–Hf–Ta diagram to problems of tectonomagmatic classification and to establishing the nature of crustal contamination of basaltic lavas of the British Tertiary volcanic province. Earth and Planetary Science Letters 50, 11–30.
Xia, X.P., Sun, M., Geng, H.Y., Sun, Y., Wang, Y.J., Zhao, G.C., 2011. Quasi-simultaneous determination of U–Pb and Hf isotope compositions of zircon by excimer laser-ablation multiple-collector ICPMS. Journal of Analytical Atomic Spectrometry 26, 1868–1871.
Xiao, W.J., Santosh, M., 2014. The western Central Asian Orogenic Belt: a window to accretionary orogenesis and continental growth. Gondwana Research 25, 1429–1444.
Xiao, W.J., Windley, B.F., Badarch, G., Sun, S., Li, J., Qin, K., Wang, Z., 2004. Palaeozoic accretionary and convergent tectonics of the southern Altaids: implications for the growth of Central Asia. Journal of the Geological Society (London) 161, 339–342.
Xiao, W.J., Windley, B.F., Huang, B.C., Han, C.M., Yuan, C., Chen, H.L., Sun, M., Sun, S., Li, J.L., 2009a. End-Permian to mid-Triassic termination of the accretionary processes of the southern Altaids: implications for the geodynamic evolution, Phanerozoic continental growth, and metallogeny of Central Asia. International Journal of Earth Sciences 98, 1189–1217.
Xiao, W.J., Windley, B.F., Yuan, C., Sun, M., Han, C.M., Lin, S.F., Chen, H.L., Yan, Q.R., Liu, D.Y., Qin, K.Z., Li, J.L., Sun, S., 2009b. Paleozoic multiple subduction–accretion processes of the southern Altaids. American Journal of Science 309, 221–270.
Xiao, W.J., Windley, B.F., Sun, S., Li, J.L., Huang, B., Han, C.M., Yuan, C., Sun, M., Chen, H., 2015. A tale of amalgamation of three Permo–Triassic collage systems in Central Asia: oroclines, sutures, and terminal accretion. Annual Review of Earth and Planetary Sciences 43, 477–507.
Yakubchuk, A., 2004. Architecture and mineral deposit settings of the Altaid orogenic collage: a revised model. Journal of Asian Earth Sciences 23, 761–779.
Yanshin, A.L., 1965. Tectonic structure of Eurasia (in Russian). Geotektonika 5, 3–35.
Yarmolyuk, V.V., Kovalenko, V.I., Anisimova, I.V., Sal'nikova, E.B., Kovach, V.P., Kozakov, I.K., Kozlovsky, A.M., Kudryashova, E.A., Kotov, A.B., Plotkina, Y., Terent'eva, L.B., Yakovleva, S.Z., 2008. Late Riphean alkali granites of the Zabhan microcontinent: evidence for the timing of Rodinia breakup and formation of microcontinents in the Central Asian Fold belt. Doklady Earth Sciences 420, 583–588.
Yarmolyuk, V.V., Kovach, V.P., Kovalenko, V.I., Sal'nikova, E.B., Kozlovskii, A.M., Kotov, A.B., Yakovleva, S.Z., Fedoseenko, A.M., 2011. Composition, sources, and mechanism of continental crust growth in the Lake Zone of the Central Asian Caledonides: I. Geological and geochronological data. Petrology 19, 55–78.
Yogodzinski, G.M., Lees, J.M., Churikova, T.G., Dorendorf, F., Wörner, G., Volynets, O.N., 2001. Geochemical evidence for the melting of subducting oceanic lithosphere at plate edges. Nature 409, 500–504.
Žák, J., Paterson, S.R., Janoušek, V., Kabele, P., 2009. The Mammoth Peak sheeted complex, Tuolumne Batholith, Sierra Nevada, California: a record of initial growth or late thermal contraction in a magma chamber? Contributions to Mineralogy and Petrology 158, 447–470.
Zandt, G., Gilbert, H., Owens, T.J., Ducea, M., Saleeby, J., Jones, C.H., 2004. Active foundering of a continental arc root beneath the southern Sierra Nevada in California. Nature 431, 41–46.
Zhang, Y., Sun, M., Yuan, C., Xu, Y., Long, X.P., Tomurhuu, D., Wang, C., He, B., 2015. Magma mixing origin for high Ba–Sr granitic pluton in the Bayankhongor area, central Mongolia: response to slab roll-back. Journal of Asian Earth Sciences 113, 353–368.
Zhu, M.S., Baatar, M., Miao, L., Anaad, C., Zhang, F., Yang, S., Li, Y., 2014a. Zircon ages and geochemical compositions of the Manlay ophiolite and coeval island arc: implications for the tectonic evolution of South Mongolia. Journal of Asian Earth Sciences 96, 108–122.
Zhu, M.S., Miao, L., Baatar, M., Zhang, F., Anaad, C., Yang, S., Li, Y., 2014b. Zircon ages and geochemical data of the Biluutiin ovoo ophiolite: implication for the tectonic evolution of South Mongolia. International Geology Review 56, 1769–1782.
Zhu, M.S., Miao, L., Baatar, M., Zhang, F., Anaad, C., Yang, S., Li, X., 2016. Early Paleozoic oceanic inliers and reconstruction of accretionary tectonics in the Middle Gobi region, Mongolia: evidence from SHRIMP zircon U–Pb dating and geochemistry. Journal of Asian Earth Sciences 127, 300–313.
Zonenshain, L.P., 1973. The evolution of Central Asiatic geosynclines through sea-floor spreading. Tectonophysics 19, 213–232.
Zonenshain, L.P., Kuzmin, M.I., 1978. The Khan-Taishir ophiolitic complex of Western Mongolia, its petrology, origin and comparison with other ophiolitic complexes. Contributions to Mineralogy and Petrology 67, 95–109.
Zonenshain, L.P., Kuzmin, M.I., Moralev, V.M., 1976. Global Tectonics, Magmatism and Metallogeny (in Russian). Nedra, Moscow.
Zorin, Y., 1999. Geodynamics of the western part of the Mongolia–Okhotsk collisional belt, Trans-Baikal region (Russia) and Mongolia. Tectonophysics 306, 33–56.

Chapter III

Early Palaeozoic sedimentary record and provenance of flysch sequences in the Hovd Zone (western Mongolia): Implications for the geodynamic evolution of the Altai accretionary wedge system

by Igor Soejono, Pavel Čáp, Jitka Míková, Vojtěch Janoušek, David Buriánek, Karel Schulmann

Graphical abstract

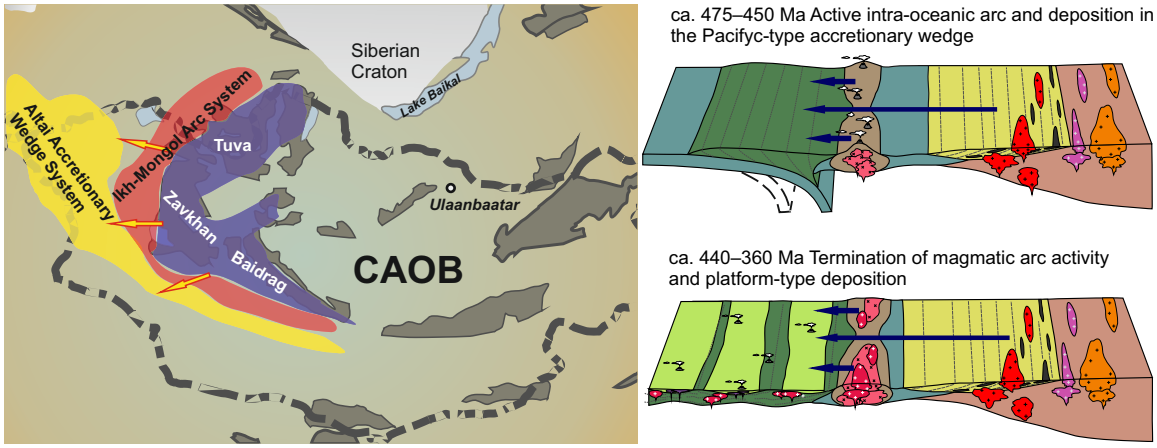

Keywords: *Altai accretionary wedge, magmatic-arc activity, crustal extension, U–Pb detrital zircon dating, Central Asian Orogenic Belt*

Supplementary materials are available at https://doi.org/10.1016/j.gr.2018.07.005

Gondwana Research 64 (2018) 163–183

Contents lists available at ScienceDirect

Gondwana Research

journal homepage: www.elsevier.com/locate/gr

Early Palaeozoic sedimentary record and provenance of flysch sequences in the Hovd Zone (western Mongolia): Implications for the geodynamic evolution of the Altai accretionary wedge system

Igor Soejono [a,b,*], Pavel Čáp [a], Jitka Míková [a], Vojtěch Janoušek [a,b], David Buriánek [a], Karel Schulmann [a]

[a] Czech Geological Survey, Klárov 3, 118 21 Prague 1, Czech Republic
[b] Institute of Petrology and Structural Geology, Faculty of Science, Charles University, Albertov 6, 128 43 Prague 2, Czech Republic

ARTICLE INFO

Article history:
Received 12 February 2018
Received in revised form 26 June 2018
Accepted 9 July 2018
Available online 14 September 2018

Handling Editor: I. Safonova

Keywords:
Altai accretionary wedge
Magmatic-arc activity
Crustal extension
U–Pb detrital zircon dating
Central Asian Orogenic Belt

ABSTRACT

Sedimentological and detrital zircon provenance study of the Lower Palaeozoic Zuunnuruu, Tsetseg and Sagsai sedimentary formations was carried out in the eastern part of the Hovd Zone in western Mongolia. Sedimentological analysis has revealed two distinct and consecutive types of sedimentary environments. The Lower Ordovician–earliest Silurian sediments had dominantly volcano-sedimentary character, interpreted as reflecting deposition in a proximal part of a Pacific-type accretionary wedge. The upper, mainly Devonian part of the profile has generally siliciclastic flysch-like nature and indicates platform-type depositional setting related to the syn-extensional thinning of the accretionary wedge-system. Detrital zircon age populations of all the three studied formations uniformly show a dominant Neoproterozoic–Ordovician age group at ca. 560–460 Ma, a broad Neo- to Mesoproterozoic peak at ca. 1050–720 Ma, several minor Meso- to Palaeoproterozoic age clusters at ca. 1.4, 1.9 and 2.4 Ga and ca. 400–360 Ma peaks in the youngest Devonian formation. The early Palaeozoic part of the age spectra is interpreted as detritus mainly derived from the magmatic rocks of the Cambrian–Ordovician Ikh-Mongol Arc System within the nearby Lake Zone and the youngest ages from the neighbouring Devonian granites. The other sources were identified as more distal Tonian magmatic-arc complexes, Rodinia break-up-related volcanic rocks and basement of the Precambrian Zavkhan and Baidrag continental blocks even further east. The maximum sedimentary ages, determined by the youngest detrital zircons, shift the end of deposition of the Sagsai Formation at least to the latest Devonian. Nearly identical detrital zircon age spectra from Lower Palaeozoic sequences of the Hovd Zone and other parts of the Altai belt support an existence of a single giant accretionary complex developed along the entire outer margin of the Ikh-Mongol Arc System. The change in the sedimentary style suggests the latest Ordovician–earliest Silurian termination of magmatic-arc activity in the western Lake Zone, marking the onset of late Silurian–Devonian crustal extensional period in the Altai accretionary system.

1. Introduction

The giant Central Asian Orogenic Belt (CAOB) (Kröner, 2015; Mossakovsky et al., 1994; Windley et al., 2007) classically named as Altaids by Şengör et al. (1993), represents one of the most important accretionary orogens in the Earth's geological history. A fundamental feature of this orogenic system was multi-stage closure of oceanic domains and progressive involvement of microcontinental blocks, magmatic arcs and accretionary wedges (Kröner et al., 2017; Safonova et al., 2011; Wilhem et al., 2012; Xiao and Santosh, 2014). However, some fundamental issues such as duration of arc magmatism, age and extent of sedimentary wedge and subduction polarity during early Palaeozoic are still discussed (Janoušek et al., 2018; Jiang et al., 2017; Safonova et al., 2017; Windley et al., 2007; Xiao et al., 2004). Although these issues have been mainly addressed in the current southern part of Altai accretionary wedge, the northern part of this giant sedimentary structure adjacent to the Mongolian continental blocks has been little investigated so far. At the same time, the study of this proximal area would allow better understanding of the dynamics of early Palaeozoic subduction system in the Mongolian tract of the CAOB.

In general, different types of sediments, reflecting basin characteristics, nature of the source material and geodynamic position, can be deposited in an accretionary complex of an active margin (Meschede, 2014; Scholl et al., 1980). Detailed field observations, petrography and provenance analysis of stratigraphically well-categorized sedimentary sequences provide unique insight into the age, tectonic setting, and

* Corresponding author at: Czech Geological Survey, Klárov 3, 118 21 Prague 1, Czech Republic.
E-mail address: igor.soejono@geology.cz (I. Soejono).

https://doi.org/10.1016/j.gr.2018.07.005
1342-937X/

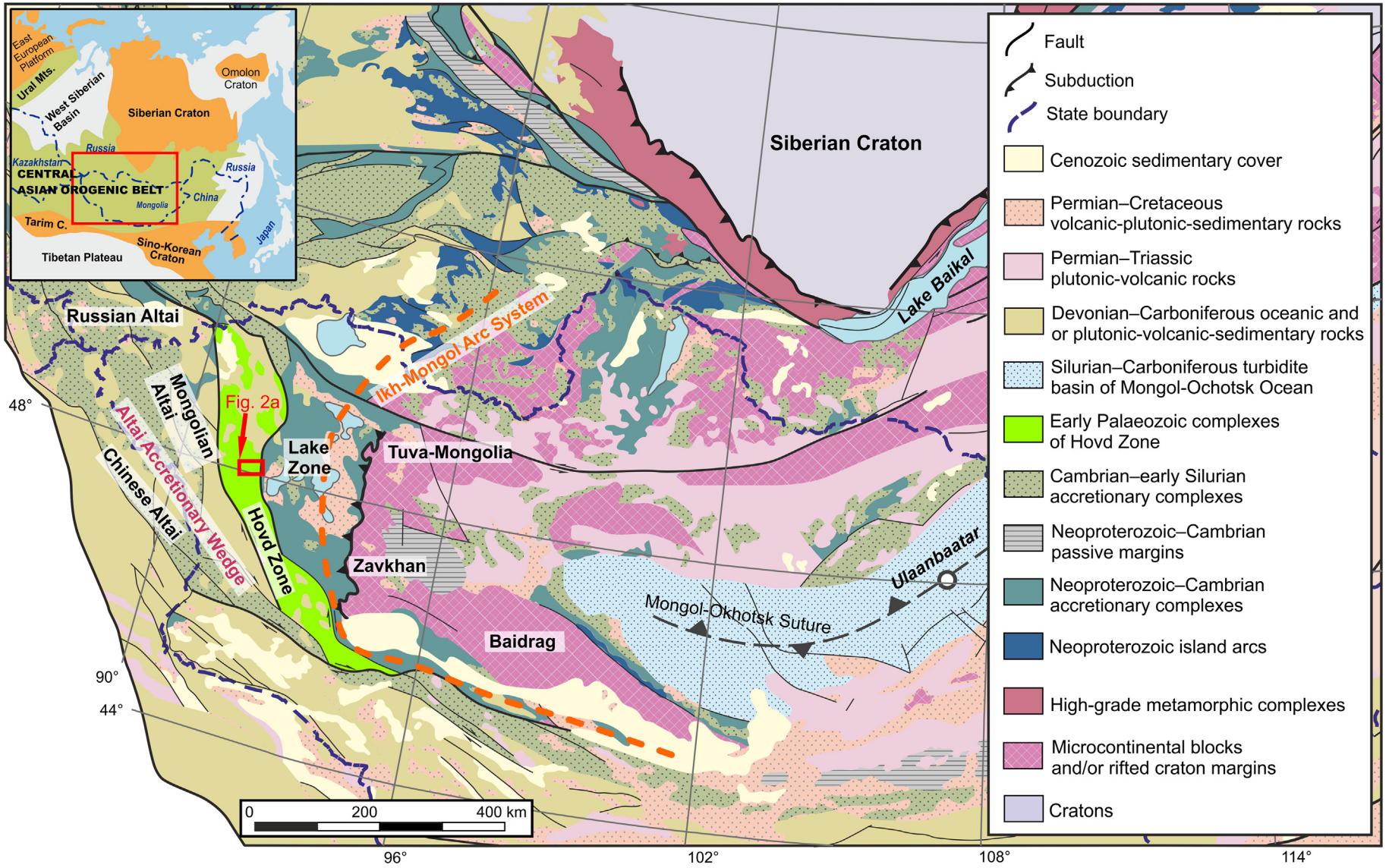

Fig. 1. Simplified tectonic map of the central CAOB showing major units in western Mongolia (modified from Parfenov et al., 2003 and Jiang et al., 2017). Study area location is indicated. Inset map shows a schematic tectonic setting of the Central Asian Orogenic Belt (after Şengör et al., 1993).

source areas of detritus, as well as their development in space and time. U–Pb dating of detrital zircons is very often used to depict the original sources of clastic material. However, several recent studies showed that correct application of detrital zircon data is complicated by sampling and separation biases (Sláma and Košler, 2012; Vermeesch, 2004; Zimmermann et al., 2015) and warned against overestimating the provenance effect and neglecting sedimentary processes (Andersen et al., 2016). Provenance interpretations could be highly speculative, especially for the subsequently fragmented crustal domains and "far-travelled terrains". Nevertheless, the link between the detailed field knowledge and realistic assessment of detrital zircon populations in the general tectonic context allows understanding dynamics of well-preserved orogenic systems, such as the CAOB.

Altai accretionary wedge, a giant Lower Palaeozoic sedimentary succession extending from Russian part of the CAOB to southern Mongolia (Fig. 1), borders the western margin of an extensive chain of Cambrian–Ordovician arc-related magmatic complexes (recently termed Ikh-Mongol Arc System by Janoušek et al., 2018), and representing a southern continuation of Kuznetsk-Alatau arc described in western Sayan (e.g. Buslov et al., 2002). These arc and accretionary wedge formed above a huge, northeast (in recent coordinates) dipping subduction system (e.g. Buriánek et al., 2017; Xiao et al., 2015). Recent studies in the Chinese Altai (Long et al., 2010; Wang et al., 2014), Mongolian Altai (Jiang et al., 2017) and Russian Altai (Chen et al., 2015) recorded very similar detrital zircon age populations of the widespread Lower Palaeozoic flysch-like sedimentary sequences (Fig. 1). Accordingly, the idea of the single early Palaeozoic Pacific-type accretionary prism for these units was proposed (Chen et al., 2014; Jiang et al., 2017; Long et al., 2012). However, such a provenance study has not yet been carried out in the northernmost part of the Altai wedge possibly representing the most proximal area with respect to potential source area. This peripheral part, located closest to the arc-belt, sensitively records both the nearby magmatic activity and diversity of detritus sources and is important for tracing provenance and overall depositional evolution of the Altai wedge system.

In this paper, we present results of the sedimentological analysis combined with U–Pb dating of detrital zircons aiming to establish the early Palaeozoic evolution of sedimentary sequences in the Hovd Zone, representing a key section of the Mongolian Altai. The studied successions cover nearly whole lifespan (Ordovician–Devonian) of the Hovd Zone sedimentary system and thus should continuously record changes in deposition style and tectonic setting of the source area during its complete evolution. Detrital zircon age data constrain depositional age of the studied formations and timing of the activity in the nearby magmatic arc. We also compare our geochronological data with those known from magmatic complexes in the potential source areas and discuss the possible sediment transport directions. These results allow us to constrain history of the Altai accretionary wedge and better understand the timing of the related early Palaeozoic Ikh-Mongol Arc System.

2. Geological setting

2.1. Regional overview of the western Mongolia

The Mongolian tract of the CAOB is located between the Siberian, the Tarim and the Sino-Korean cratonic blocks (Fig. 1, insert) (Safonova et al., 2011; Windley et al., 2007). Its western part consists of amalgamated Archean to early Neoproterozoic continental segments (Bold et al., 2016; Demoux et al., 2009a; Kozakov et al., 2007; Kröner et al., 2017) and Neoproterozoic to late Palaeozoic magmatic-arcs, accretionary complexes and back-arcs (Badarch et al., 2002; Kröner et al., 2010; Windley et al., 2007; Safonova et al., 2017).

Western Mongolia is composed of four major lithotectonic units differing mainly in age and lithology (Kröner et al., 2010; Mossakovsky et al., 1994; Parfenov et al., 2003; Wilhem et al., 2012; Xiao et al., 2004), also named terranes by Badarch et al. (2002): Mongolian continental blocks in the east, Lake Zone, and Hovd with Altai zones in the west (Fig. 1). The Zavkhan and Baidrag Precambrian microcontinents, belonging to the Mongolian continental blocks, are covered by the late Proterozoic and early Cambrian passive margin sediments (e.g. Bold et al., 2016; Buriánek et al., 2017). The Lake Zone consists of Neoproterozoic ophiolites (Buriánek et al., 2017; Dijkstra et al., 2006; Jian et al., 2014; Zonenshain and Kuzmin, 1978) and accretionary wedge volcano-sedimentary rocks (Kovach et al., 2011; Windley et al., 2007) intruded by Cambrian–Ordovician arc (Janoušek et al., 2018; Rudnev et al., 2012; Soejono et al., 2016; Yarmolyuk et al., 2011). The Hovd and Altai zones are mainly composed of the early Palaeozoic sedimentary sequences and low- to high-grade metamorphic complexes (Badarch et al., 2002; Jiang et al., 2015; Soejono et al., 2017; Xiao et al., 2004) intruded by Devonian–Permian granitic plutons (Buriánek et al., 2016; Cai et al., 2015; Jiang et al., 2016). The Ordovician sediments (Habahe Group in China and Tugrug Formation in Mongolia) were recently interpreted as a large early Palaeozoic sedimentary accretionary wedge (Chen et al., 2014; Jiang et al., 2017; Long et al., 2010, 2012).

Accretionary evolution of the Mongolian part of the CAOB could be summarised by the late Proterozoic amalgamation of the Mongolian microcontinents and mid-Proterozoic ophiolites to the Siberian margin (Cocks and Torsvik, 2007; Khain et al., 2003; Şengör et al., 1993), early Cambrian thrusting of Neoproterozoic ophiolites over these microcontinents (Buriánek et al., 2017; Dijkstra et al., 2006; Štípská et al., 2010) and subsequent development of southerly early Palaeozoic subduction system and associated magmatic-arc belt, the so-called Ikh-Mongol Arc System (Janoušek et al., 2018). Original zonation was lately rotated into an orocline, due to the late Palaeozoic opening (e.g. Xiao et al., 2017) and Permian to Jurassic closure (Lehmann et al., 2010; Xiao et al., 2015) of the Mongol-Okhotsk Ocean.

2.2. Hovd Zone

The Hovd Zone was earlier considered as a fragment of island-arc system (Şengör and Natal'in, 1996), turbidite belt (Tomurtogoo, 1997) or accretionary wedge (Hovd Terrane of Badarch et al., 2002). In contrast, the southerly Mongolian and Chinese Altai successions (Gobi Altai Terrane of Badarch et al., 2002) were seen as back-arc systems. More recently, the Hovd Zone was interpreted, together with the Mongolian Altai Zone, as a single accretionary wedge (Long et al., 2012; Xiao et al., 2004), while locally outcropping high-grade basement may be understood as a reworked margin of the Lake Zone island-arc system (Soejono et al., 2017).

The sedimentary succession studied in this work represents an Ordovician–Devonian cover of the easternmost part of the Hovd Zone close to its boundary with the Lake Zone (Fig. 1), and occupies the southern part of the Huh Serh Range in the western Mongolian Altai. The study area consists of four major lithological units (Fig. 2a): mostly Ordovician (meta-) igneous rocks of the Khuurai Tsenkher Gol Complex (Soejono et al., 2017); metasedimentary rocks of the Bij Group (Enkhbayar et al., 2003; Soejono et al., 2017; Žáček et al., 2016); Ordovician–Devonian flysch sequences (Baatarhuyag and Gansukh, 1999) and late Devonian–early Carboniferous granitic Zuun Bulgan Pluton (Gavrilova et al., 1975; Žáček et al., 2016).

The studied Lower Palaeozoic sedimentary succession has previously been subdivided, from older to younger, into the Zuunnuruu Formation, Tsetseg Formation and Sagsai Formation (Ariunchimeg et al., 2012; Luvsandanzan, 1970). These strata are composed of various types of rocks, including volcano-sedimentary, siliciclastic and carbonate sequences and also contain numerous bodies of volcanic rocks (Žáček et al., 2016). However, the depositional age of these units has remained uncertain because of the lack of fossils. The stratigraphy of these formations has been hence based mainly on the rare fossil occurrences and lithological similarities with distant regions (Ariunchimeg et al., 2012; Baatarhuyag and Gansukh, 1999; Luvsandanzan, 1970).

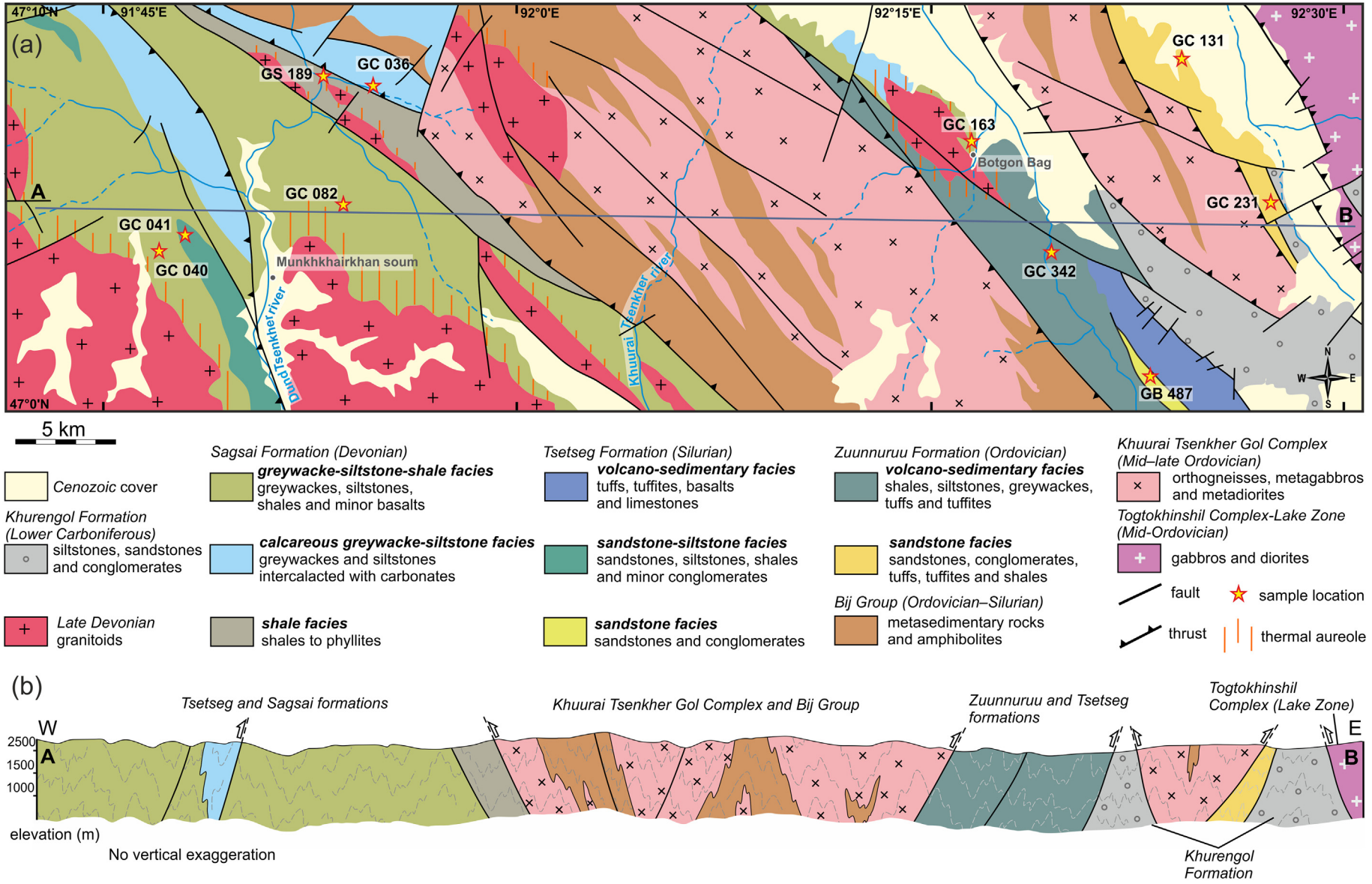

Fig. 2. (a) Geological map of the study area (modified from Žáček et al., 2016) with localizations of the detrital zircon samples. (b) Idealized structural cross-section along the line A–B. Dashed lines show foliation in the basement rocks and bedding in the sedimentary rocks.

3. Field relations, stratigraphy and sedimentology

The sedimentary sequences exposed in the study area form three NW–SE trending domains (Fig. 2a) separated by the Khuurai Tsenkher Gol Complex and Bij Group high-grade belts (Soejono et al., 2017), as well as Carboniferous sediments of the Khurengol Formation and Cenozoic basins (Baatarhuyag and Gansukh, 1999; Jelínek and Žáček, 2018). The sedimentary rocks of all three sequences (Fig. 3) are heterogeneously deformed and generally unmetamorphosed, only locally affected by very low-grade metamorphism in sub-greenschist facies (Figs. 4, 5). The whole succession was intensively folded into upright folds and affected by NW–SE trending thrust faults and NE–SW trending strike-slip faults (Fig. 2a–b). Extensive, ca. 100–1000 m wide thermal aureoles surround the abundant late Devonian granitic intrusions. The contact of the Zuunnuruu and the basal part of the Tsetseg formations with the overlying main part of the Tsetseg and Sagsai successive formations is unconformable (Žáček et al., 2016); however, there is no reported significant hiatus between them (Ariunchimeg et al., 2012; Baatarhuyag and Gansukh, 1999). An unequivocal recognition of individual formations in the field is sometimes difficult as they both share similar lithologies, suffered intense refolding and lack fossils.

3.1. Zuunnuruu Formation

The Ordovician Zuunnuruu Formation is exposed in the eastern part of the area (Fig. 2) and, based on lithology, can be divided into the volcano-sedimentary and the sandstone facies (Fig. 3). The occurrences of the both facies are tectonically restricted and thus their exact position within the formation is not entirely clear.

The prevailing *volcano-sedimentary facies* consists of shales, siltstones and sandstones (Fig. 4a) irregularly alternating with basic tuffs and tuffites. This lithofacies also contains minor bodies of basaltic pillow lavas and, rarely, small lenses of limestones. Abundant deformed fine-grained tuffs and tuffites, with variable content of clastic component, contain mostly plagioclases, lithic clasts of very fine-grained volcanic rocks and equally fine-grained groundmass (Fig. 6a, b). The sandstones are well-sorted and medium- to fine-grained, composed of rounded clasts of quartz, fine-grained volcanic rocks, fine argillaceous matrix and carbonate or quartz cement. Finer grained members are moderately-sorted shales to quartz-siltstones often containing varying amounts of volcanic material.

The subordinate *sandstone facies* is represented by a complex of nearly pure sandstones with intercalations and lenses of conglomerates (Fig. 4b), locally associated with minor rhyolite lavas and ignimbrites dated at ca. 462 Ma (Žáček et al., 2016). The well-sorted quartz sandstones are fine- to medium-grained and include lenses and intercalations of conglomerates, ignimbrites and rhyolite lavas. Clast-supported quartz sandstones contain mainly sub-rounded quartz clasts and minor portion of micas. Polymictic conglomerates are composed of quartz clasts (mono- and polycrystalline) and lithic fragments (acid volcanic rocks, clastic sedimentary rocks and granitoids).

3.2. Tsetseg Formation

The Silurian Tsetseg Formation forms several narrow belts in the western and central part of the studied area and is composed by three sedimentary facies: mutually independent volcano-sedimentary and sandstone facies, and dominant sandstone-siltstone facies (Figs. 2–3). The first two are lithologically identical to the underlying Zuunnuruu Formation.

The *volcano-sedimentary facies* dominates the eastern part of the studied area and mainly consists of the tuffites, basaltic lavas and limestone bodies. Laminated fine-grained tuffites are composed mainly by lithic fragments of volcanic rocks, quartz clasts and very fine-grained groundmass (Fig. 6a). Tuffites moreover enclose isolated lenses of relatively pure bioclastic limestones (Fig. 4c) containing recrystallized Silurian crinoidal columns and rugose corals (after Baatarhuyag and Gansukh, 1999).

The *sandstone lithofacies* forms a fault-bound body, analogous to older sandstones from the Zuunnuruu Formation, mainly composed of sandstones and conglomerates intercalated with rhyolite and ignimbrite. The quartz-sandstones are well-sorted and fine to medium-grained (Fig. 6c). The coarse-grained polymictic conglomerates are poorly sorted and composed by quartz and acid tuffs pebbles (Fig. 6d).

The prevailing *sandstone–siltstone facies* is exposed in the westerly located isolated belts surrounded by the younger Devonian rocks of the Sagsai Formation, representing uncovered stratigraphical footwall in the core of large-scale antiforms (Fig. 2). This lithofacies consists of sandstones, siltstones, shales and minor conglomerates. Sandstones (greywackes) and siltstones are predominant lithologies and they are usually developed as a flysch sequence defined by regularly alternated layers of coarser and finer grained clastic material. The content of tuffitic material is limited in the generally clastic sedimentary rocks. Nevertheless, it does not show as rhythmical character as the younger Sagsai Formation. Most of sandstones are medium- to fine-grained, immature greywackes to arkose sandstones. Fine-grained, moderately sorted siltstones locally continuously pass into massive shales. The polymictic conglomerates are coarse-grained with pebbles-size up to 50 cm and sandy matrix (Fig. 4d).

3.3. The Sagsai Formation

The Sagsai Formation is exposed mainly in the western part of the area in close contact with the late Devonian granitic pluton (Fig. 2) and has mostly a flysch-type character (Fig. 5a–c). It can be divided into three distinct sedimentary facies: greywacke–siltstone–shale facies, shale facies and calcareous greywacke–siltstone facies. At the exocontacts of the granitic bodies, these rocks were significantly affected by thermal metamorphism.

The predominant *greywacke–siltstone–shale lithofacies* is defined by rhythmical alternations of greywacke with siltstone or shale layers (Fig. 5c), locally interbedded with conglomerates and limestones or cherts. Rock association of this sedimentary facies also includes basaltic pillow lavas, however lacks their volcano-sedimentary equivalents (tuffs and tuffites). Main component of the facies are usually fine-grained, poorly-sorted and immature greywackes (Fig. 6e, f). The finer grained part of this facies is predominantly characterized by alternations of moderately sorted and slightly foliated shales and siltstones, and frequently their transitions. Petromictic conglomerates are typically medium- to coarse-grained and form intercalations or lenses within the surrounding sandstones and siltstones (Fig. 5d).

The *shale lithofacies* occurs as a narrow, fault-bound belt in the central part of the study area and contains mainly well-sorted, fine-grained shales with sandy intercalations. The *calcareous greywacke–siltstone facies* forms several bodies exposed especially in the northern part of the studied area (Fig. 2) and is mainly built by greywackes and siltstones with abundant calcareous sandstones to siltstones and shales to limestones (Figs. 3, 5a, b). Limestones with remnants of a shallow-water fauna, related to the shallower parts of the basin, are present as up to several meters big clasts (olistoliths) enclosed within coarse-grained conglomerates.

4. Samples and methods

Ten samples of typical lithologies from the studied successions were systematically collected for detrital zircon U–Pb dating. Brief petrological descriptions and localities are given in Table 1 and microphotographs of dated samples are shown in Supplementary Material A (see also Figs. 2a, 3 for sample locations). Modal framework grain analysis of 11 representative sandstone samples from the Zuunnuruu, Tsetseg and Sagsai formations have been determined by a standard 500 point counting of thin-sections.

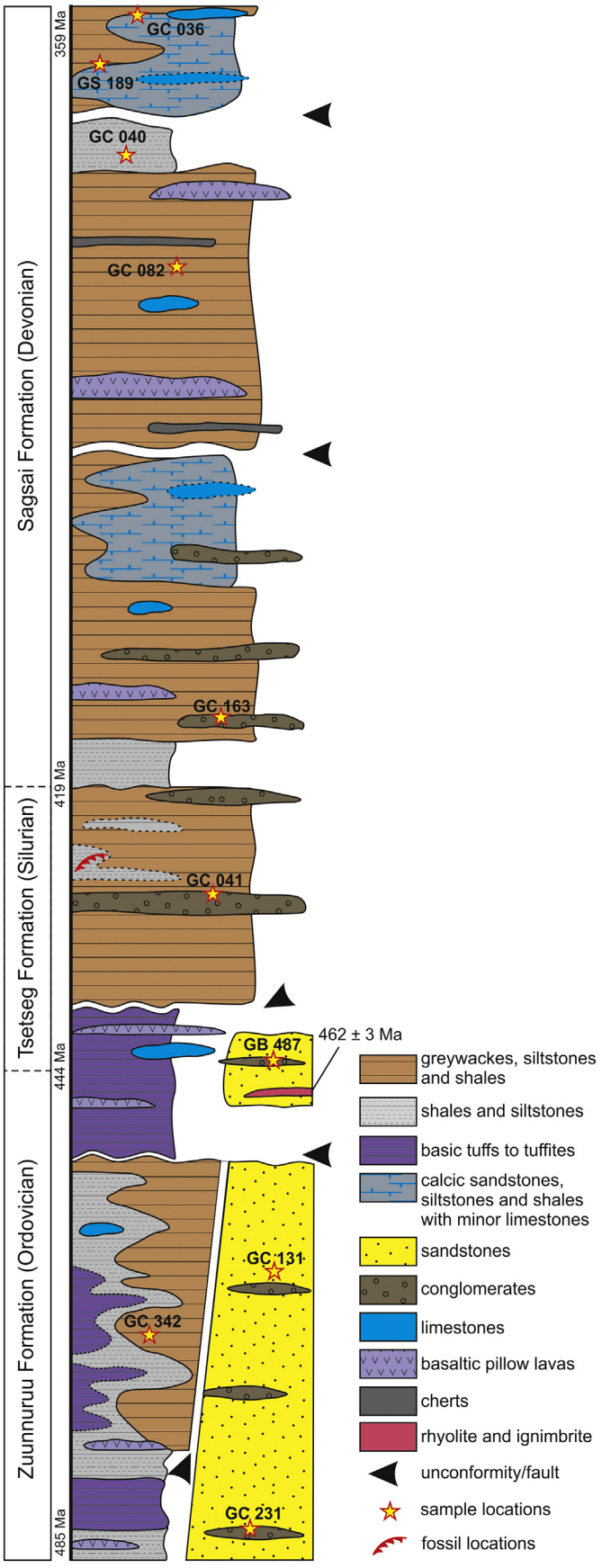

Fig. 3. Reconstructed lithostratigraphic chart of the Zuunnuruu, Tsetseg and Sagsai formations based on the field observations and fossils occurrences (Žáček et al., 2016). The positions of the dated samples are located according to the youngest detrital zircon ages.

About 10–15 kg of fresh rock per sample were collected and zircon grains were separated using conventional techniques: crushing, Wilfley concentration table, and finally, magnetic and heavy liquid separations in the Central Geological Laboratory and in Laboratory of the Geological Investigation Center in Ulaanbaatar, Mongolia. After that, zircon concentrates were handpicked for morphological types, grains mounted in one-inch epoxy discs, ground and finally polished. Internal zircon structure and zoning patterns in individual grains were checked by cathodoluminescence (CL) imaging using scanning electron microscope at the Czech Geological Survey in Prague and Institute of Petrology and Structural Geology, Charles University in Prague.

The U–Pb dating of detrital zircons was performed by using an *Analyte Excite* 193 nm excimer laser-ablation system (LA; Proton Machines), equipped with a two-volume HelEx ablation cell, in tandem with an *Agilent 7900x* ICPMS (Agilent Technologies Inc., Santa Clara, USA) at the Czech Geological Survey in Prague. Samples were ablated in He atmosphere (0.8 l min^{-1}) at a pulse repetition rate of 5 Hz using a spot size of 25 μm and laser fluence of 7.59 J cm^{-2}. Each measurement consisted of 20 s of blank acquisition followed by ablation of the sample for further 40 s of signal collection at masses ^{202}Hg, ^{204}Pb, ^{206}Pb, ^{207}Pb, ^{208}Pb, ^{232}Th and ^{238}U using the SEM detector, with one point per mass peak and the respective dwell times of 10, 10, 15, 30, 20, 10 and 15 ms per mass (total sweep time of 0.134 s). Instrumental drift was monitored by repeat measurements of 91500 reference zircon (Wiedenbeck et al., 1995) after every 20 unknowns. Data reduction using Iolite software followed the method described by Paton et al. (2010), including an 'on peak' gas blank subtraction followed by correction for laser-induced elemental fractionation (LIEF) by comparison with the behaviour of the 91500 reference zircon (Wiedenbeck et al., 1995). The concordia age for reference materials has been calculated by Isoplot (Ludwig, 2008). For primary reference material 91500, a zircon age of 1063 ± 1.4 Ma was obtained. No common Pb correction was applied as useful data could not be obtained for ^{204}Pb due to the high level of isobaric Hg interferences derived from the carrier gases. In addition zircon reference samples GJ-1 (~609 Ma, Jackson et al., 2004) and Plešovice (~337 Ma, Sláma et al., 2008) were analysed periodically during this study and yielded concordia ages of 608.5 ± 1 Ma and 337.8 ± 1 Ma (2σ), respectively.

Isotopic data from analysed detrital zircons are given in Supplementary Material B. The presented zircon ages comprise only data <10% discordant. The zircon age populations are presented in the form of concordia diagrams (Ludwig, 2008), histograms with kernel density estimates (Vermeesch, 2012) and cumulative distribution plots (Andersen et al., 2017).

5. Results

5.1. Modal analysis

The statistic results of petrographic modal analysis of selected samples are listed in Table 2 and presented in ternary diagrams (Dickinson, 1985; Dickinson and Suczek, 1979) (Fig. 7). The sandstones from the Zuunnuruu and Tsetseg formations are dominated by lithic fragments and quartz grains, whereas samples from the Sagsai Formation contain a greater amount of feldspars (e.g., Fig. 7a, b). Quartz grains in all the samples are mostly monocrystalline, feldspars consist mainly of plagioclases and lithic fragments are dominantly volcanic and metamorphic (Table 2). The samples from the Zuunnuruu and Tsetseg formation fall into the recycled orogen (Fig. 7a, b) provenance fields (Dickinson, 1985). The Sagsai Formation sandstones form large cluster spanning from recycled orogen to the dissected magmatic arc sources (Fig. 7a, b). Moreover, the Qm–F–Lt plot shows a progressively increasing contribution of feldspars (Fig. 7b).

Unlike the above-mentioned plots, the Qp–Lv–Ls diagram of Dickinson and Suczek (1979), distinguishing different type of lithic clasts, indicates rather uniform magmatic-arc sources for sandstones

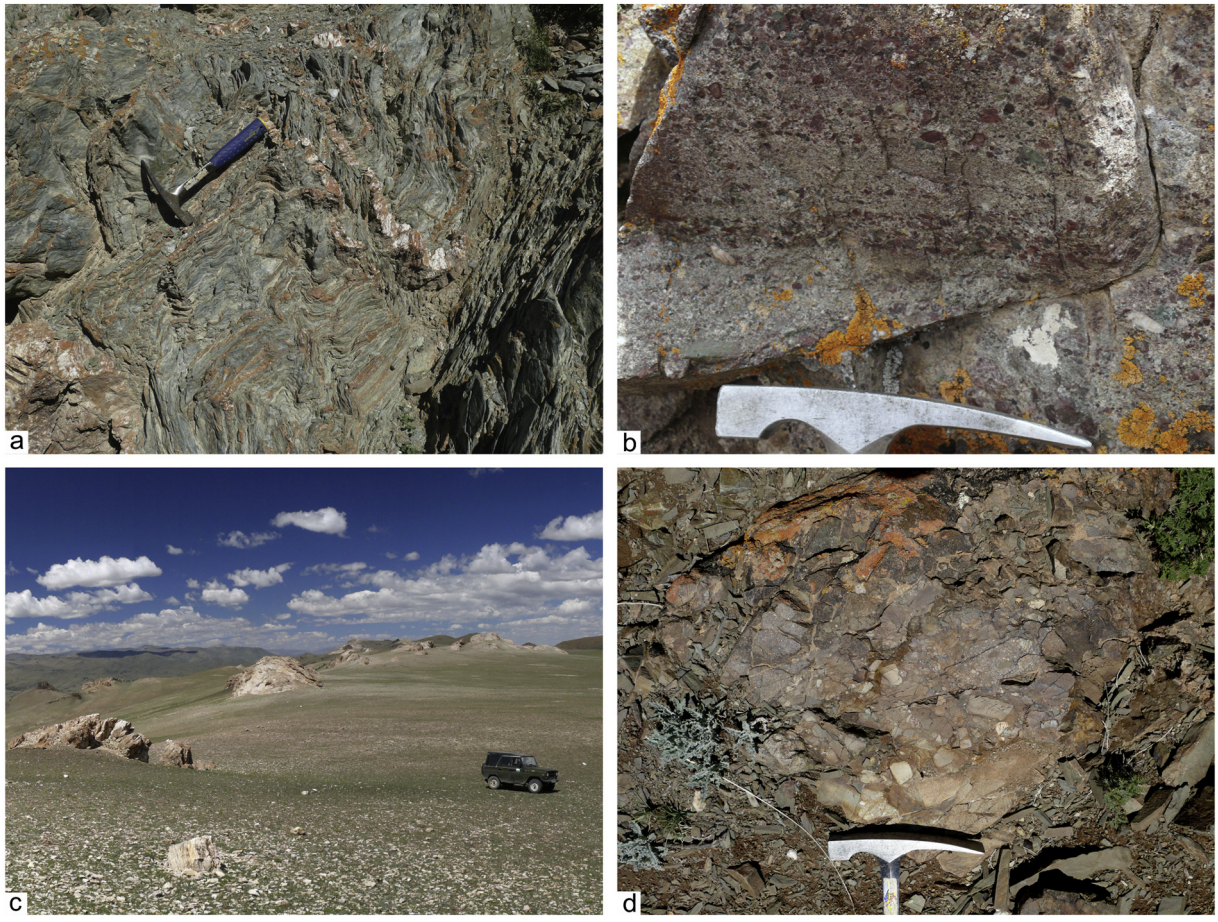

Fig. 4. Field photographs of the Zuunnuruu (a, b) and Tsetseg (c, d) formations outcrops. (a) Weakly metamorphosed and folded alternation of tuffs and shales (GC 074). (b) Graded bedding in the fine-grained conglomerate (GC 231). (c) Outcrops of limestone lenses linearly arranged in the NW–SE direction (GC 133). (d) Poorly sorted conglomerate (GC 041).

from all the three formations (Fig. 7c). Only the sample GB 194, falling close to the Qp apex of the diagram (Fig. 7c), was likely recycled from a quarzitic sedimentary rock. The Qp–Lv–Ls diagram also clearly shows that the samples from the Sagsai Formation are essentially free of the sedimentary lithic fragments and contain more volcanic clastic material than the older formations (Fig. 7c). Feldspars are, in most samples, almost exclusively plagioclases; only some samples from the Sagsai Formation display a small share of K-feldspars (Fig. 7d).

5.2. Results of U–Pb detrital zircon dating

5.2.1. Zuunnuruu Formation

Zircon grains from the sample *GC 231* are 100–200 μm long, colourless or light brown and shortly prismatic or stubby. Most of grains exhibit well-preserved crystal shapes and oscillatory zoning in CL (Fig. 8a). U–Pb dating of 50 grains yielded age population with the highest proportion of ages around ca. 520 Ma and two subordinate peaks at ca. 780 Ma and ca. 900 Ma (Fig. 9a). Some individual ages appear also at ca. 1.3 Ga, 1.5 Ga, 1.9 Ga and 2.7 Ga.

Zircons in the sample *GC 342* are mostly ca. 60–150 μm long, transparent to pale pink and generally prismatic with rarely rounded crystal faces. Most of the zircon grains have well-preserved, but often truncated, oscillatory or sector zoning (Fig. 8b). Analyses of 151 grains yielded ages dominantly clustering at ca. 520 Ma, with another significant peak between ca. 750 Ma and 1.0 Ga and several small peaks between 1.0 Ga and 3.0 Ga (Fig. 9b).

Sample *GC 131* contains generally shortly prismatic, pink to pale brown zircon grains, mostly ca. 80–200 μm long. Most grains are subhedral and display, sometimes truncated, igneous oscillatory zoning (Fig. 8c). Age population (120 analyses) of this sample shows wide spectrum of data, with a major peak at ca. 510 Ma and a broad minor peak at interval of 1000–700 Ma as well as a few data between ca. 1.2 Ga and 1.5 Ga, around 1.9 Ga and at ca. 3.0 Ga (Fig. 9c).

5.2.2. Tsetseg Formation

Sample *GB 487* contains 100–300 μm long, transparent, milky pink and brown zircons. Short-prismatic grains with well-preserved crystal faces dominate over long-prismatic and barrel-shaped ones. The crystals of the last type have often rounded edges. Most of the zircons display oscillatory zoning and some grains have angular cores discordantly overgrown by thick outer parts (Fig. 8d). Age spectrum obtained from the sample GB 487 (136 analyses) shows one significant peak at ca. 465 Ma. The remaining analyses cluster in two wide intervals of ca. 1.0–0.7 Ga and 2.2–1.4 Ga (Fig. 9d).

Zircons extracted from the sample *GC 041* are mostly subhedral, pale brown to pink, short prismatic and 800–200 μm long with relicts of crystal faces. CL images display often indistinct oscillatory or patchy zoning (Fig. 8e). Analyses of 51 grains yielded a nearly unimodal age population with a single main peak at ca. 470 Ma and somewhat smaller subpeak at ca. 500 Ma, as well as several individual ages at ca. 400 Ma, 600 Ma and around 1.0 Ga (Fig. 9e).

5.2.3. Sagsai Formation

Sample *GC 040* contains 150–300 μm long, transparent and light brown zircon grains. Most of them are euhedral, long prismatic and display non-concentric oscillatory zoning. Nevertheless, several zircons also contain sub-rounded cores, with chaotic internal patterns, overgrown by thick oscillatory-zoned rims (Fig. 8f). Analyses of 20 grains

Fig. 5. Field photographs of the Sagsai Formation outcrops. (a) Folded alternation of calcareous and clastic flysch sequences affected by thrust faulting. Height of the slope approximately 300 m. (b) Grey limestone and calcic siltstone layers alternating in a flysch sequence (GC 035). (c) Typical flysch development – regularly alternating shales and (massive) greywackes (GC 082). (d) Lenticular intercalation of deformed conglomerate with matrix supported clasts (GC 163).

from the sample GC 040 provided age spectrum showing a peak at ca. 390 Ma and two single ages at ca. 430 Ma and ca. 550 Ma (Fig. 10a). However, the absence of additional age peaks, detected in the other samples, could be caused by a small number of extracted zircons.

Zircons from the sample *GC 163* are 80–250 μm long, clear, pink or pale brown and have either long-prismatic, euhedral or stubby, rounded shapes. Most of the grains show truncated, concentric oscillatory zoning (Fig. 8g). Dating of the zircons from this sample (50 analyses) provided a wide age range. Most of the ages fall in the interval between ca. 400 Ma and 550 Ma, with a dominant peak at ca. 540 Ma (Fig. 10b). Remaining analyses cluster at 1.2–0.75 Ga and 1.85–1.25 Ga; two individual data appear around 2.8 Ga.

Sample *GC 082* includes two distinct types of zircon crystals. The prevailing, pale brown, 80–200 μm long, stubby zircons have strongly abraded edges whereas colourless, long-prismatic, 120–250 μm long grains have well-preserved crystal faces. CL imaging revealed concentric oscillatory or sector zoning or corroded inherited cores with dark overgrowths (Fig. 8h). Age population obtained from this sample (117 analyses) reveals a major peak at ca. 500 Ma, a smaller one at ca. 390 Ma and a broad, less significant group at ca. 0.7 Ma–1.1 Ga. The rest of data is distributed between 1.2 Ga and 2.1 Ga (Fig. 10c).

Zircons separated from the sample *GS 189* are generally 100–250 μm long and mainly have shortly-prismatic to stubby, subhedral shapes and pink to dark brown colour and show concentric oscillatory, but also faint zoning (Fig. 8i). Analyses of 84 grains from the sample GS 189 yielded an age spectrum resembling the previous sample. The data form a dominant peak at ca. 500 Ma and another important broad peak at ca. 900 Ma (Fig. 10d). Remaining data define minor peaks at ca. 390 Ma and 760 Ma and individual ages at ca. 1.2 Ga, 1.8 Ga and 2.7 Ga.

Sample *GC 036* contains 100–200 μm long, transparent to light brown zircons with mostly shortly-prismatic sub-rounded shapes. These mostly have oscillatory zoning or complex internal structures (Fig. 8j). Age population of 42 grains shows a single large peak at ca. 470 Ma and an individual age of ca. 1.0 Ga (Fig. 10e).

5.2.4. Summary of detrital zircon age populations of the Hovd Zone flysch sequences

Detrital zircon age populations of the studied samples display, except the youngest ages that correspond to their maximum stratigraphic age, dominant Neoproterozoic–Ordovician age peak, a broad but important Neo- to Mesoproterozoic peak at ca. 1050–720 Ma and several minor Meso- to Palaeoproterozoic age clusters at ca. 1.4, 1.9 and 2.4 Ga. The samples from the all three studied formations show very similar age patterns.

Only the sample GC 040 contains almost exclusively data in interval of ca. 420–360 Ma and lacks older ages (Fig. 10a) but this could be simply due to a relatively small number of zircons extracted. However, the other samples yielded sufficient numbers of grains (Košler et al., 2013 and references therein) and thus the whole datasets for individual formations are robust enough to allow the provenance study.

6. Discussion

6.1. Depositional setting

Based on the field observations, petrographic and sedimentological characteristics, the early Palaeozoic depositional environment and character of source rocks of the eastern Hovd Zone Basin can be established. The prevailing, mostly volcano-sedimentary development of the Zuunnuruu Formation and lowermost section of the Tsetseg Formation, defined by tuffs, shales, siltstones and greywackes, could be interpreted as related to the deeper, distal part of the basin. The more mature,

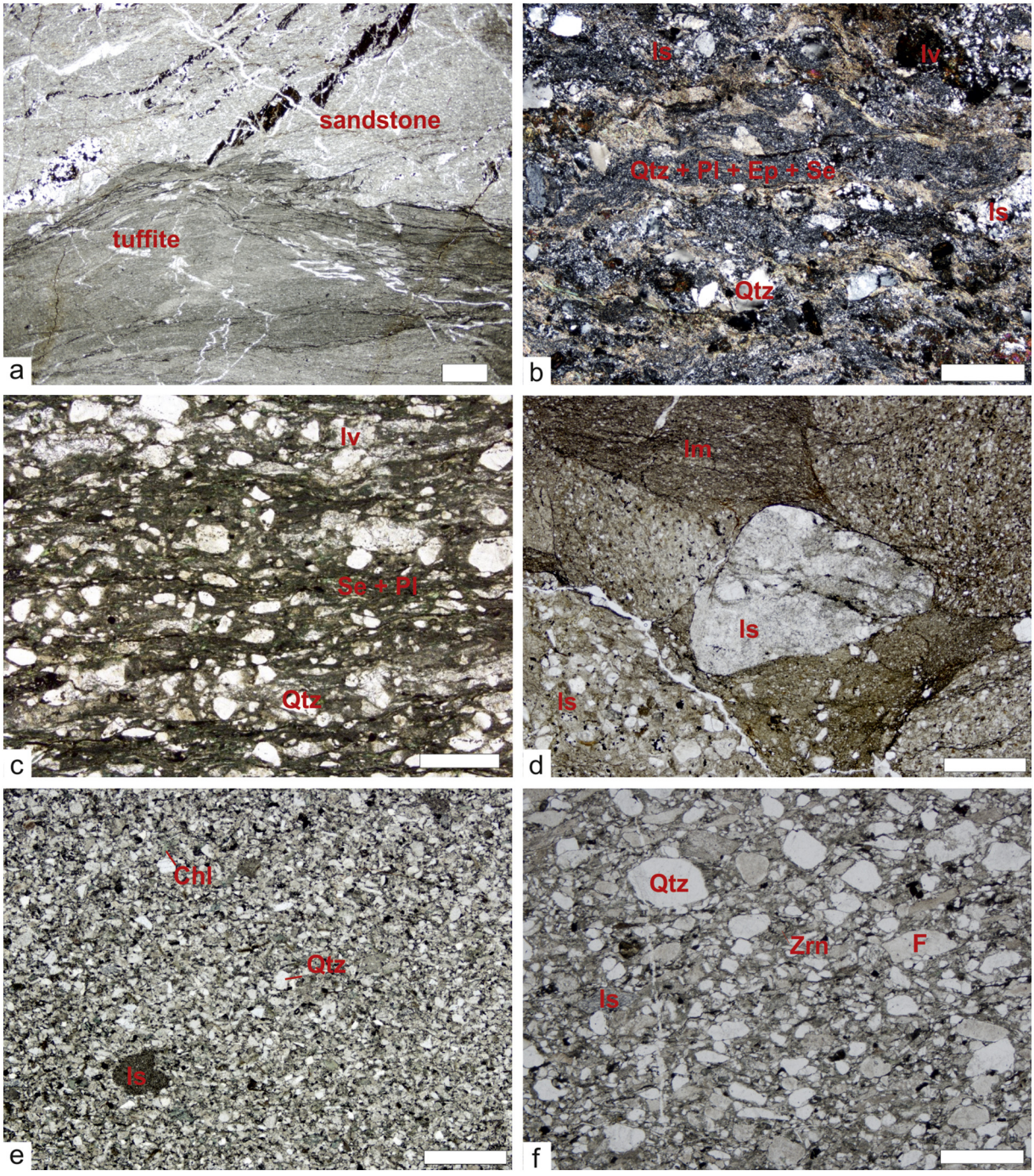

Fig. 6. Photomicrographs showing the rocks from the Zuunnuruu (a–b), Tsetseg (c–d) and Sagsai formations (e–f). (a) Alternation of slightly metamorphosed tuffite and very fine-grained metasandstone (upper part) (PPL, GC 262). (b) Deformed very fine-grained (meta-) tuffite with quartz and volcanic lithic clasts and quartz–feldspar–epidote–sericite matrix (XPL, GS 298). (c) Foliated unsorted sandstone with quartz clasts, lithic fragments of acid volcanic rocks and mostly sericite matrix (PPL, GB 200). (d) Polymictic conglomerate with silty–sandy matrix (PPL, GC 041). (e) Well sorted fine-grained greywacke (PPL, GC 082). (f) Moderately sorted medium-grained greywacke (PPL, GC 026). Scale bar = 1 mm; ls: sedimentary lithic fragment, lm: metamorphic lithic fragment, lv: volcanic lithic fragment, F: feldspar (symbols for rock-forming minerals after Kretz, 1983).

siliciclastic facies probably records deposition within a shallower, marginal part of the basin. The presence of well-sorted psammitic material suggests an important contribution from relatively remote sources, whereas the local intercalations of conglomerates, and small bodies of rhyolites and ignimbrites can be related to occasional gravity, lava and pyroclastic flows from the volcanic belt into the margin of the sedimentary basin. Limestone and basalt bodies present within the basal part of the Tsetseg Formation could be interpreted either as reef limestones possibly covering volcanic elevations or as a calcareous material redeposited from the shallower water levels.

This development evolved into the mostly siliciclastic uppermost part of the formation, which could be interpreted as a more proximal part of the prevailing turbiditic sedimentation. Shales dominating basal and uppermost Sagsai Formation were deposited in the deepest part of the basin and did not originate in a flysch regime, whereas the majority of the succession records alternations of shorter and non-periodical debris-flow events in a long-lasting period of classic flysch-type deposition. Relatively high content of volcanic lithic clasts in generally siliciclastic rocks of the Sagsai Formation is related to the associated basaltic lavas and most likely also to the sedimentary recycling of the

Table 1
Brief petrological and sedimentological description and location of geochronological samples from the Zuunnuruu, Tsetseg and Sagsai formations.

Sample	Latitude (N)	Longitude (E)	Petrology	Youngest age
Zuunnuruu Formation (Ordovician)				
GC 231	47.087638	92.450995	Fine-grained polymict conglomerate, moderately sorted with graded bedding, silicified Composed mainly of quartz (25%), lithic clasts (25%), feldspars (10%), micas, chlorite and sandy matrix (45%)	491 Ma
GC 342	47.147232	92.400781	Medium- to fine-grained sandstone, well sorted, carbonate cemented and silicified Composed mainly of quartz (30%), lithic clasts (20%), feldspar and clayey matrix (40%)	480 Ma
GC 131	47.065284	92.321480	Medium- to fine-grained sandstone, well sorted, partly silicified and laminated Composed mainly of quartz (50%), lithic clasts (up to 10%), micas and silty matrix (40%)	452 Ma
Tsetseg Formation (Silurian)				
GB 487	47.018035	92.379478	Coarse-grained polymict conglomerate, unsorted and foliated Composed mainly of quartz (65%), lithic clasts (25%; esp. acid tuffs) and sandy matrix (10%)	442 Ma
GC 041	47.065338	91.805255	Coarse-grained polymict conglomerate, unsorted Composed mainly of lithic clasts (85%), quartz (5%) and silty to fine-sandy matrix (10%)	415 Ma
Sagsai Formation (Devonian)				
GC 163	47.111721	92.271125	Medium-grained metaconglomerate, poorly sorted, silicified and strongly foliated Composed mainly of quartz (40–50%), lithic clasts (20%), actinolite and sandy to clayey matrix (20–25%)	398 Ma
GC 040	47.060500	91.798614	Siltstone locally passed into the silty shale, moderately sorted and slightly foliated Composed mainly of clayey to silty matrix (90%) and clastic quartz (2%)	366 Ma
GC 082	47.089345	91.892847	Fine-grained greywacke, well sorted Composed mainly of quartz (25%), lithic clasts (15%), feldspars (10%), micas and clay-silty matrix (45%)	377 Ma
GS 189	47.138560	91.880387	Very fine-grained metasandstone, moderately sorted and foliated Composed of quartz (60–80%), micas (3%; up to 20% in fine-grained domains) and clayey matrix (20%)	385 Ma
GC 036	47.131771	91.911621	Very fine-grained sandstone, moderately sorted and strongly foliated Composed mainly of quartz and silty to fine-sandy matrix (50%)	359 Ma

older underlying volcano-sedimentary strata. Lack of limestones and calcareous components within most of the flysch sequences indicates the dominant sedimentation environment under the CCD (carbonate compensation depth). On the contrary, the calcareous flysch portion of the formation most likely built a shallower level of the basin, most of the time above the CCD. The presence of basaltic bodies is related to the Devonian intra-basin volcanism (Buriánek, unpublished data).

In summary, the Zuunnuruu Formation and lowermost section of the Tsetseg Formation developed in the marine basin, where the prevailing volcanic material was transported together with the subordinate siliciclastic one. These sedimentological features suggest that the Ordovician to Lower Silurian section of the succession most likely represents a proximal (forearc) section of the sedimentary accretionary wedge, close to an active magmatic arc. This finding corresponds to the concept of Dobretsov et al. (1995) assuming that the Lower Palaeozoic terrigenous sequences of the Mongolian Altai and the Hovd Zone were deposited in a forearc basin.

Sedimentological characteristics imply that the most of the Tsetseg and Sagsai formations originated in a variable environment, but predominantly indicate turbiditic siliciclastic sedimentation. These parts of succession could be interpreted as having been generated in a Silurian to Devonian basin developed on margin of the former accretionary wedge system, during the extensional post-arc stage. The immature lithological character (Fig. 7d) and relatively well-preserved shape of clasts as well as most of the zircon grains (Figs. 6, 8) are in accord with a short transport and rapid deposition, pointing to turbiditic flysch-type of deposition.

Table 2
Modal analyses from sandstones of the Zuunnuruu, Tsetseg and Sagsai formations.

Sample	Matrix	Qm	Qp	P	K	Lm	Lv	Ls
Zuunnuuru Formation								
GC 231	48.4	65.7	1.6	1.7	0.0	5.0	23.3	2.8
GC 342	43.8	44.2	0.0	18.0	0.0	24.9	8.1	4.8
Tsetseg Formation								
GB 194	39.2	91.2	8.0	0.8	0.0	0.0	0.0	0.0
GB 200	51.2	60.0	0.0	9.0	0.0	15.8	10.5	4.7
GB 487A	46.0	43.3	0.0	6.9	2.6	23.7	22.8	0.8
Sagsai Formation								
GB 021	33.4	21.4	0.0	38.3	0.0	2.4	37.9	0.0
GB 050	65.8	54.0	1.3	28.1	0.7	7.8	6.7	1.4
GB 103B	24.4	33.0	0.0	26.4	0.2	19.5	20.9	0.0
GC 026	46.0	51.0	0.0	14.6	4.0	13.0	17.4	0.0
GC 082	50.2	48.0	0.0	26.6	1.4	15.3	8.7	0.0
GC 013	39.8	39.6	0.0	11.7	4.1	13.9	30.0	0.7

Abbreviations: Qm: monocrystalline quartz, Qp: polycrystalline quartz, P: plagioclase, K: K-feldspar, Lm: metamorphic lithic fragments, Ls: sedimentary lithic fragments, Lv: volcanic lithic fragments.

6.2. Depositional age

Ariunchimeg et al. (2012) with Baatarhuyag and Gansukh (1999) reported an Ordovician age for the Zuunnuruu Formation and a Silurian age for the Tsetseg Formation, whereas the Lower Devonian cessation of sedimentation has been suggested for the Sagsai Formation already by Luvsandanzan (1970). However, depositional ages of the studied sequences have been previously determined only based on the rare fossil occurrences and sedimentological analogies with the relatively remote areas.

Age populations presented in this study prove the youngest ages from three samples of the Zuunnuruu Formation in interval between ca. 491 and 452 Ma (Fig. 9a–c) and thus confirm its Ordovician age. This result is consistent with the U–Pb zircon magmatic age 462 ± 3 Ma of rhyolite from this sequence (Žáček et al., 2016). Similarly, the youngest zircon ages (442 Ma and 415 Ma; Fig. 9d, e) corroborate the Silurian (to the earliest Devonian) age of the Tsetseg Formation, also supported by the graptolite find, representing most likely the *Oktavites spiralis* Zone (Žáček et al., 2016). On the contrary, the most samples from the Sagsai Formation revealed significantly younger zircon ages (398–366 Ma; Fig. 10) and the sample GC 036 yielded even younger age of ca. 360 Ma. These youngest detrital zircon ages imply that the sedimentation lasted considerably longer than has been proposed previously (e.g., the Sagsai Fm. is marked as “Lower Devonian” on existing geological maps), at least until the latest Devonian, or even the earliest Carboniferous.

6.3. Possible source regions for the Lower Palaeozoic flysch sequences in the Hovd Zone

Determination of tectonic setting of source area, based on the petrographic modal analyses of sandstones from the studied formations, is not entirely unambiguous and the recycled orogen and/or magmatic-

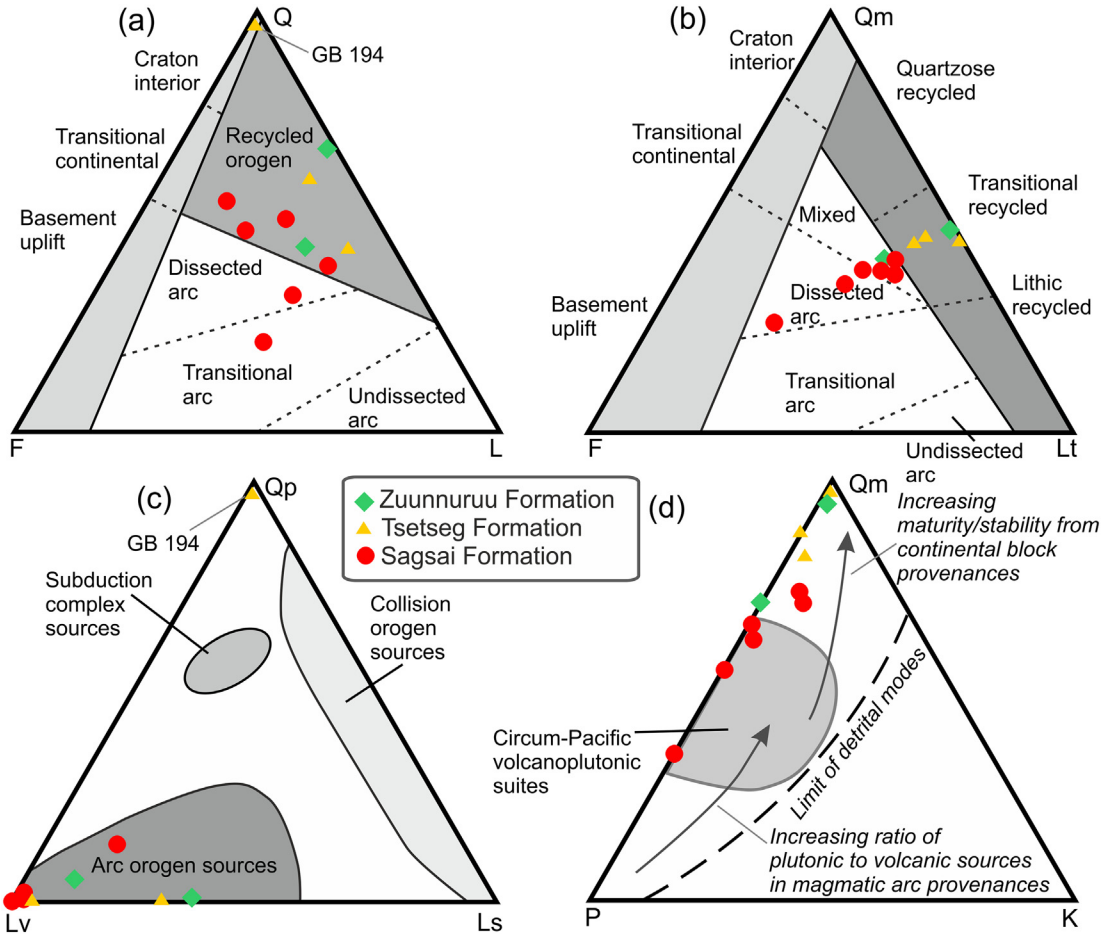

Fig. 7. Geotectonic diagrams of clastic provenance for sandstones from the Zuunnuruu, Tsetseg and Sagsai formations showing geotectonic setting of source rocks. (a) Q–F–L diagram. (b) Qm–F–Lt diagram. (c) Qp–Lv–Ls diagram. (d) Qm–P–K diagram. Provenance fields for a, b, d after Dickinson (1985) and c after Dickinson and Suczek (1979). Abbreviations: Q: total quartz, Qm: monocrystalline quartz, Qp: polycrystalline quartz, P: plagioclase, K: K-feldspar, F: feldspar (plagioclase and K-feldspar), L: total lithic fragments, Ls: sedimentary lithic fragments, Lt: total lithic fragments and polycrystalline quartz, Lv: volcanic lithic fragments.

arc provenance with progressively increasing share of plutonic rocks is established (Fig. 7). However, the sandstones, used for the modal analysis, represent just one of the lithologies in sedimentary associations of the studied sedimentary rocks (Fig. 3). Basaltic volcanites, tuffs and tuffites are abundant and volumetrically significant rock types of the Zuunnuruu and the lowermost part of the Tsetseg formations. The detrital modes aided by geotectonic diagrams (Fig. 7) do not fully reflect neither possible lithological complexity of the source region nor the sedimentary and deformational biases (Garzanti, 2016).

The general volcano-sedimentary character of the Zuunnuruu and the lowermost part of the Tsetseg formations implies that main source was an active volcanic arc. Moreover, all the samples are dominated by detrital zircon ages close to their age of sedimentation. This is typical of an active-margin setting, as documented by the cumulative distribution plot of Cawood et al. (2012) (Fig. 11b). Increasing share of feldspathic detritus in the sandstones of the generally siliciclastic Sagsai Formation indicates a derivation mostly from eroded products of an extinct volcanic arc (or its freshly exposed plutonic sections) as well as the adjacent Devonian granitic plutons.

The youngest Devonian sequences show a significant peak at 398–359 Ma. Most of the Cambrian and younger zircons have igneous-looking internal structures and subhedral to euhedral shapes (Fig. 8) implying a short transport. In contrast, the Neoproterozoic–Archean ages were detected especially in the sub-rounded or corroded grains or cores, indicating their longer transport and/or recycling. The proportion of recycled sedimentary detritus is difficult to determine; however, the cannibalisation of the underlying sedimentary wedge could have played an important role for much of the Tsetseg and Sagsai formations.

Still, the youngest age peak at ca. 400–360 Ma, detected in the samples from the Sagsai Formation, could be interpreted as a clastic material coming directly from the neighbouring Devonian granitic bodies (Cai et al., 2015; Soejono et al., 2016).

Dominant zircon age group at ca. 560–460 Ma matches well the main period of the magmatic-arc activity of the Ikh-Mongol Arc System within the Lake Zone of ca. 570–460 Ma (Janoušek et al., 2018; Kovach et al., 2011; Rudnev et al., 2012; Soejono et al., 2016, 2017), the Neoproterozoic–early Cambrian ophiolites (Dijkstra et al., 2006; Jian et al., 2014; Khain et al., 2003) along its eastern margin and also the Neoproterozoic passive margin sedimentary sequences in the Lake Zone (Buriánek et al., 2017). Remarkably small proportion of K-feldspars in the lower part of the succession is in line with the rock types (andesites/quartz diorites) likely dominating the inferred sedimentary source – Cambrian–Ordovician intra-oceanic arcs in the Lake Zone.

Broad subordinate peak at ca. 1050–720 Ma can be linked with the early Neoproterozoic (Tonian) continental-arc magmatism (Buriánek et al., 2017; Demoux et al., 2009a; Kröner et al., 2010) and Rodinia break-up related volcanism (Bold et al., 2016; Kozakov et al., 2011; Levashova et al., 2010; Yarmolyuk et al., 2008) in the Zavkhan and Baidrag microcontinental segments further east. Moreover, several minor Meso- to Palaeoproterozoic age clusters at ca. 1.4, 1.9 and 2.4 Ga could have been contributed directly by these Precambrian basements (Bold et al., 2016; Demoux et al., 2009b; Kozakov et al., 1993;

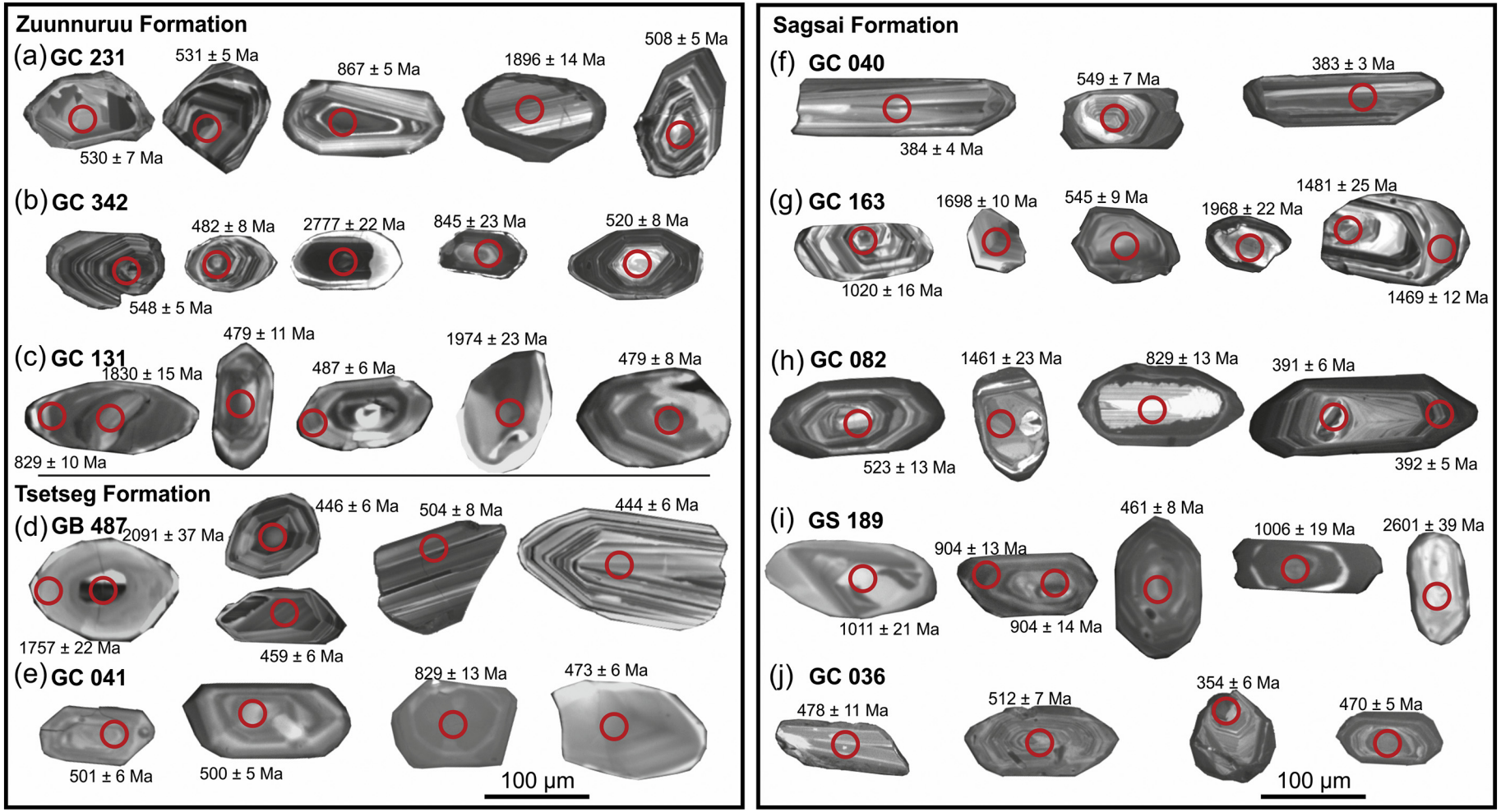

Fig. 8. Cathodoluminescence images of representative zircon grains from the studied samples. Laser-ablation ICP-MS analysis spots are marked with concordant $^{206}Pb/^{238}U$ ages with 2σ uncertainties.

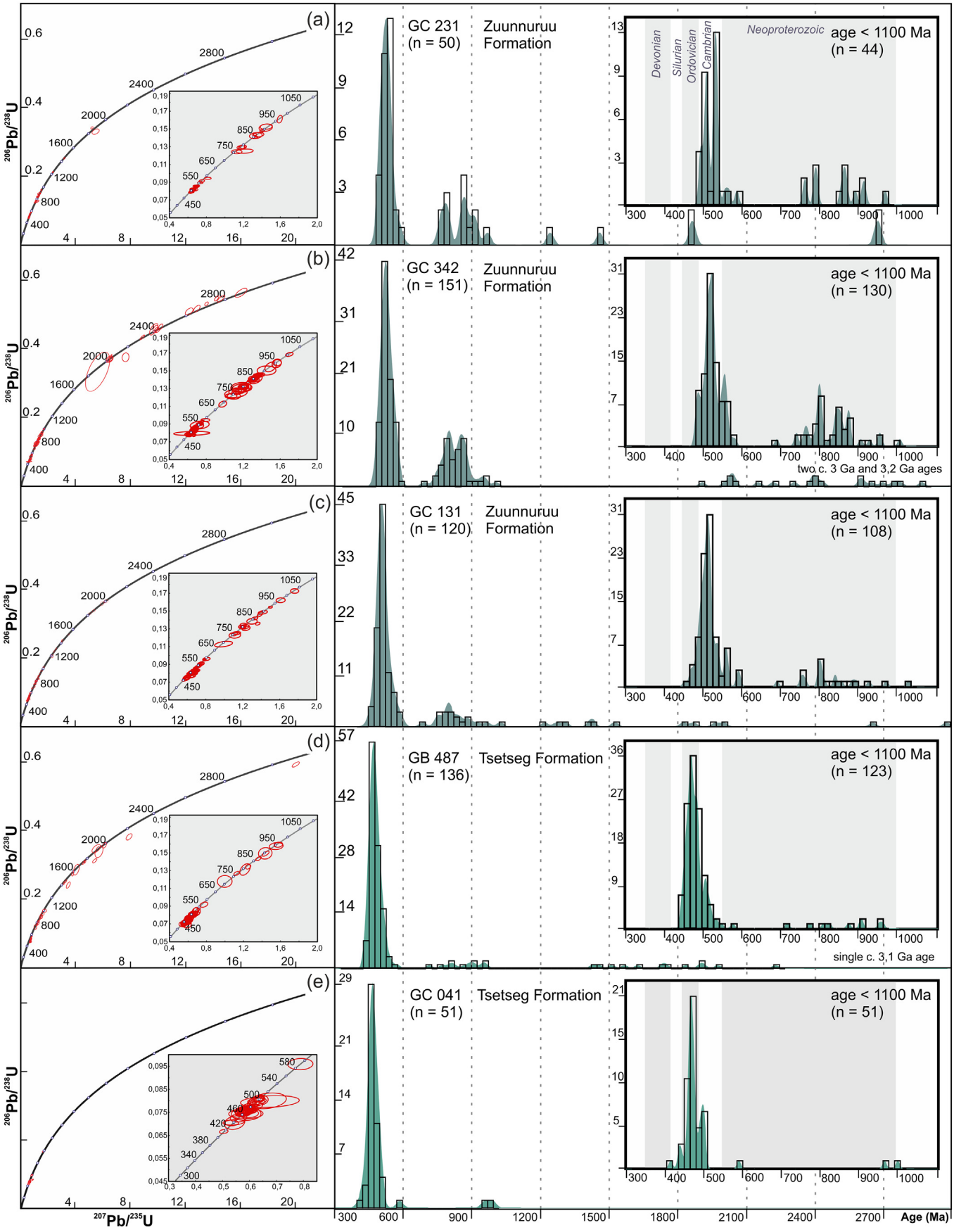

Fig. 9. Concordia diagrams and frequency histograms with kernel density estimates (filled curves) showing detrital ($^{206}Pb/^{238}U$) zircon age distributions in the studied samples from the Zuunnuruu and Tsetseg formations; n – number of analyses. Only data <10% discordant were used.

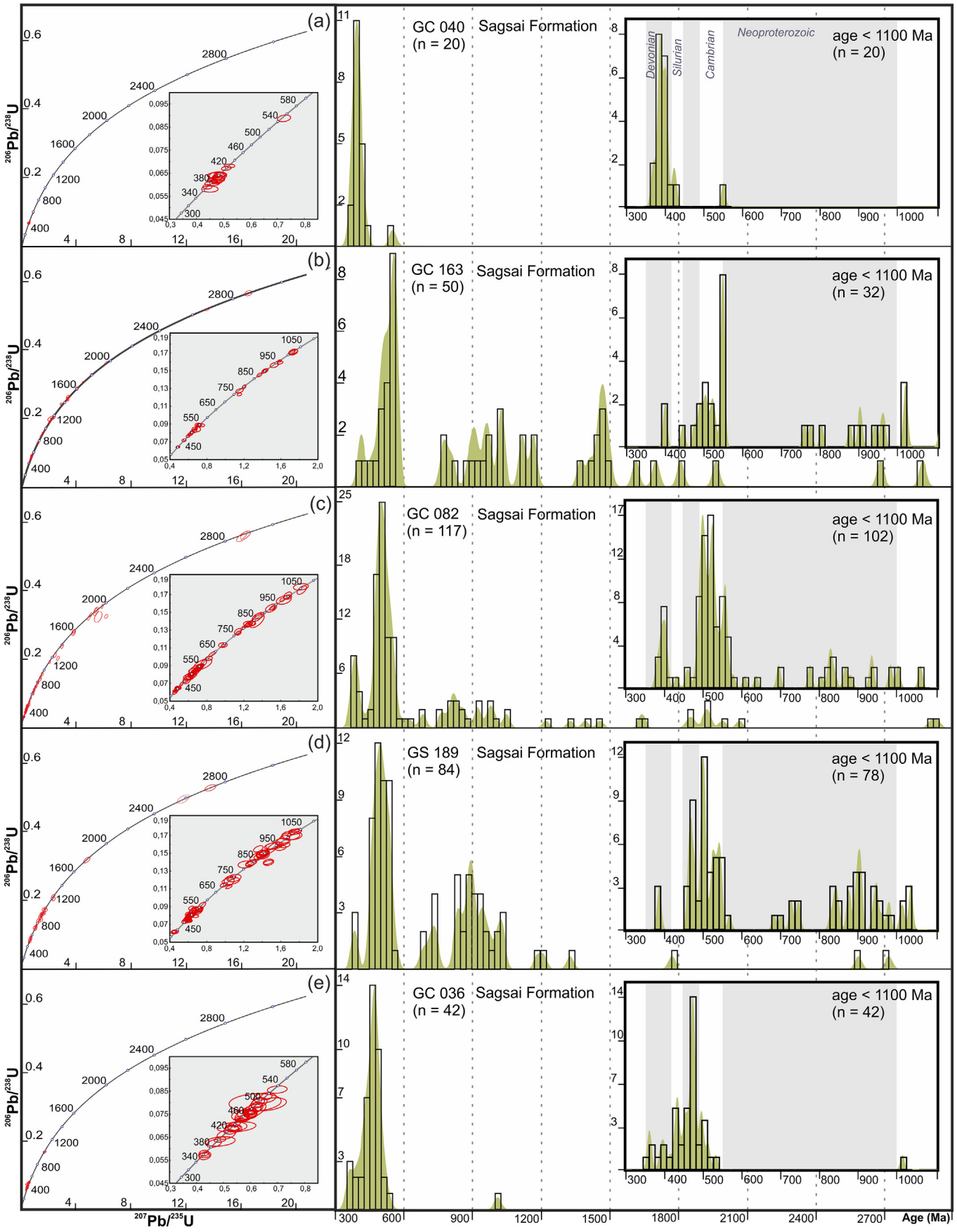

Fig. 10. Concordia diagrams and frequency histograms with kernel density estimates (filled curves), showing detrital ($^{206}Pb/^{238}U$) zircon age distributions in the studied samples from the Sagsai Formation; n – number of analyses. Only data <10% discordant were used.

Kröner et al., 2015). Short transport of the Palaeozoic zircons and the longer transport or recycling of the older, based on the zircons shapes and internal features support the idea of derivation of the clastic material from these sources.

In summary, clastic material for the studied formations was derived mainly from the neighbouring Lake Zone and also contributed from the margins of the Mongolian continental blocks (Fig. 11a, 12). This confirms the westward (in the western Mongolia, present-day coordinates) transport of sedimentary material from the central CAOB. Such an idea has been proposed previously not only for the Mongolian (Jiang et al., 2017), but also for the Chinese (Long et al., 2012) and Russian (Chen et al., 2015) Altai.

6.4. Comparison with detrital zircon data from the surrounding areas

Metasedimentary rocks of the directly adjacent Bij Group (Fig. 2) (Soejono et al., 2017) yielded detrital zircon age patterns generally indistinguishable from those obtained here from the studied flysch sequences (Fig. 13a, b). Based on this resemblance and its mostly volcano-sedimentary nature, the Bij Group could be interpreted as a metamorphosed equivalent of the Zuunnuruu Formation.

Nearly identical detrital zircon age spectra were reported also from the Lower Palaeozoic accretionary wedge-related (meta-) sedimentary rocks of the Mongolian, Russian and Chinese Altai (Figs. 11, 13) (Chen et al., 2015; Jiang et al., 2017; Long et al., 2010; Wang et al., 2014). These striking similarities in detrital zircon age populations seem a typical feature of (meta-) sedimentary rocks in the Altai accretionary wedge. This fact indicates a common provenance and shared transport direction of clastic material within the whole accretionary system.

Comparison of all these units reveals only small differences between zircon crystallization ages and depositional ages, which is consistent with the convergent margin environment (Fig. 11b), namely an origin in supra-subduction sedimentary accretionary prism. These sedimentary basins belong to the giant early Palaeozoic Altai accretionary wedge stretching from Mongolia to Russia (Chen et al., 2014; Jiang et al., 2017; Long et al., 2012; Xiao et al., 2004) that decorated the entire western and southwestern margin of the Ikh-Mongol Arc System.

6.5. Timing of magmatic-arc activity in the western Lake Zone

The abrupt change from dominantly volcano-clastic to mainly siliciclastic sedimentary mode within the Tsetseg Formation indicates

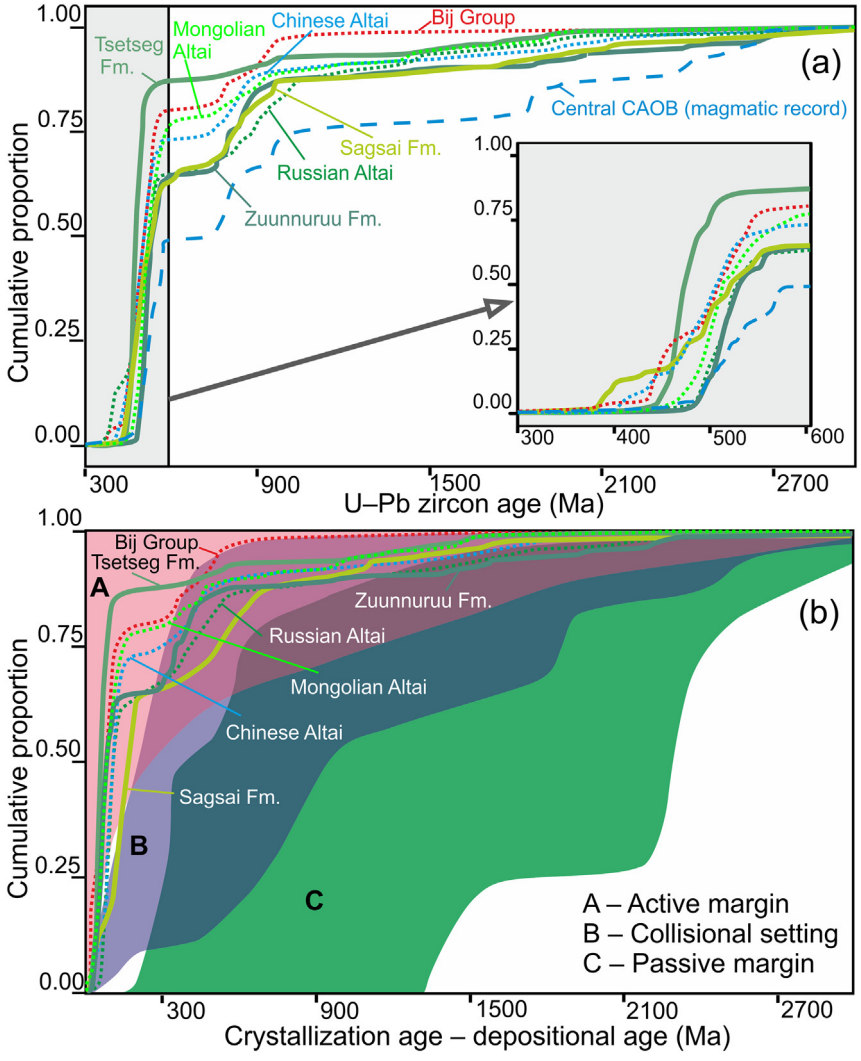

Fig. 11. (a) Cumulative distribution curves of detrital zircon age spectra from the Zuunnuruu, Tsetseg and Sagsai formations (solid lines – this study) and published data (dotted lines) from the Bij Group (Soejono et al., 2017), Chinese (Long et al., 2010; Wang et al., 2014), Mongolian Altai (Jiang et al., 2017) and Russian Altai (Chen et al., 2015). The U–Pb data from magmatic complexes from the central CAOB (Lake Zone, Zavkhan, Baidrag and Tuva-Mongolia continental blocks; dashed line – same data sources as in Fig. 13) are plotted for comparison. (b) Cumulative distribution curves of differences between the crystallization ages (CA) and the depositional ages (DA) of detrital zircons from the Zuunnuruu, Tsetseg and Sagsai formations (this study) and published data from the Bij Group, Chinese, Mongolian and Russian Altai (the same sources as in panel a). Depositional ages of individual units are inferred from the youngest detrital zircon ages. Colour fields representing different tectonic settings of deposition are after Cawood et al. (2012).

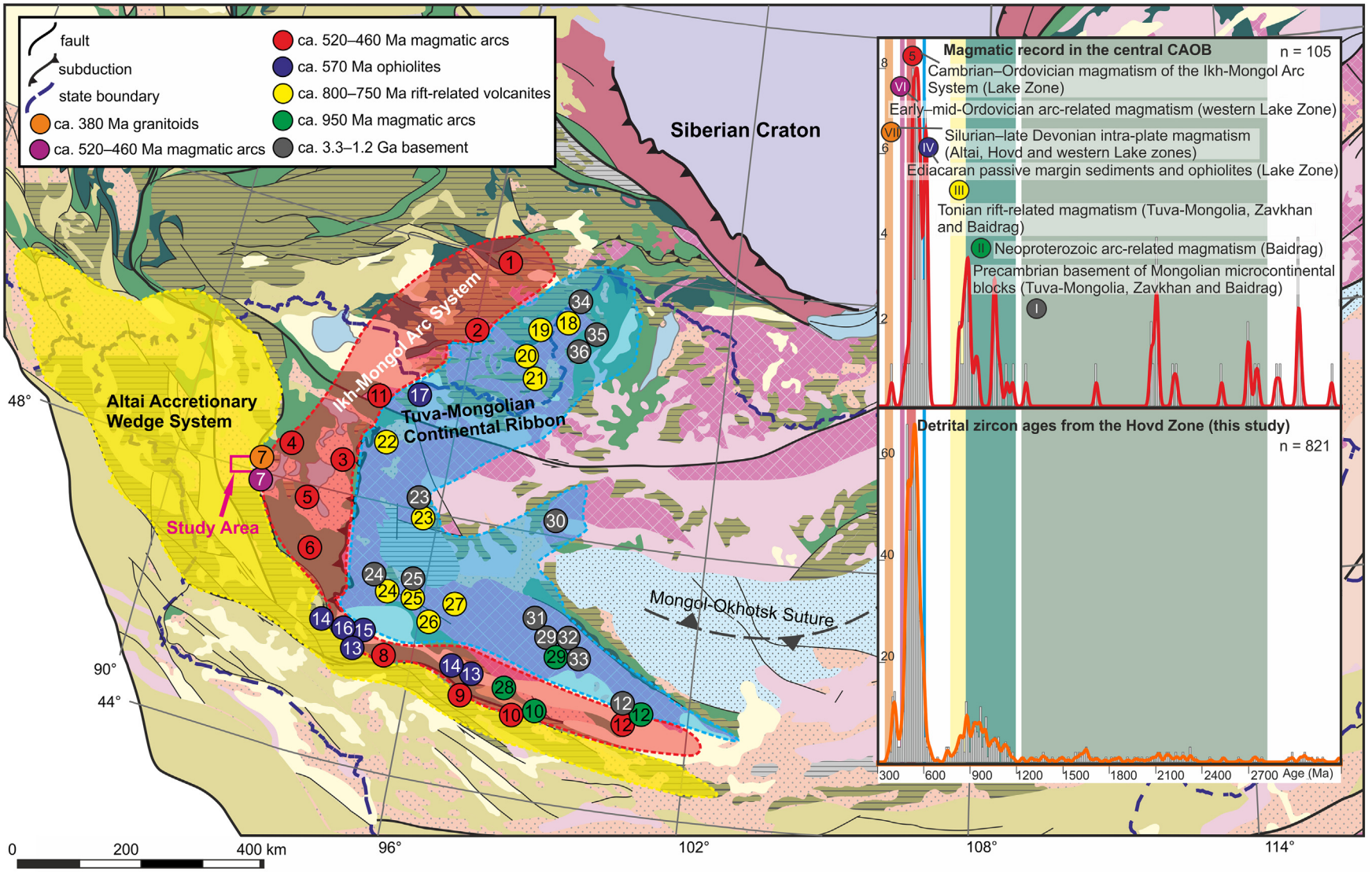
fault
subduction
state boundary
ca. 380 Ma granitoids
ca. 520–460 Ma magmatic arcs
ca. 520–460 Ma magmatic arcs
ca. 570 Ma ophiolites
ca. 800–750 Ma rift-related volcanites
ca. 950 Ma magmatic arcs
ca. 3.3–1.2 Ga basement
Siberian Craton
Altai Accretionary Wedge System
Ikh-Mongol Arc System
Tuva-Mongolian Continental Ribbon
Mongol-Okhotsk Suture
Study Area
48°
90°
44°
96°
102°
108°
114°
0
200
400 km
Magmatic record in the central CAOB
n = 105
Cambrian–Ordovician magmatism of the Ikh-Mongol Arc System (Lake Zone)
Early–mid-Ordovician arc-related magmatism (western Lake Zone)
Silurian–late Devonian intra-plate magmatism (Altai, Hovd and western Lake zones)
Ediacaran passive margin sediments and ophiolites (Lake Zone)
Tonian rift-related magmatism (Tuva-Mongolia, Zavkhan and Baidrag)
Neoproterozoic arc-related magmatism (Baidrag)
Precambrian basement of Mongolian microcontinental blocks (Tuva-Mongolia, Zavkhan and Baidrag)
Detrital zircon ages from the Hovd Zone (this study)
n = 821
Age (Ma)
Cenozoic sedimentary cover
Permian–Cretaceous volcanic-plutonic-sedimentary rocks
Permian–Triassic plutonic-volcanic rocks
Devonian–Carboniferous oceanic and or plutonic-volcanic-sedimentary rocks
Silurian–Carboniferous turbidite basin of Mongol-Ochotsk Ocean
Cambrian–early Silurian accretionary complexes
Neoproterozoic–Cambrian passive margins
Neoproterozoic–Cambrian accretionary complexes
Neoproterozoic island arcs
High-grade metamorphic complexes
Microcontinental blocks and/or rifted craton margins
Cratons

that the volcanic detritus was depleted in the source area. This result provides a unique possibility to constrain the upper age limit for an arc-related magmatic activity in the region. The real extinction of the active volcanic-arc system had to take place somewhat earlier than evidenced by the sedimentary record.

Mid-Ordovician magmatic-arc rocks were recently documented from the nearby boundary of the Lake and Hovd zones (Soejono et al., 2016, 2017). The western margin of the Lake Zone most likely was a member of the Cambro–Ordovician Ikh-Mongol Arc System, driven by the continuous Pacific-type subduction of the oceanic domain (Janoušek et al., 2018; Jiang et al., 2017).

The switch in the sedimentary style, recorded by the Tsetseg Formation, implies the latest Ordovician–earliest Silurian termination of magmatic-arc activity in the Ikh-Mongol Arc System and transition from the wedge-type volcano-sedimentary deposition into the platform siliciclastic flysch-type development with intra-basin volcanism.

6.6. Tectonic implications

Recognition of the central CAOB as the source area of the detrital material for the flysch sequences of the Hovd Zone and their equivalents in the Chinese and Mongolian Altai is essential for better understanding of early Palaeozoic tectonic evolution. Determined westward transport of clastic material indicates that the westerly area was then most likely occupied by an oceanic domain and thus supports east-dipping (in the present-day coordinates) oceanic-plate subduction beneath the Lake Zone and the Precambrian microcontinents. The eastward subduction is in accord with the model of westward younging magmatic-arc system, driven by continuous slab retreat (Janoušek et al., 2018; Soejono et al., 2017).

While the onset of this subduction and formation of the associated accretionary wedge system is relatively well constrained by the early Cambrian arc magmatism (Janoušek et al., 2018), timing their termination is more challenging. The youngest known Mid-Ordovician member of the Ikh-Mongol Arc System (Soejono et al., 2016) and its waning activity, recorded in the studied succession, suggest that the arc magmatism lasted at least until the late Ordovician or early Silurian. Furthermore, the presence of thick Silurian–Devonian siliciclastic sequences accompanied by carbonate platforms throughout the Mongolian and Chinese Altai (Ariunchimeg et al., 2012; Badarch et al., 2002; Kröner et al., 2010; Long et al., 2008) can be considered as equivalents of the majority of the Tsetseg and Sagsai formations.

The formation of late Silurian to Devonian extensional basins can be related to important lithospheric extension, associated with exceptionally high heat flow and causing HT–LP metamorphism (Broussolle et al., 2015; Burenjargal et al., 2014; Jiang et al., 2015) and, ultimately, widespread crustal anatexis leading to granitic plutonism and acid volcanism (Cai et al., 2011; Hanžl et al., 2016; Jiang et al., 2015, 2016; Wang et al., 2011) in both the Chinese and Mongolian Altai. Mid-Silurian intra-plate magmatism occurred also directly in the studied area where it has been considered an expression of the starting crustal extension (Soejono et al., 2017); the basaltic volcanism recorded in the Sagsai Formation (Buriánek, unpublished data) thus likely reflected its advanced, Devonian stage. Different mechanisms such as asthenospheric upwelling triggered by ridge subduction/slab window formation (Cai et al., 2011; Long et al., 2010) or crustal thinning of a supra-subduction system, perhaps in back-arc position (Hanžl et al., 2016; Jiang et al., 2016), have been proposed. However, a direct link between this important extensional event and the deposition of enormous amounts of Silurian to Devonian, mostly flysch-like, sedimentary rocks in the Altai region is obvious.

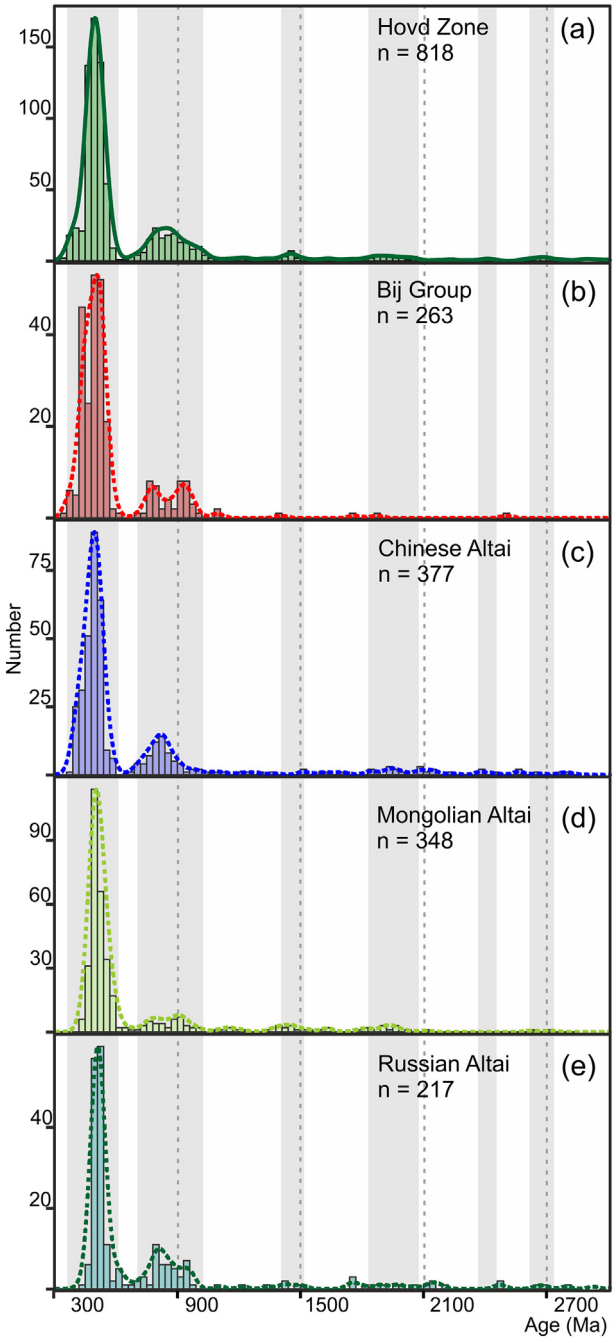

Fig. 13. Comparison of detrital zircon ages from (a) Zuunnuruu, Tsetseg and Sagsai formations (Hovd Zone; this study) with published detrital zircon ages from (b) the Bij Group (Soejono et al., 2017), (c) the Chinese Altai (Long et al., 2010; Wang et al., 2014), (d) the Mongolian Altai (Jiang et al., 2017) and (e) the Russian Altai (Chen et al., 2015) (meta-) sedimentary rocks.

Fig. 12. Simplified tectonic map of the central CAOB showing main lithotectonic domains (modified from Parfenov et al., 2003 and Jiang et al., 2017). Spatial distribution of possible magmatic sources of clastic material in the Hovd Zone Basin is marked. Inset shows a comparison of detrital zircon ages from Hovd Zone with published magmatic ages from the Lake Zone and the Mongolian microcontinents (central CAOB). Age peaks and possible source areas are labeled by numerals. Data sources: 1 – Mongush et al. (2011); 2 – Rudnev et al. (2006); 3 – Rudnev et al. (2009); 4 – Izokh et al. (2011); 5 – Yarmolyuk et al. (2011); 6 – Rudnev et al. (2012); 7 – Soejono et al. (2016); 8 – Rudnev et al. (2013); 9 – Janoušek et al. (2018); 10 – Buriánek et al. (2017); 11 – Sal'nikova et al. (2001); 12 – Demoux et al. (2009a); 13 – Khain et al. (2003); 14 – Jian et al. (2014); 15 – Dijkstra et al. (2006); 16 – Kozakov et al. (2002); 17 – Pfänder et al. (1999); 18 – Kuzmichev and Larionov (2011); 19 – Kuzmichev et al. (2001); 20 – Kuzmichev et al. (2007); 21 – Kuzmichev et al. (2005); 22 – Kozakov et al. (2014); 23 – Kozakov et al. (2011); 24 – Bold et al. (2016); 25 – Burashnikov (1990); 26 – Levashova et al. (2010); 27 – Yarmolyuk et al. (2008); 28 – Kröner et al. (2010); 29 – Demoux et al. (2009b); 30 – Kröner et al. (2015); 31 – Kotov et al. (1995); 32 – Kozakov et al. (1993); 33 – Mitrofanov et al. (1985); 34 – Khain et al. (1999); 35 – Kovach et al. (2004); 36 – Khain et al. (1995).

Finally, our results enable us to characterize the early Palaeozoic sedimentary evolution of the studied successions, within the framework of the tectonic evolution of the west Mongolian part of the CAOB. During the Ordovician to early Silurian, the Zuunnuruu Formation and the basal part of the Tsetseg Formation developed in an arc-proximal part of a Pacific-type accretionary prism, above the eastward subducting oceanic plate. The basin was fed mainly by the adjacent active magmatic-arc and other sources in the easterly Lake Zone and Mongolian continental segments (Fig. 14a). Thereafter, most likely at the end of the Ordovician but not later than in early Silurian, the activity of this magmatic arc-system terminated and the depositional setting changed into a generally siliciclastic platform sedimentation in the extension-related basins developed on the former accretionary wedge. Until the late Devonian, the Tsetseg and Sagsai formations, accompanied by intra-basin volcanism, were more or less continuously deposited within the easternmost part of the attenuated Altai accretionary complex (Fig. 14b). Basinal system was continuously filled by material derived from still the same source areas.

In conclusion, we suggest that the depositional history of the Hovd Zone Basin as well as the overall geodynamic evolution of the west Mongolian part of the CAOB during much of early Palaeozoic were driven by a long-lasting subduction, associated accretionary prism formation and following crustal extension. However, additional comparative studies both of large detrital zircon populations and/or dating of potential source rocks are needed for shaping a more detailed and better constrained model of the sediment provenance, basinal development, and tectonic evolution of the Hovd Zone and surrounding regions.

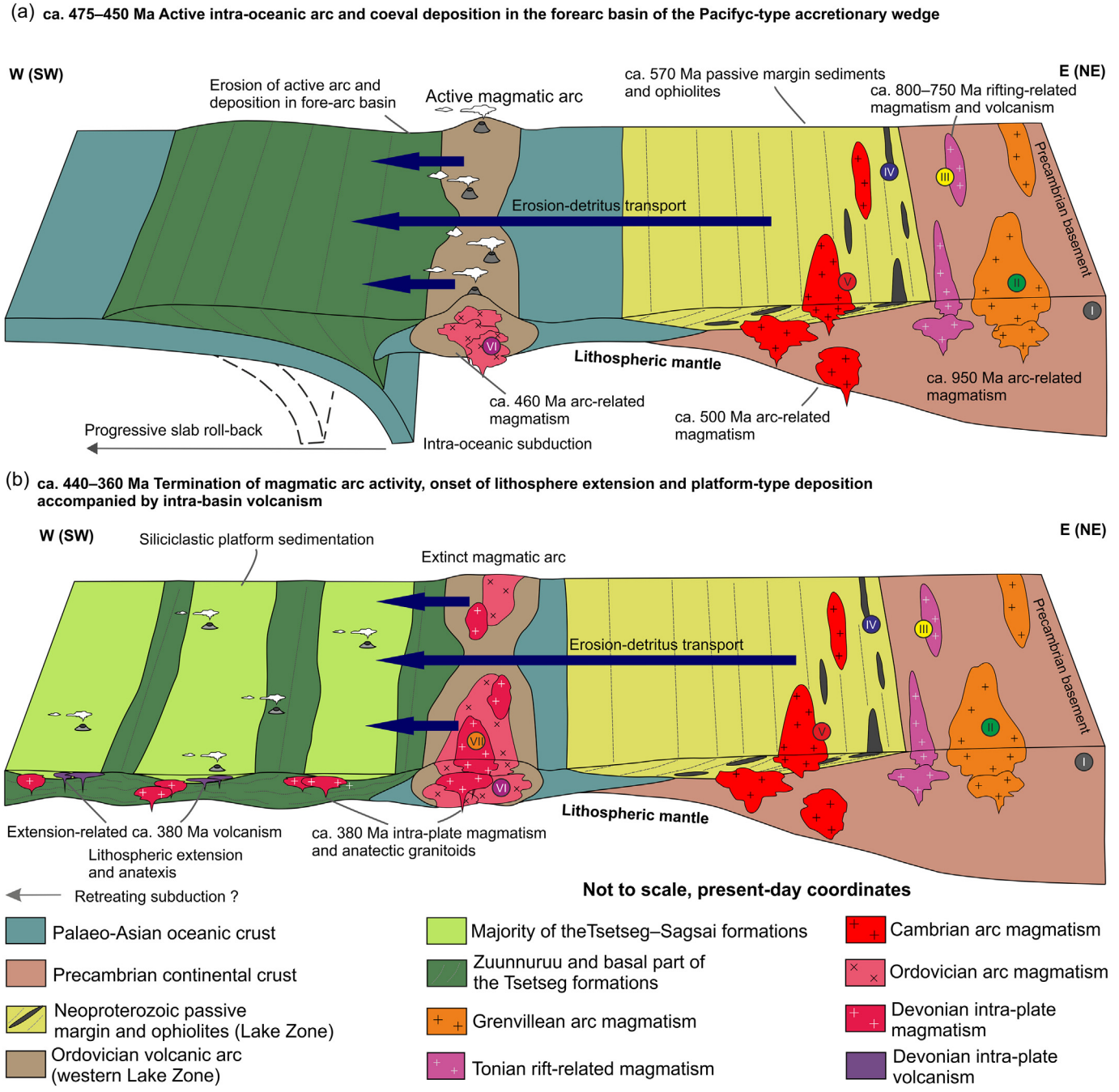

Fig. 14. Schematic geodynamic model for evolution of the western Mongolian tract of the CAOB. (a) Accretionary wedge stage in the Ordovician–earliest Silurian. (b) Platform stage in the earliest Silurian–late Devonian. Possible sources of detritus are labeled according to Fig. 13.

7. Conclusions

Combining our new sedimentological analyses and the detrital zircon dating of the Lower Palaeozoic sequences from the eastern Hovd Zone in western Mongolia with published geochronological, geochemical and tectonic studies, we can propose the following conclusions:

1) Two main sedimentary stages have been distinguished in the early Palaeozoic evolution of the Hovd Zone sedimentary system: (i) volcano-clastic deposition in a proximal part of the accretionary wedge (Ordovician–earliest Silurian), (ii) siliciclastic flysch-type deposition in platform mode (late Silurian–late Devonian).
2) This switch of the sedimentary regime implies the latest Ordovician–earliest Silurian termination of magmatic-arc activity in the western Lake Zone and the onset of crustal extensional period.
3) The detrital zircon geochronology shifts the end of deposition at least to late Devonian.
4) The clastic material for the Altai accretionary wedge basin was uniformly derived from the easterly situated central segment of the CAOB.
5) Comparison of detrital zircon age populations from different parts of the Altai confirms the model of the giant early Palaeozoic accretionary wedge along the entire current western and southwestern margins of the Ikh-Mongol Arc System.
6) Established general westward (in the present-day coordinates) sedimentary transport indicates the east-dipping Pacific-type subduction of oceanic plate in the early Palaeozoic.

Supplementary data to this article can be found online at https://doi.org/10.1016/j.gr.2018.07.005.

Acknowledgements

We are grateful to M. Racek, P. Halodová and O. Pour for CL images. We also thank S. Vrána for help with microscopy, L. Maštera for modal analysis and V. Žáček, T. Vorel, V. Fürych, O. Oyun-Enkh, and B. Janzanpagma for field assistance. We also acknowledge I. Safonova for editorial handling and three journal referees for their constructive comments. This work was supported by the internal grant of Czech Geological Survey no. 321700 and by the Czech Science Foundation (GAČR) (17-17540S to K. Schulmann and O. Lexa). This manuscript benefited from our discussions with O. Lexa, Y.D. Jiang, P. Hanžl and A. Guy.

References

Andersen, T., Kristoffersen, M., Elburg, M.A., 2016. How far can we trust provenance and crustal evolution information from detrital zircons? A South African case study. Gondwana Research 34, 129–148. https://doi.org/10.1016/j.gr.2016.03.003.

Andersen, T., Kristoffersen, M., Elburg, M.A., 2017. Visualizing, interpreting and comparing detrital zircon age and Hf isotope data in basin analysis – a graphical approach. Basin Research 38, 42–49. https://doi.org/10.1111/bre.12245.

Ariunchimeg, Ya., Badamgarav, D., Byamba, J., Dorjnamjaa, D., Makhbadar, Ts., Minjin, Ch., Narantsetseg, Ts., Orolmaa, D., Sersmaa, G., 2012. Geology and Mineral Resources of Mongolia. vol. 1. Stratigraphy, Soëmbo, Ulaanbaatar, pp. 1–562 (in Mongolian).

Baatarhuyag, A., Gansukh, L., 1999. Geological Map of the Mongolia on the Scale 1:200 000, Map Sheet L-46-IX. Geological Information Center, MRAM, Ulaanbaatar (in Mongolian).

Badarch, G., Cunningham, W.D., Windley, B.F., 2002. A new terrane subdivision for Mongolia: implications for the Phanerozoic crustal growth of Central Asia. Journal of Asian Earth Sciences 21, 87–110. https://doi.org/10.1016/S1367-9120(02)00017-2.

Bold, U., Crowley, J.L., Smith, E.F., Sambuu, O., Macdonald, F.A., 2016. Neoproterozoic to early Paleozoic tectonic evolution of the Zavkhan Terrane of Mongolia: implications for continental growth in the Central Asian Orogenic Belt. Lithosphere 8, 729–750. https://doi.org/10.1130/L549.1.

Broussolle, A., Štípská, P., Lehmann, J., Schulmann, K., Hacker, B.R., Holder, R., Kylander-Clark, R.C., Hanžl, P., Racek, M., Hasalová, P., Lexa, O., Hrdličková, K., Buriánek, D., 2015. P–T–t–D record of crustal-scale horizontal flow and magma-assisted doming in the SW Mongolian Altai. Journal of Metamorphic Geology 33, 357–383. https://doi.org/10.1111/jmg.12124.

Burashnikov, V.V., 1990. Tectonics of the Urgamal Zone, Early Caledonides of Western Mongolia. (Unpublished Ph.D. Thesis). Geological Institute, Russian Academy of Sciences, Moscow.

Burenjargal, U., Okamoto, A., Kuwatani, T., Sakata, S., Hirata, T., Tsuchiya, N., 2014. Thermal evolution of the Tseel Terrane, SW Mongolia and its relation to granitoid intrusions in the Central Asian Orogenic Belt. Journal of Metamorphic Geology 32, 765–790. https://doi.org/10.1111/jmg.12090.

Buriánek, D., Janoušek, V., Hanžl, P., Jiang, Y., Schulmann, K., Lexa, O., Altanbaatar, B., 2016. Petrogenesis of the Late Carboniferous Sagsai Pluton in the SE Mongolian Altai. Journal of Geosciences 61, 67–92. https://doi.org/10.3190/jgeosci.207.

Buriánek, D., Schulmann, K., Hrdličková, K., Hanžl, P., Janoušek, V., Gerdes, A., 2017. Geochemical and geochronological constraints on distinct Early-Neoproterozoic and Cambrian accretionary events along southern margin of the Baydrag Continent in western Mongolia. Gondwana Research 47, 200–227. https://doi.org/10.1016/j.gr.2016.09.008.

Buslov, M.M., Watanabe, T., Saphonova, I., Iwata, K., Travinl, A., Akiyama, M., 2002. A Vendian–Cambrian Island Arc System of the Siberian Continent in Gorny Altai (Russia, Central Asia). Gondwana Research 5, 781–800. https://doi.org/10.1016/S1342-937X(05)70913-8.

Cai, K., Sun, M., Yuan, C., Zhao, G., Xiao, W., Long, X., Wu, F., 2011. Prolonged magmatism, juvenile nature and tectonic evolution of the Chinese Altai, NW China: evidence from zircon U–Pb and Hf isotopic study of Paleozoic granitoids. Journal of Asian Earth Sciences 42, 949–968. https://doi.org/10.1016/j.jseaes.2010.11.020.

Cai, K., Sun, M., Jahn, B., Xiao, W., Yuan, C., Long, X., Chen, H., Tumurkhuu, D., 2015. A synthesis of zircon U–Pb ages and Hf isotopic compositions of granitoids from southwest Mongolia: implications for crustal nature and tectonic evolution of the Altai Superterrane. Lithos 232, 131–142. https://doi.org/10.1016/j.lithos.2015.06.014.

Cawood, P.A., Hawkesworth, C.J., Dhuime, B., 2012. Detrital zircon record and tectonic setting. Geology 40, 875–878. https://doi.org/10.1130/G32945.1.

Chen, M., Sun, M., Cai, K., Buslov, M.M., Zhao, G., Rubanova, E.S., 2014. Geochemical study of the Cambrian–Ordovician meta-sedimentary rocks from the northern Altai-Mongolian Terrane, northwestern Central Asian Orogenic Belt: implications on the provenance and tectonic setting. Journal of Asian Earth Sciences 96, 69–83. https://doi.org/10.1016/j.jseaes.2014.08.028.

Chen, M., Sun, M., Cai, K., Buslov, M.M., Zhao, G., Rubanova, E.S., Voytishek, E.E., 2015. Detrital zircon record of the early Paleozoic meta-sedimentary rocks in Russian Altai: Implications on their provenance and the tectonic nature of the Altai–Mongolian Terrane. Lithos 233, 209–222. https://doi.org/10.1016/j.lithos.2014.11.023.

Cocks, L.R.M., Torsvik, T.H., 2007. Siberia, the wandering northern terrane, and its changing geography through the Palaeozoic. Earth-Science Reviews 82, 29–74. https://doi.org/10.1016/j.earscirev.2007.02.001.

Demoux, A., Kröner, A., Liu, D., Badarch, G., 2009a. Precambrian crystalline basement in southern Mongolia as revealed by SHRIMP zircon dating. International Journal of Earth Sciences 98, 1365–1380. https://doi.org/10.1007/s00531-008-0321-4.

Demoux, A., Kröner, A., Badarch, G., Jian, P., Tomurhuu, D., Wingate, M.T.D., 2009b. Zircon ages from the Baydrag Block and the Bayankhongor Ophiolite Zone: time constraints on Late Neoproterozoic to Cambrian subduction- and accretion-related magmatism in Central Mongolia. Journal of Geology 117, 377–397. https://doi.org/10.1086/598947.

Dickinson, W.R., 1985. Interpreting provenance relations from detrital modes of sandstones. In: Zuffa, G.G. (Ed.), Provenance of Arenites. Springer Netherlands, Dordrecht, pp. 333–361. https://doi.org/10.1306/2F9188FB-16CE-11D7-8645000102C1865.

Dickinson, W.R., Suczek, C.A., 1979. Plate tectonics and sandstone compositions. American Association of Petroleum Geologists Bulletin 63, 2164–2182 (doi:0149-1423/79/B012-0003$03.00/0).

Dijkstra, A., Buchan, C., Dijkstra, A., Brouwer, F., Cunningham, W., Badarch, G., Mason, P., 2006. Late Neoproterozoic proto-arc ocean crust in the Dariv Range, Western Mongolia: a supra-subduction zone end-member ophiolite. Journal of the Geological Society of London 163, 363–373. https://doi.org/10.1144/0016-764904-156.

Dobretsov, N.L., Berzin, N.A., Buslov, M.M., Ermakov, V.D., 1995. General aspects of the Altai region interrelationships between its basement pattern and neotectonic structural development. Russian Geology and Geophysics 36, 3–15.

Enkhbayar, B., Bolormaa, Kh., Barsbold, Ts, 2003. Origin of Bij metamorphic complex. Mongolian Geoscientist 20, 2–7 (in Mongolian).

Garzanti, E., 2016. From static to dynamic provenance analysis – sedimentary petrology upgraded. Sedimentary Geology 336, 3–13. https://doi.org/10.1016/j.sedgeo.2015.07.010.

Gavrilova, S.P., Zaitsev, N.S., Pavlov, V.P., Yashina, R.M., 1975. Granitoid and alkaline formations in the structures of Western and Northern Mongolia. Transactions. vol. 14. Nauka, Moscow (in Russian).

Hanžl, P., Schulmann, K., Janoušek, V., Lexa, O., Hrdličková, K., Jiang, Y., Buriánek, D., Altanbaatar, B., Ganchuluun, T., Erban, V., 2016. Making continental crust: origin of Devonian orthogneisses from SE Mongolian Altai. Journal of Geosciences 61, 25–50. https://doi.org/10.3190/jgeosci.206.

Izokh, A.E., Vishnevskii, A.V., Polyakov, G.V., Shelepaev, R.A., 2011. Age of picrite and picrodolerite magmatism in western Mongolia. Russian Geology and Geophysics 52, 7–23. https://doi.org/10.1016/j.rgg.2010.12.002.

Jackson, S.E., Pearson, N.J., Griffin, W.L., Belousova, E.A., 2004. The application of laser ablation-inductively coupled plasma-mass spectrometry to in situ U–Pb zircon geochronology. Chemical Geology 211, 47–69.

Janoušek, V., Jiang, Y.D., Buriánek, D., Schulmann, K., Hanžl, P., Soejono, I., Kröner, A., Altanbaatar, B., Erban, V., Lexa, O., Ganchuluun, T., Košler, J., 2018. Cambrian–Ordovician magmatism of the Ikh-Mongol Arc System exemplified by the Khantaishir Magmatic Complex (Lake Zone, south–central Mongolia). Gondwana Research 54, 122–149. https://doi.org/10.1016/j.gr.2017.10.003.

Jelínek, J., Žáček, V., 2018. Assessment of a catastrophic rock avalanche in the West Mongolian Altai Mountains. Engineering Geology 233, 38–47. https://doi.org/10.1016/j.enggeo.2017.12.003.

Jian, P., Kröner, A., Jahn, B.M., Windley, B.F., Shi, Y., Zhang, W., Zhang, F., Miao, L., Tomurhuu, D., Liu, D., 2014. Zircon dating of Neoproterozoic and Cambrian ophiolites in West Mongolia and implications for the timing of orogenic processes in the central part of the Central Asian Orogenic Belt. Earth-Science Reviews 133, 62–93. https://doi.org/10.1016/j.earscirev.2014.02.006.

Jiang, Y.D., Štípská, P., Sun, M., Schulmann, K., Zhang, J., Wu, Q.H., Long, X.P., Yuan, C., Racek, M., Zhao, G.C., Xiao, W.J., 2015. Juxtaposition of Barrovian and migmatite domains in the Chinese Altai: a result of crustal thickening followed by doming of partially molten lower crust. Journal of Metamorphic Geology 33, 45–70. https://doi.org/10.1111/jmg.12110.

Jiang, Y.D., Schulmann, K., Sun, M., Štípská, P., Guy, A., Janoušek, V., Lexa, O., Yuan, C., 2016. Anatexis of accretionary wedge, Pacific type magmatism, and formation of vertically stratified continental crust in the Altai Orogenic Belt. Tectonics 35, 3095–3118. https://doi.org/10.1002/2016TC004271.

Jiang, Y.D., Schulmann, K., Kröner, A., Sun, M., Lexa, O., Janoušek, V., Buriánek, D., Yuan, C., Hanžl, P., 2017. Neoproterozoic–Early Paleozoic peri-Pacific accretionary evolution of the Mongolian collage system: insights from geochemical and U–Pb zircon data from the Ordovician sedimentary wedge in the Mongolian Altai. Tectonics 36, 2305–2331. https://doi.org/10.1002/2017TC004533.

Khain, E.V., Neimark, L.A., Amelin Yu, V., 1995. The Caledonian stage of remobilization of the Precambrian basement of the Gargan Block, the Eastern Sayan (isotopic geochronological data). Doklady Akademii Nauk 342, 776–780 (in Russian).

Khain, E.V., Bibikova, E.V., Degtyarev, K., Gibsher, A.S., Didenko, A.N., Klochko, A.N., Rytsk, E.Y., Sal'nikova, E.B., Fedotova, A.A., 1999. The Paleo-Asian Ocean in the Neoproterozoic and early Paleozoic: new isotope geochronological data. Geological Development of Proterozoic Pericratonic and Palaeoceanic Structures of Northern Eurasia, pp. 175–181 (Abstract Volume. St. Petersburg).

Khain, E.V., Bibikova, E.V., Sal'nikova, E.B., Kröner, A., Gibsher, A.S., Didenko, A.N., Degtyarev, K.E., Fedotova, A.A., 2003. The Palaeo-Asian Ocean in the Neoproterozoic and early Palaeozoic: new geochronologic data and palaeotectonic reconstructions. Precambrian Research 122, 329–358.

Košler, J., Sláma, J., Belousova, E., Corfu, F., Gehrels, G.E., Gerdes, A., Horstwood, M.S.A., Sircombe, K.N., Sylvester, P.J., Tiepolo, M., Whitehouse, M.J., Woodhead, J.D., 2013. U–Pb detrital zircon analysis – results of an inter-laboratory comparison. Geostandards and Geoanalytical Research 37, 243–259. https://doi.org/10.1111/j.1751-908X.2013.00245.x.

Kotov, A.B., Kozakov, I.K., Bibikova, E.V., Sal'nikova, E.B., Kirnozova, T.I., Kovach, V.P., 1995. Duration of regional metamorphic episodes in areas of polycyclic endogenic processes – a U–Pb geochronological study. Petrology 3, 567–575 (in Russian).

Kovach, V.P., Matukov, D.I., Berezhnaya, N.G., 2004. Tectonics of Precambrian mobile belts. The 32nd IGC Florence, Session: T31.01, p. 1263.

Kovach, V.P., Yarmolyuk, V.V., Kovalenko, V.I., Kozlovskyi, A.M., Kotov, A.B., Terent'eva, L.B., 2011. Composition, sources, and mechanisms of formation of the continental crust of the Lake Zone of the Central Asian Caledonides. II. Geochemical and Nd isotope data. Petrology 19, 399–425. https://doi.org/10.1134/S0869591111030064.

Kozakov, I.K., Bibikova, E., Neymark, L.A., Kimozova, T.I., 1993. The Baydaric Block. In: Rudnik, B.A., Sokolov, Y.M., Filatova, L.I. (Eds.), The Early Precambrian of the Central Asian Fold Belt. Nauka, St. Petersburg, pp. 118–137.

Kozakov, I.K., Sal'nikova, E.B., Khain, E.V., Kovach, V.P., Berezhnaya, N.G., Yakovleva, S.Z., Plotkina, Y.V., 2002. Early Caledonian crystalline rocks of the Lake Zone in Mongolia: formation history and tectonic settings as deduced from U–Pb and Sm–Nd datings. Geotectonics 36, 156–166.

Kozakov, I.K., Sal, E.B., Wang, T., Didenko, A.N., Plotkina, Y.V., Podkovyrov, V.N., 2007. Early Precambrian crystalline complexes of the Central Asian Microcontinent: age, sources, tectonic position. Stratigraphy and Geological Correlation 15, 121–140. https://doi.org/10.1134/S0869593807020013.

Kozakov, I.K., Kozlovsky, A.M., Yarmolyuk, V.V., Kovach, V.P., Bibikova, E.V., Kirnozova, T.I., Plotkina, Y.V., Zagornaya, N.Y., Fugzan, M.M., Erdenejargal, C., Lebedev, V.I., Eenjin, G., 2011. Crystalline complexes of the Tarbagatai block of the Early Caledonian superterrane of Central Asia. Petrology 19, 426–444. https://doi.org/10.1134/S0869591111040047.

Kozakov, I.K., Kovach, V.P., Bibikova, E.V., Kirnozova, T.I., Lykhin, D.A., Plotkina, Y., Tolmacheva, E.V., Fugzan, M.M., Erdenezhargal, C., 2014. Late Riphean episode in the formation of crystalline rock complexes in the Dzabkhan microcontinent: geological, geochronologic, and Nd isotopic-geochemical data. Petrology 22, 480–506. https://doi.org/10.1134/S0869593808040023.

Kretz, R., 1983. Symbols for rock-forming minerals. American Mineralogist 68, 277–279.

Kröner, A. (Ed.), 2015. The Central Asian Orogenic Belt. Geology, Evolution, Tectonics, and Models. Schweizerbart Science Publishers, Stuttgart (313 pp.).

Kröner, A., Lehmann, J., Schulmann, K., Demoux, A., Lexa, O., Tomurhuu, D., Štípská, P., Liu, D., Wingate, M.T.D., 2010. Lithostratigraphic and geochronological constraints on the evolution of the Central Asian Orogenic Belt in SW Mongolia: Early Paleozoic rifting followed by Late Paleozoic accretion. American Journal of Science 310, 523–574.

Kröner, A., Kovach, V.P., Kozakov, I.K., Kirnozova, T., Azimov, P., Wong, J., Geng, H.Y., 2015. Zircon ages and Nd–Hf isotopes in UHT granulites of the Ider Complex: a cratonic terrane within the Central Asian Orogenic Belt in NW Mongolia. Gondwana Research 27, 1392–1406. https://doi.org/10.1016/j.gr.2014.03.005.

Kröner, A., Kovach, V., Alexeiev, D., Wang, K., Wong, J., Degtyarev, K., Kozakov, I., 2017. No excessive crustal growth in the Central Asian Orogenic Belt: further evidence from field relationships and isotopic data. Gondwana Research 50, 135–166. https://doi.org/10.1016/j.gr.2017.04.006.

Kuzmichev, A.B., Larionov, A.N., 2011. The Sarkhoi Group in East Sayan: Neoproterozoic (~770–800 Ma) volcanic belt of the Andean type. Russian Geology and Geophysics 52, 685–700. https://doi.org/10.1016/j.rgg.2011.06.001.

Kuzmichev, A.B., Bibikova, E.V., Zhuravlev, D.Z., 2001. Neoproterozoic (~800 Ma) orogeny in the Tuva–Mongolia Massif (Siberia): island arc–continent collision at the northeast Rodinia margin. Precambrian Research 110, 109–126. https://doi.org/10.1016/S0301-9268(01)00183-8.

Kuzmichev, A.B., Kröner, A., Hegner, E., Dunyi, L., Yusheng, W., 2005. The Shishkhid ophiolite, northern Mongolia: a key to the reconstruction of a Neoproterozoic island-arc system in central Asia. Precambrian Research 138, 125–150. https://doi.org/10.1016/j.precamres.2005.04.002.

Kuzmichev, A.B., Sklyarov, E., Postnikov, A., Bibikova, E., 2007. The Oka Belt (Southern Siberia and Northern Mongolia): a Neoproterozoic analog of the Japanese Shimanto Belt? Island Arc 16, 224–242. https://doi.org/10.1111/j.1440-1738.2007.00568.x.

Lehmann, J., Schulmann, K., Lexa, O., Corsini, M., Kröner, A., Štípská, P., Tomurhuu, D., Otgonbator, D., 2010. Structural constraints on the evolution of the Central Asian Orogenic Belt in SW Mongolia. American Journal of Science 310, 575–628. https://doi.org/10.2475/07.2010.02.

Levashova, N.M., Kalugin, V.M., Gibsher, A.S., Yff, J., Ryabinin, A.B., Meert, J.G., Malone, S.J., 2010. The origin of the Baydaric microcontinent, Mongolia: Constraints from paleomagnetism and geochronology. Tectonophysics 485, 306–320. https://doi.org/10.1016/j.tecto.2010.01.012.

Long, X., Sun, M., Yuan, C., Xiao, W., Cai, K., 2008. Early Paleozoic sedimentary record of the Chinese Altai: implications for its tectonic evolution. Sedimentary Geology 208, 88–100. https://doi.org/10.1016/j.sedgeo.2008.05.002.

Long, X., Yuan, C., Sun, M., Xiao, W., Zhao, G., Wang, Y., Cai, K., Xia, X., Xie, L., 2010. Detrital zircon ages and Hf isotopes of the early Paleozoic flysch sequence in the Chinese Altai, NW China: new constrains on depositional age, provenance and tectonic evolution. Tectonophysics 480, 213–231. https://doi.org/10.1016/j.tecto.2009.10.013.

Long, X., Yuan, C., Sun, M., Xiao, W., Wang, Y., Cai, K., Jiang, Y., 2012. Geochemistry and Nd isotopic composition of the Early Paleozoic flysch sequence in the Chinese Altai, Central Asia: evidence for a northward-derived mafic source and insight into Nd model ages in accretionary orogen. Gondwana Research 22, 554–566. https://doi.org/10.1016/j.gr.2011.04.009.

Ludwig, K.R., 2008. User's Manual for Isoplot v. 3.6, a Geochronological Toolkit for Microsoft Excel. vol. 4. Berkeley Geochronological Center Special Publications, pp. 1–77.

Luvsandanzan, B., 1970. Stratigraphy of the Paleozoic of the Mongolian Altai. Stratigraphy and Tectonics of the Mongolian National Republic. Nauka, Moskva, pp. 62–98 (in Russian).

Meschede, M., 2014. Accretionary wedge. In: Harff, J., Meschede, M., Petersen, S., Thiede, J. (Eds.), Encyclopedia of Marine Geosciences. Springer Netherlands, Dordrecht, pp. 1–5 https://doi.org/10.1007/978-94-007-6644-0_101-1.

Mitrofanov, F.P., Bibikova, E.V., Gracheva, T.V., Kozakov, I.K., Sumin, L.V., Shuleshko, I.K., 1985. Archaean isotope age of tonalite ("grey") gneisses within the Caledonian structures of Central Mongolia. Doklady Akademii Nauk 284, 670–674 (in Russian).

Mongush, A.A., Lebedev, V.I., Kovach, V.P., Sal'nikova, E.B., Druzhkova, E.K., Yakovleva, S.Z., Plotkina, Y., Zagornaya, N.Y., Travin, A.V., Serov, P.A., 2011. The tectonomagmatic evolution of structure-lithologic complexes in the Tannu-Ola Zone, Tuva, in the late Vendian–early Cambrian (from geochemical, Nd isotope, and geochronological data). Russian Geology and Geophysics 52, 503–516. https://doi.org/10.1016/j.rgg.2011.04.003.

Mossakovsky, A.A., Ruzhentsev, S.V., Samygin, S.G., Kheraskova, T.N., 1994. Central Asian Fold Belt: geodynamic evolution and formation history. Geotectonics 27, 445–474.

Parfenov, L.M., Khanchuk, A.I., Badarch, G., Miller, R.J., Naumova, V.V., Nokleberg, W.J., Ogasawara, M., Prokopiev, A.V., Yan, H., 2003. Preliminary Northeast Asia geodynamics map, sheet 2, scale 1:5,000,000. U.S. Geological Survey Open-File Report 03–205.

Paton, C., Woodhead, J.D., Hellstrom, J.C., Hergt, J.M., Greig, A., Maas, R., 2010. Improved laser ablation U–Pb zircon geochronology through robust downhole fractionation correction. Geochemistry, Geophysics, Geosystems 11, 1–36. https://doi.org/10.1029/2009GC002618 (Q0AA06).

Pfänder, J., Jochum, K.P., Todt, W., Kröner, A., 1999. Relationships between the mantle, lower crust and upper crust within the Agardagh-Tes Chem Ophiolite, Central Asia: evidence from petrologic, trace element, and isotopic data. Ofioliti 24, 151–152. https://doi.org/10.4454/ofioliti.v24i1b.73.

Rudnev, S.N., Vladimirov, A.G., Ponomarchuk, V.A., Bibikova, E.V., Sergeev, S.A., Plotkina, Y.V., Bayanova, T.B., 2006. The Kaakhem polychronous granitoid batholith, eastern Tuva: composition, age, sources, and geodynamic setting. Litosfera 200, 3–33 (in Russian).

Rudnev, S.N., Izokh, A.E., Kovach, V.P., Shelepaev, R.A., Terent'eva, L.B., 2009. Age, composition, sources, and geodynamic environments of the origin of granitoids in the northern part of the Ozernaya Zone, western Mongolia: growth mechanisms of the Paleozoic continental crust. Petrology 17, 439–475. https://doi.org/10.1134/S0869591109050026.

Rudnev, S., Izokh, E., Borisenko, S., Shelepaev, R., Orihashi, Y., Lobanov, K., Vishnevsky, V., 2012. Early Paleozoic magmatism in the Bumbat-Hairhan area of the Lake Zone in western Mongolia (geological, petrochemical, and geochronological data). Russian Geology and Geophysics 53, 425–441. https://doi.org/10.1016/j.rgg.2012.03.004.

Rudnev, S.N., Kovach, V.P., Ponomarchuk, V.A., 2013. Vendian–early Cambrian island-arc plagiogranitoid magmatism in the Altai-Sayan folded area and in the Lake Zone of western Mongolia (geochronological, geochemical, and isotope data). Russian Geology and Geophysics 54, 1272–1287. https://doi.org/10.1016/j.rgg.2013.09.010.

Safonova, I., Seltmann, R., Kröner, A., Gladkochub, D., Schulmann, K., Xiao, W., Kim, J., Komiya, T., Sun, M., 2011. A new concept of continental construction in the Central Asian Orogenic Belt. Episodes 34, 186–196.

Safonova, I., Kotlyarov, A., Krivonogov, S., Xiao, W., 2017. Intra-oceanic arcs of the Paleo-Asian Ocean. Gondwana Research 50, 167–194. https://doi.org/10.1016/j.gr.2017.04.005.

Sal'nikova, E.B., Kozakov, I.K., Kotov, A.B., Kröner, A., Todt, W., Bibikova, E.V., Nutman, A., Yakovleva, S.Z., Kovach, V.P., 2001. Age of Palaeozoic granites and metamorphism

in the Tuvino-Mongolian Massif of the Central Asian Mobile Belt: loss of a Precambrian microcontinent. Precambrian Research 110, 143–164. https://doi.org/10.1016/S0301-9268(01)00185-1.
Scholl, D.W., Von Huene, R., Vallier, T.L., Howell, D.G., 1980. Sedimentary masses and concepts about tectonic processes at underthrust ocean margins (subduction). Geology 8, 564–568. https://doi.org/10.1130/0091-7613(1980)8<564:SMACAT>2.0.CO.
Şengör, A.M.C., Natal'in, B.A., 1996. Turkic-Type Orogeny and its role in the making of the continental crust. Annual Review of Earth and Planetary Sciences 24, 263–337.
Şengör, A., Natal'in, B., Burtman, V., 1993. Evolution of the Altaid tectonic collage and Paleozoic crustal growth in Eurasia. Nature 364, 299–307.
Sláma, J., Košler, J., 2012. Effects of sampling and mineral separation on accuracy of detrital zircon studies. Geochemistry, Geophysics, Geosystems 13, 1–17. https://doi.org/10.1029/2012GC004106.
Sláma, J., Košler, J., Condon, D.J., Crowley, J.L., Gerdes, A., Hanchar, J.M., Horstwood, M.S.A., Morris, G.A., Nasdala, L., Norberg, N., Schaltegger, U., Schoene, B., Tubrett, M.N., Whitehouse, M.J., 2008. Plešovice zircon – a new natural reference material for U–Pb and Hf isotopic microanalysis. Chemical Geology 249, 1–35.
Soejono, I., Buriánek, D., Svojtka, M., Žáček, V., Čáp, P., Janoušek, V., 2016. Mid-Ordovician and Late Devonian magmatism in the Togtokhinshil Complex: new insight into the formation and accretionary evolution of the Lake Zone (western Mongolia). Journal of Geosciences 61, 5–23. https://doi.org/10.3190/jgeosci.208.
Soejono, I., Buriánek, D., Janoušek, V., Svojtka, M., Čáp, P., Erban, V., Ganpurev, N., 2017. A reworked Lake Zone margin: chronological and geochemical constraints from the Ordovician arc-related basement of the Hovd Zone (western Mongolia). Lithos 295, 112–132. https://doi.org/10.1016/j.lithos.2017.08.014.
Štípská, P., Schulmann, K., Lehmann, J., Corsini, M., Lexa, O., Tomurhuu, D., 2010. Early Cambrian eclogites in SW Mongolia: evidence that the Palaeo-Asian Ocean suture extends further east than expected. Journal of Metamorphic Geology 28, 915–933. https://doi.org/10.1111/j.1525-1314.2010.00899.x.
Tomurtogoo, O., 1997. A new tectonic scheme of the Paleozoides in Mongolia. Mongolian Geoscientist 3, 12–19.
Vermeesch, P., 2004. How many grains are needed for a provenance study? Earth and Planetary Science Letters 224, 441–451. https://doi.org/10.1016/j.epsl.2004.05.037.
Vermeesch, P., 2012. On the visualisation of detrital age distributions. Chemical Geology 341, 190–194. https://doi.org/10.1016/j.chemgeo.2013.01.010.
Wang, Y., Yuan, C., Long, X., Sun, M., Xiao, W., Zhao, G., Cai, K., Jiang, Y., 2011. Geochemistry, zircon U–Pb ages and Hf isotopes of the Paleozoic volcanic rocks in the northwestern Chinese Altai: petrogenesis and tectonic implications. Journal of Asian Earth Sciences 42, 969–985. https://doi.org/10.1016/j.jseaes.2010.11.005.
Wang, Y., Long, X., Wilde, S.A., Xu, H., Sun, M., Xiao, W., Yuan, C., Cai, K., 2014. Provenance of Early Paleozoic metasediments in the central Chinese Altai: implications for tectonic affinity of the Altai-Mongolia Terrane in the Central Asian Orogenic Belt. Lithos 210, 57–68. https://doi.org/10.1016/j.lithos.2014.09.026.
Wiedenbeck, M., Alle, P., Corfu, F., Griffin, W.L., Meier, M., Oberli, F., von Quadt, A., Roddick, J.C., Spiegel, W., 1995. Three natural zircon standards for U–Th–Pb, Lu–Hf, trace element and REE analyses. Geostandards Newsletter 19, 1–23.
Wilhem, C., Windley, B.F., Stampfli, G.M., 2012. The Altaids of Central Asia: a tectonic and evolutionary innovative review. Earth-Science Reviews 113, 303–341.
Windley, B.F., Alexeiev, D.V., Xiao, W.J., Kröner, A., Badarch, G., 2007. Tectonic models for accretion of the Central Asian Orogenic Belt. Journal of the Geological Society of London 164, 31–47.
Xiao, W.J., Santosh, M., 2014. The western Central Asian Orogenic Belt: a window to accretionary orogenesis and continental growth. Gondwana Research 25, 1429–1444.
Xiao, W.J., Windley, B.F., Badarch, G., Sun, S., Li, J., Qin, K., Wang, Z., 2004. Palaeozoic accretionary and convergent tectonics of the southern Altaids: implications for the growth of Central Asia. Journal of the Geological Society of London 161, 339–342.
Xiao, W.J., Windley, B., Sun, S., Li, J., Huang, B., Han, C., Yuan, C., Sun, Chen, H., 2015. A tale of amalgamation of three Permo–Triassic collage systems in Central Asia: oroclines, sutures, and terminal accretion. Annual Review of Earth and Planetary Sciences 43, 477–507. https://doi.org/10.1146/annurev-earth-060614-105254.
Xiao, W.J., Windley, B.F., Han, C., Liu, W., Wan, B., Zhang, J., Ao, S., Zhang, Z., Song, D., 2017. Late Paleozoic to early Triassic multiple roll-back and oroclinal bending of the Mongolia collage in Central Asia. Earth-Science Reviews, https://doi.org/10.1016/j.earscirev.2017.09.020 (in print).
Yarmolyuk, V., Kovalenko, V., Anisimova, I., Sal'nikova, E., Kovach, V., Kozakov, I., Kozlovsky, A., Kudryashova, E., Kotov, A., Plotkina, Y., Terent'eva, L., Yakovleva, S., 2008. Late Riphean alkali granites of the Zabhan microcontinent: evidence for the timing of Rodinia breakup and formation of microcontinents in the Central Asian Fold belt. Doklady Earth Sciences 420, 583–588. https://doi.org/10.1134/S1028334X08040132.
Yarmolyuk, V.V., Kovach, V.P., Kovalenko, V.I., Sal'nikova, E.B., Kozlovskii, a.M., Kotov, a.B., Yakovleva, S.Z., Fedoseenko, a.M., 2011. Composition, sources, and mechanism of continental crust growth in the Lake Zone of the Central Asian Caledonides: I. Geological and geochronological data. Petrology 19, 55–78. https://doi.org/10.1134/S0869591111010085.
Žáček, V., Břízová, E., Bohdálek, P., Buriánek, D., Čáp, P., Enkhjargal, M., Franců, J., Gelegjamts, A., Guy, A., Hanžl, P., Havlíček, P., Henrion, E., Hošek, J., Jelének, J., Knésl, I., Karenová, J., Kociánová, L., Kotková, J., Krejčí, Z., Mixa, P., Mrlina, J., Pecina, V., Pécskay, Z., Prudhomme, A., Soejono, I., Svojtka, M., Šimůnek, Z., Škoda, R., Verner, K., Vondrovic, L., Vorel, T., Vrána, S., Čopjaková, R., 2016. Geological Mapping 1: 50,000 and Assessment of Economic Potential of Selected Region in Western Mongolia (Mongol Altai 50, Ma-50), Final Report, Czech Geological Survey, Prague, Mineral Resources Authority of Mongolia. pp. 1–518.
Zimmermann, U., Andersen, T., Madland, M.V., Larsen, I.S., 2015. The role of U–Pb ages of detrital zircons in sedimentology – an alarming case study for the impact of sampling for provenance interpretation. Sedimentary Geology 320, 38–50. https://doi.org/10.1016/j.sedgeo.2015.02.006.
Zonenshain, L.P., Kuzmin, M.I., 1978. Khan-Taishir ophiolite complex in western Mongolia and problems of ophiolites. Geotectonics 1, 19–42.